A report for the

Commonwealth Department of Climate Change and Energy Efficiency (DCCEE)

Extreme windspeed baseline climate investigation project

April 2011

Editor: John Ginger, Cyclone Testing Station

Task 1: Bob Cechet, Augusto Sanabria, Geoscience Australia

Task 2: Jeff Kepert, Bureau of Meteorology; John Holmes, JDH Consulting

Task 3: John Ginger, David Henderson, Cyclone Testing Station, James Cook University

Extreme Windspeed Baseline Climate Investigation Project

A report for the
Commonwealth Department of Climate Change and Energy Efficiency
(DCCEE)

Final Report
28 April, 2011

Report Editor and Project Manager: John Ginger
Cyclone Testing Station
School of Engineering and Physical Sciences
James Cook University
Queensland, 4811, Australia

www.jcu.edu.au/cts

Task 1: Bob Cechet, Augusto Sanabria, Geoscience Australia

Task 2: Jeff Kepert, Bureau of Meteorology; John Holmes, JDH Consulting

Task 3: John Ginger, David Henderson, Cyclone Testing Station, James Cook University

Extreme Windspeed Baseline Climate Investigation Project

EXECUTIVE SUMMARY

The project aim was to establish the difference in response characteristics and appropriate correction factors for the Dines anemometer formerly used, and the currently used cup anemometers. The project has achieved this with the development of correction factors for various wind speeds and instrument types through investigation of historical wind records, theoretical modelling of the anemometers and experimental testing.

Starting in about the mid 1980's, the standard anemometers used by the Bureau of Meteorology to record wind speeds, including the maximum daily gusts, have been changed from the Dines anemometers to 3-cup Synchrotac anemometers. The Dines anemometer had been the mainstay of wind speed measurements since the 1930's and forms the majority of the historical wind record in Australia.

The Dines uses a pressure tube head, with the pressure changes in the tube related to the wind velocity raising and lowering a shaped float in a water chamber. Three types of Dines were used; the main two being the low-speed or standard (measuring to 100 knots) in non-cyclonic regions and the high-speed (measuring to 200 knots) in cyclonic regions. There were also a few examples of an intermediate instrument that measured to 150 knots, including in Darwin, during Cyclone Tracy. From the few occasions that the cup and Dines anemometers were operating in parallel during a storm event, the responses of the Dines and 3-cup differed; for example, the Dines peak gust reading was about 15% higher than that recorded by the 3-cup during Cyclone 'Vance' at Learmonth, WA and Cyclone Tessi in Townsville, Qld.

The Australian and New Zealand wind actions Standard AS/NZS 1170.2 uses historical data records from the Bureau of Meteorology stations, fitted to appropriate extreme value probability distributions, to stipulate the design wind speed to be applied when designing a structure. Reliable wind speed measurements are important for estimating extreme wind speeds in regions across the country given in AS/NZ1170.2, for the forensic analysis of assessing structural damage following windstorms to evaluate building code performance and for use in hazard-vulnerability models, and for analysing climate change impacts.

This project was carried out to determine the response of the two main types of Dines instruments and compare gust (i.e. peak) wind speeds measured against the replacement 3-cup anemometers. The activity established the difference in response characteristics and produced appropriate correction factors for the former Dines and the current Synchrotac anemometers used by the Bureau of Meteorology to measure wind speed, that will enable the establishment of a valid baseline for Australian wind speed data.

The project comprised three tasks.

Task 1: Statistical analysis of the maximum gust wind speed observations conducted by employing extreme value statistical theory to examine two datasets:

(1) time-series of daily maximum wind gust observations (Dines and cup anemometer with no overlap)

(2) coincident Dines and cup anemometer observations (30 minute time slices for 89 years of observational record at seven Bureau of Meteorology stations considered).

The observed data allowed us to consider gust wind speeds up to 60 m/s (the EVD's tend to asymptote above this range for the data considered). The Dines anemometer has a tendency to read about 5% higher than the cup anemometer at gust wind speeds of 40m/s increasing to about 15% higher at gust wind speeds of 60 m/s. These systematic differences are consistent with those reported previously, and confirm concerns about the consistency of the peak gust wind speed observational database which underpins the wind actions standard AS/NZS 1170.2.

Task 2: Review of previous studies of response characteristics of the Dines anemometer system (both low speed and high-speed) and the development of a validated numerical model of the Dines anemometer.

The literature review found published material on the dynamic response of the Dines anemometers –but this mainly early work from the U.K., was unpublished, or was available in a 'second-hand' form. A paper from Portugal describing laboratory measurements of the float motion was identified as useful to the project. Little published material directly comparing the response of anemometer types to short-term *gusts* was found. One reason for this is the change to wind speeds for structural design averaged over a longer period (e.g. 1-hour) in the U.K., for the last 15-20 years. However, a useful comparative study from Ireland from the 1980s was found to have particular relevance to the project.

This study found that the effect of the tubing on the overall response of the Dines system, (for the tubing dimensions used in Australian applications), was negligible, because of the dominant influence of the float dynamics.

Dynamical modelling of the response of the Dines anemometer to fluctuating winds found that the instrument possesses two resonant frequencies. In one, the float and water in the float chamber move in phase, and in the other, they move out of phase. The response characteristics of both Dines instruments are not highly dependent on the magnitude of the mean and peak wind speeds. A random process approach to gust factors and Dines/cup gust ratios gave good agreement with measured values of gust ratios, and enabled adjustment for varying parameters such as mean wind speed, turbulence intensity, turbulence length scale, and distance constant of the cup anemometer. The dynamical modelling produced excellent agreement with the laboratory measurements.

The analytical results indicate that the low-speed Dines overshoots the 3-cup by about 3 to 5% at a mean wind speed of 25 m/s and turbulence intensity of 9%. The high speed Dines overshoots the 3-cup by about 7% at a mean wind speed of 35 m/s and turbulence intensity of 20%. These are quite consistent with the experimental results and field comparisons. However, the effect of applying a 3-sec moving average filter to the 3-cup anemometer output, as recommended by the WMO, is to greatly increase the overshoot ratio of the Dines, doubling it at lower speeds and trebling it at higher

speeds, and introducing a greater difference than that arising from differences between the anemometer types.

Task 3: Experimental testing of the Dines pressure tube and float dynamic characteristics (Low-Speed and High Speed) using a Pressure Loading Actuator (PLA).

The objectives of the Task were to measure the response of the low-speed and high-speed Dines when excited by a known pressure signal at the head. A series of tests were conducted on the low-speed Dines at the CTS in Townsville, followed by the high-speed Dines at the Bureau of Meteorology located at Townsville Airport. A range of pressure signals (static, sinusoidal, white noise) were generated using a Pressure Loading Actuator (PLA) and applied to the Dines instruments.

The tests showed that the mean wind speed is accurately measured by both Dines types with the movement of the float rod. Application of fluctuating pressures (i.e. gust velocities) to the system indicated that the 10m tube amplifies pressures at a high frequency (> 5Hz). The response of the float and rod immersed in water in the chamber generates a double peak spectrum creating a slight amplification at low frequencies, a trough at about 1Hz followed by a peak at higher frequencies. The low-frequency peak occurred at about 0.5 Hertz for the low-speed Dines, and 0.3 Hertz for the high-speed Dines. These experimental results were satisfactorily modeled in Task 2. Both Dines instruments satisfactorily "follow" the fluctuating wind gusts, and nominally give a peak representative of a value averaged over a period of less than 3sec (the 'response time' depends on the definition used).

OUTCOMES OF THE PROJECT

- The mean wind speed averaged over 1 to 10 mins is accurately measured by low- and high-speed Dines anemometers.
- The response of the Dines anemometer is mainly governed by the dynamics of the float system, with the connecting 10m tubing having negligible effect. The instrument natural frequencies at < 1.0 Hz, affects their response to wind gusts, and the maximum gust recorded in a defined period.
- Because of the resonance in the float system, the Dines anemometer records higher gusts than the (unfiltered) cup anemometer used by the Bureau of Meteorology.
- The application of a 3-second moving average filter to the cup anemometer outputs in the Automatic Weather Stations (AWS) reduces the peaks recorded by the that instrument, and has resulted in a further increase in the *apparent* average overshoot of the Dines anemometers relative to the cup anemometer to 7-13% for the low-speed type, and to 12-21% for the high-speed type.
- Correction factors for comparison of Dines to 3-cup peak gusts for increasing mean wind speeds are given in Tables III and IV of Appendix II-4

RECOMMENDATIONS OF THE PROJECT

- The definition of peak gust used in the Australian/New Zealand Standard for wind actions (AS/NZS1170.2) should be reviewed by Standards Australia, since a significantly lower gust is currently being recorded by the Bureau of Meteorology. The latter has resulted from the decision of the Bureau, following a World Meteorological Office recommendation, to apply a 3-second moving-average filter applied in the Automatic Weather Stations to recorded daily gusts in Australia. The current description of the maximum gust in the Standard as a '3-second gust' is

misleading, as it was based on an earlier definition of the averaging time of the gust recorded by the Dines anemometers, and is not a moving-average time.

- Factors have been derived to allow corrections to be made to daily maximum gusts formerly generated by the Dines anemometers (both low-speed and high-speed types), and currently being generated by Automatic Weather Stations in Australia. These correction factors should be applied before extreme value analyses are undertaken to develop revised design wind speeds for structures.
- The Bureau of Meteorology should provide details of instrument changeover including dates and described relevant methods of measurement and recording, and provide correction factors for users of wind speed Metadata.
- Develop standardized procedures for developing a baseline wind speed dataset from the correction factors given in this project.
- The Bureau of Meteorology should consider collecting daily maximum *10-minute* averaged winds from the Automatic Weather Stations. This would provide an alternative set of data to the 3-second-averaged gusts for extreme value analyses, that is not sensitive to anemometer response, or is affected by the digital filtering

ACKNOWLEDGEMENTS

The Extreme Windspeed Baseline Investigation Project is a collaboration between the Cyclone Testing Station at James Cook University, the Bureau of Meteorology, John Holmes Consulting and Geoscience Australia. The authors gratefully acknowledge the financial support from the Department of Climate Change and Energy Efficiency (DCCEE) and the Australasian Wind Engineering Society (AWES) and the Bureau of Meteorology for the support and valued assistance.

The authors would like to thank;

Jim Davidson, Director, Bureau of Meteorology, Queensland
Doug Fraser and Mats Einerman, Bureau of Meteorology, Townsville
Dave Edwards, Paul Leigh and Jim Easson, Bureau of Meteorology, Melbourne
Ian Muirhead, Bureau of Meteorology, National Climate Centre, Melbourne
Sean Carson, Bureau of Meteorology, Canberra
Murray Morrison, University of Western Ontario
Rachael Dempsey (now Murray Darling Basin Authority)
Antonio Mozqueira (now Office of Australian Chief Scientist)
Anthony Swirepik from the Department of Climate Change and Energy Efficiency

This report was reviewed by Dr. Craig Miller (University of Western Ontario, Canada), Dr. Chris Letchford (Rensselaer Polytechnic Institute, USA) and Dr. Bruce Harper (GHD, Australia). The authors are grateful for the reviewers' comments and suggestions.

Extreme Windspeed Baseline Climate Investigation Project

TABLE OF CONTENTS

INTRODUCTION

This project aims to establish the response characteristics of the now obsolete Dines Anemometer and the Synchrotac 3-cup anemometers currently used by the Bureau of Meteorology. Three types of Dines anemometers (mainly high speed in cyclone areas and low-speed in non-cyclone areas, plus a few intermediate speed instruments) were used at a number of sites in Australia, and these have been progressively replaced by 3-cup anemometers commencing in the mid 1980s. In addition, new sites have been added to the network by the Bureau of Meteorology. The Bureau of Meteorology advises that at a number of sites, the cup and Dines instruments have collected data in parallel, notwithstanding that only the data from one instrument may be in the official data record (Metadata). Both instruments are still operational at a few sites. Hence, wind speed data from each instrument at selected sites, and importantly any overlapping data were analyzed, noting any local influences especially if the instruments were not located close to each other.

From the few occasions that cup and Dines anemometers were operating in parallel during a storm event it is apparent that the responses of these two to extreme wind gusts can differ significantly. For example, a 15% difference in the peak gust was recorded by the two anemometer types situated no more than 20 metres apart during Cyclone 'Vance' at Learmonth, WA in 1999. A similar difference between anemometers was found during Cyclone 'Tessi' and also Cyclone 'Yasi' in Townsville.

The long-term observational wind speed data recorded by the Bureau of Meteorology at their weather station sites is statistically analyzed for deriving regional design wind speeds given in the wind loading standard AS/NZS1170.2. These design wind speeds are specified in terms of peak (i.e. gust) wind speed with return period. The aim for this project is to assess the response of the Dines and compare it with the response of the new 3-cup anemometer to ascertain if there is a systematic trend or bias in the data records that are periodically analyzed and used for revising the wind load standard. The data of interest are the peak wind speeds exceeding some threshold value. Data available when both instruments are operating in parallel are used for direct comparisons.

This project commenced on 1 July 2009, and was carried out by a team from the Bureau of Meteorology, Geoscience Australia, JDH Consulting and the Cyclone Testing Station (CTS) at James Cook University. Standards Australia was represented by team members from JDH Consulting and the CTS. A steering committee comprising a number of stakeholders assisted the team in setting the scope, and reviewed a draft of this report and provided comment. Their feedback has been addressed in this final report.

OVERVIEW

The project comprising of three Tasks progressed mostly according to plan, with some minor adjustments; i.e. overlap of Tasks, early starts of some Tasks and some delays due to issues outside the control of the team. Table 1 provides a summary of Tasks and reporting outcomes. This Final Report has been prepared following review of the Draft Report by representatives of the stakeholders. The project team and stakeholders met twice to formulate the project. Since the commencement a further two meetings and three teleconference meetings have been held. A final meeting is planned following the submission of the report to the Department of Climate Change and Energy Efficiency (DCCEE).

Table 1. Summary description of Tasks and Project Outputs

Task	Lead Agency/ Contact	Progress Reporting	Draft Reporting	Final Reporting
• Statistical comparison of historical daily gust data from those cases where the two anemometer systems were operating in parallel.	Geoscience Australia Bob Cechet and Augusto Sanabria	Progress report submitted to DCCEE in March 2010	Draft report submitted to DCCEE in December 2010	Final report submitted to DCCEE in April 2011
• An extensive review of previous studies of response characteristics of the Dines anemometer system (both low-speed and high-speed systems) and the development of a validated numerical model of the Dines anemometer (to be supported by experimental testing in Task 3).	Bureau of Meteorology Jeff Kepert JDH Consulting John Holmes	Progress report submitted to DCCEE in April 2010	Draft report submitted to DCCEE in December 2010	Final report submitted to DCCEE in April 2011
• Experimental testing of the Dines pressure tube and float dynamic characteristics using a rapid pressure actuator (Testing of low- and high-speed Dines Systems).	Cyclone Testing Station John Ginger and David Henderson	Progress report submitted to DCCEE in April 2010	Draft report submitted to DCCEE in December 2010	Final report submitted to DCCEE in April 2011

The Report is produced in parts related to each Task. These parts comprise of a brief description of each Task followed by a summary of accomplishments in each Task. The detailed work carried out in each Task is presented in separate Appendices.

The Dines anemometer is a pressure tube type instrument that measures the difference in pressure between moving air bought to rest and a reference static pressure. The system consists of; a head (or pitot) and vane typically located in open terrain at a standard height of 10m, a float that sits in a chamber containing water, and pipes (or tubes) connecting the head and static port to the chamber. A pen attached to an arm fixed to the float rod connected to the float records the motion of the float which responds to changes in the wind speed (i.e. pressure differences across the float) on a chart attached to a rotating drum. There are two main types of Dines systems; the low-speed (Standard)type used in non-cyclonic regions and the high-speed type used in cyclonic regions. The differences in the two systems relate to a taller chamber and heavier float of the high -speed system giving it the ability to measure higher wind speeds. A schematic diagram of the Dines obtained from the operations manual is given in Figure 1.

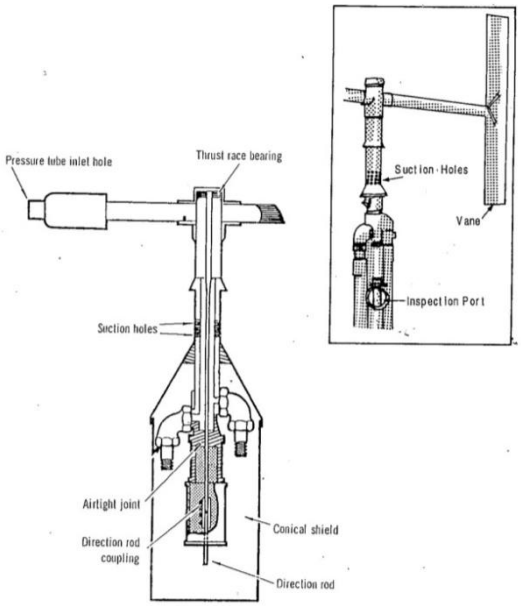

a) Dines Head and Vane

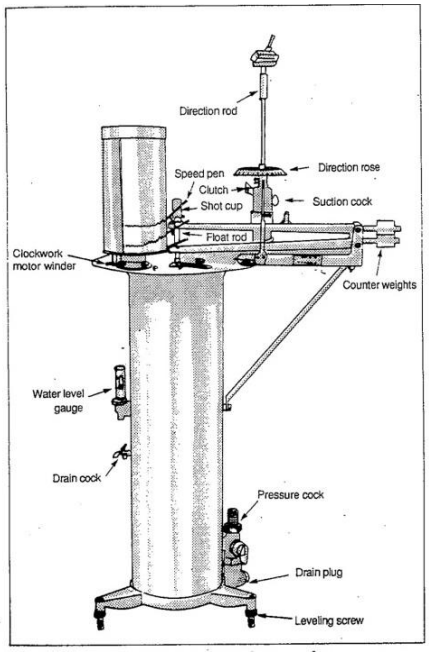

b) Float chamber and speed recorder

Figure 1. Schematic diagram of Dines (Meteorological-Office (1956), "Handbook of meteorological instruments Part 1: Instruments for surface observations" A. Ministry, ed., Her Majesty's Stationery Office, London)

TASK 1: STATISTICAL COMPARISON OF HISTORICAL DAILY GUST DATA FROM THOSE CASES WHERE THE TWO ANEMOMETER SYSTEMS WERE OPERATING IN PARALLEL

This task sought to examine the observed record of peak gust wind speed (daily maximum gust wind speed) in order to establish the existence of a bias between the early part of the record (obtained using pressure-tube Dines anemometers) and the later part of the record (obtained using 3-cup anemometers). All observational data as well as metadata was obtained from the Bureau of Meteorology. The 38 recording stations considered were all situated at airports and were in the most part staffed by Bureau of Meteorology officers. To isolate the issue of anemometer replacement (i.e. reduce concerns regarding consistent instrument exposure), only observing stations located at airports and with more than 30 years of record were considered.

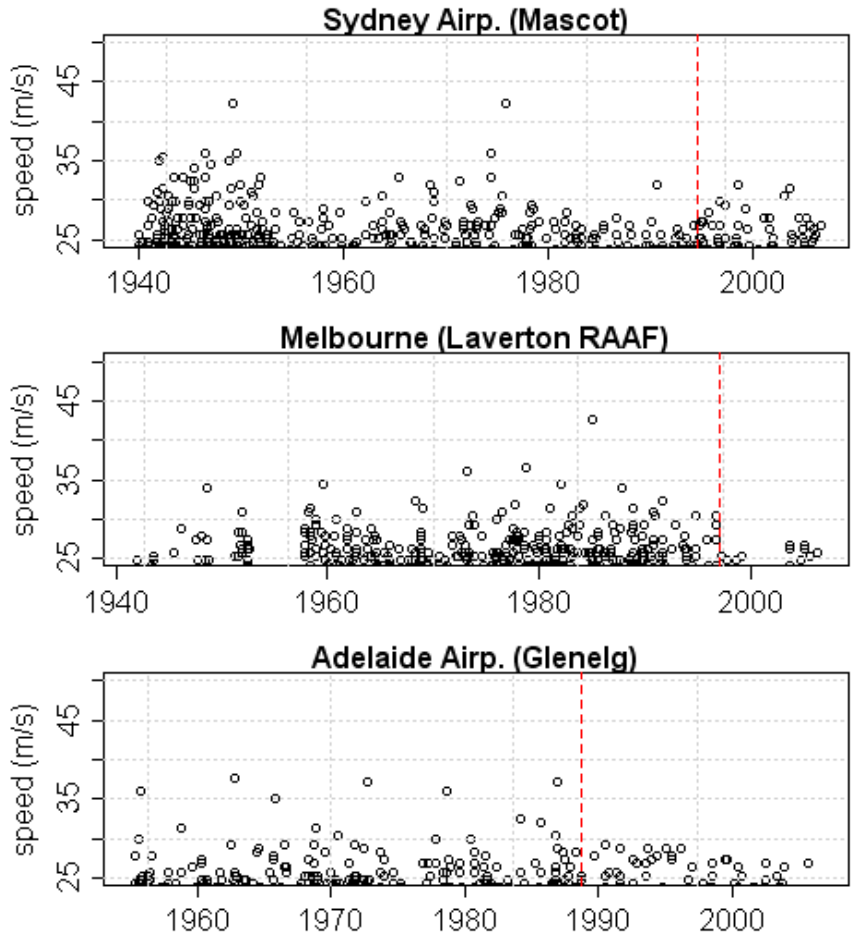

Figure 1-1. Time-series plots of the daily maximum gust wind speed (above a threshold of 25 m/s) for the Sydney, Melbourne and Adelaide (airport) meteorological observing station. The broken vertical line indicates the replacement of the Dines anemometer with a 3-cup anemometer.

The visual inspection of the observed daily peak gust wind speed time-series for most of the Bureau of Meteorology observing sites considered in this study is sufficient to indicate that in general *"the early part of the record (Dines measurements) contains a higher frequency of extreme events, and also the largest amplitude extreme events."* Figure 1-1 shows time-series plots of the daily maximum gust wind speed (above a threshold of 25 m/s) for the Sydney, Melbourne and Adelaide meteorological observing stations. Visual inspection indicates that the early part of the record (Dines anemometer) contains a greater number and also higher amplitude extreme events compared to the later part of the record (replacement cup anemometer).

Statistical analysis of the daily maximum gust wind speed observations was conducted by employing extreme value distribution (EVD) statistical theory to examine two datasets:

(1) time-series of Dines & cup anemometer observations (with no overlap in the observational record);
(2) coincident Dines & cup anemometer observations.

Analysis of time-series of Dines and cup anemometer observations (no overlap)

We have evaluated both the daily maximum gust and 3PM mean wind speed 500-year return period (500RP) exceedance levels for the total (*combined*) wind speeds for the 31 wind observing stations selected (within AS/NZS 1170.2 Region A). Observations have been segmented into the Dines and cup anemometer observing periods. The 95% confidence interval (95CI) has been determined for both gust and 3PM mean wind speeds for the Dines anemometer segment of the record. For the cup anemometer 500RP exceedance level gust wind speed estimates, there are 17 observing stations where the cup anemometer estimates fall below the lower 95% confidence interval (95CI) for the Dines segment of the observing record. For 24 of the 31 observing stations the cup anemometer estimate falls below the corresponding Dines segment estimate. Considering the 3PM mean wind speeds, there are 18 observing stations where the cup anemometer estimate falls below the lower 95CI for the Dines segment of the observing record.

The statistical analysis utilising extreme value distributions (EVD's) resulted in more than half of the observing stations considered (later part of the time-series record) having both 500-year RP gust wind speed (17 of 31) and 3PM mean wind speed (18 of 31) exceedance level estimates being in the lower tail of the distribution for the early part of the observing record (period prior to equipment upgrade from Dines to cup anemometer). We should be cautious in interpreting the differences in the return period hazard for the two segments of the record. It is possible that the frequency of extreme wind speeds has actually declined (Smits *et al*. 2005). The most recent part of the record has been dominated by a number of large El Nino events and only one La Nina event, where thunderstorms are known to be more prevalent (Kuleshov *et al*. 2002). The importance of the non-stationary climate needs to be considered when conducting a time series analysis. Circulation changes as discussed in (Plummer *et al.* 1999; Alexander *et al.* 2010), possibly driven by anthropogenic climate change, could also affect the frequency and amplitude of extreme winds. The cup anemometer part of the record is generally much shorter (10-25 years) than the Dines segment and it is possible that the very high maximum wind speeds have just not yet been sampled, although the reduced frequency of extreme events in the later part of the record is of concern. Even considering these issues, this analysis suggests that the consistency of the combined peak gust wind speed dataset is suspect, and that the problem requires further examination via analysis of coincident measurements. This analysis indicates that it appears unlikely that the later part of the observing record can be considered consistent with the initial (Dines) segment of the record.

Analysis of coincident Dines and cup anemometer observations

Coincident gust wind speed measurements at 7 northern Australian observing stations were analysed to determine the magnitude of the direct bias. Only Dines "high-speed range" anemometers (0-200 knots) were considered for observing stations where extreme wind gusts are dominated by thunderstorm and tropical cyclone events. The stations examined were Cairns, Townsville, Brisbane, Darwin, Gove, Broome and Learmonth. Cup anemometer data was available in digital form (maximum gust wind speed for each 30 minute interval) whereas the maximum gust wind speed for the Dines anemometer record was scaled directly off the chart record by recording the maximum peak each 30 minute period. A threshold of 15 m/s over the 30 minute period for the cup anemometer was selected so that only thunderstorm and tropical cyclone events were considered (i.e. no synoptic wind events were considered; gusts were independent events).

Coincident probability distributions (PDF's) of the gust wind speed ((Dines & cup anemometer; 15 m/s threshold) for the seven sites considered display some interesting characteristics:

- PDF's are broader for the Dines instrument (all cases) indicating an elevated level of noise compared with the cup anemometer. This noise may be partly made up of random error (instruments not coincident in position; separated by between 25m and 100m) and also instrument error (issues such as the Dines float resonance and the Dines wind vane not parallel to gust direction as well as others such as the Dines float level not being maintained at the correct position). This confirms both theoretical and laboratory testing undertaken within other tasks of this study which indicated that the Dines instrument was more "noisy" compared to cup anemometers. It is possible that instrument error is the cause of "extreme value bias" between the two instruments
- Focusing on the peak of the PDF's, there appears to be some systematic bias between Dines and cup anemometers for some of the observing stations. The PDF peak appears slightly low for the Dines at Darwin compared to the cup anemometer and too high for Learmonth and Townsville. Agreement is excellent for Cairns.

Time-series plots of the bias between the Dines and cup anemometer measurements show no time dependent relationships. The bias is uni-directional for some extreme cases where the cup anemometer recorded an event that the Dines either captures to a much lesser extent or misses altogether. The size of thunderstorm gust fronts can cause significant differences in wind speed over 10's to 100's of metres. The uni-directional nature of the extreme bias is due to events captured by the Dines but not the cup anemometer not being considered by the analysis technique (which was driven by the digital record).

The data on the extreme gust wind speeds for the 7 sites were combined into one dataset and extreme value statistical theory (Generalised Pareto Distributions; GPD's) were used to investigate the return period exceedence levels for the combined dataset. Figure 1-2 shows the return period plots of coincident maximum gust wind speed (above a threshold of 15 m/s for 30 minute time sections) for the combined 7 northern Australian observing stations obtained over a total coincident measurement period of 89 years. In addition, 95% confidence limits for the GPD fit to the Dines extreme gust wind observations are also shown.

Table 1-1 details the percentage bias between the cup anemometer and Dines return period estimates (including the 95% confidence limits regarding the fitting of the extreme value distribution to the Dines gust observations). The observed data allows us to consider gust wind speeds between 45 and 70 m/s. When considering gust wind speeds at about 45 m/s, the Dines anemometer has a tendency to read about 5 to 10% higher than the cup anemometer (considering coincident data at 30

minute intervals); this increases to about 12 to 17% higher at gust wind speeds around 60 m/s. These systematic differences are consistent with those reported by Reardon *et al*. (1999) and Reardon (2000), and confirm concerns about the consistency of the peak gust wind speed observational database which underpins the Australian wind loading standard (AS/NZS 1170.2, 2010).

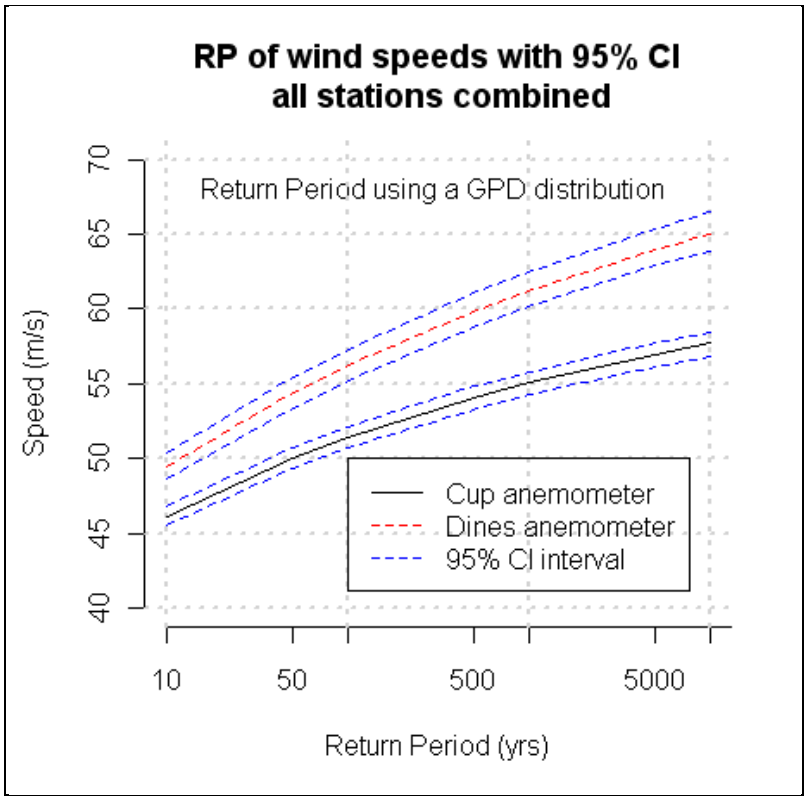

Figure1-2. Return period plots of coincident maximum gust wind speed (above a threshold of 15 m/s for 30 minute time sections) for the combined 7 northern Australian observing stations over a total coincident measurement period of 89 years. 95% confidence limits for the GPD fit to the Dines anemometer observations are also provided.

Table 1-1. Percentage difference (return period gust wind speed) between the Dines anemometer and cup anemometers over a range of wind speeds, considering coincident extreme wind gust measurements at 7 observing sites over a total coincident measurement period of 89 years. The asymptotic nature of the GPD fit to the observations does not allow a comparison for gust wind speeds above 60 m/s.

Cup anemometer gust wind speed	Dines anemometer gust wind speed	Dines; Lower 95% confidence limit	Dines; Upper 95% confidence limit
45 m/s	+7 %	+5 %	+9 %
50 m/s	+9%	+7 %	+11 %
55 m/s	+11 %	+9 %	+13.5 %
60 m/s	+14 %	+12 %	+17 %
65 m/s	N/A	N/A	N/A

Recommendation from Task 1

- This analysis allows the calculation of factors which will provide corrections to be made to daily maximum gust wind speed data in order to obtain a uniform record. It appears that a significantly lower amplitude wind gust is currently being recorded by the Bureau of Meteorology (BoM). This is chiefly the result of a decision of the BoM (based on W.M.O. advice) to apply a 3-second moving average filter to the 3-cup Synchrotac anemometer recorded daily gusts (see further explanation later in the report). It is recommended that experimental evidence detailing the impact of the "digital filtering" on the cup anemometer measurements should be acquired to quantify this bias and determine its significance with regards to the issue of correction factors.

References for Task 1

Alexander L.V., Uotila P., Nicholls N. and Lynch A. 2010. A New Daily Pressure Dataset for Australia and Its Application to the Assessment of Changes in Synoptic Patterns during the Last Century, *Journal of Climate 23:5* 1111-1126

AS/NZS 1170.2 2002. *Structural design actions, Part 2: Wind actions* Australian/New Zealand Standard

Kuleshov Y., de Hoedt, G., Wright W. and Brewster A. 2002. Thunderstorm distribution and frequency in Australia, *Aust. Met. Mag*. 51, 145-154

Plummer N., Salinger M.J., Nicholls N., Suppiah R., Hennessy K.J., Leighton R.M., Trewin B., Page C.M. and Lough J.M. 1999. Changes in Climate Extremes Over the Australian Region and New Zealand During the Twentieth Century, *Climate Change*, *42* 183-202

Reardon G.F., Henderson D. and Ginger J.D.1999. *A structural assessment of the effects of Cyclone Vance on houses in Exmouth WA,* Technical report, James Cook University of North Queensland. Cyclone Testing Station, No. 48

Reardon G.F. 2000. *Anemometers: Dines vs. AWS,* Australasian Wind Engineering Society Newsletter, May 2000

Smits A., Klein Tank A.M.G. and Konnen G.P. 2005. Trends in storminess over the Netherlands, 1962-2002, *Int J Climatology, 25* 1331-1344

TASK 2: REVIEW OF PREVIOUS STUDIES OF RESPONSE CHARACTERISTICS OF THE DINES ANEMOMETER SYSTEM (BOTH LOW-SPEED AND HIGH-SPEED) AND THE DEVELOPMENT OF A VALIDATED NUMERICAL MODEL OF THE DINES ANEMOMETER.

(a) Literature review of Dines anemometer response and related studies

A review of previous studies from the early 1930s to the 1980s on the dynamic response of the Dines anemometer was carried out. These included experimental studies of the response to sinusoidal pressure fluctuations and step inputs, and comparative studies of the gusts recorded by Dines anemometers and rotating cup anemometers operating in parallel in the natural wind.

Studies of the dynamic response of the Dines anemometer system, although intensive in the 1920s to 1930s period, have been sparse ever since. The early studies seemed to focus on the effect of the tubing, which the present project has found is only a problem if very long, or very narrow, tubes are used. A useful paper reviewed is that of Borges (1968), who focused on the response characteristics of the float movement, and identified the two natural frequencies associated with in-phase and out-of-phase motion of the float and the water; these aspects have been further studied experimentally and theoretically in the present project. The paper from Ireland by Logue (1986), in which statistical comparisons of gusts recorded over a year were compared, and higher readings of peak gusts by the Dines anemometer on average, was also particularly useful for the present project.

The general conclusion was that the Dines anemometer was generally believed to be more responsive than most cup anemometers, but there was no definitive conclusion on the appropriate correction factors, and on the variations for the different versions of the instrument. There was also some inconclusive evidence on the effect of the connecting tubing on the response. All these issues have been addressed and resolved in the present project.

A paper from Beljaars (1987) from the 1980s has led to the re-definition of 'effective gust duration', and to recommendation of a 2 to 5- second moving average filter by the World Meteorological Organization and adoption of it the Bureau of Meteorology. With hindsight, this has had a greater effect on the reported maximum gusts, than has the change from Dines to cup anemometers. A paper-by-paper summary is given in Appendix II-1.

(b) Modelling of the tubing response

In this Sub-Task, the response of the connecting tubing from the Dines anemometer head to the float chamber to sinusoidal pressure fluctuation was studied, using a well-established theory from the 1960s. It was found that the theory agreed quite well with the measured response, obtained in Task 3, of tubing of typical length and diameter used in Australian applications of the instrument, using a representative 'rigid' volume at the end of the tubing. However, the frequencies, at which significant amplification of the response by the tubing occurred, were found to be significantly greater than those of the float chamber, and hence the influence of the tubing on the anemometer response was judged to be quite small. This conclusion was confirmed by measurements carried out as part of Task 3.

Good agreement between theoretical predictions, based on laminar fluctuating flow, of the frequency response of tubing typical of that used in the Dines system with experiments, lead to the conclusion that the flow in the tubing system is essentially laminar. This contradicts a conclusion of an early Japanese study, which suggested that the flow would be better modelled as turbulent flow.

Details of this work are given in Appendix II-2.

(c) Statistical comparison of peak velocities recorded by Dines, cup and sonic anemometers using time histories

In this Sub-Task, using time histories of Dines float movement generated experimentally in Task 3, a statistical comparison of peak velocities recorded by the Dines anemometer a 3-cup anemometer and a sonic anemometer was made. This was achieved by processing of a time series of wind velocity which was used to drive the float system of a low-speed Dines anemometer.

This work indicated that the Dines anemometer under-estimated the 'true' peaks that would have been recorded by a sonic anemometer by 5-10%, but over-predicted the peaks recorded by the cup anemometer by 2-5%. This work is discussed in detail in the Appendix II-3.

However, in order to derive appropriate correction factors for past recordings of daily gusts in Australia, it is necessary to account for the 3-second moving average filter applied in the Automatic Weather Stations by the Bureau of Meteorology in accordance with the WMO standard. This aspect was investigated in another Sub-Task, described following.

(d) Gust factors for Dines and cup anemometers using the spectral approach

A spectral approach based on random process and linear systems theory was applied to calculate expected gust factors for the two types of Dines anemometers and a cup anemometer, as a function of mean wind speed, turbulence intensity and sample time. This approach allowed Dines/cup gust ratios to be calculated, and gave good agreement with independently obtained values of gust ratios.

Hence comparisons were made of the average gust factors and gust ratios recorded by the Dines and those expected from the type of cup anemometer currently used by the Bureau of Meteorology in their Automatic Weather Stations, with the 3-second moving average filter applied. As a result of the analysis, significant 'overshoots' in measured gust wind speeds are expected to occur – up to 13% for the low- speed Dines anemometer, and up to 21% for the high-speed Dines, relative to the cup anemometer. These are compatible with statistical analyses by Geoscience Australia carried out under Task 1, and with anecdotal evidence from individual stations in the cyclone regions, where the instruments have operated in parallel.

The adoption of the 3-second moving average gust definition by the Bureau of Meteorology will require a re-consideration of the peak gust definition used in Australian/New Zealand Standard AS/NZS1170.2 since 1971.

(e) Modelling of the Dines Manometer

Two physical models of the Dines manometer have been developed. The first model includes two significant simplifications, namely that the float sides are assumed parallel instead of flared, and the tubing effects are not included. Analytical solutions of the linearised undamped equations, and numerical solutions of the full equations have been obtained. The key advantage of this simplified model is that analytical solutions, with their concomitant physical insight, are obtainable. A detailed report on the properties of the first model is attached as section 2 of Appendix II-5, the main conclusions from which are summarised below.

These analytical solutions of the linearised undamped equations have two solutions, a low-frequency oscillation in which the water and float move in phase, and a higher-frequency oscillation in which they move exactly out of phase. The frequencies and for the relative amplitudes of the

oscillation in the water and of the float are given by equations 22 to 25 of Appendix II-5. These frequencies depend upon several factors, including the mean wind speed. These oscillations have been noted in a few of the historical laboratory test reports, notably Borges (1968), but have not been previously analysed mathematically.

Numerical solutions were obtained using a fourth-order Runge-Kutta scheme, with a sample simulation is shown here as Figure 2.1. In this sample, both the in-phase and out-of-phase oscillations are clearly present, with a periodic transfer of energy between the two.

In reality, Dines anemometers possess several sources of friction, which acts to damp the motion of the float and water. These dampings include of the float directly (due e.g. to friction of the pen arm), and of the water directly (due to friction between the water and the tank). However, the most significant damping is believed to be due to the passage of water in and out of the float bottom, where a "choke", shown in Figure 15 of Appendix II-5, significantly impedes the flow. All three sources of damping are represented in the equations derived to model the system as first-order linear dampings characterised by individual time constants (see equations 1 to 5 of Appendix II-5).

The solution to the forced damped equations depends on the relationship between the forcing, strength of the damping, and the resonant frequencies. Forcing near the resonance produces the strongest response. The amplitude of the response can vary from zero to several times the amplitude of the forcing, depending on the degree of the damping and the frequency of the forcing.

Response curves are shown for a sample configuration in Figure 2-2. These curves show the relative amplitude and phase of the oscillation as a function of forcing frequency, with the blue curve representing the float and the green, the water. The amplitudes have been scaled by the forcing amplitude, so that amplitude=1, phase=0 means the float exactly follows the varying wind speed. The magenta diamonds indicate the linear undamped frequencies, and are clearly close to the resonant peaks. At low frequencies, the float closely follows the wind speed, with a rising response to the out-of-phase oscillation near the lower resonant frequency, and a second weaker peak near the higher resonance, with a weak trough between. The phase response shifts from in-phase at low frequencies, to out-of-phase at high.

The dual peak in the response curve significantly complicates attempts to calculate the "gust period" or "response time" that the Dines anemometer measures. Such calculations are straightforward for the more usual first-order systems, but not for those one, let alone two, significant resonances. Accordingly, due care is urged in interpreting such calculations.

Figure 2-2 is in very good agreement with the measurements of Borges (1968). Figure 2-3 reproduces a similar curve (of the float motion only) from his laboratory experiments, showing good quantitative agreement with the model. Both the amplitude and phase of the response are well represented (some tuning of the damping in the model was necessary to achieve this good agreement). The results in Figure 2-3 are similarly in good agreement with the measurements taken by the CTS as part of Task 3 of this project, although here the agreement is more qualitative than quantitative as the higher-frequency peak is stronger. Close agreement with the Dines measurements is possible with re-tuning of the physical constants in the model equations, implying that the Fuess anemometer used by Borges has some significant differences from the Dines anemometer.

The second model removes the simplifications to the geometry made in the above model and is described in section 2 of Appendix II-5. Figure 2-4 summarises the behaviour of the system, configured to model a low-speed Dines anemometer, in the absence of damping. As for the U-tube analogue, there are two dominant resonant frequencies, with the water moving in- or out-of-phase with the float. The figure shows that the lower-frequency oscillation, in which the float and water

inside it move in phase, has a frequency of 0.49 Hz at a mean wind speed of 10 m/s which increases slowly with wind speed to 0.75 Hz at 50 m/s. The higher-frequency, out-of-phase motion, has a frequency that increases from about 1 to 3 Hz as the mean wind speed increases from 10 to 50 m s^{-1}. At a mean wind speed of 20 m s^{-1}, similar to that of the laboratory measurements conducted by the Cyclone Testing Station, the two frequencies are about 0.55 Hz and 1.45 Hz, within about 0.1 Hz of the measured resonant frequencies. This is excellent agreement; the small discrepancy is probably due to some simplifying assumptions in the model, the difficulty of measuring the response frequencies to high precision in the laboratory, that damping may slightly shift the frequencies, and experimental uncertainty in the measured resonant frequencies. As with the first model, there are also weaker spectral peaks at harmonics and interharmonics of the dominant resonances.

The strong agreement with the laboratory measurements provides considerable confidence in the model. There is no tuning of these results, they were obtained simply by inserting the correct float geometry and mass and chamber geometry into the equations. Calibration of the second model would be assisted by detailed drawings and specifications of the float and chamber, particularly for the rarer 150 and 200 m.p.h. models of the instrument. The former manufacturer of the Dines anemometer, R.M. Munro, very kindly agreed to search their archives for such drawings, unfortunately without success.

In the absence of firm information, a hypothetical configuration of the model for a high-speed instrument was attempted. This utilised some measurements of the outside of the tank, together with reasonable estimates of the float characteristics, as detailed in Appendix II-5. Compared to the low-speed instrument, the dominant oscillation shifts to a lower frequency, about 0.3 Hz with a weak increase at higher wind speeds, while the higher-frequency oscillation increases in frequency. The reduction in frequency of the in-phase oscillation is in good agreement with the laboratory measurements and is consistent with the approximate doubling of the oscillating mass. However, the increase in frequency of the out-of-phase oscillation seems somewhat larger than found in the laboratory measurements. However, until firm information on the physical characteristics of the high-speed float become available, the cause for this discrepancy cannot be determined.

This sensitivity of the results to the physical characteristics of the instrument implies that care will be needed in interpreting the results of this study to ensure that the appropriate model of Dines anemometer is considered. Of the three versions used, the most common were the low-speed and high-speed measured as part of Task 3, which had maximum readings of 100 and 200 miles per hour respectively. However, there was also an intermediate instrument, with a maximum reading of 150 m.p.h., no examples of which survive in Australia. It is apparent from the surviving chart that the winds in Cyclone Tracy were measured by the 150 m.p.h. instrument, and there is physical and anecdotal evidence for one having been previously installed at Learmonth. In addition, the Bureau's instrument laboratory have published test results on such an instrument. Unfortunately, more detailed documentary evidence has proved elusive.

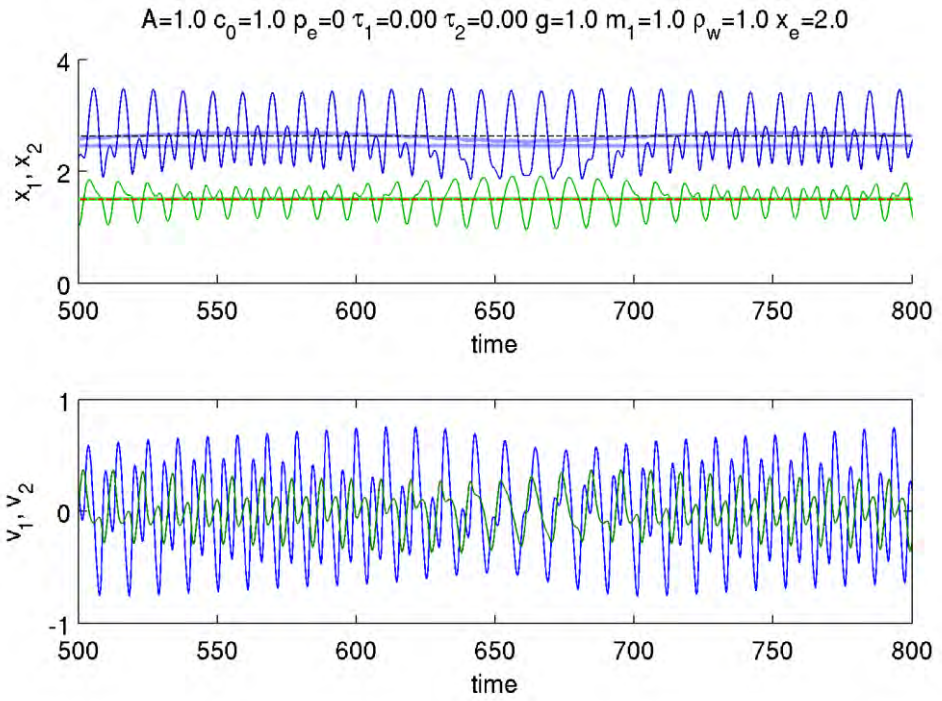

Figure 2- 1. Time-series of unforced, undamped numerical solutions to the full nonlinear equations for the simplified model. The upper panel shows the float (blue) and water (green) positions, and the lower panel their velocities. The thin curves show the instantaneous positions and velocities, both in-phase and out-of-phase oscillations are clearly present. In the top panel, the thick blue curve shows the low-pass filtered float position, showing the long-period oscillation due to a nonlinear interaction between the in-phase and out-of-phase oscillations. The thick blue line the mean position for that wind speed with no fluctuations, and the thin dashed line is the actual mean float position. The difference between these curves indicates that the instrument is "overspeeding".

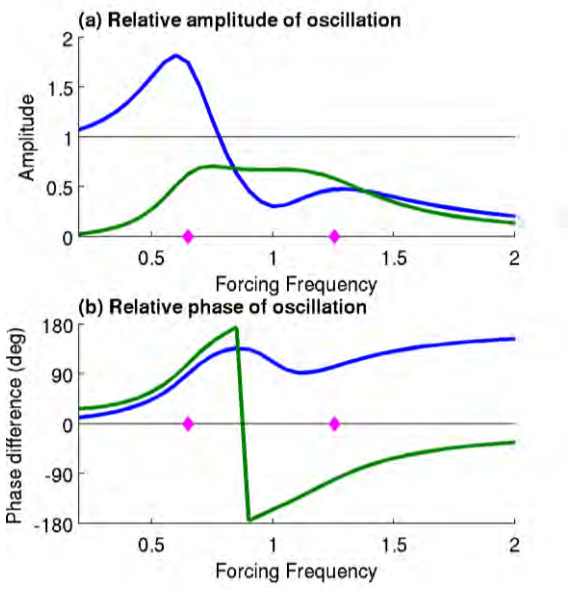

Figure 2-2. The (a) amplitude and (b) phase of the anemometer response in float motion (blue) and water motion (green), as a function of dimensionless forcing frequency in the simplified model. The curves have been normalised by the forcing, so an amplitude of 1 and phase of 0 implies that the float exactly follows the fluctuating wind at that frequency. The magenta diamonds show the resonant frequencies from the linear undamped theory.

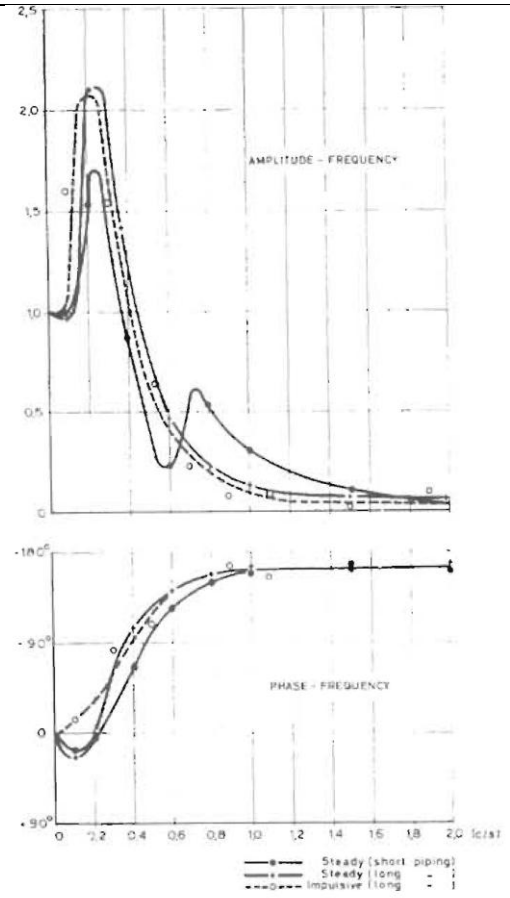

Figure 2-3. The relative amplitude (top) and phase (bottom) of the float movement, as a function of forcing frequency, for a Fuess anemometer with various tubing lengths. From Borges (1968).

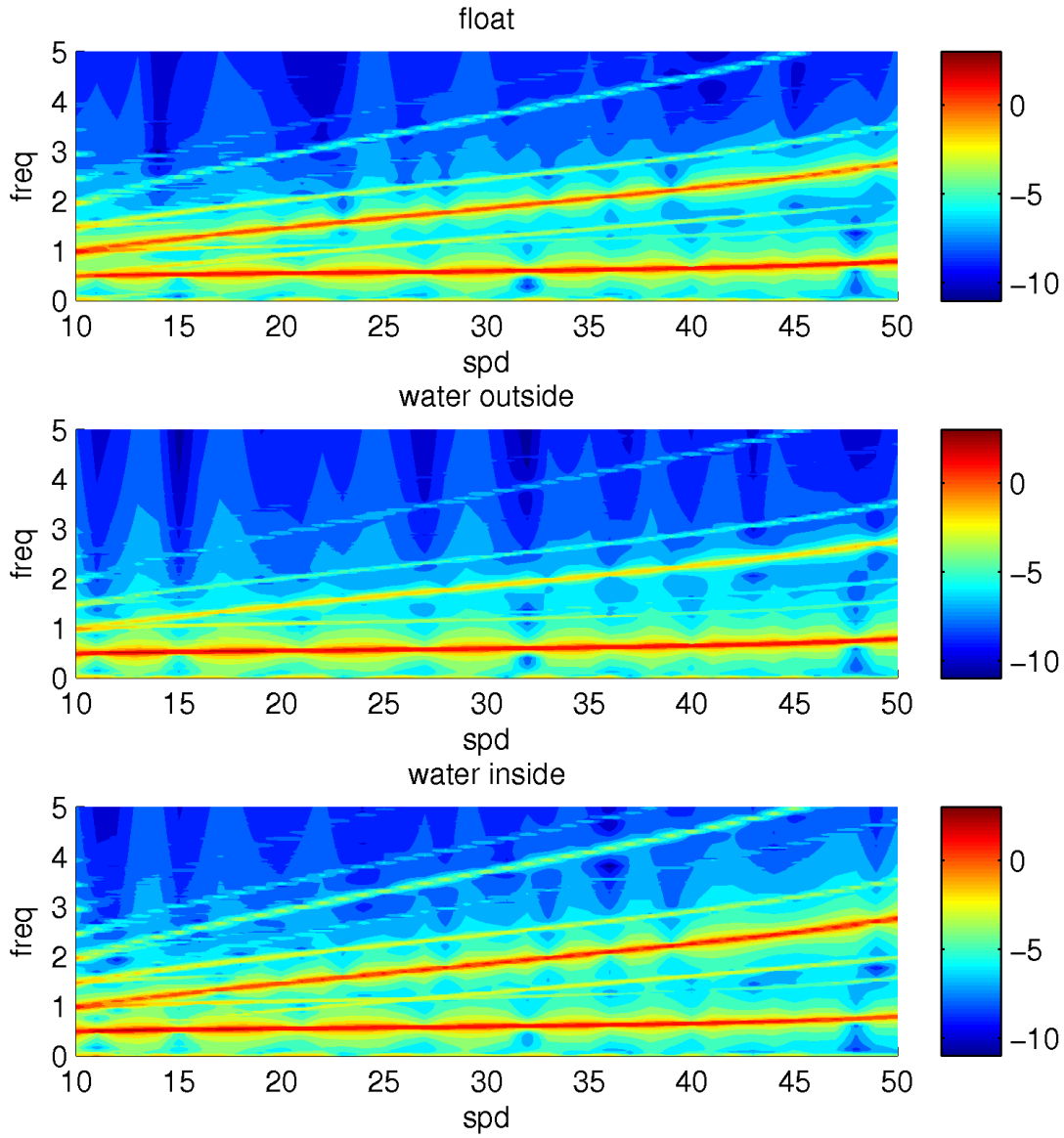

Figure 2-4. Logarithm base-10 of the power spectral density of the position of the float (top), water level in the tank (middle), and water level inside the float (bottom), as a function of the mean wind speed, for the model with the full geometry configured for the low-speed instrument. The wind speeds are in m s^{-1} and the frequencies in Hz.

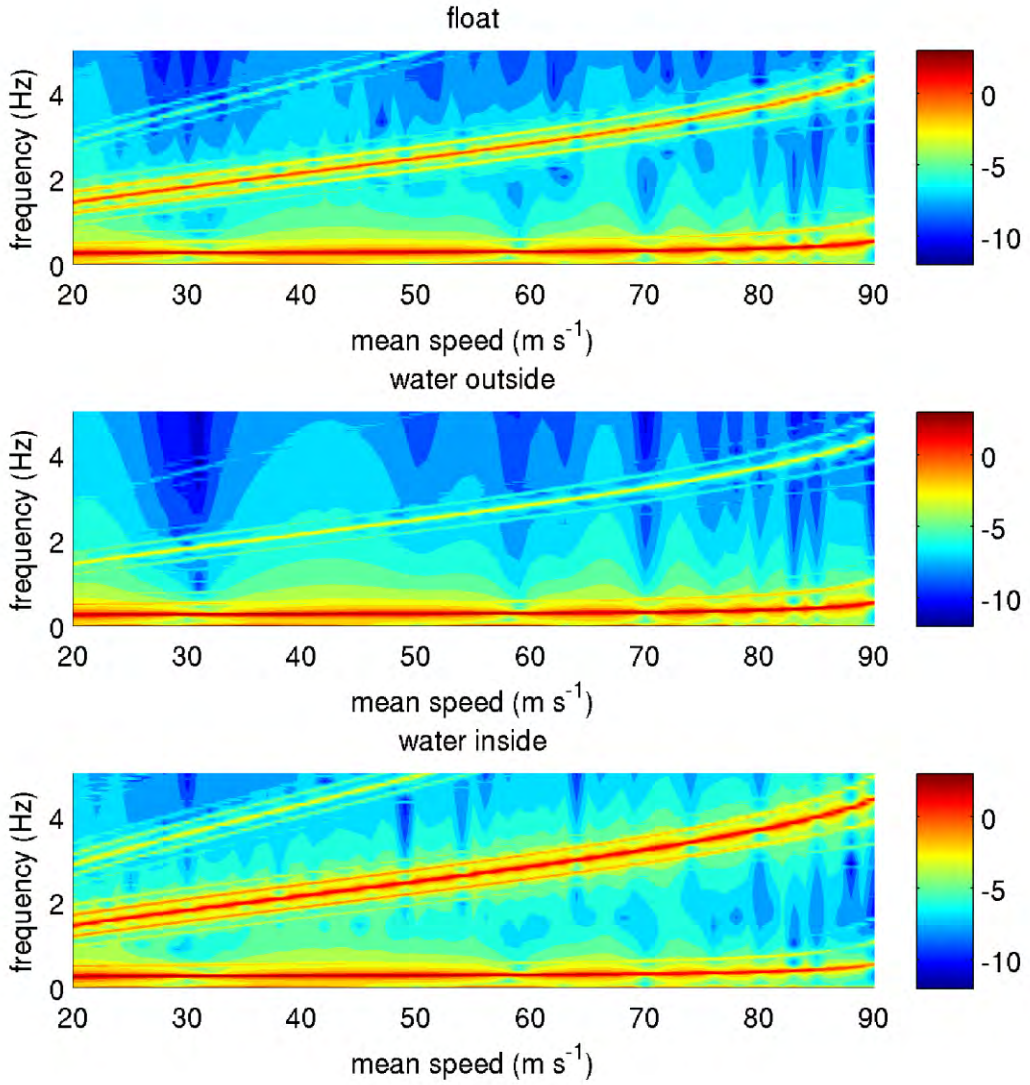

Figure 2-5. As for Figure 2-4, except with the full-geometry model configured for a hypothetical high-speed instrument.

Conclusions from Task 2

- The response of the Dines anemometer is primarily governed by the dynamics of the float system, with the effect of the connecting tubing having a minor role. The lowest natural frequency of about 0.5 Hertz for the low-speed type, and 0.3 Hertz for the high-speed type, has the greatest effect on the response of the instrument to wind gusts, and on the maximum gust recorded in a defined period.
- Because of the resonance in the float system, the low-speed Dines anemometer records higher gusts than the (unfiltered) standard cup anemometer used by the Bureau of Meteorology (BoM) with average 'overshoots' of 3-5% (depending on mean wind speed and turbulence intensity). The incremental overshoot for the high-speed version of the Dines anemometer is 5-8%.

- The application of a 3-second moving average filter to the cup anemometer outputs in the Automatic Weather Stations (AWS) by the BoM in accordance with international practice has resulted in a further increase in the *apparent* average overshoot of the Dines anemometers to 7-13% for the low-speed type, and to 12-21% for the high-speed type.
- The 3-second moving average in the AWSs has led to 'double-filtering' of the wind turbulence. It has resulted in a 'mismatch' between the definition of maximum gust used for design for wind loading in Australia since 1971. However, we note that this averaging follows the recommended procedure by the World Meteorological Organisation, and is consistent with international practice. In principle, it should be possible to adjust gusts measured under this averaging to other averaging periods, or to no averaging, provided that the relevant anemometer characteristics are known.

Recommendations from Task 2

- The definition of peak gust used in the Australian/New Zealand Standard for wind actions should be reviewed by Standards Australia, since a significantly lower gust is currently being recorded by the Bureau of Meteorology (BoM). The latter has resulted from the decision of the BoM to apply a 3-second moving average filter applied in the Automatic Weather Stations to recorded daily gusts in Australia.
- Factors have been derived to allow corrections to be made to daily maximum gusts formerly generated by the Dines anemometers (both low-speed and high-speed types), and currently being generated by Automatic Weather Stations in Australia. These correction factors should be applied before extreme value analyses are undertaken to develop revised design wind speeds for structures.

References for Task 2

A.R.J. Borges, 1968: On the frequency response of floater-type anemographs, Tecnica, No. 379, pp505-511.

J.J. Logue, 1986: Comparison of wind speeds recorded simultaneously by a pressure-tube anemograph and a cup-generator anemograph. *Met. Mag.*, **115,** pp 178-185.

TASK 3: EXPERIMENTAL TESTING OF THE DINES PRESSURE TUBE AND FLOAT FOR DYNAMIC CHARACTERISTICS USING A RAPID PRESSURE LOADING ACTUATOR (PLA).

Introduction

The response of low-speed and high-speed Dines instruments were studied by testing these, as part of Task 3 of the project. The objectives were to measure the response of the Low Speed and High Speed Dines float when excited by a known pressure signal applied to the head. Various pressure signals with differing frequencies and amplitudes were generated using a Pressure Loading Actuator (PLA) capable of applying rapidly fluctuating realistic wind pressures.

Figures 3-1 to 3-3 show the high speed Dines anemometer tower at the site, and the float chamber with paper record drum float rod and recorder. The Dines anemometer in Townsville was replaced by the 3-cup Synchrotac anemometer and direction vane, as the official wind speed measurement device in the early 1990s. Figure 3-4 shows the Bureau of Meteorology 3-cup anemometer at the Townsville Airport. However, the Dines has been kept operational as an unofficial wind speed recording device to-date, as noted by Reardon *et al* (1999). This provides an opportunity to compare the "performance" of both instruments which are located about 100m apart, at Townsville Airport,.

A low-speed Dines anemometer, including the head and vane, float and chamber, from Glenlitta Victoria was loaned to the CTS by the Bureau of Meteorology. The low-speed units were typically used in non-cyclonic regions (and in cyclonic regions prior to the mid-70s). This system was set-up in the laboratory at the CTS and series of experiments were conducted prior to testing the high-speed system at the Airport in Townsville. This enabled any potential difficulties to be identified and rectified in controlled lab conditions before conducting tests in the field.

Tests were carried out on these two instruments over a period of about five months in 2010. Details of these tests and results are provided in Appendix III of this report. The focus of these tests were to ascertain the response of these two Dines instruments, and provide test results to Task 2 for calibration and validation of the mathematical models. The analysis carried out in Task 1 is also assessed against these test results.

Experiments and Data Collection

Recent development of the advanced Pressure Loading Actuator (PLA) that can simulate realistic fluctuating wind pressures allow the response of the Dines anemometers to be assessed for a wide range of frequencies including actual fluctuating winds. Several configurations, isolating each component in turn; the Dines head, the float chamber and the 10 m tubing (the typical height of the head above ground level), were tested for assessing their contributions to the overall response of the instrument. The dynamic response of the Dines is complex and is dependent on the characteristics of the applied pressure fluctuations and the mass of the float/rod and the column of water in the chamber. These complex interactions along with the effect of mean, range and form of the pressures applied in Task 3, are modeled in Task 2.

Figure 3-1 Dines anemometer

Figure 3-2. High Speed Float Chamber

Figure 3-3. Float rod and speed recorder

Figure 3-4. 3-cup anemometer

Pressure input to the Dines and Dines output

Tests were conducted to assess for the mean (time averaged) response of the Dines to static step pressures (i.e. steady velocity) and the fluctuating (i.e. dynamic) response. A range of test pressure time traces were applied to the various Dines test configurations. The traces ranged from varying ”static” step traces, sinusoidal, square wave and dynamic pressure signals representing actual velocity fluctuations. White noise pressures were used to determine the frequency response characteristics of the Dines instruments.

A manifold was fabricated from PVC pipe to adapt the PLA outlet hose to the Dines inlet at the head/vane unit as shown in Figure 3-5. The input pressure from the PLA was measured with two

pressure transducers located in the manifold immediately in front of the inlet of the Dines head. One pressure transducer (PT) was used by the PLA for controlling the valve to achieve the requested pressure trace. The second PT output was recorded using the same data acquisition (DAQ) module that recorded the response of the LVDT attached to the float. The DAQ used a simultaneous sampling system ensuring that the input and output (i.e. PT and LVDT measurements) were synchronized.

The output of the Dines float chamber is measured by the vertical rise and fall of a float rod attached to the top of the float chamber. The vertical movement is typically transcribed directly onto a chart rotated by clockwork. The chart is located adjacent to the float rod. The robust and reliable operation of the Dines and provision of repeatable output is reliant on initial and ongoing maintenance procedures, such as ensuring the free running of the float in the chamber slides and the balancing of the float chamber via the lead-shot cup on top of the rod.

The response of the float chamber to the applied pressure was measured using a linear variable differential transformer (LVDT) connected to the shot-cup on top of the float rod as shown in Figure 3-6. A small universal joint was used to connect the shot-cup to the LVDT. A crucial requirement was to ensure that the weight of the universal joint, modified shot-cup and LVDT shaft was equal to the weight of the original shot-cup, lead shot and pen.

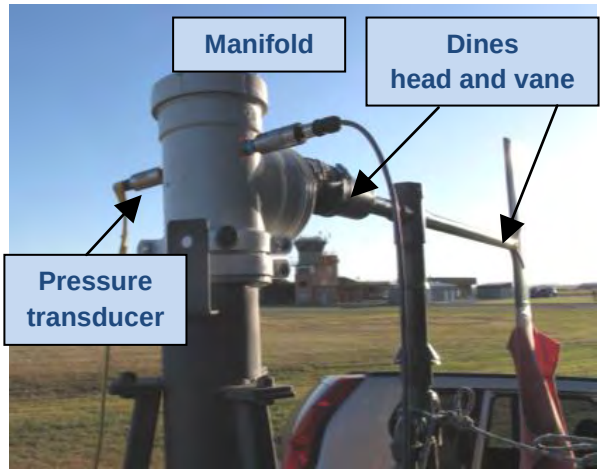

Figure 3-5. Manifold and stand for connection PLA to Dines head/vane. Note the two pressure transducers located at the inlet of the Dines head

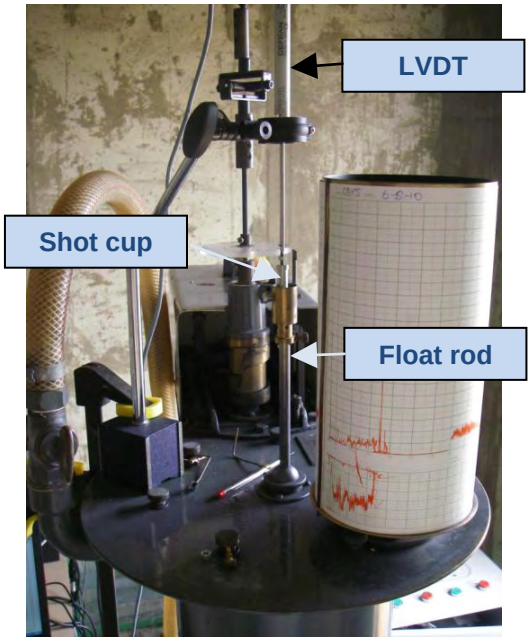

Figure 3-6. LVDT measuring movement of float rod

Test configurations

A range of test configurations were set-up to examine the contribution of each component of the Dines systems to the overall frequency response. The tests included assessing the response of both the high-speed and low-speed Dines float chambers, as well as investigating the contribution of the Dines Head (with associated bends), and the connecting tubing to the overall response of the system.

The test configurations were;

1. PLA connected to 10 m PVC pipe (30 mm internal diameter) with 225 mm long 100 mm internal diameter *fixed* float volume at the output end (i.e. Dines head and float chamber not used)
2. PLA connected to Dines head (including right angle bends) to 8.1 m PVC pipe (30 mm internal diameter) with 225 mm long 100 mm internal diameter *fixed* float volume at end (total "length of tubing" from Dines head to fixed volume remains 10 m)
3. PLA connected to Dines head (including right angle bends) to 225 mm long 100 mm internal diameter *fixed* float volume at output end (using only short flexible tube of ~ 2m)
4. PLA connected to Dines head (including right angle bends) to 10 m PVC pipe (30 mm internal diameter) with Low Speed Dines float chamber at the output end
5. PLA connected to Dines head (including right angle bends) to low-speed Dines float chamber (using only short flexible tube of ~ 2 m)
6. PLA connected to Dines head (including right angle bends) to high-speed Dines float chamber (using only short flexible tube of ~ 2 m)

A summary of the tests, analysis, results and discussion is presented in this section. A detailed list of tests and results is presented in Appendix III.

Results and Discussion

The low-speed and high-speed Dines instruments were calibrated for their mean (time averaged) response to static pressures (i.e. steady velocity). The static pressure test provided a calibration factor that relates the vertical displacement of the float rod (in mm) to the applied pressure difference (in Pa) which is converted to the velocity in m/s. The calibration factors obtained are used in the series of fluctuating pressure tests (i.e. sinusoidal, square waves, white noise and pressure signals representing actual velocity), to determine their dynamic response.

The float chamber of the Dines anemometer is designed in such a way that it produces a linear displacement of the float/rod proportional to the measured velocity. The Dines anemometer responds by sensing the wind pressure at the head and relating the pressure difference between the head and reference port, Δp (in Pa) to velocity, U (in m/s) using Equation 3-1, as described in the "Handbook of meteorological instruments Part 1: Instruments for surface observations" (1956). Here, K =1.49 is a constant factor (i.e. a 'pressure coefficient') based on the shape and dimensions of the head, ρ is the density of air in kg/m^3.

$$\Delta p = \tfrac{1}{2} \rho K U^2 \qquad (3\text{-}1)$$

Following Equation 3-1, the displacement of the Dines float rod (i.e. the wind speed recorded) is calibrated against the pressure applied to the head. An increasing then decreasing 30 sec step

pressure trace was applied to the systems. The vertical displacement of the float rod measured by the LVDT (in mm) was recorded vs Δp and converted to an equivalent velocity using Equation 3-1. Figures 3.7 and 3.8 show the measured response of the low- and high-speed Dines float chambers respectively, obtained by applying the "static" pressure traces. The linear relationship between the velocity, and the low- and high-speed Dines responses are 0.29 and 0.59 ms^{-1}/mm, respectively. The vertical axis (wind speed) of the actual Dines paper chart measured 177 mm for the maximum speed of 100 and 200 knots, thus each mm on the standard and high speed charts is equivalent to 0.290 and 0.583 m/s. Following calibration of the float rod with the LVDT, the vertical movement of the float rod was converted to the equivalent wind speed and then to pressure allowing direct comparison with the fluctuating input pressure traces.

Dynamic Response

The measured frequency response (transfer function) $|H(n)|^2$ of the low-speed and high-speed Dines have been utilized as a validation of the numerical analysis described in Task 2. Outcomes from these tests are summarized as;

- The 10 m length of tube connecting the inlet head to the float chamber amplifies the input signal at frequencies above 5Hz. Application of an input sinusoidal trace at this frequency showed a 90° phase change (indicating resonance), and a small lag.
- The response of low-speed and high-speed Dines systems were dominated by their respective float chambers. Pressure fluctuations greater than 2 Hz were effectively damped by the float.
- The analysis of the low-speed and high-speed (float) response spectra to input sinusoidal, white noise and wind traces showed characteristic double peaks; an amplified peak at low frequency (< 0.8 Hz) followed by a trough and a second peak at a higher frequency (~1.2Hz). These low and high frequency peaks relates to the in and out of phase motion of the float with the water column in the chamber. The response of the Dines instruments are also discussed in Task 2

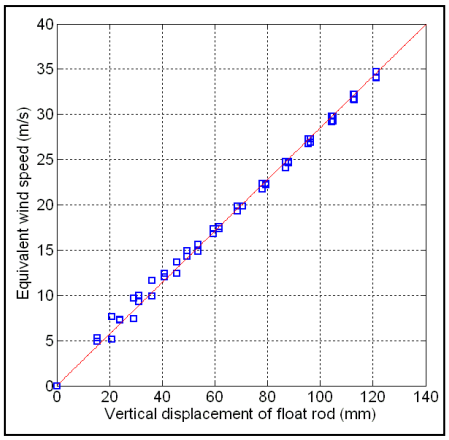

Figure 3-7. Wind speed converted from applied PLA pressure vs vertical displacement of float rod (measured by LVDT) – low-speed Dines

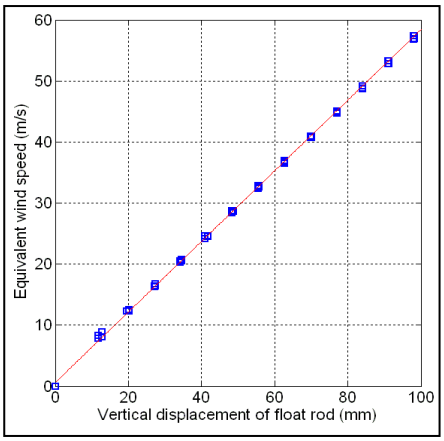

Figure 3-8. Wind speed converted from applied PLA pressure vs vertical displacement of float rod (measured by LVDT) – high-speed Dines

The Low-Speed and High Speed Dines instruments were subjected to a range of input fluctuating pressures derived from wind speeds measured by a sonic anemometer and in a wind tunnel. The mean wind speeds were 20, 25 and 30 m/s for the Low speed Dines and higher than 50 m/s for the High Speed Dines. The turbulence intensities varied from ~10 to 20%. Figure 3-9 shows a portion of the Sonic anemometer input and Low Speed Dines response for a mean velocity of 25 m/s and turbulence intensity of 10%. The Dines "follows" the wind speed time trace. The mean wind speed is accurately represented by the Dines and peaks are influenced by the float response.

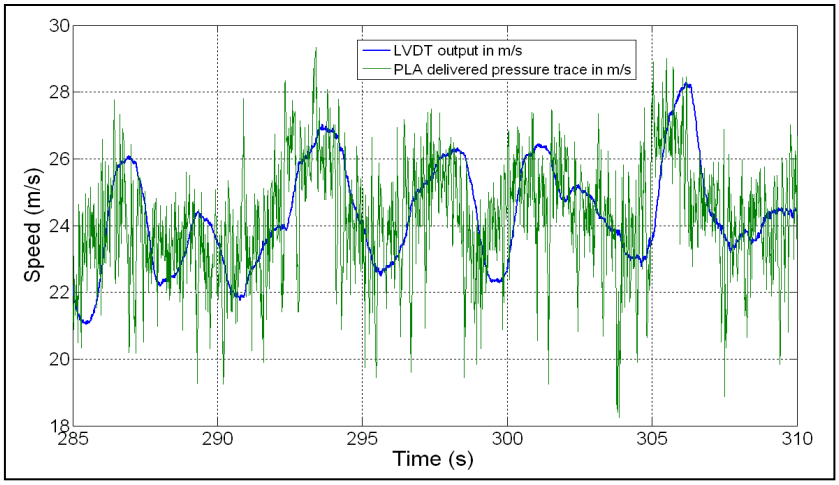

Figure 3-9.Input pressure trace representative of sonic anemometer and the Low-speed Dines output

Conclusions for Task 3

Experiments were conducted on a low-speed and a high-speed Dines anemometer using a Pressure Loading Actuator capable of simulating realistic wind pressures.

Both the low speed and high speed Dines units replicated mean winds speeds accurately. However, with the application of oscillating pressures such as sinusoidal or fluctuating pressures such as white noise or simulated wind traces, both types of Dines float chambers exhibited amplification and attenuation of some of the input signal peaks. The amount of the attenuation or amplification depended on the frequency, amplitude and mean of the input signal. The dynamical modelling in Task 2 of the complex system produced excellent agreement with the laboratory measurements demonstrating the model's capability to produce realistic anemometer correction factors.

References for Task 3

Borges, A. R. J. (1968). "On the frequency response of floater-type anemographs." Technica, 379, 7.

Meteorological-Office. (1956). "Handbook of meteorological instruments Part 1: Instruments for surface observations." A. Ministry, ed., Her Majesty's Stationery Office, London.

Reardon, G., Henderson, D., and Ginger, J., (1999) "A structural assessment of the effects of Cyclone Vance on houses in Exmouth WA", Technical Report 48, Cyclone Testing Station, James Cook University, Townsville.

Australian extreme windspeed baseline climate investigation project

APPENDIX I.

Intercomparison of time-series and coincident

Dines & cup anemometer observations.

NOTE: This report is to be published as a Geoscience Australia Record

GA Record 2011/xx:

by R.P. Cechet[1] and L.A. Sanabria[1]

Australian Government

Geoscience Australia

1. Risk and Impact Analysis Group, Geoscience Australia

Department of Resources, Energy and Tourism
Minister for Resources and Energy: The Hon. Martin Ferguson, AM MP
Secretary: Mr Drew Clarke

Geoscience Australia
Chief Executive Officer: Dr Chris Pigram

ISSN 1448-2177
ISBN 0 642 XXXXX X

GeoCat # XXXXX

Bibliographic reference: Cechet R.P. and L.A. Sanabria (2011) Australian extreme wind baseline climate investigation. Geoscience Australia Record 2011/XX, GeoCat #xxxxx

Dines anemometer (image supplied by Cyclone Testing Station, James Cook University)

3-cup Synchrotac anemometer (image supplied by Cyclone Testing Station, James Cook University)

Executive Summary

This study has examined the observed record of **peak gust wind speed** (daily maximum 3-second averaged gust wind speed) in order to establish the existence of bias between the early part of the record (measurements obtained using pressure-tube Dines anemometers) and the later part of the record (measurements obtained using cup anemometers).

All observational data as well as metadata was obtained from the Bureau of Meteorology. The 38 recording stations considered were all situated at airports and were in the most part staffed by Bureau of Meteorology officers. To isolate the issue of anemometer replacement, only observing stations located at airports (i.e. those with consistent exposure) and with more than 30 years of record were considered. The visual inspection of the observed daily peak gust wind speed time-series for most of the Bureau of Meteorology observing sites considered in this study is sufficient to indicate that in general the early part of the observing record contains a higher frequency of extreme events, and also the largest amplitude extreme events.

Statistical analysis of the daily maximum gust wind speed observations was conducted by employing extreme value distribution (EVD) statistical theory to examine the difference between two datasets:

(1) time-series of Dines & cup anemometer observations (no overlap for each station)
(2) coincident Dines & cup anemometer observations

Analysis of time-series of Dines & cup anemometer observations (no overlap)
We have evaluated both the daily maximum gust and 3PM mean wind speed 500-year return period (500RP) exceedance levels for the *combined* wind speeds for the 31 wind observing stations selected (within AS/NZS 1170.2 Region A). Observations have also been segmented into the Dines and replacement cup anemometer observing periods. The 95% confidence interval (95CI) has been determined for both gust and 3PM mean wind speeds for the Dines anemometer time-series segment of the record. For the replacement anemometer 500RP exceedance level gust wind speed estimates, there are 17 observing stations where the replacement anemometer estimates fall below the lower 95% confidence interval (95CI) for the Dines segment of the observing record. For 24 of the 31 observing stations the replacement anemometer estimate falls below the corresponding Dines segment estimate. Considering the 3PM mean wind speeds, there are 18 observing stations where the replacement anemometer estimate falls below the lower 95CI for the Dines segment of the observing record.

The statistical analysis utilising extreme value distributions (EVD's) resulted in more than half of the observing stations considered (post cup anemometer instalation) having both 500RP gust wind speed (17 of 31) and 3PM mean wind speed (18 of 31) exceedance level estimates being in the lower tail of the distribution for the early part of the observing record (period prior to equipment upgrade from Dines to cup anemometer). Interpretation of the differences in the return period hazard for the two segments of the record should be done with caution. It is possible that the frequency of extreme wind speeds has actually declined (Smits *et al*. 2005). The most recent part of the record has been dominated by a number of large El Nino events and only one La Nina event, where thunderstorms are known to be more prevalent (Kuleshov *et al*. 2002). The importance of the non-stationary climate needs to be considered when conducting a time series analysis. Circulation changes as discussed in (Plummer *et al.* 1999; Alexander *et al.* 2010), possibly driven by anthropogenic climate change, could also affect the frequency and amplitude of extreme winds. The replacement cup anemometer part of the record is generally much shorter (10-25 years) than the Dines segment and it is possible that the very high maximum wind speeds have not yet been sampled, although the reduced frequency of extreme events in the later part of the record is of concern. Even considering these issues, the analysis outlined above suggests that the consistency of the peak gust wind speed dataset is suspect, and that the problem required further examination via analysis of coincident measurements. The analysis indicates that it appears unlikely that the later part of the observing record can be considered consistent with the initial (Dines) segment of the record.

Coincident Dines & cup anemometer observations

Coincident gust wind speed measurements at 7 northern Australian observing stations were analysed to determine the magnitude of the direct bias. Only Dines "high-speed range" anemometers (0-200 knots) were considered for observing stations where extreme wind gusts are dominated by thunderstorm and tropical cyclone events. The stations examined were Cairns, Townsville, Brisbane, Darwin, Gove, Broome and Learmonth. Coincident probability distributions (PDF's) of the gust wind speed ((Dines & cup anemometer) for the seven sites display systematic bias with regards to the peak of the distribution for some of the observing stations. The peak of the Dines anemometer PDF appears slightly low for Darwin and too high for Learmonth and Townsville in comparison to the cup anemometer. Agreement is excellent for Cairns. In general, the time-series plots of the bias between the Dines and cup anemometer measurements show no time dependent relationships.

The data on the extreme gust wind speeds for the 7 sites (total period of coincident measurement of 89 years) were combined into one dataset and extreme value statistical theory (Generalised Pareto Distributions; GPD's) was used to investigate the return period exceedence levels for the combined dataset. In addition, 95% confidence limits for the GPD fit to the Dines extreme gust wind observations are also calculated. Table 1 details the percentage bias between the cup anemometer and Dines return period estimates (including the 95% confidence limits regarding the fitting of the extreme value distribution to the Dines gust observations). The observed data allows us to consider gust wind speeds between 45 and 60 m/s. When considering gust wind speeds at about 45 m/s, the Dines anemometer has a tendency to read about 5 to 10% higher than the cup anemometer (considering coincident data at 30 minute intervals); this increases to about 12 to 17% higher at gust wind speeds around 60 m/s. These systematic differences are consistent with those reported by Reardon *et al*. (1999) and Reardon (2000), and confirm concerns about the consistency of the peak gust wind speed observational database which underpins the Australian wind loading standard (AS/NZS 1170.2, 2002).

Cup anemometer gust wind speed	Dines anemometer gust wind speed	Dines; Lower 95% confidence limit	Dines; Upper 95% confidence limit
45 m/s	+7 %	+5 %	+9 %
50 m/s	+9%	+7 %	+11 %
55 m/s	+11 %	+9 %	+13.5 %
60 m/s	+14 %	+12 %	+17 %

Table 1. Percentage difference between the Dines anemometer and cup anemometers over a range of wind speeds, considering coincident extreme wind gust measurements at 7 observing sites over a total coincident measurement period of 89 years. The asymptotic nature of the GPD fit to the observations does not allow a comparison for wind gust speeds above 60 m/s.

This study has provided the engineering community with the outputs (knowledge and tools) to improve our understanding of the baseline extreme wind climatology within Australia. Based on this study, it will be possible to develop corrections based on this information and also to develop a reanalysed peak gust wind speed observing record which can inform an improved understanding of wind loading for the Australian region.

Contents

1. Introduction

Climate change is expected to increase severe wind hazard in many regions of the Australian continent with consequences for exposed infrastructure and human populations. Severe wind is one of the major hazards facing Australia. While cyclonic winds are the major source of wind hazard in the northern states, non-cyclonic winds driven by synoptic lows, thunderstorms and tornadoes affect the southern states. Severe winds are responsible for about 40% of damage to Australian buildings (see Figure 1; combination of cyclone, gust and tornado). Tropical cyclones pose a significant threat to life and property around Australia's northern coastline; average annual losses are estimated at around A$260 million (BTE 2001) and nearly A$700 million (Waters et al., 2010; direct impacts [replacement value] of severe wind, storm surge and damage to contents). Over 80% of the nation's population reside within 25 km of the coastline (Chen and McAneney 2006) and continued rapid growth in the northern parts of the country is increasing the population exposed to in particular severe thunderstorms and tropical cyclones. Hence it is important that the observational record of gust wind speeds that underpins Australia's wind loading standard (AS/NZS 1170.2) is both consistent and precise.

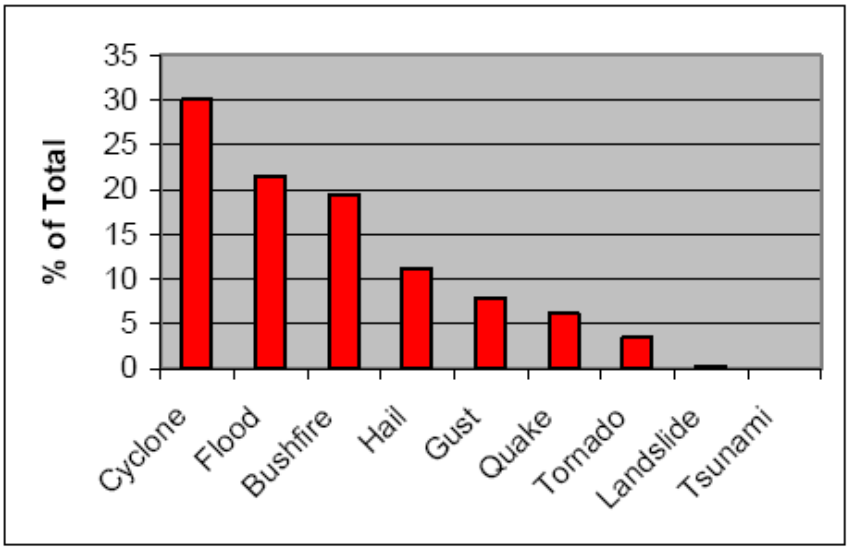

Figure 1. Proportion of total building damage (1900 – 2003) attributed to each of nine natural hazards (from Chen 2004). Note that for cyclonic hazard losses are dominated by severe wind, however a small proportion of the loss is attributable to storm surge and flooding.

1.1. RATIONALE

Geoscience Australia (GA) in collaboration with the Department of Climate Change and Energy Efficiency (DCCEE) has conducted a preliminary study (the National Wind Risk Assessment; NWRA) to investigate severe wind risk to residential buildings both under current climate and also for a range of climate change scenarios (Cechet *et al* 2011). The study was established to identify communities subject to high wind risk under present climate, and also those communities which will be most susceptible to any climate change related exacerbation of local wind hazard, requiring an adaptation response. The NWRA highlighted the issues of both calibration and also consistency of the extreme wind speed observational record which underpins the NWRA study and also the Australian/New Zealand wind loadings Standard (AS/NZS 1170.2:2002).

To provide a benchmark measure of severe wind hazard nationally (current climate), this study has investigated the

- consistency of the time-series observations of extreme wind speed;
- comparison of coincident observations from the "old" and "new" types of observing instruments.

1.2. BACKGROUND

The Australian Government, through the Australian Building Codes Board (ABCB), has responsibility for maintenance of the Building Code of Australia (BCA). The BCA establishes performance requirements that buildings must satisfy when subjected to the actions of, among other hazards, severe winds. In relation to wind actions, the BCA references two Standards to establish the performance requirements – AS/NZS 1170.2:2002 *Structural design actions Part 2; Wind actions* and AS 4055:2006 *Wind loads for housing*. In each State and Territory, the BCA forms part of the building regulations, enforced through legislation at that level.

For design of engineered and residential buildings, the Australian Standard/New Zealand Standard AS/NZS 1170.2 (2002) *Structural design actions Part 2; Wind actions* sets out the gust wind speeds (that relate to the performance levels specified in the BCA) that must be used in calculating loads on structures in different regions of the country, together with modification factors to account for directionality, terrain roughness, shielding and topographic effects. Design wind speeds are equivalent to wind hazard (in that they are described in terms of a gust wind speed for a return period), and the levels are set in an effort to equalise the risk between the low and high hazard regions across the country.

The BCA regulations stipulate that the 500 year return period hazard be used as the design wind speed for residential housing in all Australia states, For this reason, this study employs this metric (the 500 year return period for gust wind speed) as the geophysical variable for comparing both the time-series observations and also for comparing the coincident measurements from the "old" and "new" types of observing instruments (anemometers).

The Australian Bureau of Meteorology (BoM) has been recording peak gust wind speed observations in the Australian region for over 70 years. The current wind loading code and hence the performance of our infrastructure against severe wind hazard is based primarily on the Dines anemometer measurement of the peak gust wind speed. The Australia/New Zealand Wind Actions Standard (AS/NZS 1170.2, 2002) as well as the wind engineering community in general rely on these peak gust wind speed observations to determine design loads on buildings and infrastructure. The digital recording of meteorological data became prevalent in the 1990's. BoM implemented a 3-second averaged gust wind speed in the mid-1990's on a recommendation from the World Meteorological Organisation (WMO).

In the mid-1980's the Australian Bureau of Meteorology (BoM) commenced a program to replace the aging pressure tube Dines anemometer with the Synchrotac and Almos cup anemometers. Only six Dines anemometers remain in operation, mainly as backup or for high-speed measurement. During the anemometer replacement procedure, many localities had more than one type of anemometer operating, recording extreme events. The passage of Cyclone Vance through Exmouth in 1999 saw Dines and Almos anemometers, separated by 25 metres, recording peak gusts of 144 and 122 knots respectively (Reardon *et al*., 1999). A weak cyclone that passed through Townsville in April 2000 recorded a peak gust of 70 knots on the Dines and 59 knots on the Almos anemometer (Reardon, 2000). Systematic differences as demonstrated in these instances raise concerns about the consistency and utility of the peak gust wind speed database.

The visual inspection of the observed daily peak gust wind speed time-series for most of the Bureau of Meteorology observing sites considered in this study is sufficient to indicate that in general *"the early part of the record contains a higher frequency of extreme events, and also the largest amplitude extreme events"*. Figure 2 shows time-series plots of the daily maximum gust wind speed (above a threshold of 25 m/s) for the Sydney, Melbourne and Adelaide meteorological observing stations. Visual inspection indicates that the early part of the record (Dines anemometer) contains a greater number and also higher amplitude extreme events compared to the later part of the record (replacement cup anemometer). Time-series plots of gust wind speed for all stations considered are shown in Appendix I-A.

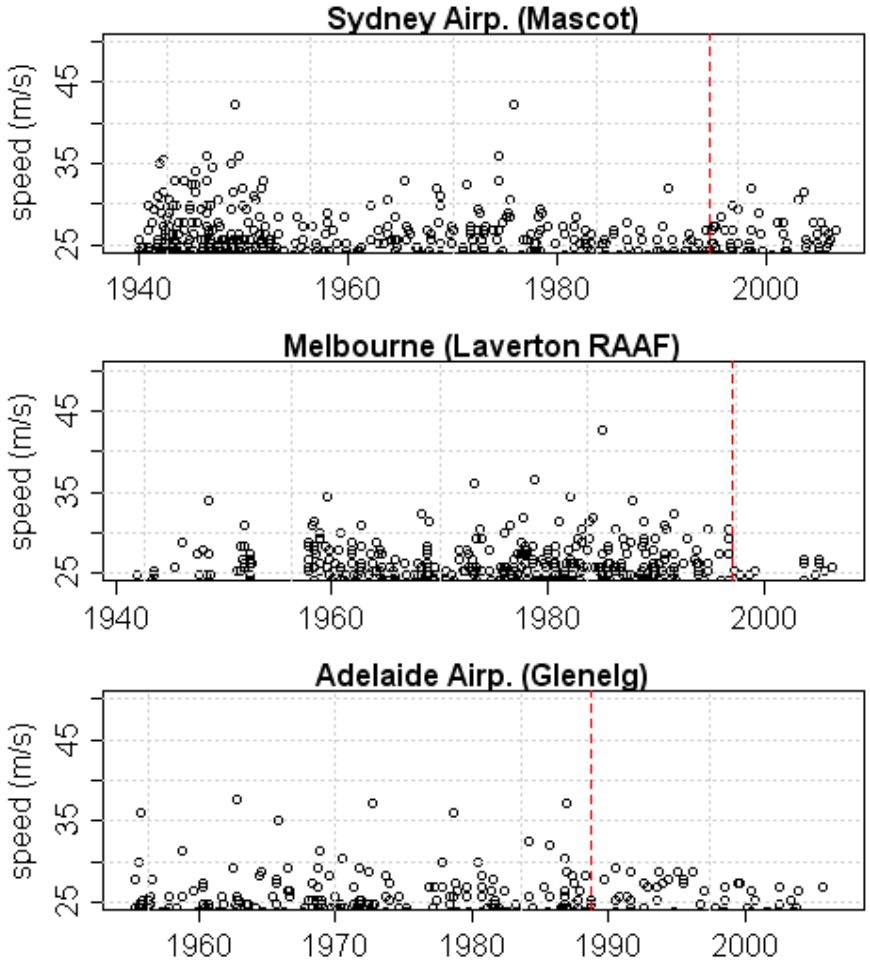

Fig. 2. Time-series plots of the daily maximum gust wind speed (above a threshold of 25 m/s) for the Sydney, Melbourne and Adelaide (airport) meteorological observing station. The broken vertical line indicates the replacement of the Dines anemometer with a cup anemometer.

The installation of the pressure-tube (Dines) anemometer (described in Jacobson, 2005; Knowles and Spilhaus, 1953) commenced at Australian sites in the 1930's. The Dines anemometers were factory calibrated under steady state conditions (mean wind speeds); however their response to transient wind conditions (gusts) was not determined. The BoM anemometer replacement program, which commenced in the 1980's, replaced the pressure-tube Dines instruments (paper chart recording) with cup anemometers (digital recording). This replacement program had the potential to drastically change the characteristics of observed wind speed. It was well known that the Dines had a high minimum start-up speed (i.e. minimum speed before the instrument registers a reading) whilst the cup anemometers suffered from overspeeding (i.e. cups keep rotating even though wind has dropped; see Gorman, 2004).

A number of intercomparisons involving Dines and cup anemometers have been undertaken over the last 50 years or so; see for example (Smith, 1981). Logue (1986) compared both mean and gust wind speeds measured using a Dines co-located with a standard cup anemometer at the Irish Meteorological Service's Galway observing site during 1984. Overall the mean wind speeds from the two instruments compared well. However, the cup anemometer significantly underestimated the gust wind speeds when compared to those obtained using the Dines. The cup anemometer used by Logue is similar in design to the BoM instruments (i.e. heavy construction). These types of anemometers have a large distance constant (length of fluid flow past the sensor required to cause it to respond) compared to lightweight cup anemometers found on automatic weather stations (Sparks, 1997).

1.3. OBJECTIVE AND OUTLINE

The study focused on the problem of whether the introduction of cup anemometers has introduced a bias into the gust wind speed observational database.
Section 2 of this report presents the methodology employed to analyse the return-period hazard extreme wind hazard levels and the confidence limits associated with these estimates.
Section 3 presents the data and metadata obtained from the Bureau of Meteorology for the study.
Section 4 presents the results of the analysis of both the time-series and coincident measurements.
Section 5 provides a discussion of the analysis whilst Section 6 provides conclusions.
Future directions and recommendations are provided in Section 7.

2. Methodology

2.1. STATISTICAL MODEL

The results presented here were generated using a statistical model of severe winds developed by Geoscience Australia (Sanabria & Cechet, 2007). Although statistical models have limitations, they are useful for the assessment of potential severe winds at discrete points in a region and are fundamental for the calculation of hazard from records of observational gust wind speed datasets. Statistical methods are extensively utilised in the current Australian wind loadings standard (AS/NZS 1170.2, 2002).

The main limitation of statistical models is their dependency on the quality of the observational data utilised. One of the issues affecting the quality is the small size of the datasets available for analysis; the largest dataset used in this study has only 60 years of data whilst it is required to predict the 500 year return period for gust wind hazard. The ability to calculate reliable confidence intervals for the results is also an issue of further research.

The core of the statistical model is the calculation of return periods for extreme gust speeds. This is carried out by fitting a extreme value distribution to the given gust speed dataset. Extreme value distributions are asymptotic functions that allow modellers to extrapolate limited data samples to maximum possible values. The theory behind extreme value distributions is similar to the Central Limit Theorem (CLT); both infer the limiting distribution of independent, identically distributed (iid) random variables. According to the CLT, the mean value of a sample of iid random variables converges to a standard normal distribution. Similarly if the maxima of a large number of iid random variables converge to a distribution, this distribution has to be a member of the Extreme Value Distributions (Jagger and Elsner, 2006).

Although the extreme value distributions have been derived considering a set of infinite data samples, they are regarded as good approximations to the behaviour of limited data. There are two basic types of functions to fit extreme values: Generalised Extreme Value distributions (GEV) and the Generalised Pareto Distribution (GPD).

Whittingham (1964) conducted the first analysis of extreme gust wind speeds in Australia. He analyzed annual maximum gusts at each station irrespective of their source, and did not specifically extract those produced by tropical cyclones. For the extreme value analysis he drew contour maps for extremes at various return periods up to 100 years. In most cases, Whittingham's predictions of return period wind gusts were based on quite short record lengths, compared with current values in AS/NZS 1170.2. For the observing stations considered by Whittingham with regards to extreme value analysis, the maximum number of years of data was 21, and in one case as few as 7 years of data were considered.

2.2 GENERALISED EXTREME VALUE DISTRIBUTION

A unifying expression to represent the family of extreme value distributions was introduced by Jenkinson in 1955; it is known as the Generalised Extreme Value (GEV) distribution (Coles, 2001) and is given by,

$$G(z) = \exp\{-[1 + \xi(z - \mu)/\sigma]^{-1/\xi}\} \qquad (1)$$

the expression is defined on the set $\{z : 1 + \xi(z - \mu)/\sigma > 0\}$
where: ξ = shape parameter
μ = location parameter
σ = scale parameter

These parameters must satisfy; $-\infty < \mu < \infty$, $\sigma > 0$, and $-\infty < \xi < \infty$, and the value of the shape parameter defines which specific distribution is being fitted to the given data:,

- If $\xi < 0$, a GEV type III or ***Weibull*** distribution is used. This distribution has a convex (bounded) curve.

- If $\xi > 0$, a GEV type II or ***Frechet*** distribution is used. This distribution has a concave (unbounded) curve.

- If $\xi = 0$, a GEV type I or ***Gumbel*** distribution which is a straight line, is used.

A number of techniques to fit these distributions to the given data have been developed. The most effective are the maximum likelihood and the method of moments. Figure 3 shows the Sydney airport data fitted using seven different techniques: maximum likelihood (mle), method of moments (moments), unbiased probability weighted moments (pwmu), biased probability weighted moments (pwmb), minimum density power divergence (mdpd), medians (med) and likelihood moment (lme). Although in most cases they give similar results, other examples (not presented here) show that the most effective technique to fit GEV distributions to wind speed datasets is the 'mle' method. Palutikoff et al., (1999) and Seguro and Lambert (2000) report similar results; for this reason the 'mle' technique will be used throughout this work.

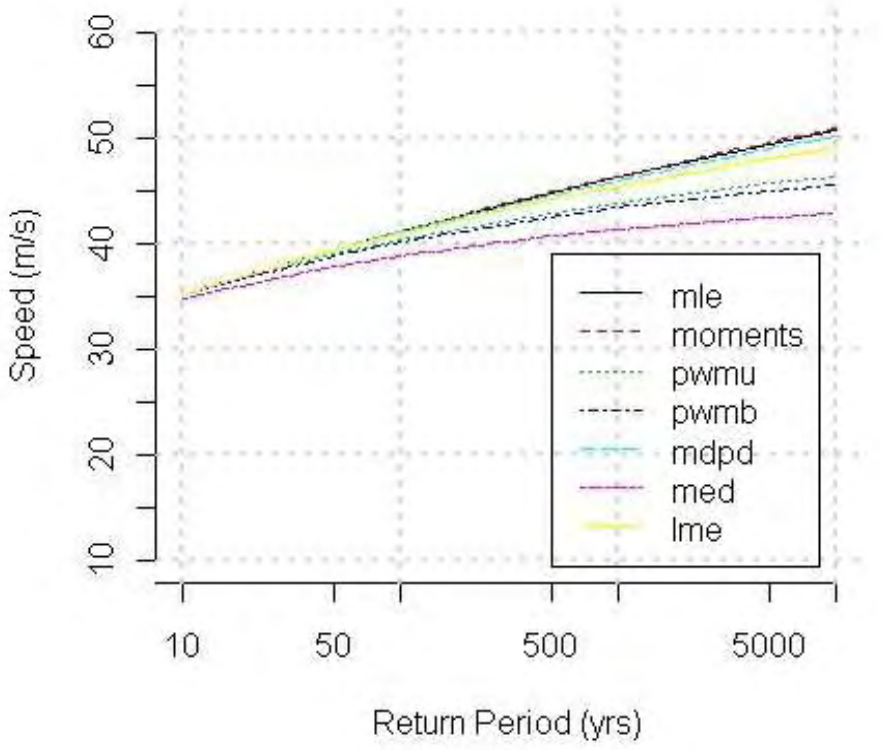

Figure 3. Fitting the GEV to gust wind speeds using a number of techniques.

2.3. GENERALISED PARETO DISTRIBUTION (GPD)

The Generalised Pareto Distribution (GPD) belongs to a family of extreme value distributions. The GPD utilises all values of a dataset exceeding a given threshold. It has certain advantages over the Generalised Extreme Value Distributions (GEV); first it uses significantly more data than the GEV; secondly by setting the threshold high enough, the data will be better distributed in time, so it is likely that the observations are independent from each other, one of the conditions of extreme value distributions (Coles, 2001). The GPD is defined by the expression,

$$H(y) = 1 - (1 + \xi * y/\check{s})^{-1/\xi} \qquad (2)$$

defined in $\{y : y > 0$ and $(1 + \xi * y/\check{s}) > 0$

where: $\check{s} = \sigma + \xi * (u - \mu)$

$\check{s}$ is the scale parameter of the GPD

u = threshold value
σ = scale parameter of GEV
μ = location parameter of GEV
ξ = shape parameter of GEV

Note that μ and ξ are also the parameters of the GEV, i.e. if the original data can be fitted with a GEV distribution, values above the threshold can be fitted with a GPD,

In Sanabria & Cechet (2007) a number of wind datasets were modelled by both methods: GEV and GPD. The results produced by the GEV distributions were considered too poor for wind hazard applications so this report focuses only on results produced by the GPD.

2.3.1 Threshold selection

One of the issues found in fitting a GPD to given wind speed datasets is the selection of the appropriate threshold value ‘u’. High threshold values result in the selection of only a few data points, most likely not enough for a good fitting of the distribution. Low values result in too many samples which are most likely not independent from each other. Return period calculation using GPD distributions are very sensitive to the threshold selection.

Although there are methods to help modellers select the appropriate threshold for a given dataset they are mostly visual, subjective techniques, prone to producing inaccurate results and inappropriate for large scale applications. In these studies the computer-based, automatic algorithm discussed in Sanabria & Cechet (2007) was used.

2.3.2 Confidence Interval

Calculation of return periods of wind gusts should be considered incomplete if a confidence interval (CI) for the results is not presented. A confidence interval shows the range of values in which the true value of the return period lies for a given probability. The confidence interval depends on the amount and structure of the dataset, particularly the variance-covariance matrix which measures the spread of the samples around their mean. In this study we are interested in finding confidence intervals with 95% probability, in other words, we want to find the return period of wind speeds with the interval in which the true value of the return period can be found in 95% of cases.

There are two basic algorithms for calculation of the confidence intervals of results produced by extreme value distributions: The `Delta' method and the `Profile Likelihood' method. Both methods have been implemented in the R environment by Gilleland and Katz (2005a) based on Coles (2001).

Applying the methods to temperature data, Gillelland and Katz found out that the Profile-likelihood method gives better results because it considers the asymmetry of the data (Gilleland and Katz 2005b). Figure 4 shows the RP of the Sydney Airport combined winds (black line) with 95% Confidence Interval calculated using the Profile-likelihood method (blue dashed line), the asymmetry of the interval with respect to the calculated RP can be clearly seen. The exceedance levels for the 500-year RP with its 95% confidence interval is shown in red, this is the prescribed wind speeds for design of structures in Australia (AS/NZS 1170.2, 2002). Note that the CI substantially increases as the RP years increase indicating a higher degree of uncertainty when making inferences far beyond the range of the data (66 years).

Since wind speed data is highly asymmetric the Profile-likelihood method has been used in this study. Both the upper and lower bounds for the RP will be shown since they are asymmetric with respect to the value of the RP.

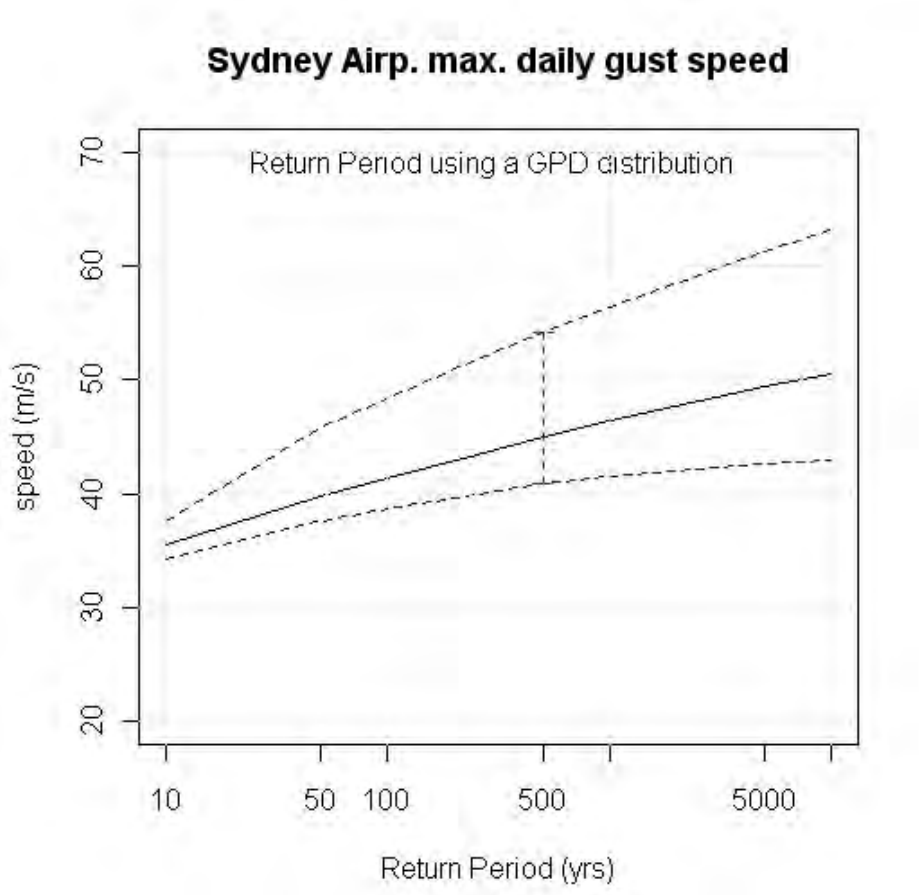

Figure 4. Sydney Airport daily maximum gust wind speed return period (RP). Also shown in broken lines are the 95% confidence limits (CI)

2.4. R- PROGRAMMING ENVIRONMENT

The software utilised for this study was developed using the R-programming environment on a computer running the Linux operating system. One of the main advantages of R is the large collection of specific-purpose packages developed by the user community. For this project extensive use of R-programming environment packages for extreme value analysis were used (Stephenson 2004; Gilleland and Katz, 2005a).

The methodology used in this study can be summarised in the following steps:

- Select a particular wind recording station with available maximum daily wind speed and weather description datasets,
- Merge the wind dataset with the corresponding weather description dataset,
- From the merged dataset, extract thunderstorm wind speeds and construct a thunderstorm wind dataset. The remainder of the original dataset is termed the synoptic wind dataset. The original dataset is called combined wind dataset,
- Fit an Extreme Value (EV) Distribution to each one of the datasets (combined, thunderstorm and synoptic winds). To do this,
- Calculate the parameters to fit the distribution to the given data (in practice a Generalised Pareto Distribution (GPD) was used for reasons explained in Section 3.2),
- Using the GPD calculate and plot return periods (RP) for these datasets. Plot return periods for all wind types, i.e. combined, thunderstorm and synoptic wind speeds in the same plot to observe the relationship between them,
- Calculate confidence interval for the RP, and present the RP in plots and/or tables.

If annual observations are used the return period (RP) gives the maximum wind speed that could be exceeded on average once a year. Thus a 500year return period wind speed has a probability of exceedance of “one in fifty” (years) or equivalently 0.2% in any single year.

3. Data

This study has examined the observed record of **peak gust wind speed** (daily maximum gust wind speed) in order to establish the existence of a bias between the early part of the record (obtained using pressure-tube Dines anemometers) and the later part of the record (obtained using cup anemometers). All observational data (38 observing stations considered) as well as all the metadata was obtained from the Bureau of Meteorology. All recording stations considered were situated at airports which were in the most part staffed by Bureau of Meteorology officers. To isolate the issue of anemometer replacement, only observing stations located at airports (consistent exposure) and with more than 30 years of record were considered.

3.1 GUST WIND SPEED DATA

All wind datasets used in this study were acquired by GA from the Australian Bureau of Meteorology (BoM). The wind speed data contains six types of datasets from 134 recording stations (not all types available for all stations):

- `1min'. - contain one-minute averaged wind speed records,
- `3hour'. - contain three-hourly observations of wind speed (10 minute average),
- `hhourly'. - contain half-hourly observations of wind speed (10 minute average), and
- `MxDai'. - contain maximum daily gust wind speed records.
- `weatherd'. - contain 3-hourly weather description records,
- `metadata'. - contain a comprehensive description of wind station characteristics and an explanation of the type of data recorded by the station.

Each dataset type comes with two metadata files called `*_Notes_*.txt' and `*_StnDet_*.txt', where the * should be replaced by the data type and a BoM ID number (eg. 99999999299892) respectively. "*_Notes" provides a detailed explanation of the data format for the data type, including a description of the recording instrument, time and reading frequency. File "*_StnDet_*.txt" provides further information about the dataset type including station reference number and name, location (in lat, long); and more importantly, the starting date for the records. In cases in which the station has been closed the final recording date is also presented.

BoM publishes a three-hour interval classification of weather conditions according to the W.M.O. code (BoM, 1982). The present weather is described by 100 symbols abridged from the W.M.O. code indicating the type of weather conditions during the past hour. These symbols are numbered from 0 to 99. From this classification, 12 weather classes that can be considered as thunderstorms were identified. They are classes 17, 27, 29 and classes 91 to 99 as presented in Table 1 Classes 9, 33, 34 and 35 refer to short-period dust storms or sand storms but they have also been included because they impede visibility and hence are related to nearby mesoscale phenomena because of the sudden change in wind conditions (Sanabria & Cechet, 2007a).

Ten symbols for the past weather are also given to represent the most significant weather conditions within the past three hours of observation but not during the most recent hour. BoM numbers these symbols from 0 to 9 (see Table 2).

Table 1. Present weather description

Present weather number	Description
17	Thunder heard but no precipitation at the station.
27	Showers of hail, or of hail and rain during past hour, but no at time of obs.
29	Thunderstorm (with or without precip) during past hour, but not at time of obs.
91	Slight rain at time of obs; thunderstorm during past hour not at time of obs.
92	Moderate or heavy rain at time of obs; TS during past hour not at time of obs.
93	Slight snow and/or rain/hail at time of obs; TS during past hour not at time of obs.
94	Moderate or heavy snow and/or rain/hail at time of obs; TS past hour not at obs time.
95	Slight or moderate thunderstorm without hail but with rain and/or snow at obs time.
96	Slight or moderate thunderstorm with hail at time of obs.
97	Heavy thunderstorm without hail but with rain and/or snow at time of obs.
98	Thunderstorm combined with duststorm or sandstorm at time of obs.
99	Heavy thunderstorm with hail at time of obs.
9	Duststorm or sandstorm within sight of station or at station during past hour
33	Severe duststorm of sandstorm, has decreased during past hour
34	Severe duststorm of sandstorm, no appreciable change during past hour.
35	Severe duststorm of sandstorm, has increased during past hour.

Table 2. Past weather description

Past weather number	Description
0	Clear, few clouds at observing station.
1	Partly cloudy, scattered or variable sky at obs station.
2	Cloudy (broken) or overcast at observing station.
3	Sandstorm or duststorm during past 3 hours.
4	Fog or smoke or thick dust haze during past 3 hours.
5	Drizzle.
6	Rain.
7	Snow, or rain and snow.
8	Shower(s).
9	Thunderstorm, with or without precipitation.

3.2. GUST WIND SPEED METADATA

The metadata describing the history of anemometer measurement at Bureau of Meteorology observing stations was assembled for this study (obtained by request from BoM). The metadata detailed:

- Installation and decommissioning dates
- Instrument type
- Calibration dates
- Movement of instruments
- Issues with instrument performance
- Repair of instruments

This information was used to segment the Dines and cup anemometer parts of the observing record for the observing stations considered. In addition, the metadata was very useful for determining periods where both anemometers were operational at BoM observing stations.

3.3 DINES ANEMOMETER CHART RECORDS

Analysis of the anemometer metadata from the BoM observing stations allowed the development of an understanding regarding the availability of coincident Dines and cup anemometer observations for conducting a direct comparison (bias assessment). Most observing stations had an overlap period of weeks to a few months, however some observing stations within the Australia tropical region have maintained their Dines anemometer in parallel with the cup anemometer. At the beginning of this study only six (6) Dines anemometers remained in operation in the Australian region (all at BoM observing sites). These instruments were meticulously maintained by BoM technicians even though all had ceased to be the primary wind speed observing instrument at some stage during the 1990's. They remained operational whilst spare parts were available. The robust nature of the Dines anemometer construction resulted in these instruments having a superior survivability (tropical cyclones) compared to the replacement cup anemometers.

Table 3. BoM observing stations where coincident Dines and cup anemometer measurements were available;listed are the years where coincident data were available

Station name	Years when coincident measurements considered
Brisbane	1987-01-01 to 1999-12-02
Broome	2002-12-12 to 2010-09-19
Cairns	2002-12-12 to 2010-09-19
Darwin	1990-11-21 to 2010-10-20
Gove	2007-01-16 to 2010-03-31
Learmonth	1996-01-07 to 2010-10-16
Townsville	1996-01-07 to 2010-10-16

Dines paper anemometer charts covering approximately 100 years of observation were obtained from the BoM. Table 3 provides a list of the observing stations where coincident Dines and cup anemometer measurements were available, as well as a list of the actual years where coincident data were assessed. The provision of the Dines anemometer charts was coordinated by Ian Muirhead (Data Manager, National Climate Centre, Bureau of Meteorology, Melbourne) who organised the movement of the Dines anemometer charts from the state-based National Archives centres to the Bureau of Meteorology office in Canberra (where they were analysed). The volume of charts was approximately one cubic metre.

3.4. GUST WIND SPEED DATASET CLEANING

As mentioned before, results from the statistical model are very sensitive to data quality. In particular, gust speed observations used in these studies are unreliable as instruments are calibrated for mean wind speeds; the procedure does not determine their transient response. This is a serious limitation because of the possible inconsistency and reduced accuracy between instrument types. These instruments have been developed over a period of more than 50 years and some studies have shown that differences occur with regard to their ability to measure short wind gusts (say gusts of 2-3 sec duration) (Whittingham, 1964). These short duration wind gusts are the cause of wind-related damage and thus crucial in wind hazard studies. A brief description of the data quality problem is presented below. A detailed discussion of this problem is however, beyond the scope of this report; interested readers can refer to Muirhead et al. (2008) and Miller (2008).

Wind speed dataset quality can be illustrated by considering some of the Sydney airport wind datasets available from the Australian Bureau of Meteorology. Figure 5 shows the scatter plot of the airport's maximum daily gust exceeding 15 m/s. The vertical (dotted) lines indicate the date in which the wind recording instrument was changed as shown in Table 4 (BoM, 2006). Figure 5a clearly shows three different speed regions; one from the start of the record until 31/12/1973 when the first synchrotac anemometer was installed. The second period stretches from the installation of the first synchrotac until the new synchrotac was installed (01/07/1994); the third region comprises the data after the 1994 upgrade. Observations in each region appear to be drawn from different populations; the first region in particular presents higher speeds than the other two. Regions 1 and 2 show outliers (maximum readings) at 42.2 m/s. Studies conducted by BoM show that some stations can be affected by the growth of nearby trees or housing developments, movement of the anemometer, recalibration or changes in the reading frequency (Muirhead et al., 2005).

To further examine the dataset consider the 3-hourly mean speed from the same observing station, as presented in Figure 5b. Notice that the Region 2 outliers are not present. Region 1 still provides the highest speeds in the dataset.

Table 4. Changes in anemometer instrumentation at the Sydney airport observing station.

04/01/1939	Installation	Dines
31/12/1973	Installation	Synchrotac S/N
01/07/1994	Installation	Synchrotac 706 S/N
28/04/1999	Replacement	Synchrotac 706 S/N
10/09/1999	Replacement	Synchrotac 897 S/N
28/04/2000	Installation	Mast installation
05/09/2003	Installation	Synchrotac cups 732 S/N
03/01/2006	Replacement	Synchrotac cups 732 S/N

Two more plots of the Sydney airport wind station are presented in Figures 5c and 5d, generated from the half hour sampling dataset. This dataset includes half-hour values for mean wind speed, i.e. wind speeds averaged over the 10 minutes prior to observation time; and for the maximum gust speed during this period. For automatic weather stations (AWS) the gust speed recorded is the highest 1 sec value over the last 10 min previous to observation time. During the mid-1990's, the BoM implemented a WMO directive that the gust wind speed be calculated as the 3-second moving average over the time period considered (see Discussion for further comment).

Figure 5c shows the half hour gust speed scatter plot, whilst Figure 5d shows the daily mean wind speed calculated from the half-hourly mean wind speed dataset. Figure 5e shows the relationship between gust and mean speeds as found in the half-hour dataset, the straight lines are the linear regression in regions 1, 2 & 3. The regression lines show a different trend for each speed region, with the data for the period 1972-94 showing a long-term trend towards higher values than the other two.

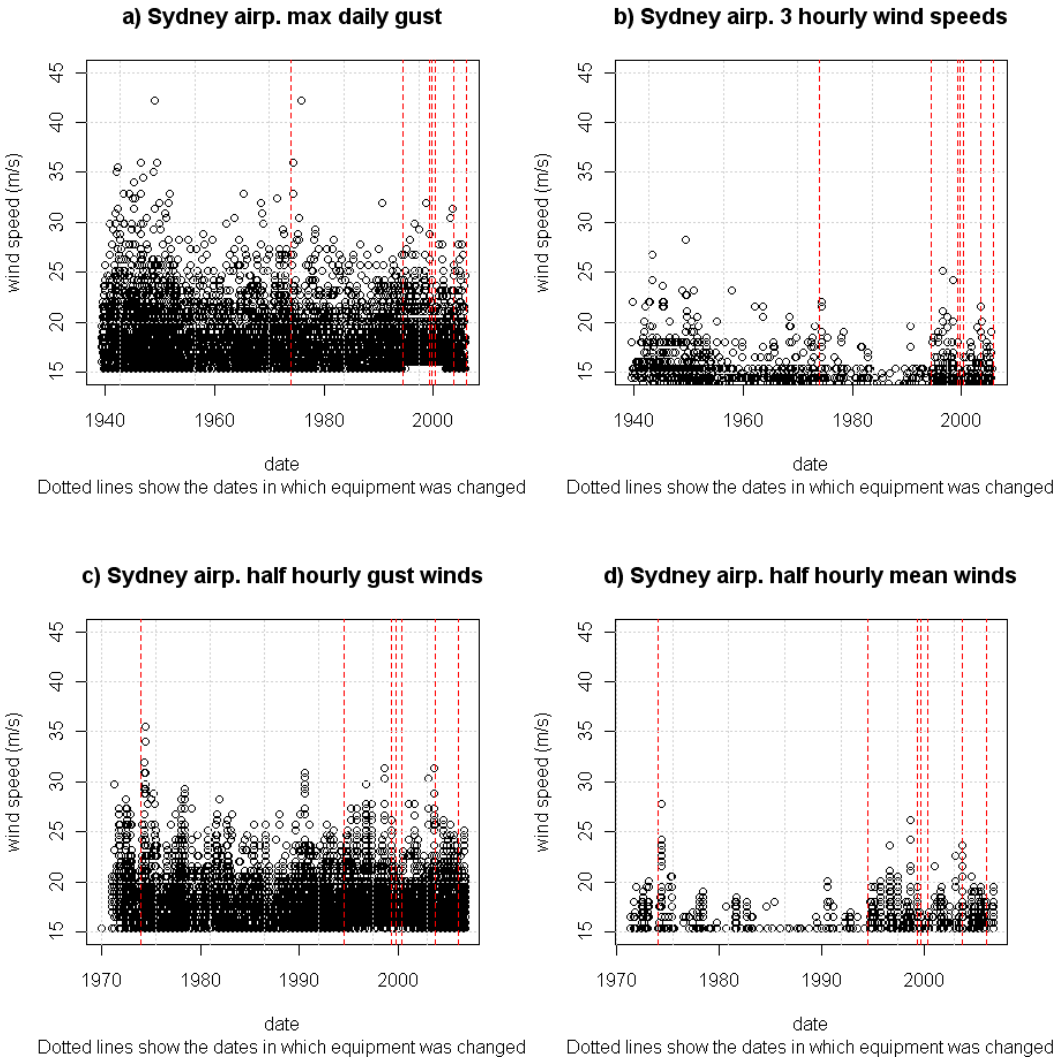

Figure 5. Four scatter plots of Sydney Airport wind speeds; (a) maximum daily gust wind speeds, (b) 3-hourly mean wind speeds, (c) half-hourly mean wind speeds, and (d) daily mean wind speed (from half-hourly observations).

Notice that the regression line for the later part of the records is in between the lines of the earlier parts indicating less extreme values; this is because the records of the later part are more reliable since automatic instrumentation and recording systems (replacing chart recordings) was installed in most BoM stations in the 1980's.

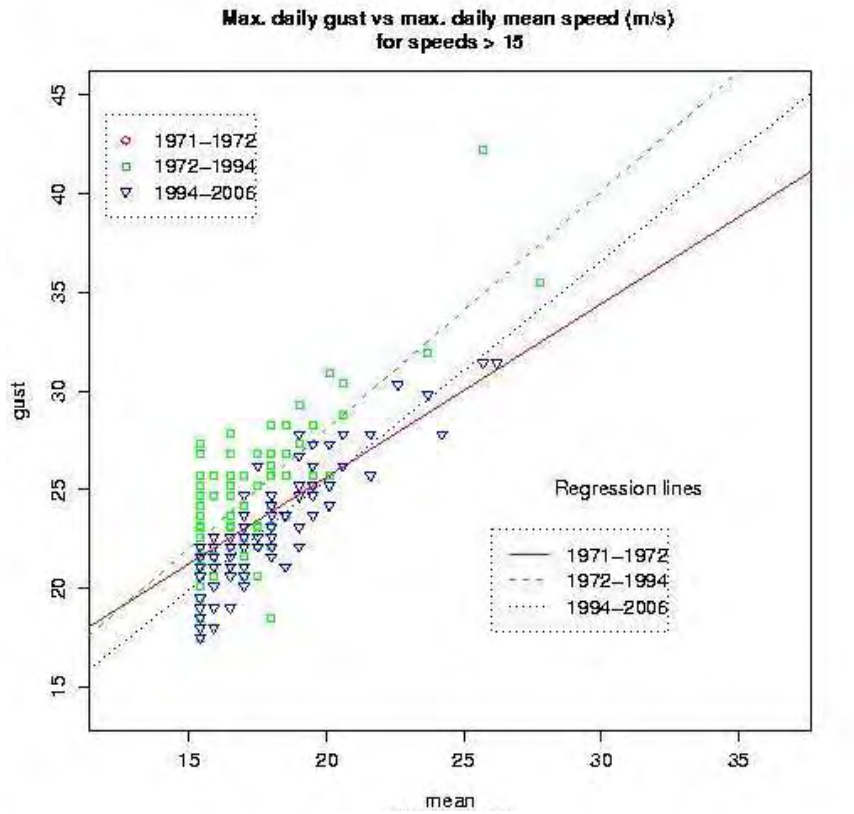

Figure 5e: Sydney airport; half-hour gust to mean wind speed ratio. All wind speeds are in m/s.

In order to obtain an estimate of the dataset quality limitations, Geoscience Australia has developed a Monte Carlo (MC) method which can generate large amounts of synthetic gust data by sampling from appropriate probabilistic functions of mean wind speed and gust to mean wind speed ratio. This synthetic data has been generated by sampling from mean wind speeds and gust factors from recent era of records (i.e. since the late 1980's). The MC technique is able to produce synthetic datasets of this period that compare well with the gust wind speed observations. The MC technique also allows the production of longer records, equivalent to thousands of years of observation, and can be used to calculate improved confidence intervals for high return period hazard. For a full description of the MC method see Sanabria & Cechet (2010).

4. Results

The analysis for decadal time-series and the separated time-series (Dines and cup anemometer sections) are presented in Sections 4.1 & 4.2. They contain the analysis of the current BoM peak gust wind speed database for the non-cyclonic region (Region A) of the Australia/New Zealand Wind Actions Standard AS/NZS 1170.2. Region A was considered for these analyses as the observed record contains a significant number of extreme events (*synoptic* and *thunderstorm*) over decadal time scales (i.e. extreme events not dominated by one or two tropical cyclone events). This analysis strategy aids in the fitting of the GPD extreme value distribution in that the confidence intervals are narrow due to the large number of extreme events with similar amplitude. A total of 31 Bureau of Meteorology (BoM) recording stations distributed throughout Region A were selected for this project as shown in Figure 6.

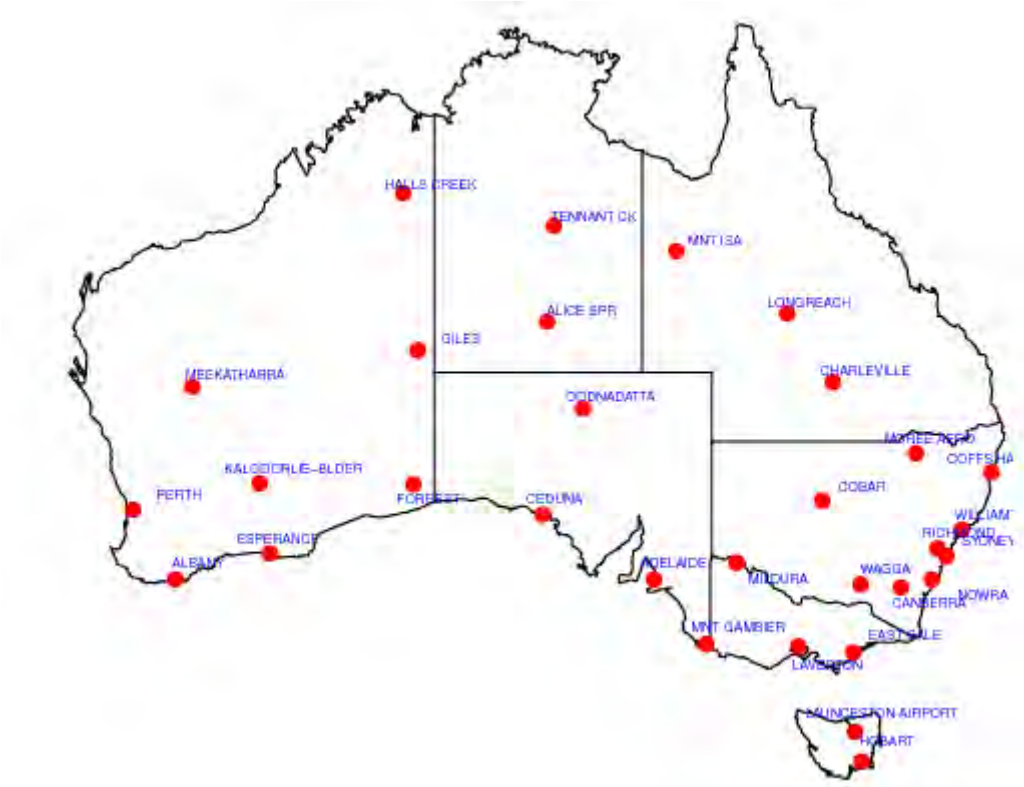

Figure 6. Location of selected wind stations

A number of researchers have recognised the need for a more detailed analysis and modelling of the different components of the wind data sets. The importance of this approach concerns not only the physical characteristics of the component mechanism but also the specific hazard that they pose to people and the built environment. More realistic results are obtained when each wind component is modelled independently (Gomes & Vickery, 1978; Holmes, 2002).

The model discussed here follows the technique proposed by Holmes (2002) which allows the extraction of thunderstorm downbursts or mesoscale winds from the dataset. The remaining dataset is termed synoptic winds and the complete dataset is called the combined wind dataset. Regions also experiencing wind gusts from tropical cyclones and/or tornadoes could have this component dealt with separately.

It is also important to separate the wind gusts into these components because wind multipliers as detailed in the Australian/NZ Wind Loadings Standard (AS/NZS 1170:2, 2002) affect these components differently. In particular, the topographic multiplier for thunderstorm downbursts is significantly reduced compared to synoptic winds. Synoptic winds travel chiefly in a horizontal direction towards a target location whereas thunderstorm downbursts have a significant vertical component and are affected to a lesser extent by topographic acceleration.

The separation of the components of the BoM dataset in order to calculate the corresponding wind hazard of thunderstorm and synoptic winds relies on the weather description dataset (see Section 3.1). The algorithm used here selects records with the present weather shown in Tables 1 & 2.

4.1. DECADAL TIME-SERIES ANALYSIS

The decadal time-series analysis was undertaken prior to receiving the anemometer metadata from BoM (i.e. prior to obtaining an understanding of when anemometers were changes from Dines to the 3-cup type). To assess data consistency, we generated RP of gust wind speeds for four sections of the datasets: a) using all records in the dataset, b) using only records after 1980, c) using records after 1990; and d) using only the initial part of the dataset (records before 1980).

Table 5 presents the gust wind exceedance levels of the 500 year return period (RP) with 95% confidence interval for the total (combined) wind speeds of the wind stations selected. The maximum daily gust wind speed dataset was used in these studies. All wind speeds are in m/s.

Appendix I-B contains the RP plots for all the observing stations considered. The corresponding curves for combined, thunderstorm and synoptic winds are shown. Notice the location of each RP curve: combined winds are higher than the corresponding thunderstorm winds but the latter tends asymptotically to the combined winds. Synoptic wind speeds are consistently lower than combined wind speeds. They are also lower than thunderstorm speeds for medium and high return periods but higher for low return periods with a crossover between the two of between 10 and 100 years in most cases. There are however curves which are separate from the trend, to illustrate the point the plots have been organised locating first those which better follow the trend. The curves which start in Appendix I-B, Figure 5 for instance, separate substantially from the trend, some show very low synoptic wind speeds. For a few observing stations the thunderstorm winds are a bit higher than the corresponding combined winds especially for high values. Most of these problems can be traced back to the quality of the dataset used, as previously explained. In cases in which the merged dataset of speed and weather show a lot of missing values the result is a synoptic wind dataset with very few - mostly low - values and hence its curve is very low with respect to the other two. The opposite is true for thunderstorm datasets, they have few, very high values and for this reason their curves can be a bit higher than the corresponding combined winds, especially for high RP.

The asymptotic behaviour of the thunderstorm winds shows that wind datasets for some locations (but not all) are dominated by these types of winds. The return period plots in Appendix I-B also show that each type of wind poses a different hazard to the environment and hence separation of the types of winds present in the dataset is important for a more realistic modelling of wind hazard.

Table 5. 500 year return period (RP) of combined gust wind with 95% CI considering the complete observed data record.

	Station name	RP	Lower 95% CI	Upper 95% CI
1	Adelaide Airp.	42.6	37.8	49.7
2	Albany Airp.	42.0	38.3	46.1
3	Alice Springs Airp.	41.6	37.3	46.0
4	Canberra Airp.	37.3	34.4	41.6
5	Ceduna AMO	39.8	37.3	42.3
6	Charleville Airp.	42.6	38.7	46.5
7	Cobar MO	39.3	33.6	51.2
8	Coffs Harbour MO	37.1	33.6	42.7
9	East Sale Airp.	41.3	38.1	45.1
10	Esperance	44.1	40.1	50.2
11	Forrest Airp.	45.5	42.8	48.4
12	Giles MO	42.0	37.4	48.1
13	Halls Creek Airp.	41.8	37.5	46.2
14	Hobart Airp.	38.6	35.2	44.1
15	Kalgoorlie-Boulder Airp.	43.8	38.8	50.0
16	Launceston Airp.	38.8	35.1	44.2
17	Laverton RAAF	42.3	38.7	45.9
18	Longreach Airp.	44.4	40.1	48.7
19	Meekatharra Airp.	41.9	38.0	45.8
20	Mildura Airp.	45.6	39.2	66.8
21	Moree Comparison	42.4	34.4	61.9
22	Mount Gambier Airp.	40.3	37.5	43.0
23	Mount Isa Airp.	43.5	36.1	57.0
24	Nowra Airp.	41.8	38.3	46.8
25	Oodnadatta Airp.	41.3	38.1	46.1
26	Perth Airp.	38.8	34.9	44.1
27	Sydney Airp.	44.8	40.6	54.4
28	Tennant Creek Airp.	37.6	34.0	41.3
29	Wagga Wagga AMO	41.0	36.7	46.8
30	Williamtown RAAF	42.2	39.1	45.4
31	Woomera Airp.	45.8	41.6	50.0

4.1.1 CONSIDERING ONLY THE OBSERVING RECORD POST- 1980

In order to address concerns over the reliability of data recorded by older, possible poorly calibrated equipment, we recalculated Table 5 using only the part of the dataset after 1980. The selection of 1980 as the cut-off point was made on a basis that it was the start of the decade about which station equipment began being migrated from Dines to cup style anemometry and onsite data recording practices were improved. It was not possible to separate according to the actual equipment used at the site due to the unavailability (at the time) of the station metadata records.

Table 6 presents the exceedance levels of the total or combined maximum daily gust speed of the 500 year RP with 95% confidence interval, data in the range 1980-2006 was used.

When comparing the exceedance levels of the 500 year RP of the gust speeds produced by the full and post 1980 station dataset, it is clear that the exceedance levels do not differ in any consistent manner across multiple stations. Most values are higher for the full dataset case although a few stations present lower values for the full dataset, see for instance station 8 'Coffs Harbour'. This is due to most of the high wind speeds for this station occuring after 1980. The presence of higher values in a smaller dataset results in higher exceedance levels for the RP.

Notice that the exceedance levels of 500 year RP of the gust speeds with the full dataset and with only the part after 1980, is within the 95% CI of either case. This indicates small variation of the exceedance levels of the 500 year RP around the mean (discussed further later in Section 4.1).

Table 6. 500 year RP of combined wind with 95% CI (observations from 1981-2006)

	Station name	RP	Lower 95% CI	Upper 95% CI
1	Adelaide Airp.	41.4	36.9	45.9
2	Albany Airp.	39.6	34.8	49.3
3	Alice Springs Airp.	41.9	34.8	46.9
4	Canberra Airp.	39.8	34.0	50.3
5	Ceduna AMO	41.6	37.3	46.1
6	Charleville Airp.	43.2	37.6	50.3
7	Cobar MO	39.8	33.7	51.4
8	Coffs Harbour MO	40.4	33.9	54.3
9	East Sale Airp.	42.2	37.9	47.6
10	Esperance	44.3	39.6	51.5
11	Forrest Airp.	43.4	36.9	49.9
12	Giles MO	43.0	37.9	48.2
13	Halls Creek Airp.	42.8	37.7	48.8
14	Hobart Airp.	40.1	36.2	44.1
15	Kalgoorlie-Boulder Airp.	40.4	36.7	44.1
16	Launceston Airp.	37.5	33.1	42.1
17	Laverton RAAF	43.7	40.0	47.5
18	Longreach Airp.	39.6	38.1	41.1
19	Meekatharra Airp.	38.7	34.6	43.2
20	Mildura Airp.	41.3	37.4	45.2
21	Moree Comparison	41.0	34.0	57.9
22	Mount Gambier Airp.	38.2	34.4	41.9
23	Mount Isa Airp.	41.7	35.5	55.8
24	Nowra Airp.	43.3	38.6	51.1
25	Oodnadatta Airp.	40.2	33.2	49.0
26	Perth Airp.	39.9	34.8	45.7
27	Sydney Airp.	39.5	35.5	43.4
28	Tennant Creek Airp.	38.6	32.6	48.0
29	Wagga Wagga AMO	38.7	33.2	44.5
30	Williamtown RAAF	39.2	34.4	46.2
31	Woomera Airp.	41.9	36.9	46.9

4.1.2 CONSIDERING ONLY THE OBSERVING RECORD POST- 1991

To further assess possible differences in results another experiment was carried out using only the latter part of the dataset, this coincides with the installation of a new generation of synchrotac-based recording equipment in most stations in Australian airports.

Table 7 presents the results for the combined gust speeds using the data in the year range 1990-2006.

Table 7. 500 year RP of combined wind with 95% CI (observations from 1991-2006)

	Station name	RP	Lower 95% CI	Upper 95% CI
1	Adelaide Airp.	34.9	29.8	42.9
2	Albany Airp.	34.4	30.4	38.9
3	Alice Springs Airp.	41.2	34.4	48.3
4	Canberra Airp.	40.1	35.8	44.3
5	Ceduna AMO	35.7	31.3	40.7
6	Charleville Airp.	31.8	28.4	36.4
7	Cobar MO	41.0	34.1	51.1
8	Coffs Harbour MO	34.8	31.3	38.3
9	East Sale Airp.	43.8	38.5	52.9
10	Esperance	43.3	39.0	47.6
11	Forrest Airp.	39.3	33.3	45.7
12	Giles MO	43.6	38.6	48.5
13	Halls Creek Airp.	40.2	32.8	50.6
14	Hobart Airp.	36.1	32.3	40.0
15	Kalgoorlie-Boulder Airp.	40.9	36.0	46.2
16	Launceston Airp.	34.8	29.3	44.9
17	Laverton RAAF	38.5	32.8	46.0
18	Longreach Airp.	37.9	36.2	39.6
19	Meekatharra Airp.	41.3	35.1	53.2
20	Mildura Airp.	35.0	30.0	42.9
21	Moree Comparison	41.6	34.7	49.9
22	Mount Gambier Airp.	36.2	30.7	43.0
23	Mount Isa Airp.	42.6	35.4	63.5
24	Nowra Airp.	44.3	38.4	54.4
25	Oodnadatta Airp.	34.7	29.5	39.9
26	Perth Airp.	40.2	36.3	44.0
27	Sydney Airp.	40.0	35.3	44.6
28	Tennant Creek Airp.	38.1	32.6	43.6
29	Wagga Wagga AMO	40.4	33.6	47.3
30	Williamtown RAAF	40.0	34.6	46.9
31	Woomera Airp.	40.6	37.7	43.4

4.1.3 CONSIDERING THE OBSERVING RECORD PRE- 1981

One more comparison was carried out using only the initial part of the dataset, ie. a subset between the start of the dataset and 1980 (including 1980) was extracted and the RP curve calculated. Notice that the start of the dataset is the start of the merged speed-weather dataset, i.e. the start of the shorter of the maximum daily wind speed and the weather description. In most cases the shorter of the two is the weather description dataset. The 'Giles MO' observing station has only two years of data before 1980, such a small sample can produce very unreliable results, and for this reason the data was not included. Similarly the 'Moree Comparison' observing station has no data prior to 1980.

Table 8 presents the results for the combined wind gust speed. 'start' is the first year of observation with regards to gust wind speed.

Table 8. 500 year RP of combined wind with 95% CI (observations prior to 1981)

	Station name	start	RP	Low CI	high CI
1	Adelaide Airp.	1962	45.9	38.1	59.3
2	Albany Airp.	1965	43.2	39.2	47.2
3	Alice Springs Airp.	1954	42.6	35.8	51.8
4	Canberra Airp.	1939	40.1	35.1	49.1
5	Ceduna AMO	1954	42.6	38.6	49.7
6	Charleville Airp.	1945	42.9	36.6	55.1
7	Cobar MO	1962	36.4	31.2	43.2
8	Coffs Harbour MO	1959	34.0	31.5	38.7
9	East Sale Airp.	1951	38.3	35.8	45.2
10	Esperance	1969	41.2	36.7	45.6
11	Forrest Airp.	1958	45.1	38.8	51.3
12	Giles MO	1978			
13	Halls Creek Airp.	1962	40.4	34.5	49.2
14	Hobart Airp.	1958	37.3	33.7	41.0
15	Kalgoorlie-Boulder Airp.	1939	43.7	38.7	48.8
16	Launceston Airp.	1941	40.2	37.0	43.4
17	Laverton RAAF	1941	40.8	36.0	53.5
18	Longreach Airp.	1966	39.8	32.8	53.7
19	Meekatharra Airp.	1957	47.0	39.6	62.3
20	Mildura Airp.	1957	41.7	37.0	46.9
21	Moree Comparison	1995			
22	Mount Gambier Airp.	1954	41.6	37.2	47.4
23	Mount Isa Airp.	1966	40.4	33.9	55.7
24	Nowra Airp.	1955	38.3	35.7	42.5
25	Oodnadatta Airp.	1954	41.1	38.4	45.2
26	Perth Airp.	1944	39.9	36.0	43.7
27	Sydney Airp.	1939	46.4	41.2	56.3
28	Tennant Creek Airp.	1969	33.8	29.3	38.3
29	Wagga Wagga AMO	1942	42.4	37.1	51.3
30	Williamtown RAAF	1942	44.3	38.5	52.4
31	Woomera Airp.	1949	47.6	43.5	51.4

4.1.4 OVERVIEW TABLE

Table 9 presents the merging into a single overview table of the exceedance levels of the 500-year RP from Sections 4.1.1 to 4.1.3 . This allows a quick comparison (single table) of results from the three sections of the dataset and the full dataset for each station..

The results indicate that the highest exceedance levels of the 500-year RP occur for the earlier part of the dataset (pre- 1981). The differences between the different sections of the dataset and the full datasets with regards to 500-year RP are not very large. Only 6 of the 31 stations go against the trend showing higher speeds in the latter part of the dataset. The largest of this group is the ’East Sale Airport` observing station with an exceedance level of 41.3 m/s using all data and 43.8 m/s using only the part of the dataset after 1990.

Table 9. 500 year RP of combined winds using all the observing record as well as segments of the record.

	Station name	All data	upto 1980	1980-2006	1990-2006
1	Adelaide Airp.	42.6	45.9	41.4	34.9
2	Albany Airp.	42.0	43.2	39.6	34.4
3	Alice Springs Airp.	41.6	42.6	41.9	41.2
4	Canberra Airp.	37.3	40.1	39.8	40.1
5	Ceduna AMO	39.8	42.6	41.6	35.7
6	Charleville Airp.	42.6	42.9	43.2	31.8
7	Cobar MO	39.3	36.4	39.8	41.0
8	Coffs Harbour MO	37.1	34.0	40.4	34.8
9	East Sale Airp.	41.3	38.3	42.2	43.8
10	Esperance	44.1	41.2	44.3	43.3
11	Forrest Airp.	45.5	45.1	43.4	39.3
12	Giles MO	42.0	-	43.0	43.6
13	Halls Creek Airp.	42.8	40.4	37.5	40.2
14	Hobart Airp.	38.6	37.3	40.1	36.1
15	Kalgoorlie-Boulder Airp.	43.8	43.7	40.4	40.9
16	Launceston Airp.	38.8	40.2	37.5	34.8
17	Laverton RAAF	42.3	40.8	43.7	38.5
18	Longreach Airp.	44.4	39.8	39.6	37.9
19	Meekatharra Airp.	41.9	47.0	38.7	41.3
20	Mildura Airp.	45.6	41.7	41.3	35.0
21	Moree Comparison	42.4	-	41.0	41.6
22	Mount Gambier Airp.	40.3	41.6	38.2	36.2
23	Mount Isa Airp.	43.5	40.4	41.7	42.6
24	Nowra Airp.	41.8	38.3	43.3	44.3
25	Oodnadatta Airp.	41.3	41.1	40.2	34.7
26	Perth Airp.	38.8	39.9	39.9	40.2
27	Sydney Airp.	44.8	46.4	39.5	40.0
28	Tennant Creek Airp.	37.6	33.8	38.6	38.1
29	Wagga Wagga AMO	41.0	42.4	38.7	40.4
31	Woomera Airp.	45.8	47.6	41.9	40.6

The ‘East Sale airport’ dataset was further investigated by examining the wind speed using the whole dataset (19,947 observations of maximum daily gust wind speed)) as well as the post- 1990 period (6,079 observations). Both datasets contain the same maximum wind speed (42.4 m/s) which occured on 1998-12-27 @18:00. Figure 7 displays the actual data points and the GPD calculated RP (lines) for both parts of the dataset. The actual exceedance levels refer to levels calculated from the observations; to distinguish them the actual exceedance levels of the whole dataset is plotted with blue points whilst the exceedance levels of the dataset after 1990 has red points. The maximum wind speed (42.4 m/s) is shown for both datasets; in the full dataset it is in blue at 55-years RP, whilst in the shorter dataset it is in red at 16-years RP.

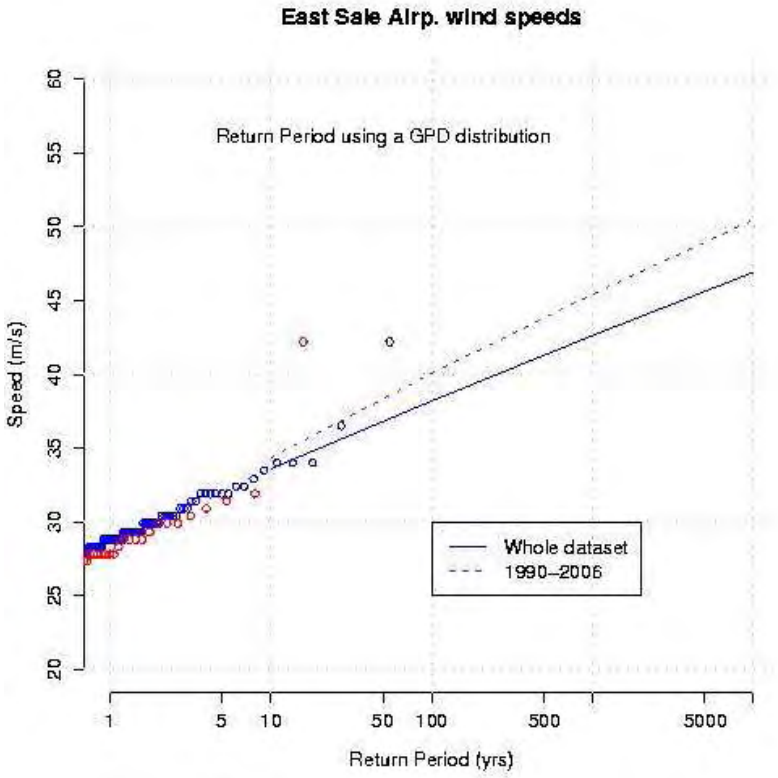

Figure 7. East Sale RP of gust wind speed considering the whole and also the latter part of the dataset (1991-2006).

The actual exceedance levels are similar for the two datasets up about 10 m/s; after this point the exceedance levels of the whole dataset utilises more data which results in the curve trending downwards. The curve produced by the post- 1990 segment of the dataset has one value at 9 m/s and the next value is at 42.4 m/s; the net result is that the use of minimal data for the RP curve trends the curve towards higher values. Wind analysts are generally aware of this characteristic of extreme value distributions. In general the presence of high values in small datasets (few years considered) tends to produce higher RP curves, which has been known to also produce higher hazard for "thunderstorm component" curves than when considering the "combined thunderstorm and synoptic component" curves. This issue is not the norm in `well-behaved` datasets which represent a climatology.

To facilitate the comparison of RP for each of the datasets considered (all observing stations), Figure 8 presents the location of all 500-yr RP with respect to the standard normal distribution N(0,1) calculated from the whole dataset. The RP presented in Table 9 have been standardized by using the expression:

$$\text{Standard\_RP} = (\text{RP} - \mu)/\sigma \qquad (3)$$

Figure 8a shows that 500-yr RP using the whole dataset (column 3 of Table 9) are located around the standard mean (0), all of them are within two standard deviations of the mean. The RP using the early part of the dataset (up to 1980) are presented in Fig 8b. This graph shows a few very high and low values well beyond one standard deviation indicating unusual values for some observing stations. The 500-yr RP of the dataset between 1981-2006, presented in Figure 8c appears well-behaved; most are located around the mean within one and a half standard deviations. The RP of the latter part of the dataset (1991-2006), presented in Figure 8d, shows some very low values which is of concern regarding the consistency of the dataset.

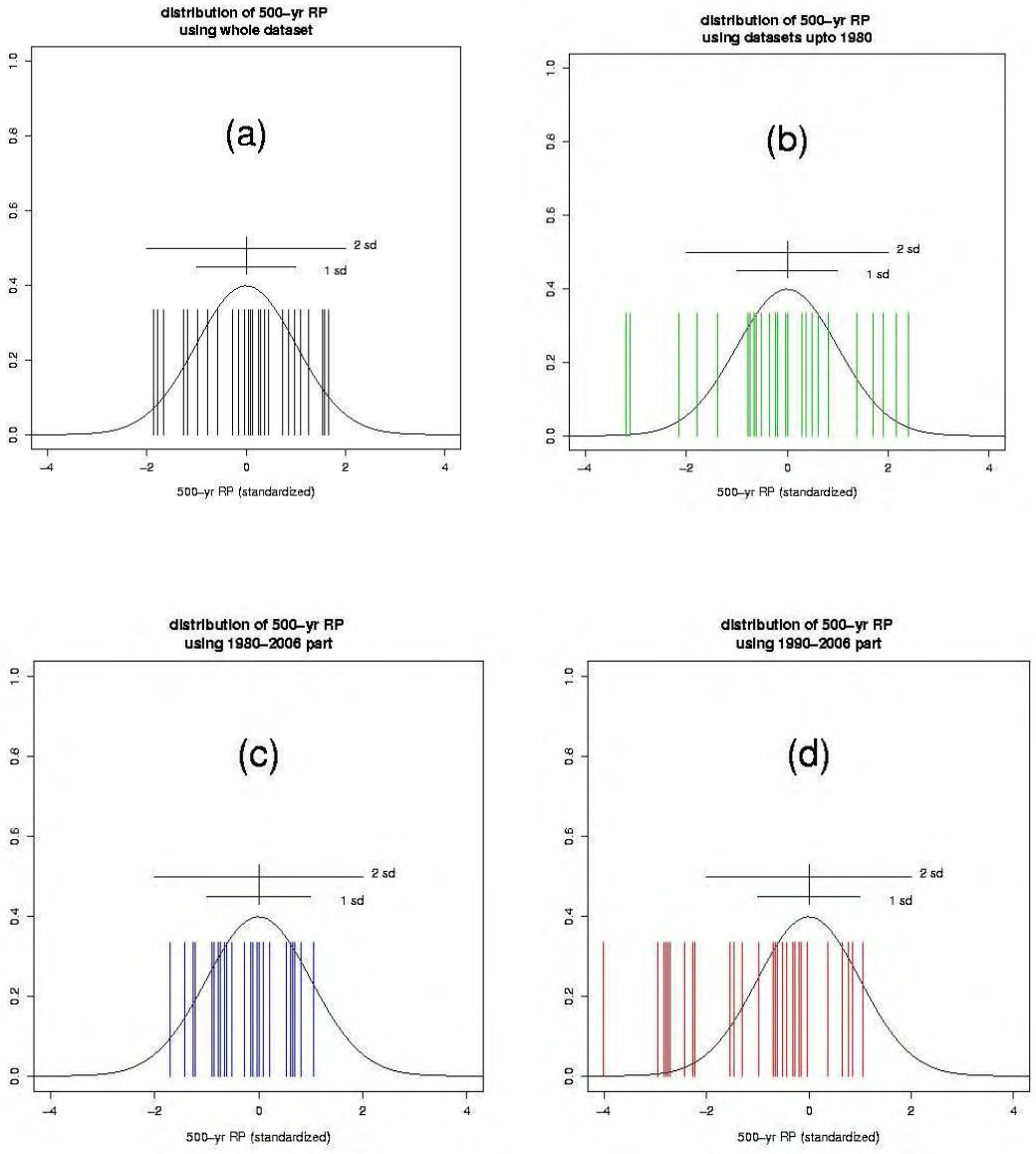

Figure 8. Distribution of the 500 year RPs presented in Table 9.

4.2. SEPARATE DINES AND CUP-ANEMOMETER TIME-SERIES

Three datasets were acquired from BoM for these studies; maximum daily gust speeds, 3PM mean wind speed and weather description. Both maximum daily gust wind speeds and 3PM mean winds are considered to examine the range of wind conditions both within and outside the instrument calibration range. 3PM mean wind speed data was chosen as the mean wind speed reaches a peak at this time in the diurnal cycle. Meta data concerning the replacement of the Dines anemometers was also obtained from BoM. We utilise as a measure of the hazard the 500-year return period (500RP) exceedance level gust wind speed. This hazard level has been chosen as it represents the wind loading design level used for the construction of most of the residential, commercial and industrial buildings in Australia and New Zealand. For this preliminary analysis we only consider the combined (complete) dataset and not the component synoptic and thunderstorm extreme winds (See Section 2).

The analysis statistically examines the issue of inconsistency in the gust wind speed record by investigating the impact of instrument upgrade within the dataset. The dataset (time-series of measurements) is segmented into the Dines and replacement anemometer observing periods, with the Dines observing period the longest in length in all cases. The latter coincides with the installation of the new generation of cup-anemometers at most observing stations (major Australian airports). All stations considered are currently operational.

Table 10 presents gust and 3PM mean wind speed 500-year return period (500RP) hazard levels for the total (combined) wind speeds for the wind stations selected. The 95% confidence interval (95CI) is provided for both gust and 3PM mean wind speeds for the Dines anemometer segment of the record. Note that the width of the confidence interval is dependent on the frequency and consistency of the extreme events considered.

Considering the replacement anemometer 500RP gust wind speed estimates (Table 10: data column 7), the values which are not within the 95% confidence limit for the Dines anemometer part of the observing record are marked in bold print. There are 17 observing stations where the replacement anemometer estimates fall below the lower 95% confidence interval (95CI) for the Dines segment of the observing record. For 24 of the 31 observing stations the replacement anemometer estimate fall below the corresponding Dines segment estimate. Considering the 3PM mean wind speeds (Table 10: data column 8), there are also 17 observing stations where the replacement anemometer estimate falls below the lower 95CI for the Dines segment of the observing record.

Figure 9 displays this information pictorially. The distribution of (a) the Dines 500-year RP gust wind speed, and (b) the Dines 500-year RP 3PM mean wind speed (data scaled by the standard deviation for each station respectively) is shown. Plotted on each distribution are blue vertical bars pictorially indicating the fit for each observing station for the section of the record acquired using the upgraded/replacement (cup) anemometer. Estimates for the later part of the record appear biases to the lower tail of the distribution for the early part of the record (Dines anemometer).

Table 10. 500 year RP of combined maximum daily gust wind speed and 3PM mean wind speed with 95% confidence limits (95CI) from the observing record segmented into Dines and Replacement cup anemometer measurement periods (last two columns of the table). All wind speeds in metres per second (m/s).

				Dines anemometer				Replacement	
	Station name (Length of record)	95CI Gust	Max Gust 500RP	95CI Gust	95CI Mean	3PM Mean 500RP	95CI Mean	Max Gust 500RP	3PM Mean 500RP
1	Adelaide Airp. (1955-)	37.9	42.3	52.8	18.3	20.5	24.8	**33.2**	19
2	Albany Airp. (1965-)	38.9	42.6	46.4	18.7	21.0	25.0	**33.1**	**16.7**
3	Alice Springs Airp. (1952-)	38.0	39.2	40.4	19.0	20.7	22.9	39.6	19.6
4	Canberra Airp. (1939-)	33.0	38.8	45.0	25.5	26.3	27.2	37.2	18.2
5	Ceduna AMO (1940-)	39.0	44.3	50.0	19.0	21.4	25.5	**35.3**	20.2
6	Charlev Airp. (1945-)	32.0	47.0	58.0	17.3	19.1	23.2	41.6	15.7
7	Cobar MO (1962-)	33.7	39.3	50.5	15.1	17.5	23.5	36.6	**14.0**
8	Coffs Harbour MO (1959-)	34.1	39.5	55.2	19.5	21.4	25.4	**31.2**	**16.2**
9	East Sale Airp. (1951-)	35.7	39.3	44.7	24.4	27.2	32.5	42.7	**24.3**
10	Esperance (1969-)	38.2	43.8	51.3	19.8	22.1	24.4	43.9	20.
11	Forrest Airp. (1958-)	43.0	45.6	48.6	28.0	31.5	38.7	**41.8**	**24.4**
12	Giles MO (1956-)	37.5	43.6	52.0	16.5	19.9	25.3	40.6	17.9
13	Halls Creek Airp. (1962-)	38.4	44.7	59.7	18.3	21.5	27.7	**36.0**	**16.2**
14	Hobart Airp. (1958-)	35.4	38.4	41.9	19.2	21.2	23.9	**34.1**	**18.9**
15	Kalgoor Airp. (1939-)	37.6	41.4	45.7	19.2	21.2	23.2	38.6	**16.4**
16	launceston Airp. (1941-)	35.2	38.9	45.7	22.0	24.2	26.9	**34.1**	**20.5**
17	laverton RAAF (1941-)	38.8	42.2	46.0	20.0	21.7	23.4	**38.4**	**15.7**
18	Longreach Airp. (1966-)	39.4	44.1	50.3	14.7	15.1	18.3	**36.1**	18.1
19	Meekatharra Airp. (1959-)	39.2	45.8	58.8	23.8	26.8	34.9	**39.2**	**16.2**
20	Mildura Airp. (1957-)	37.5	42.0	48.0	17.7	19.6	24.6	**34.1**	**16.3**
21	Moree CO (1964-)	35.6	41.6	56.3	20.0	22.6	27.3	41.8	**19.2**
22	Mount Gambier Airp. (1948-)	36.5	39.9	44.9	13.7	15.3	17.6	**33.3**	14.5
23	Mount Isa Airp. (1966-)	36.8	41.5	54.9	16.0	18.0	20.9	40.2	18.6
24	Nowra Airp. (1955-)	38.5	41.8	46.7	20.8	23.5	27.9	**38.0**	**20.6**
25	Oodnadatta Airp. (1941-)	38.9	43.1	47.9	17.4	19.5	23.6	**32.7**	18.7
26	Perth Airp. (1944-)	35.0	38.2	42.0	18.1	20.0	23.1	35.4	**17.3**
27	Sydney Airp. (1939-)	40.9	45.6	54.8	22.6	24.9	27.9	**36.6**	24.9
28	Tennant Creek Airp. (1969-)	31.8	36.2	40.8	15.0	16.5	21.4	35.6	16.6
29	Wagga Wagga AMO (1942-)	37.2	41.6	46.3	17.8	19.1	21.0	37.8	**17.7**
30	Williamtown RAAF (1942-)	38.2	42.2	46.7	27.8	30.4	33.7	38.5	**19.7**
31	Woomera Airp. (1949-)	41.8	45.1	48.5	19.8	22.0	25.1	**38.4**	22.6

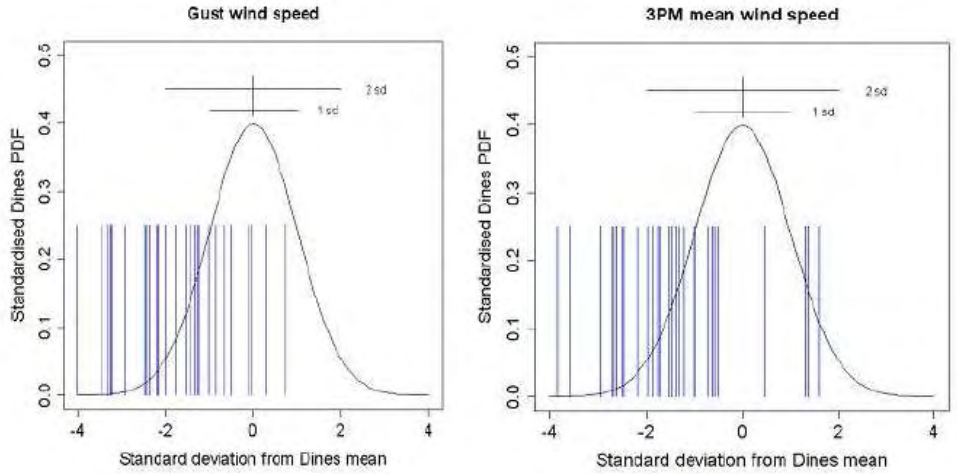

Figure 9. Distribution of (a) Dines 500 year RP gust wind speed, and (b) Dines 500 year RP 3PM mean wind speed scaled by the standard deviation (respectively) with the blue vertical bars indicating the fit for the section of the record acquired using the replacement (upgraded - cup) anemometer.

The statistical analysis resulted in more than half of the observing stations considered (later part of the time-series record) having both 500-year RP gust wind speed (17 of 31) and 3PM mean wind speed (18 of 31) exceedance level estimates being in the lower tail of the distribution for the early part of the observing record (period prior to equipment upgrade from Dines to cup anemometer). This analysis suggests that the consistency of the peak gust wind speed dataset is suspect, and that the problem requires further examination via analysis of coincident measurements. This segmented analysis (i.e. not coincident) indicates that it appears unlikely that the later part of the observing record can be considered consistent with the initial (Dines) segment of the record.

4.3 COINCIDENT DINES AND CUP-ANEMOMETER OBSERVATIONS

Coincident gust wind speed measurements at 7 northern Australian observing stations were analysed to determine the magnitude of the direct bias. Only Dines “high-speed range” anemometers (0-200 knots) were considered for observing stations where extreme wind gusts are dominated by thunderstorm and tropical cyclone events. The stations examined were Cairns, Townsville, Brisbane, Darwin, Gove, Broome and Learmonth. Cup anemometer data was available in digital form (for each 30 minute interval) whereas the 30 minute maximum gust wind speed for the Dines anemometer record was scaled directly (manually) off the chart record by selecting the maximum peak. Data for 30 minute time segments where the cup anemometer reading was greater than or equal to 15 m/s were analysed. A threshold of 15 m/s was selected so that only thunderstorm and tropical cyclone events were considered (i.e. no synoptic wind events were considered; gusts were independent events). Coincident probability distributions (PDF’s) of the gust wind speed ((Dines & cup anemometer; 15 m/s threshold) for the seven sites considered display some interesting characteristics (see Appendix I-C, Figure C1 & Discussion for further information).

Time-series plots of the bias between the Dines and cup anemometer measurements show no time dependent relationships. The bias is uni-directional for some extreme cases where the cup anemometer records the event that the Dines either captures to a much lesser extent or misses altogether. The size of thunderstorm gust fronts can cause significant differences in wind speed over 10’s of metres. The uni-directional nature of the extreme bias is due to events captured by the Dines but not the cup anemometer not being considered by the analysis techniques (which was driven by the digital record). Where the analysts found cases where the Dines recorded gusts above 15 m/s but the cup anemometer was below this threshold, the data was included (but this did not occur rigorously; i.e. every 30 minute period for every day was considered on the electronic record and only at or above the cup anemometer 15 m/s threshold for the Dines charts).

The data on the extreme gust wind speeds for the 7 sites were combined into one dataset and extreme value statistical theory (Generalised Pareto Distributions; GPD’s) were used to investigate the return period exceedence levels for the combined dataset. Figure 10 shows the return period plots of coincident maximum gust wind speed (above a threshold of 15 m/s for 30 minute time sections) for the combined 7 northern Australian observing stations obtained over a total measurement period of 89 years. In addition, 95% confidence limits (95CI) for the GPD fit to the Dines extreme gust wind observations are also shown. Table 11 details the percentage bias between the cup anemometer and Dines return period estimates (including the 95% confidence limits regarding the fitting of the extreme value distribution to the Dines gust observations).

The observed data allows us to consider gust wind speeds between 45 and 70 m/s. When considering gust wind speeds, the Dines anemometer has a tendency to read about 10 to 15% higher than the cup anemometer (considering coincident data at 30 minute intervals). These systematic differences confirm concerns about the consistency of the peak gust wind speed observational database which underpins the Australian wind loading standard (AS/NZS 1170.2, 2002).

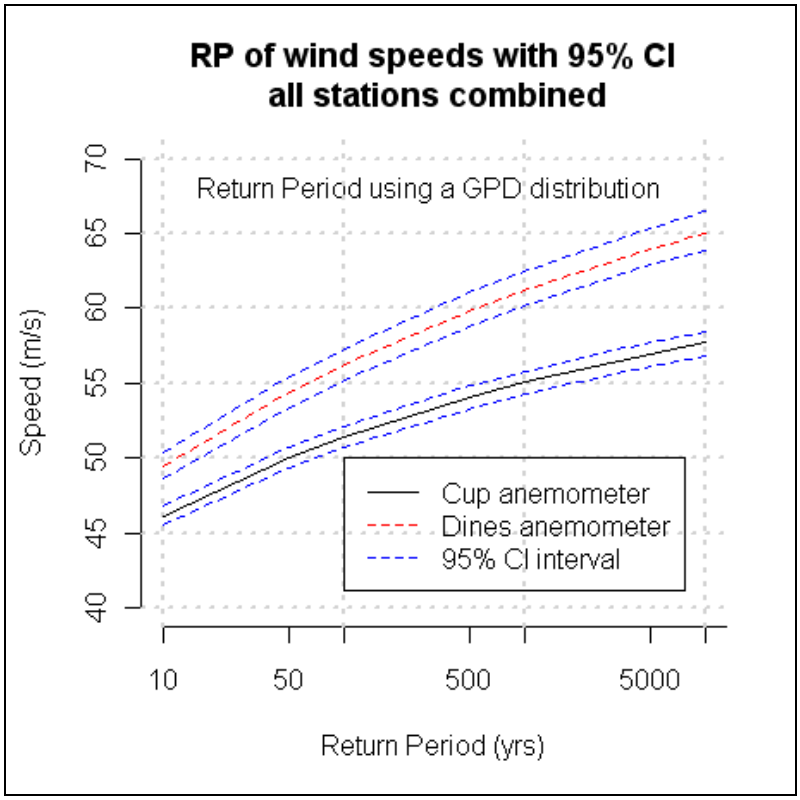

Figure 10. Return period plots of coincident maximum gust wind speed (above a threshold of 15 m/s for 30 minute time sections) for the combined 7 northern Australian observing stations over a total coincident measurement period of 89 years. 95% confidence limits for the GPD fit to the Dines anemometer observations are also provided.

Table 11. Percentage difference (return period gust wind speed) between the Dines anemometer and cup anemometers over a range of wind speeds, considering coincident extreme wind gust measurements at 7 observing sites over a total coincident measurement period of 89 years. The asymptotic nature of the GPD fit to the observations does not allow a comparison for gust wind speeds above 60 m/s.

Cup anemometer gust wind speed	Dines anemometer gust wind speed	Dines; Lower 95% confidence limit	Dines; Upper 95% confidence limit
45 m/s	+7 %	+5 %	+9 %
50 m/s	+9%	+7 %	+11 %
55 m/s	+11 %	+9 %	+13.5 %
60 m/s	+14 %	+12 %	+17 %

5. Discussion

Statistical analysis of the daily maximum gust wind speed observations was conducted by employing extreme value distribution (EVD) statistical theory. Generalised Pareto Distributions (GPD's) were fitted to:

(1) Separate time-series of Dines & cup anemometer observations (no overlap for each station)
(2) Coincident Dines & cup anemometer observations

Separate time-series of Dines & cup anemometer observations (no overlap)
We have evaluated both the daily maximum gust and 3PM mean wind speed 500-year return period (500RP) exceedance levels for the total (*combined*) wind speeds for the 31 wind observing stations selected (within AS/NZS 1170.2 Region A). Observations have been segmented into the Dines and replacement cup anemometer observing periods. The 95% confidence interval (95CI) has been determined for both gust and 3PM mean wind speeds for the Dines anemometer segment of the record. For the replacement anemometer 500RP exceedance level gust wind speed estimates, there are 17 observing stations where the replacement anemometer estimates fall below the lower 95% confidence interval (95CI) for the Dines segment of the observing record. For 24 of the 31 observing stations the replacement anemometer estimate fall below the corresponding Dines segment estimate. Considering the 3PM mean wind speeds, there are 18 observing stations where the replacement anemometer estimate falls below the lower 95CI for the Dines segment of the observing record.

The statistical analysis utilising extreme value distributions (GPD's) resulted in more than half of the observing stations considered (later part of the time-series record) having both 500-year RP gust wind speed (17 of 31) and 3PM mean wind speed (18 of 31) exceedance level estimates being in the lower tail of the distribution for the early part of the observing record (period prior to equipment upgrade from Dines to cup anemometer). We should be cautious in interpreting the differences in the return period hazard for the two segments of the record. It is possible that the frequency of extreme wind speeds has actually declined (Smits *et al*. 2005). The most recent part of the record has been dominated by a number of large El Nino events and only one La Nina event, where thunderstorms are known to be more prevalent (Kuleshov *et al*. 2002). The importance of the non-stationary climate needs to be considered when conducting a time series analysis. Circulation changes as discussed in (Plummer *et al.* 1999; Alexander *et al.* 2010), possibly driven by anthropogenic climate change, could also affect the frequency and amplitude of extreme winds. The replacement anemometer part of the record is generally much shorter (10-25 years) than the Dines segment and it is possible that the very high maximum wind speeds have just not yet been sampled, although the reduced frequency of extreme events in the later part of the record is of concern. Even considering these issues, this analysis suggests that the consistency of the peak gust wind speed dataset is suspect, and that the problem requires further examination via analysis of coincident measurements. This analysis indicates that it appears unlikely that the later part of the observing record can be considered consistent with the initial (Dines) segment of the record.

Coincident Dines & cup anemometer observations
Coincident gust wind speed measurements at 7 northern Australian observing stations were analysed to determine the magnitude of the direct bias. A threshold of 15 m/s was selected so that only thunderstorm and tropical cyclone events were considered (i.e. no synoptic wind events were considered; gusts were independent events). Coincident probability distributions (PDF's) of the gust wind speed ((Dines & cup anemometer; 15 m/s threshold) for the seven sites considered display some interesting characteristics:

(1) PDF's are broader for the Dines instrument (all cases) indicating either
   (i) an elevated level of noise compared to the cup anemometer;
   (ii) possible damping of the cup anemometer response compared to the Dines anemometer.

This difference may be due to a number of issues such as:
   (i) random error (instruments not coincident in position; separated by 25-100m);
   (ii) instrument error (issues such as the Dines float resonance and the Dines wind vane not being parallel to gust direction as well as others such as the Dines float level not being maintained at the correct position);
   (iii) the 3-second moving average filter applied to the 1-second wind speed measurements which forms the gust recorded by the BoM instrumentation.

NOTE: Theoretical and laboratory testing undertaken within other parts of this project confirm that the Dines instrument is more "noisy" compared to cup anemometers.
In addition, the magnitude of the bias appears to be a function of wind speed.

(2) Focusing on the peak of the PDF's, there appears to be some systematic bias for some of the observing stations. The peak of the PDF appears slightly low for Darwin and too high for Learmonth and Townsville. Agreement is excellent for Cairns.

As mentioned earlier in the report, the digital recording of meteorological data became prevalent in the 1990's. With regards to gust wind speed measurements, BoM implemented a 3-second averaged gust wind speed in the mid-1990's on a recommendation from the World Meteorological Organisation (WMO). The World Meteorological Association (WMO) decided to adopt a 3-second moving average gust wind speed as the de facto standard based on the Beljaars (1987) study of wind gustiness.

In practice applying a 3-second moving average to the sampled signal (one measurement each second) will filter out anything with a period of less than around 6.8 seconds, which more than doubles the effective wavelength of the measured gust wind speeds. Clearly not even a true 3-second gust is fully captured by the current filtering, and this is not consistent with the gust length scales relevant for a typical residential structure. Miller (2007) examined the response of the combination of a Munro MK IV anemometer with a chart recorder as used in the UK Meteorological Office until the mid-1970's. He found that this combination gives an effective gust duration approaching 1 second at high wind speeds (considered suitable for informing design wind speeds). Discussions with the BoM are continuing with regards to understanding the impact of this filtering on the consistency of the long-term record. It may be prudent to review the use of the 3-second moving average for gust wind speed observations (including an experimental study) in order to assess the significance of this issue.

Coincident data on the extreme gust wind speeds for the 7 sites were combined into one dataset and extreme value statistical theory (Generalised Pareto Distributions; GPD's) were used to investigate the return period exceedence levels for the combined dataset. A total coincident measurement period of 89 years was achieved. The observed data has allowed us to consider gust wind speeds between 45 and 60 m/s. When considering gust wind speeds at about 45 m/s, the Dines anemometer has a tendency to read about 5 to 10% higher than the cup anemometer (considering coincident data at 30 minute intervals); this increases to about 12 to 17% higher at gust wind speeds around 60 m/s. These systematic differences are consistent with those reported by Reardon *et al*. (1999) and Reardon (2000), and confirm concerns about the consistency of the peak gust wind speed observational database which underpins the Australian wind loading standard (AS/NZS 1170.2, 2002).

6. Conclusions

This study has examined the observed record of peak gust wind speed in order to establish the existence of a bias between the early part of the record (measurements obtained using pressure-tube Dines anemometers) and the later part of the record (measurements obtained using 3-cup anemometers). The 38 recording stations considered were all situated at airports and were in the most part staffed by Bureau of Meteorology officers. To isolate the issue of anemometer replacement, only observing stations located at airports (consistent exposure) and with more than 30 years of record were considered.

Statistical analysis of the daily maximum gust wind speed observations was conducted by employing extreme value distribution (EVD) statistical theory to examine the difference between two datasets:

(1) time-series of Dines & cup anemometer observations (no overlap for each station);
(2) coincident Dines & cup anemometer observations.

Analysis of time-series of Dines & cup anemometer observations (no overlap)
The statistical analysis resulted in more than half of the observing stations considered (later part of the time-series record) having both 500RP gust wind speed (17 of 31) and 3PM mean wind speed (18 of 31) exceedance level estimates being in the lower tail of the distribution for the early part of the observing record (period prior to equipment upgrade from Dines to cup anemometer).

Coincident Dines & cup anemometer observations
Coincident gust wind speed measurements at 7 northern Australian observing stations were analysed to determine the magnitude of the direct bias. In general, the time-series plots of the bias between the Dines and cup anemometer measurements show no time dependent relationships. The data on the extreme gust wind speeds for the 7 sites (coincident measurement period of 89 years) were considered, allowing an assessment of bias for gust wind speeds between 45 and 60 m/s. For gust wind speeds of about 45 m/s, the Dines anemometer has a tendency to read about 5 to 10% higher than the cup anemometer (considering coincident data at 30 minute intervals); this increases to about 12 to 17% higher at gust wind speeds around 60 m/s. These systematic differences are consistent with those reported by Reardon *et al*. (1999) and Reardon (2000), and confirm concerns about the consistency of the peak gust wind speed observational database which underpins the Australian wind loading standard (AS/NZS 1170.2, 2002).

7. Future Directions and Recommendations

It has been identified that the observational record attributable to the Dines anemometer provides a more extreme wind climatology than the part of the record attributable to the 3-cup anemometer. In addition, the Dines anemometer has an effective gust duration approaching 1 second, which is considered suitable for informing design wind speeds. The synchrotac anemometer has a 3-second moving average (1-second sampling) applied to the digital output for maximum wind gust measurements. This is considered the major reason as to why the cup anemometer consistently reads lower than the Dines with respect to the recording of severe wind events.

The results of the *Australian Extreme Wind Speed Baseline Climate Investigation* study indicate that there is a need to firstly review the use of the 3-second moving average for gust wind speed observations to determine the extent that this issue affects the consistency of the observing record (and will continue to do so). It does appear that the WMO standard gust is a retrograde step with regards to informing wind loading. The adoption of the WMO standard gust in the mid-1990's appears to have gone unnoticed by the wind engineering community, or possibly its impact was not fully considered at the time of implementation. The "up-side" of the WMO standard gust is that currently we do have a consistent, standardized gust definition that is being applied worldwide, and this should also eliminate variability due to instrumentation response characteristics.

In moving forward, we need to deal with the issue of improving the consistency of measurements within the gust wind speed observing record. In one very real sense this study has provided the engineering community with the outputs (knowledge and tools) to improve our understanding of the baseline extreme wind climatology within Australia. It has also developed preliminary corrections based on this information which could be utilised to develop a reanalysed observing record which can inform an improved wind loading standard for the Australian region. There remains the need to determine whether the 3-second moving average for gust wind speed is the most appropriate from wind loading considerations.

We plan to discuss these findings with the broader user and stakeholder community at the 15th Australasian Wind Engineering Society (AWES) Workshop to be held at Sydney University in February 2012. Once a broad acceptance of the study has been achieved, we would like to take the next step of implementing a strategy for correcting the gust wind speed observations to achieve a consistent extreme wind speed database for the Australian region.

RECOMMENDATION 1.
The outputs of the *Australian Extreme Wind Speed Baseline Climate Investigation* project should be workshopped at the 15th Australasian Wind Engineering Society (AWES) Workshop to be held at Sydney University in February 2012. A dedicated *Special Session* should be setup to workshop the outcomes of the study in an effort to gain broad support for the science that has been undertaken.

RECOMMENDATION 2.
The AWES Workshop *Special Session* should call for volunteers from learned society members and interested international researchers to "review the concept and use of the 3-second moving average for gust wind speed observations". A report should be drafted and presented to the WMO for consideration.

RECOMMENDATION 3.
Experimental trials (either field or high-speed wind tunnel) should be conducted to determine the impact of the 3-second moving average on gust wind speed measurements (i.e. difference between the peak wind gust and the 3-second moving average gust wind speed) . It is unlikely that BoM will deviate from W.M.O. recommendations regarding gust wind speed measurement, so it is likely that correction factors will be required to relate the 3-second averaged gust wind speed to a more appropriate metric with regards to wind loading.

Acknowledgements:

The *Australian Extreme Windspeed Baseline Investigation Project* is a collaboration between James Cook University, the Bureau of Meteorology, JDH Consulting and Geoscience Australia. A significant portion of the funding (about 60%) was obtained from the Federal Department of Climate Change and Energy Efficiency (DCCEE). The study was conducted in support of DCCEE's climate change professional development program, in the area of building standards. The team at Geoscience Australia would like to thank Rachael Dempsey, Antonio Mozqueira and Anthony Swirepik from the Department of Climate Change and Energy Efficiency for their assistance and guidance with the study.

The team at Geoscience Australia would also like to thank Ian Muirhead (Bureau of Meteorology, National Climate Centre, Melbourne) for his generous assistance with the provision of the meteorological data as well as coordinating the movement of the Dines anemometer charts from the state-based National Archives centres to the Bureau of Meteorology office in Canberra (where they were analysed). We would also like to thank Sean Carson (Bureau of Meteorology, Canberra airport office) for making us welcome at the Canberra airport office during the 4 weeks that elapsed while the Dines anemometer charts were examined.

References:

Alexander L.V., Uotila P., Nicholls N. and Lynch A. 2010. A New Daily Pressure Dataset for Australia and Its Application to the Assessment of Changes in Synoptic Patterns during the Last Century, *Journal of Climate 23:5* 1111-1126

AS 4055 2006. Wind loads for housing, Australian Standard, Available at http://www.saiglobal.com/PDFTemp/Previews/OSH/as/as4000/4000/4055-2006.pdf

AS/NZS 1170.2, 2002. Structural design actions, Part 2: Wind actions, Australian/New Zealand Standard, 2002.

Beljaars, A.C.M. 1987. The measurement of gustiness at routine wind stations – A review, KNMI scientific report WR87-11, 50pp

BTE, 2001. Economic costs of natural disasters. Bureau of Transport Economics, Canberra, Australia.

Bureau of Meteorology 1982. Department of Science and Technology (1982). Present Weather Plotting Diagram (Description abridge from W.M.O. Code). Jan. 1982.

Bureau of Meteorology 2006. Basic Climatological Station Metadata. Metadata compiled: 29 Sep 2006.

Bureau of Meteorology 2008. Severe Thunderstorms in Southeast Queensland - 20th November 2008. [Available online at http://www.bom.gov.au/qld/sevwx/ts/20081120/qldts20081120.shtml.]

Callaghan, J., and S. B. Power, 2010. Variability and decline in the number of severe tropical cyclones making land-fall over eastern Australia since the late nineteenth century. *Climate Dynamics***,** 16.

Cechet, R. P., and L. A. Sanabria, 2010. Reanalysis of wind-loading "Region A" gust wind speeds. *IOP Conf. Ser.: Earth Environ. Sci.* **11,** 012016, doi: 10.1088/1755-1315/11/1/012016

Chen K. 2004. Relative Risks Ratings for Local Government Areas. *Risk Frontiers quarterly newsletter*, Macquarie University, Australia. (3) Issue 3, March 2004.

Chen, K. and J. McAneney, 2006. High-resolution estimates of Australia's coastal population. *Geophysical Research Letters*, 33 (L16601), 4, doi:DOI:10.1029/2006GL026981.

Coles S. 2001. An Introduction to Statistical Modeling of Extreme Values (Springer series in statistics. London)

CSIRO, 2007. Climate Change in Australia – Wind Speed, Technical Report – Supplementary Material. Available online at http://climatechangeinaustralia.com.au/documents/resources/5_wind_speed.pdf.

Gillelland E. and Katz R.W. 2005a. Extremes Toolkit: Weather and Climate Applications of Extreme Value Statistics. *National Center for Atmospheric Research (NCAR). Boulder CO, USA*

Gillelland E. and Katz R.W. 2005b. Analysing Seasonal to Interannual Extreme Weather and Climate Variability with the Extremes Toolkit. National Center for Atmospheric Research (NCAR). Boulder CO, USA.

Gomes, L., and B. J. Vickery, 1978. Extreme wind speeds in mixed wind climates. *Journal of Wind Engineering and Industrial Aerodynamics*, **2,** 4, 331-344.

Gorman J. 2004. *The conversion equation of the Synchrotac 706 anemometer*, Bureau of Meteorology Instrument Test Report, No. 677

Holmes, J. D., 2002. A re-analysis of recorded extreme wind speeds in Region A. *Australian Journal of Structural Engineering*, **4,** 1.
——, 2004. Wind risk methodology and vulnerability model development review, consultancy report for Geoscience Australia, Dec 2004
——, 2007. *Wind Loading of Structures.* 2 ed. Taylor and Francis.
—— and W. W. Moriarty, 1999. Application of the generalized Pareto distribution to extreme value analysis in wind engineering. *Journal of Wind Engineering and Industrial Aerodynamics*, **83**, 1-10.

Hope, P.K. 2006. Projected future changes in synoptic systems influencing southwest Western Australia, Climate Dynamics, 26: 765–780

Jacobson M.Z. 2005. *Fundamentals of Atmospheric Modeling* (New York: Cambridge University Press, 2nd ed.) 828pp

Jagger T.H. and Elsner J.B. 2006. Climatology Models for Extreme Hurricane Winds near the United States. Journal of Climate. Vol. 19, 3220-3236.

Knowles W.E.K. and Spilhaus A.F. 1953. *Meteorological Instruments* (University of Toronto Press – Third Edition)

Kuleshov Y., de Hoedt, G., Wright W. and Brewster A. 2002. Thunderstorm distribution and frequency in Australia, *Aust. Met. Mag*. 51, 145-154

Kaplan, J., and M. DeMaria, 1995. A Simple Empirical Model for Predicting the Decay of Tropical Cyclone Winds after Landfall. *Journal of Applied Meteorology*, **34,** 2499-2512.

Logue J.J. 1986. Comparison of wind speeds recorded simultaneously by a pressure tube anemograph and a cup-generator anemograph *Meteorol. Mag., 115* 178-185

Miller, C. 2007. Defining the effective duration of a gust, Proceedings of the International Conf. on Wind Engineering (ICWE12), Cairns, Australia, 759-766

Miller C. 2008. Assessing the Impact of Anemometer Exposure and Instrumentation Changes on Measured Wind Speeds. 15th Nat. AMOS conference. Atmospheric and Oceanic Extremes. Geelong, Vic. Jan 29- Feb 2, 2008.

Muirhead I.J., Grant I.F., Jacob D. and Glowacki T.J. 2005. Developments in Climate Data for a Sustainable Future. Proceedings of the ANZSES Solar 2005 conference. Dunedin NZ. November 2005.

Muirhead I., Monnik K., and deHoedt G. 2008. Wind: Data, limitations and access. 15th Nat. AMOS conference. Atmospheric and Oceanic Extremes. Geelong, Vic. Jan 29- Feb 2, 2008.

Palutikof J.P., Brabson B.B., Lister D. H. and Adcock S.T. 1999. A Review of Methods to Calculate Extreme Wind Speeds. Meteorol. Appl. 6, 119-132.

Plummer N., Salinger M.J., Nicholls N., Suppiah R., Hennessy K.J., Leighton R.M., Trewin B., Page C.M. and Lough J.M. 1999. Changes in Climate Extremes over the Australian Region and New Zealand During the Twentieth Century, *Climate Change*, *42* 183-202

Reardon G.F., Henderson D. and Ginger J.D. 1999. *A structural assessment of the effects of Cyclone Vance on houses in Exmouth WA*, (Technical report, James Cook University of North Queensland. Cyclone Testing Station) No. 48

Reardon G.F. 2000. *Anemometers: Dines vs. AWS,* Australasian Wind Engineering Society Newsletter, May 2000
Sanabria, L. A., and Cechet, R.P. 2007. A Statistical Model of Severe Winds, Geoscience Australia Record, Geocat Number 65052.

——, 2010. Severe Wind Hazard Assessment using Monte Carlo Simulation. *Environmental Modeling and Assessment*, **15,** 2, 147-154.
——, 2010. Severe wind hazard using dynamically downscaled climate simulations, IOP Conf. Series: Earth and Environmental Science 11, 012021, doi:10.1088/1755-1315/11/1/012021

Seguro J.V. and Lambert T.W. 2000. Modern Estimation of the Parameters of the Weibull Wind Speed Distribution for Wind Energy Analysis. Journal of Wind Eng. and Industrial Aerodynamics 85 (2000) 75-84.

Smith S.G. 1981. Comparison of wind speeds recorded by pressure-tube and Meteorological Office electrical cup generator anemographs *Meteorol. Mag., 110* 288-300

Smits A., Klein Tank A.M.G. and Konnen G.P. 2005. Trends in storminess over the Netherlands, 1962-2002, *Int J Climatology, 25* 1331-1344

Sparks W. 1997. *Equations of Motion for Munro Anemometers,* Meteorological Office, Observations - Logistics and Automation, Technical Report No.11

Stephenson A 2004. A User's Guide to the 'EVD' Package (Version 2.1). Department of Statistics. Macquarie University. Australia.

Waters, D. Cechet, R.P. and Arthur, W.C. 2010. Role of exposure in projected residential building cyclone risk for the Australian region, IOP Conf. Series: Earth and Environmental Science 11, 012022, doi: 10.1088/1755-1315/11/1/012022

Whittingham, H.E. 1964. Extreme wind gusts in Australia, Bureau of Meteorology, Bulletin No. 46.

Appendix I - A.

Scatterplots of the gust wind speed datasets

Figure A presents the scatterplot of the maximum daily gust wind speed datasets used in this study. Only wind speeds greater or equal to 25 m/s, the speeds relevant for wind hazard studies, have been plotted. The vertical (dotted) lines are the dates in which the wind recording instruments were either changed, modified or moved to a new position (see anemometer metadata; Section 3.2).

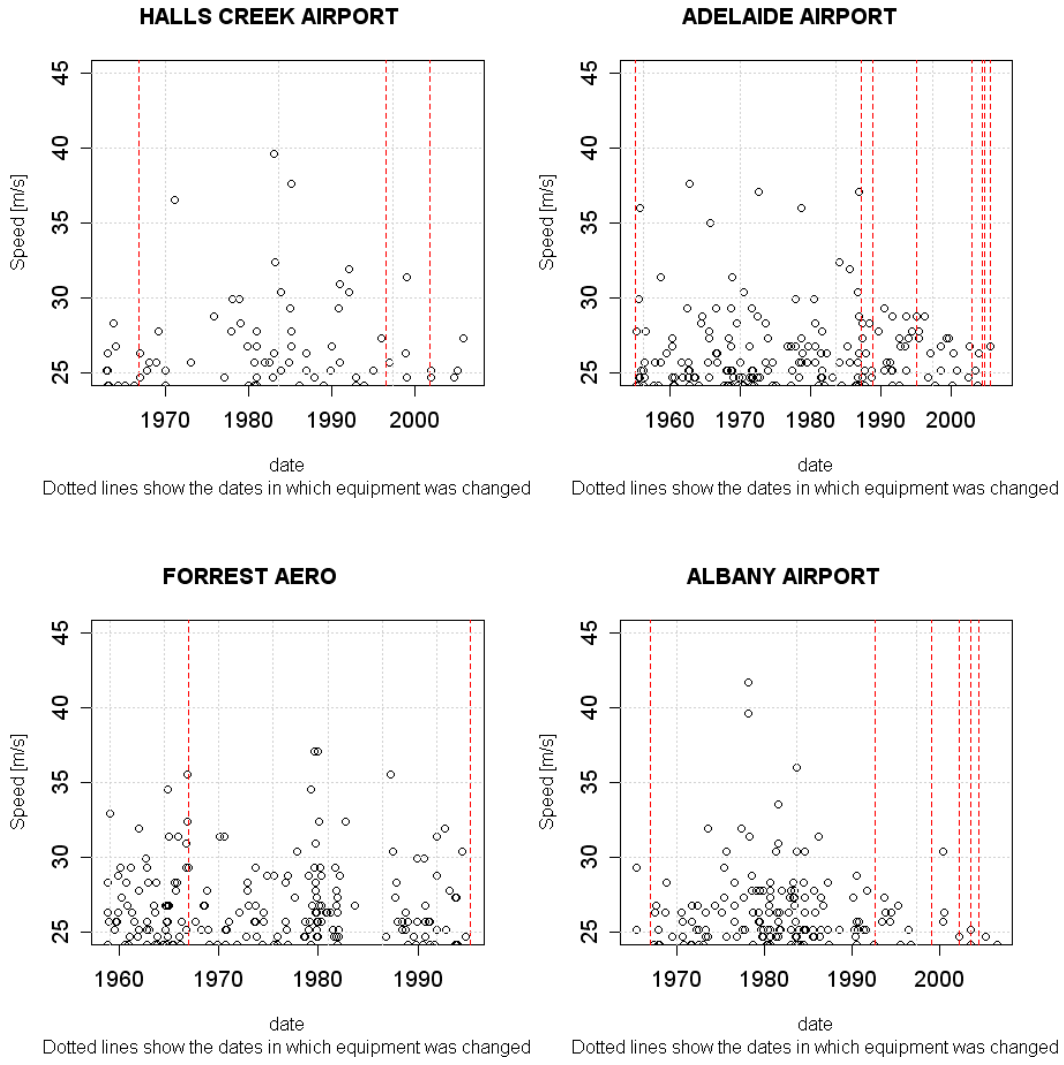

Figure A. Scatterplots of the maximum daily gust wind speeds

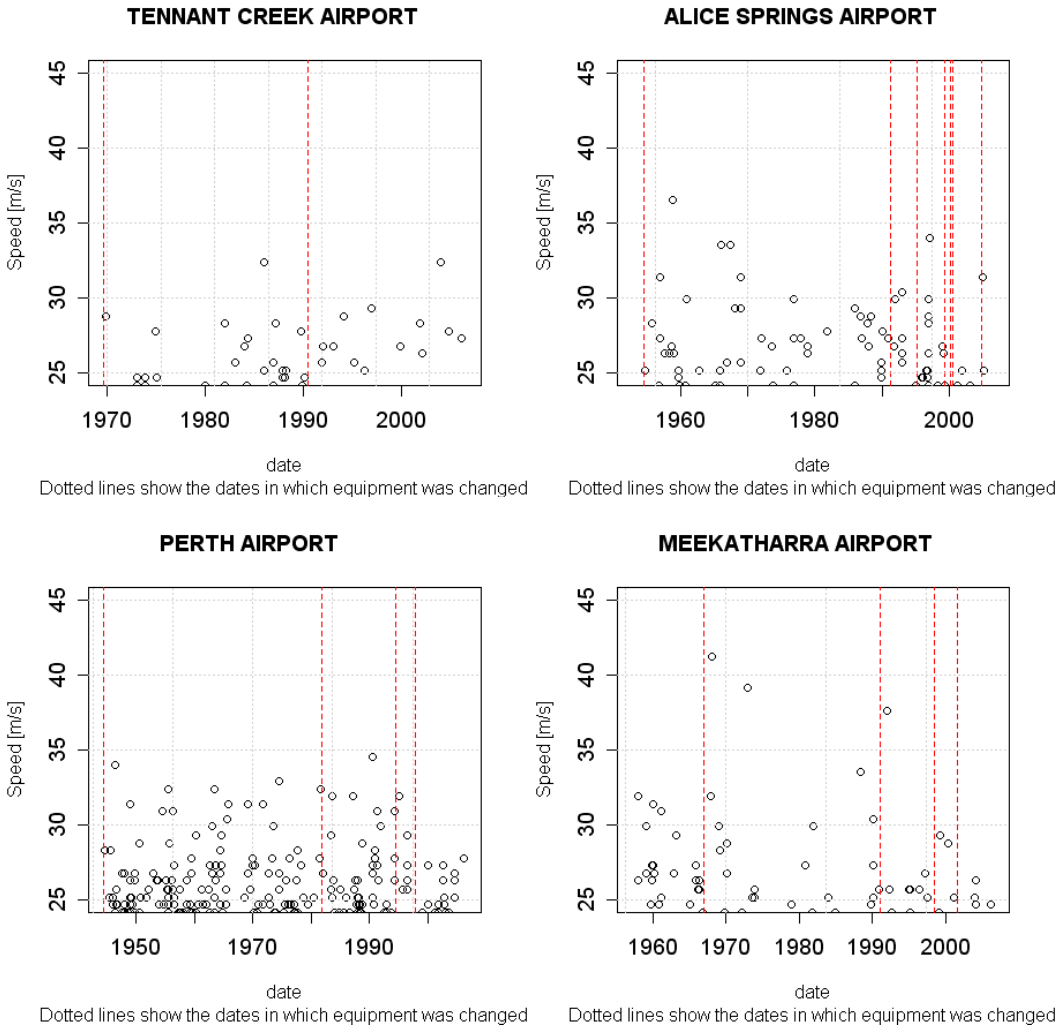

Figure A (Cont.). Scatterplots of maximum daily gust wind speeds

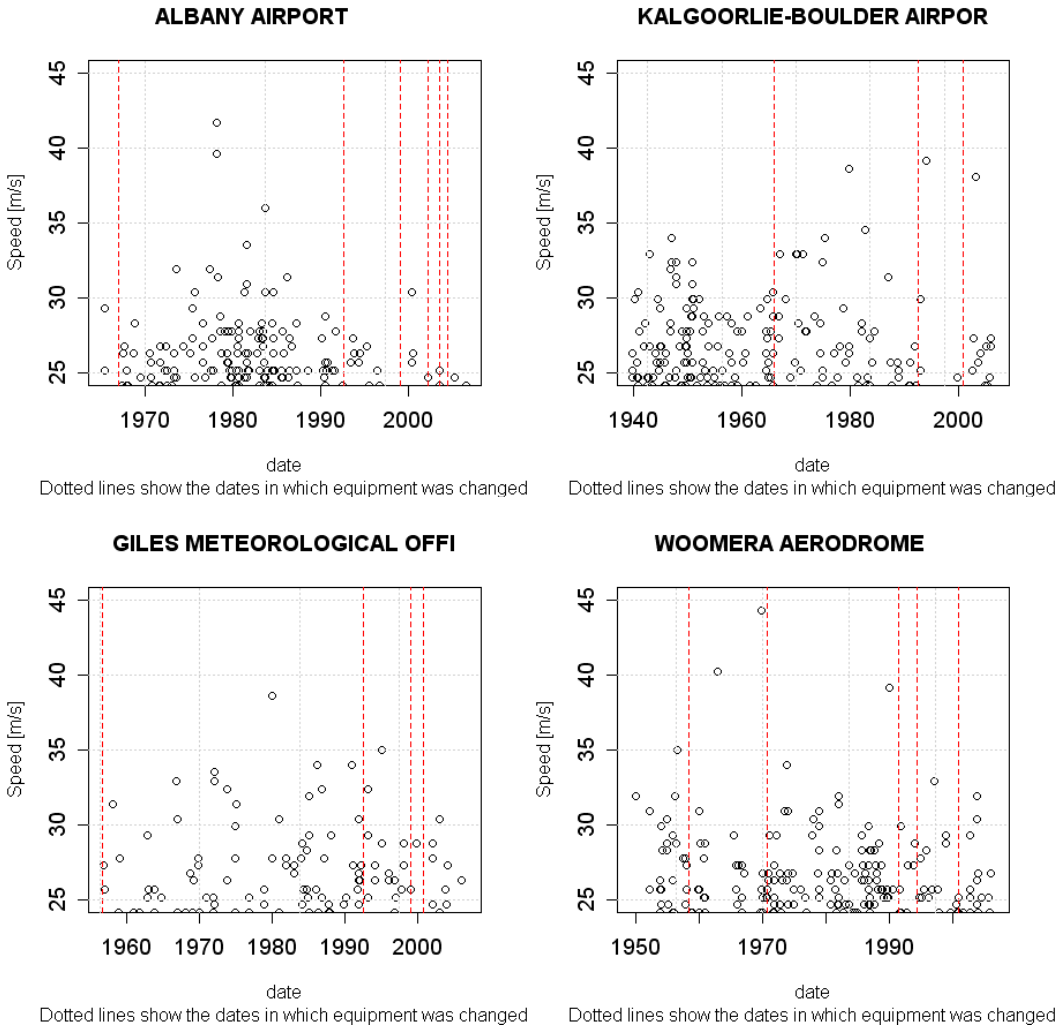

Figure A (Cont.). Scatterplots of maximum daily gust wind speeds

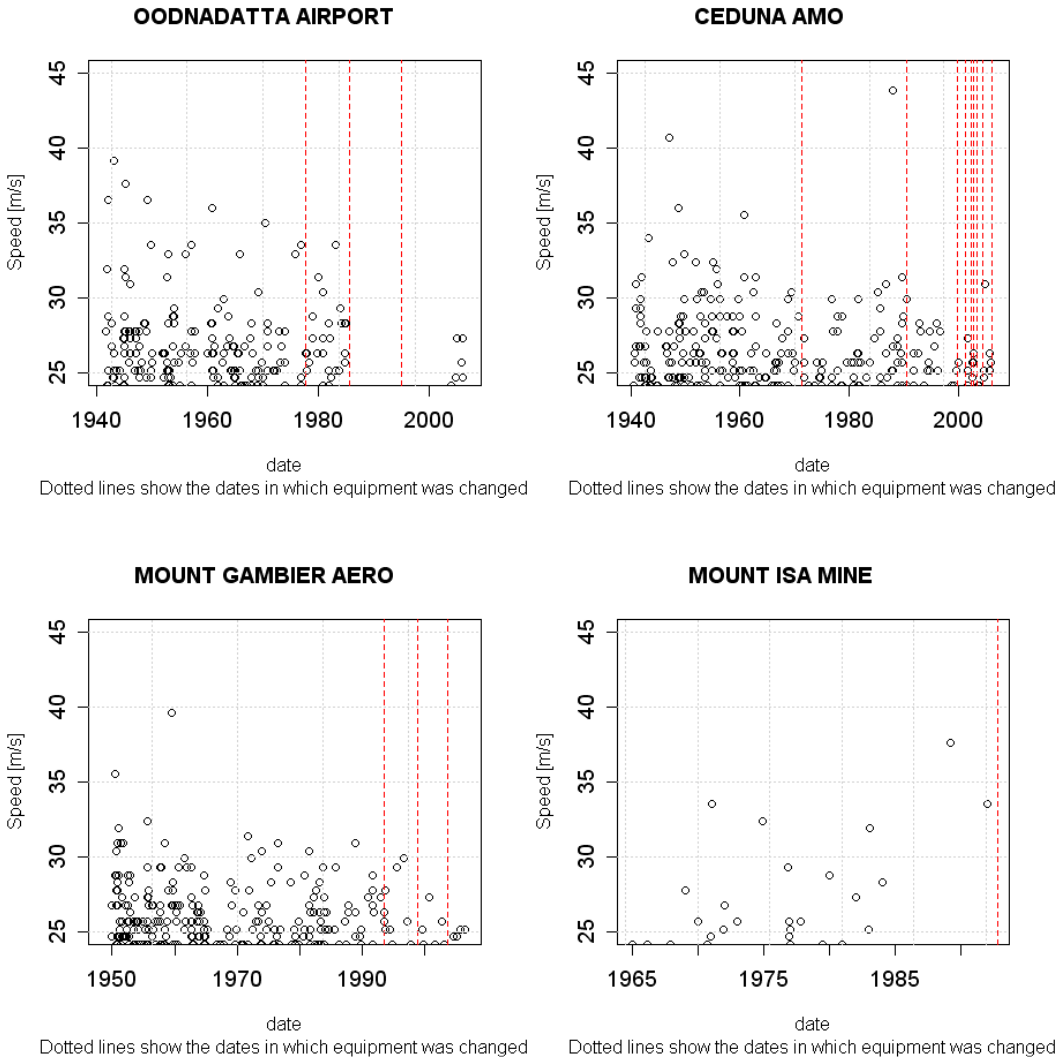

Figure A (Cont.). Scatterplots of maximum daily gust wind speeds

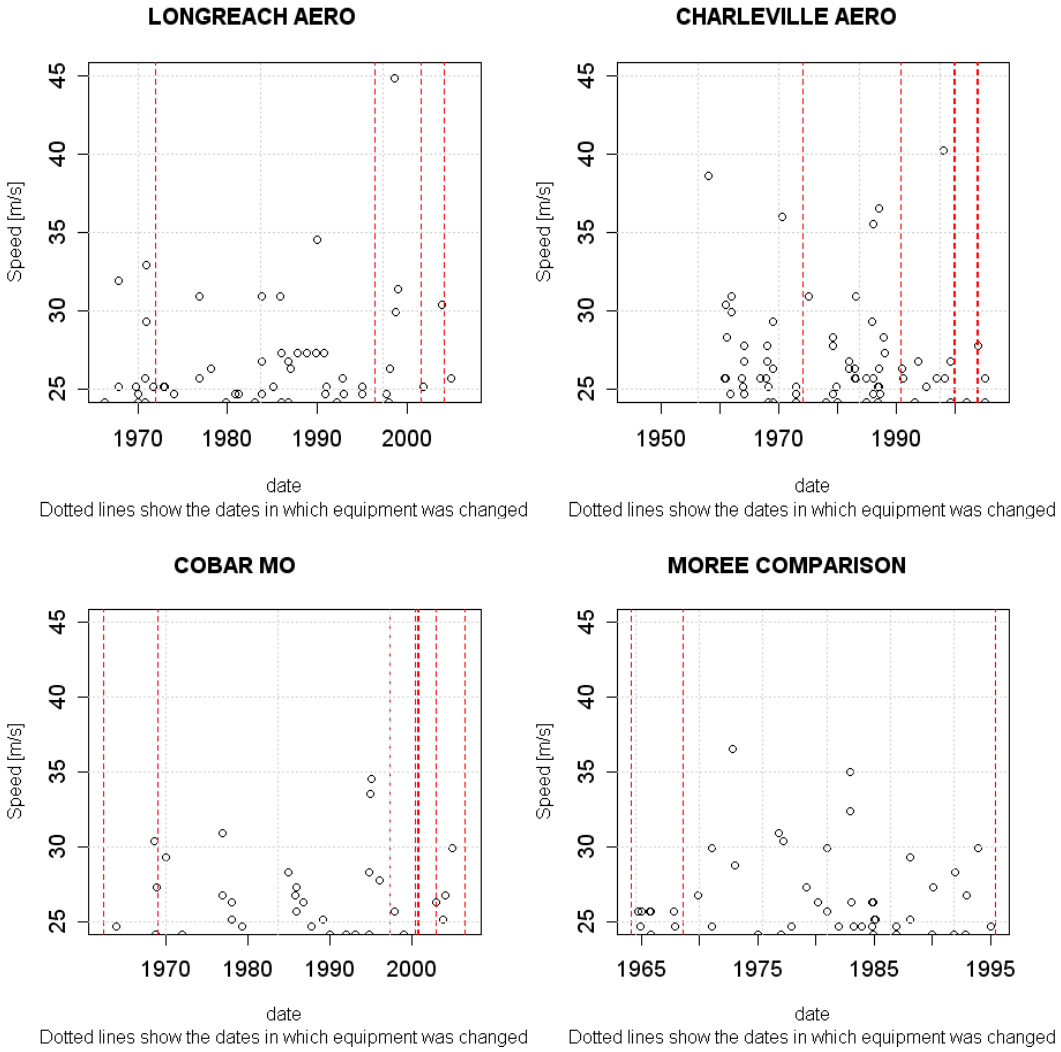

Figure A (Cont.). Scatterplots of maximum daily gust wind speeds

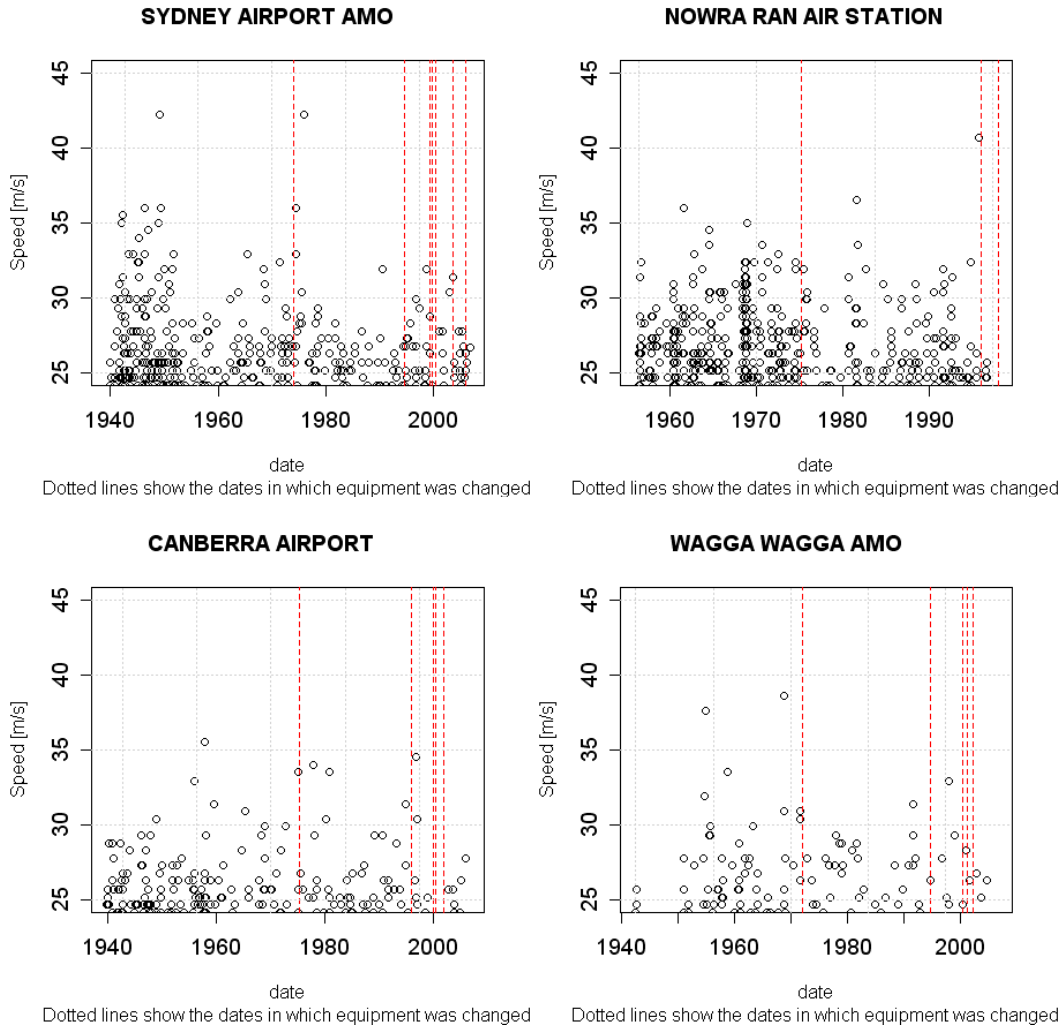

Figure A (Cont.). Scatterplots of maximum daily gust wind speeds

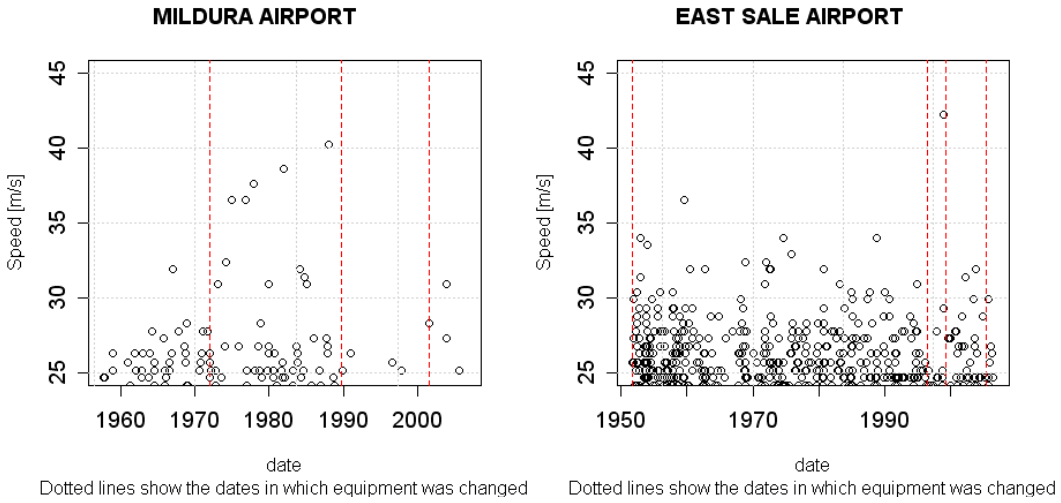

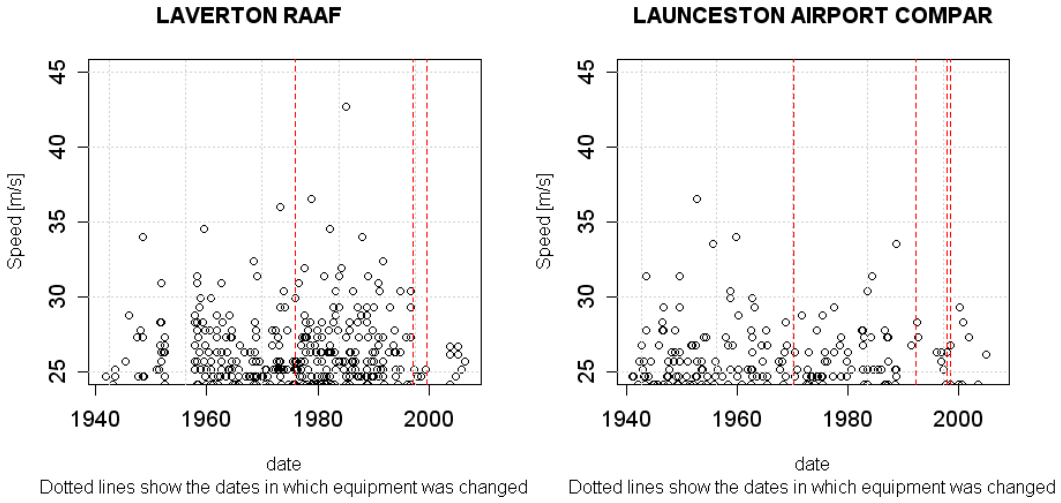

Figure A (Cont.). Scatterplots of maximum daily gust wind speeds

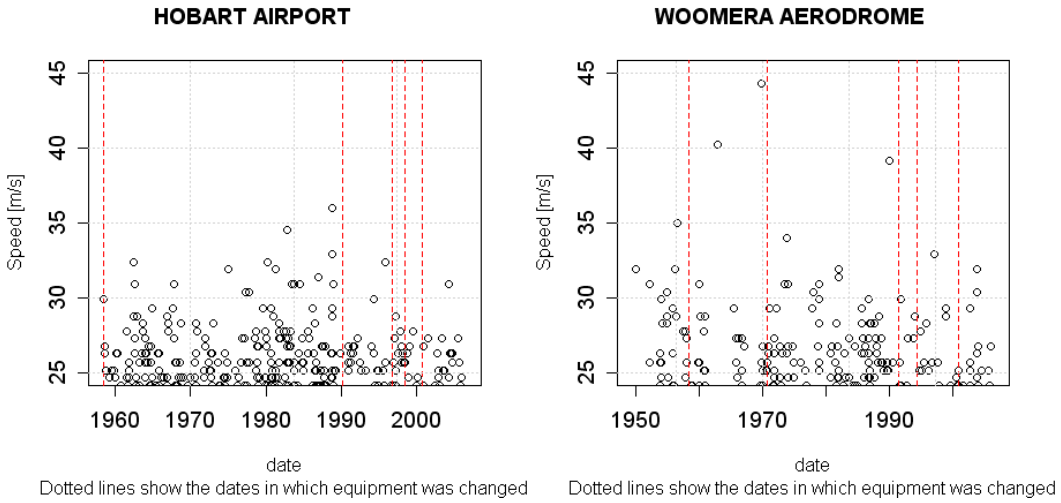

Figure A (Cont.). Scatterplots of maximum daily gust wind speeds

Appendix I - B.

Return period (RP) plots of maximum daily gust wind speed for the 31 "Region A" observing stations considered in Sections 4.1 & 4.2 (see Figure 5 for observing station locations depicted on a map of Australia).

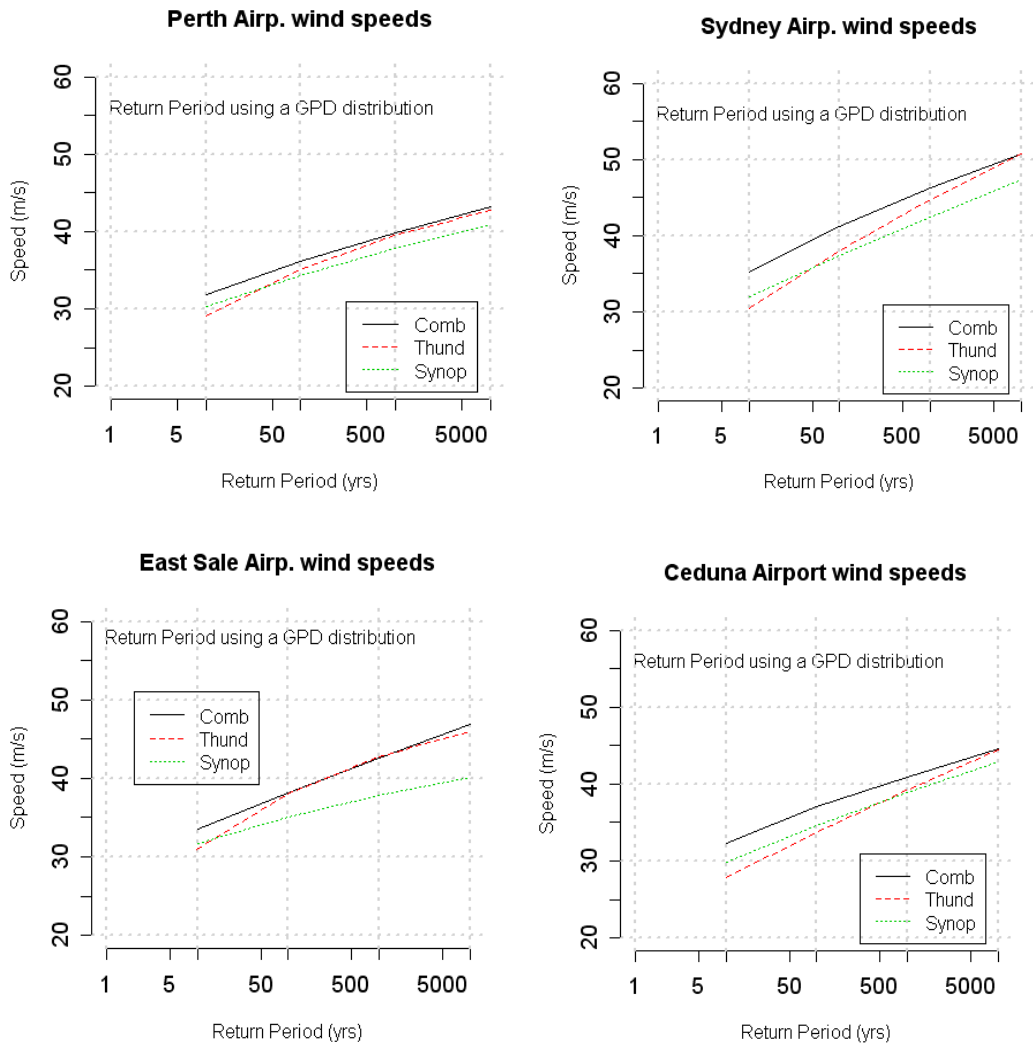

Figure B1. RP curves of the three types of winds; synoptic, thunderstorm and combined for Perth, Sydney, East Sale and Ceduna airports.

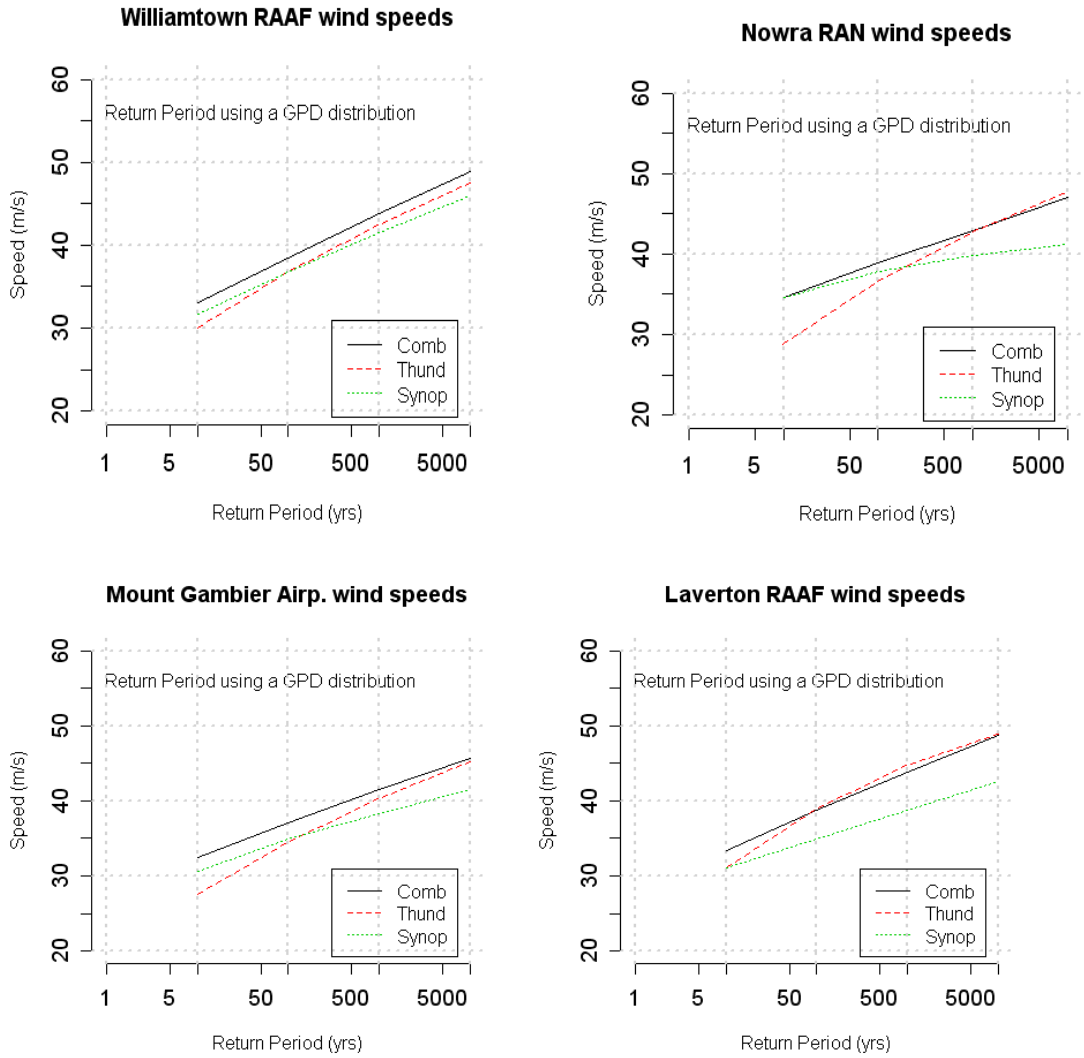

Figure B2. RP curves of synoptic, thunderstorm and combined winds for Williamtown, Nowra, Mount Gambier and Laverton airports.

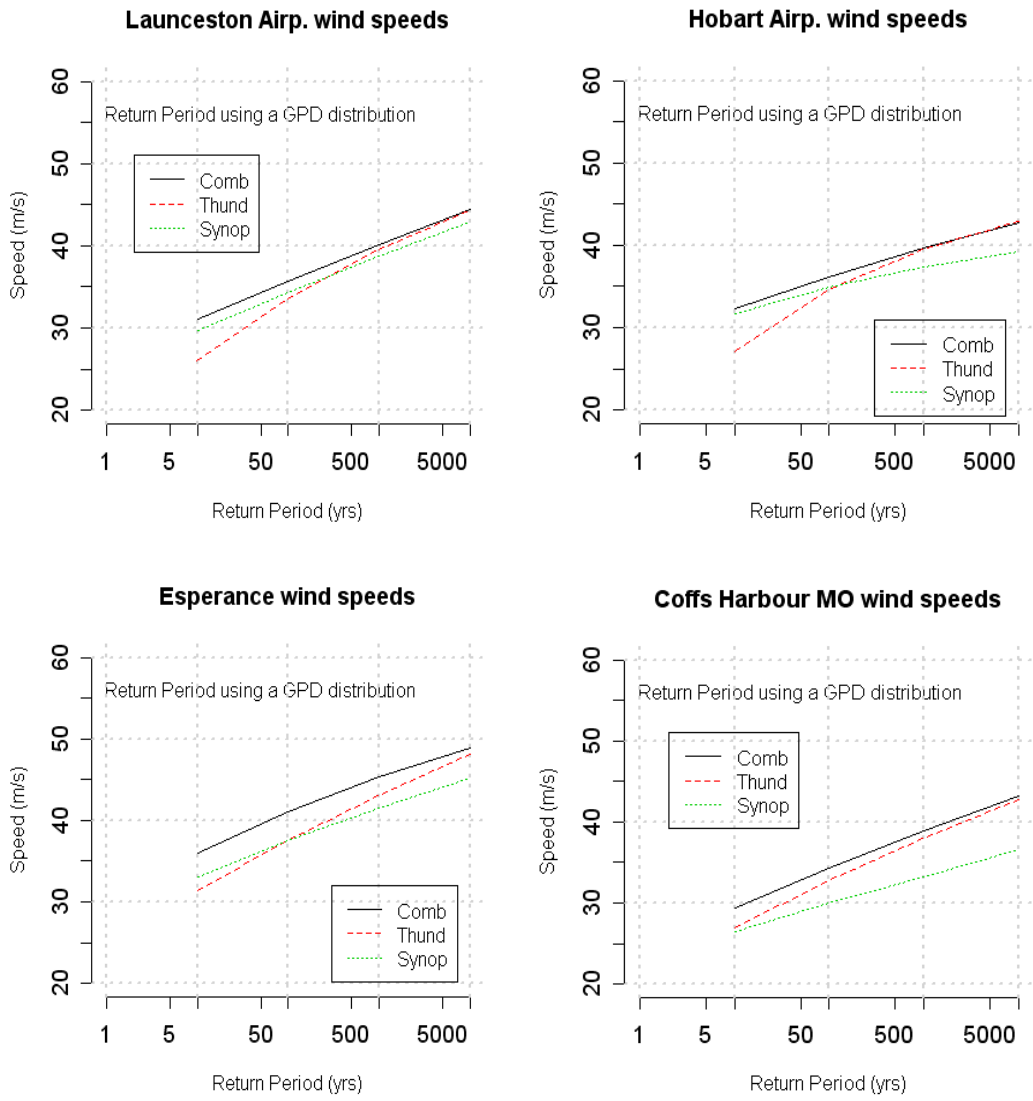

Figure B3. RP curves of synoptic, thunderstorm and combined winds for Launceston, Hobart, Esperance and Coffs Harbour airports.

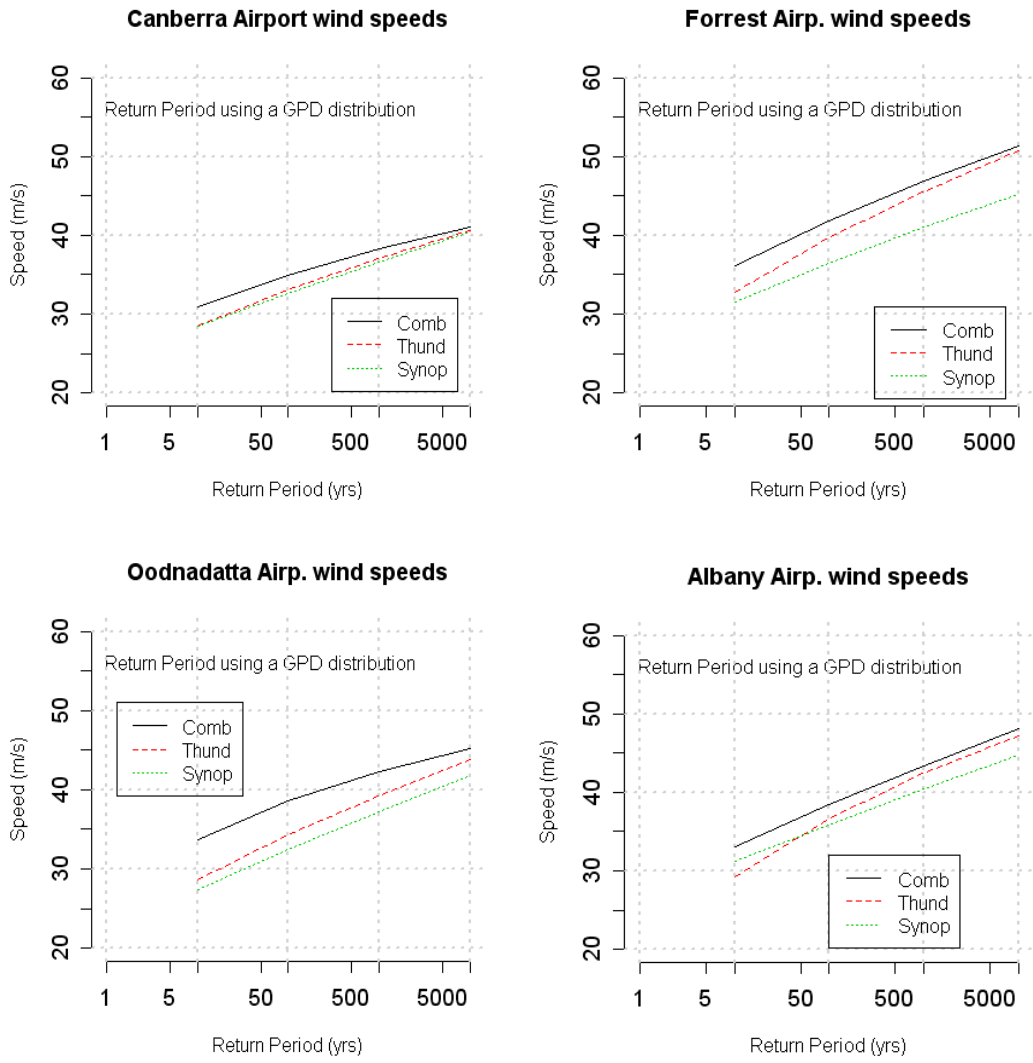

Figure B4. RP curves of synoptic, thunderstorm and combined winds for Canberra, Forrest, Oodnadatta and Albany airports

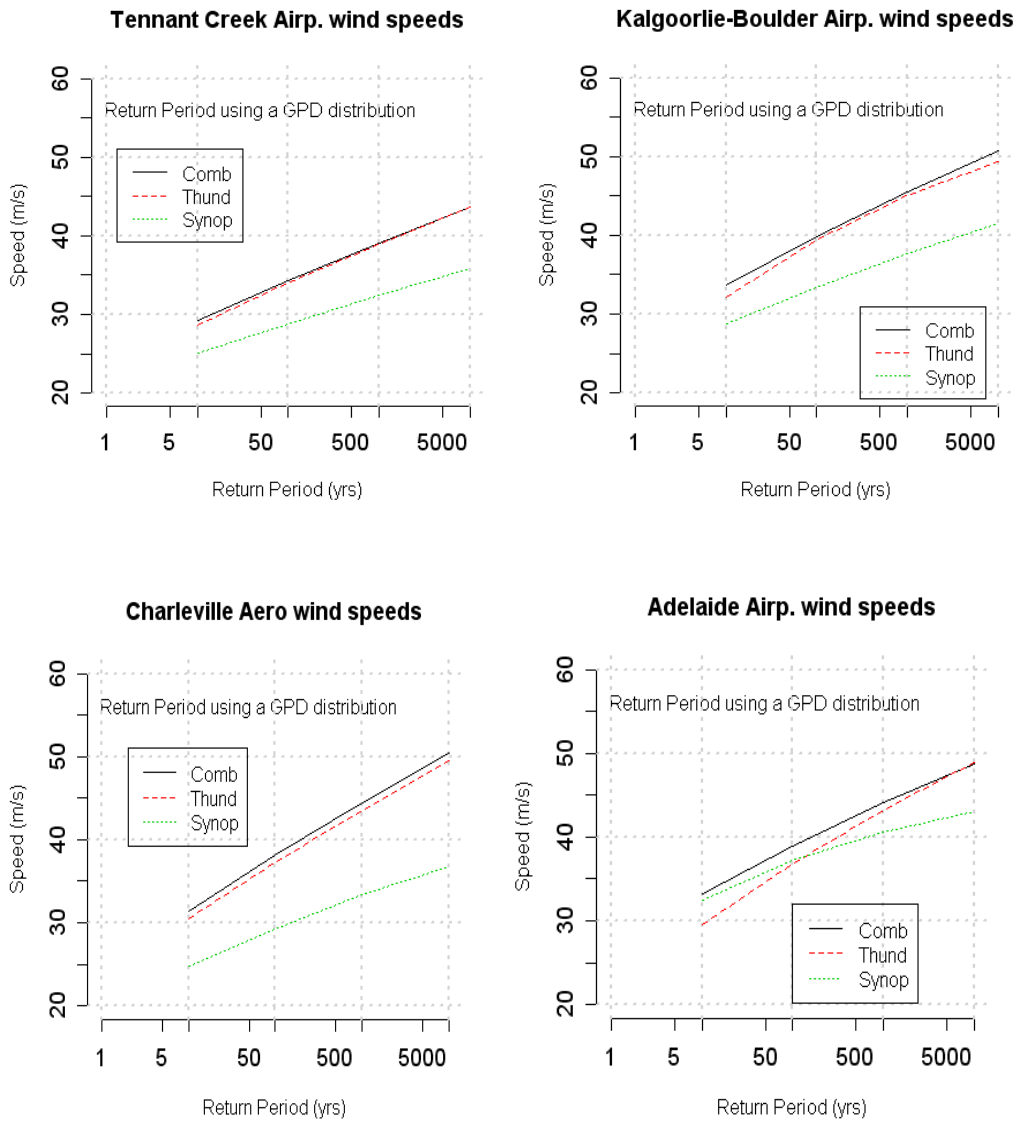

Figure B5. RP curves of synoptic, thunderstorm and combined winds for Tennant Creek, Kalgoorlie-Boulder, Charleville and Adelaide airports.

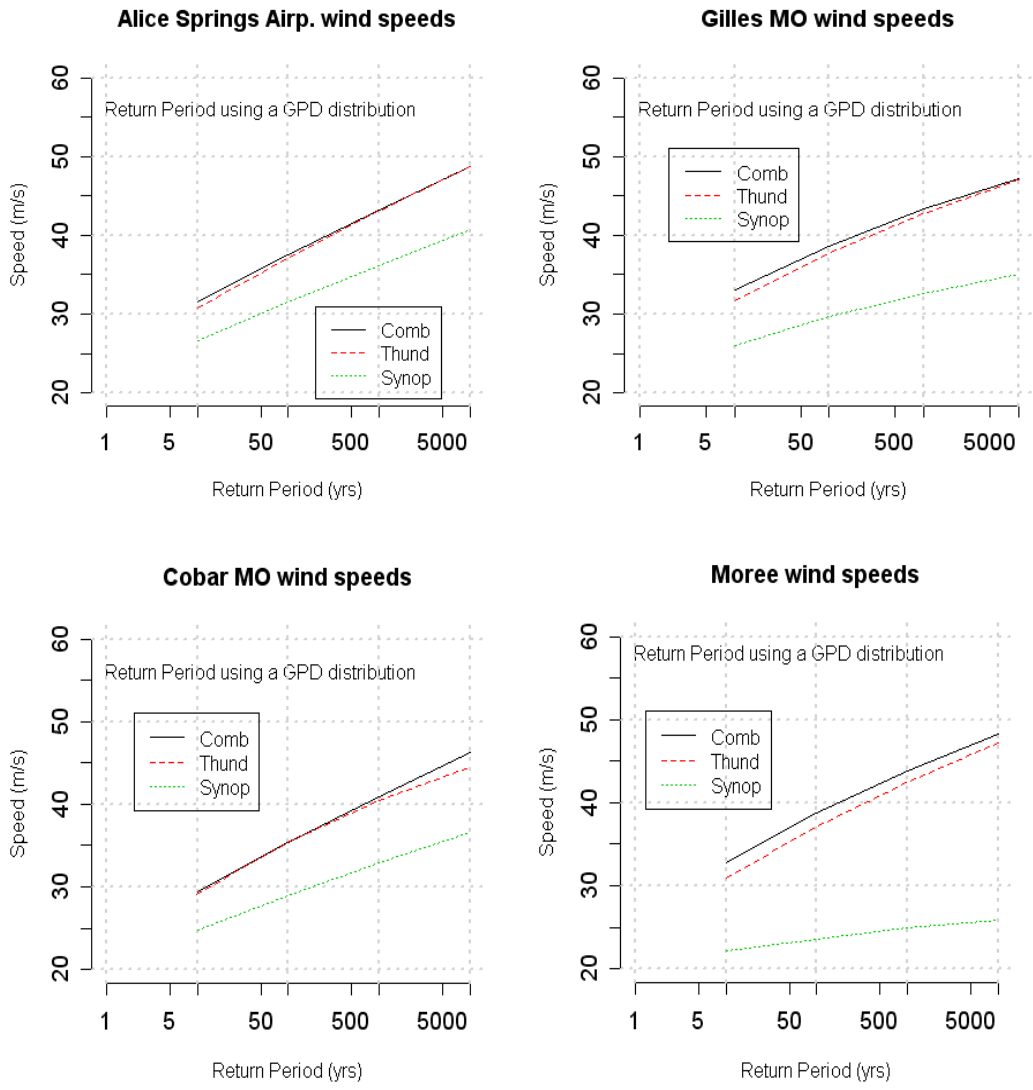

Figure B6. RP curves of synoptic, thunderstorm and combined winds for Alice Springs, Giles, Cobar and Moree airports.

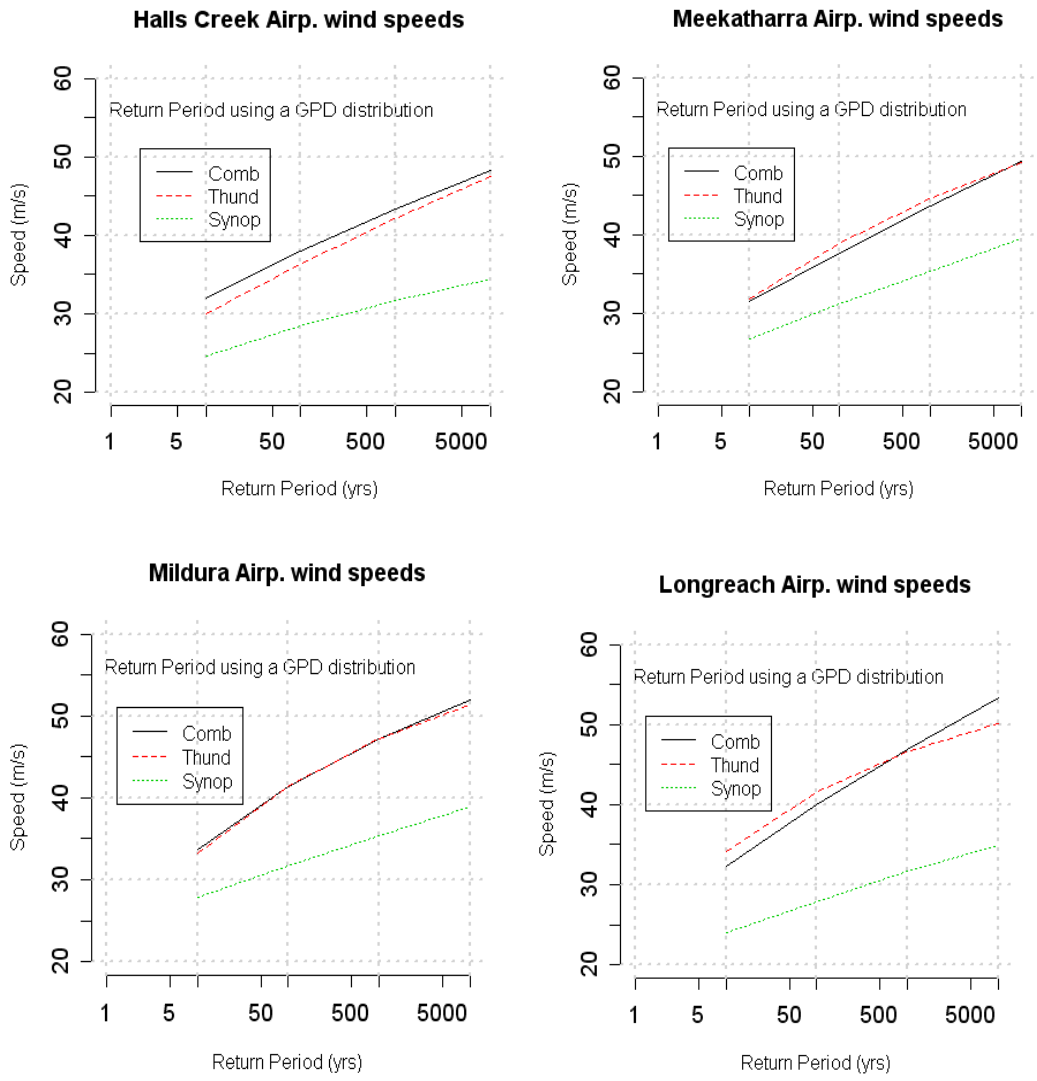

Figure B7. RP curves of synoptic, thunderstorm and combined winds for Halls Creek, Meekatharra, Mildura and Longreach airports.

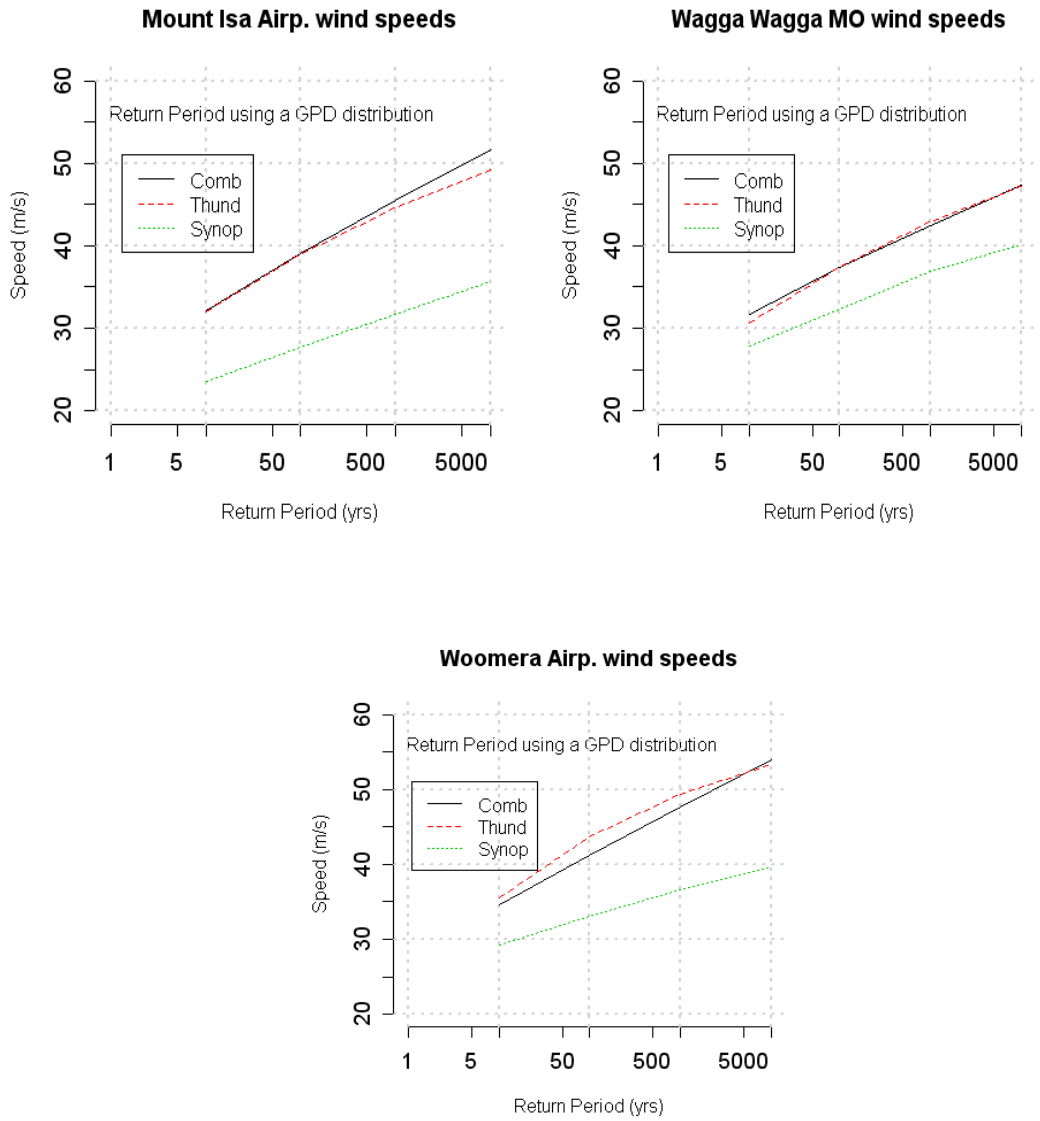

Figure B8. RP curves of synoptic, thunderstorm and combined winds for Mount Isa, Wagga Wagga and Woomera airports.

Appendix I - C.

Coincident Dines and cup anemometer observations

(i) Probability distributions of gust wind speeds

Figure C1 presents the coincident probability density function of gust wind speed measured by the Dines and the cup anemometers. The Learmonth and Townsville PDF's have been corrected (to make the mean of the Dines and the cup anemometer gust wind speeds to coincide). Note that the cup anemometer is the "Synchrotac" type for the observing stations considered.

The last plot, marked as 'All stations combined', was obtained by joining the wind speed datasets of all seven stations together into a single dataset of gust wind speeds and plotting its probability density.

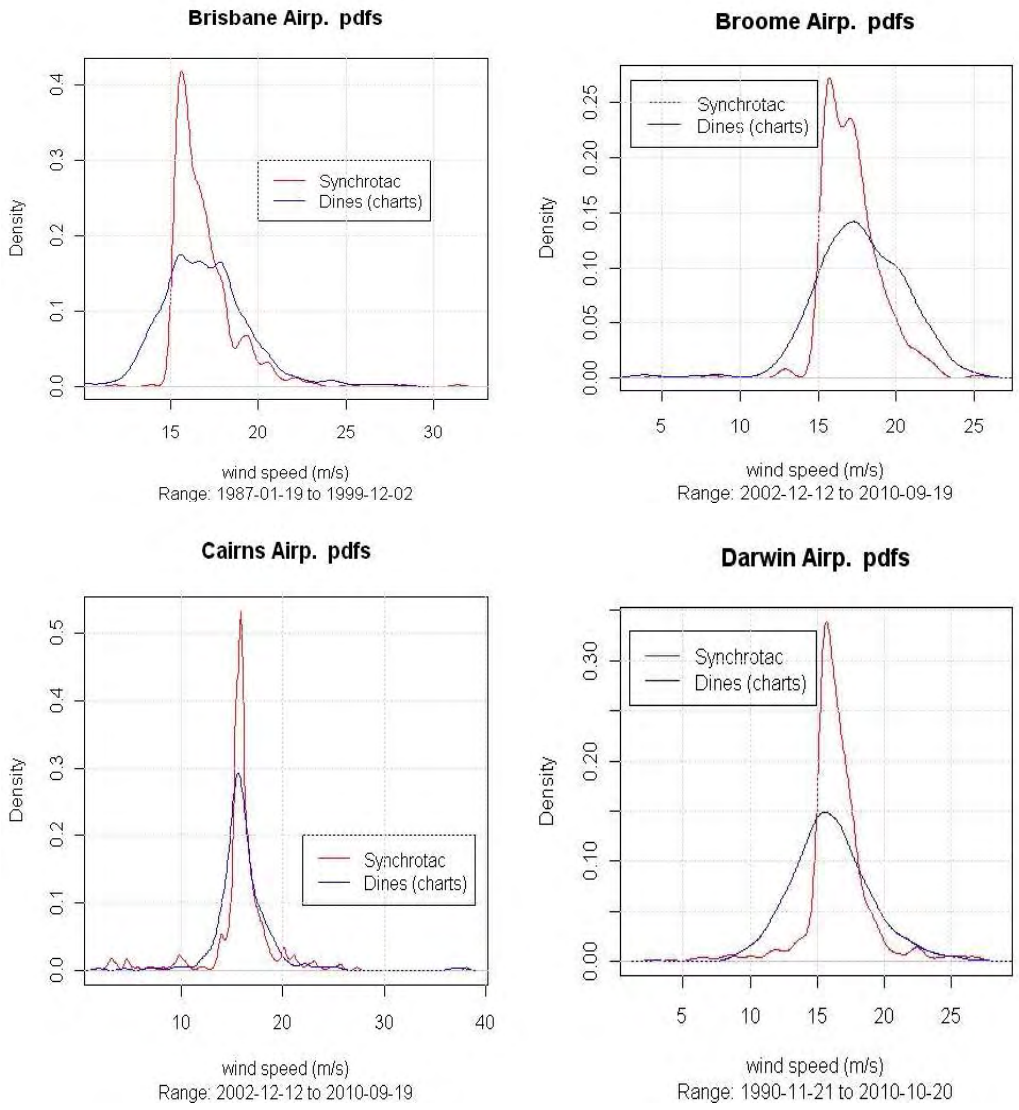

Figure C1: Probability distributions of the gust wind speeds for the coincident anemometer datasets

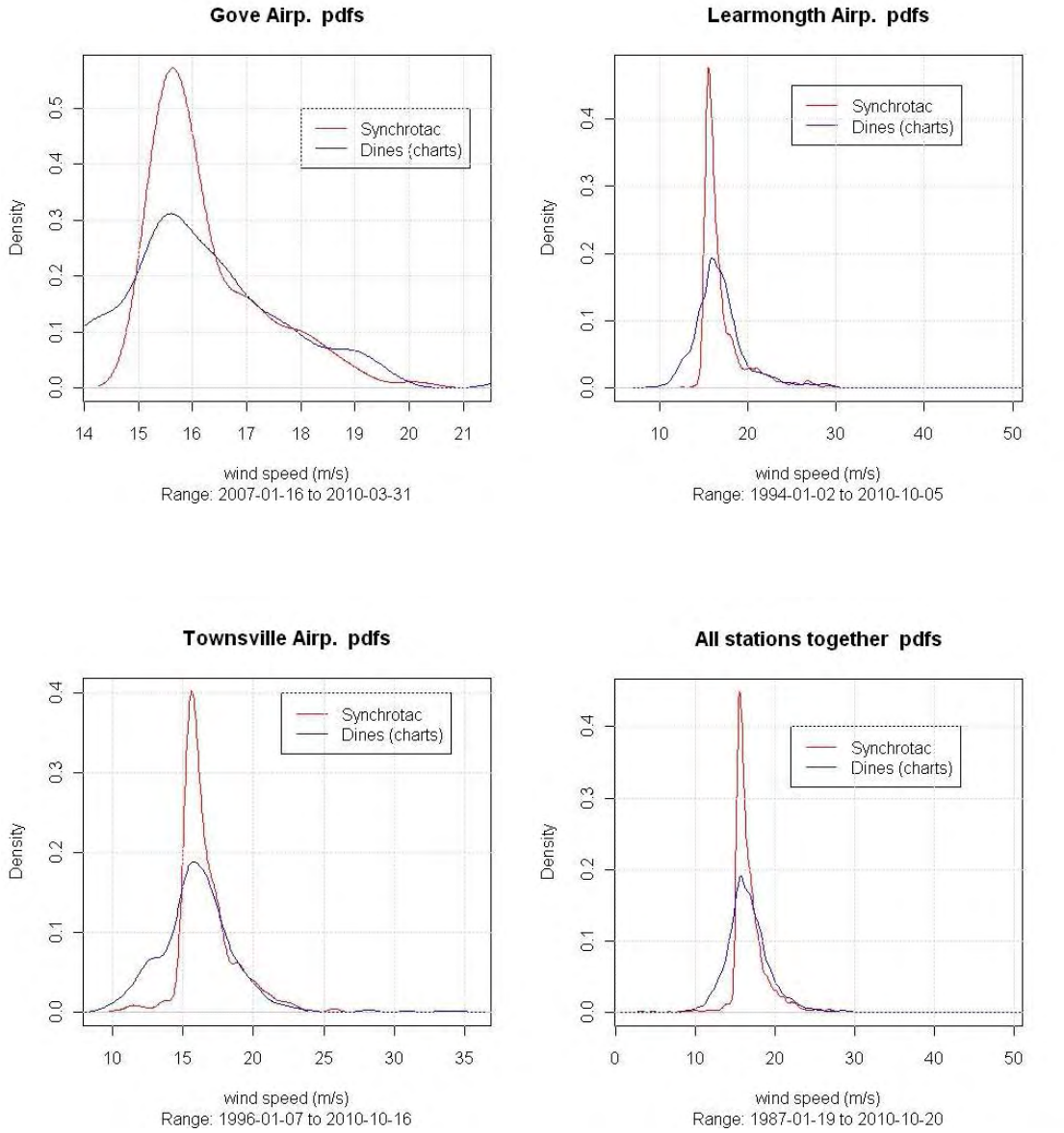

Figure C1 (cont). Probability distributions of the gust wind speeds for the coincident anemometer datasets

(ii) Bias between coincident Dines and cup anemometer observations

Figure C2 presents the time-series plot of the bias between the Dines and the cup anemometer coincident measurements. Similarly the last plot corresponds to 'All stations combined' i.e. the plot of all the station wind speed biases joined into a single dataset.

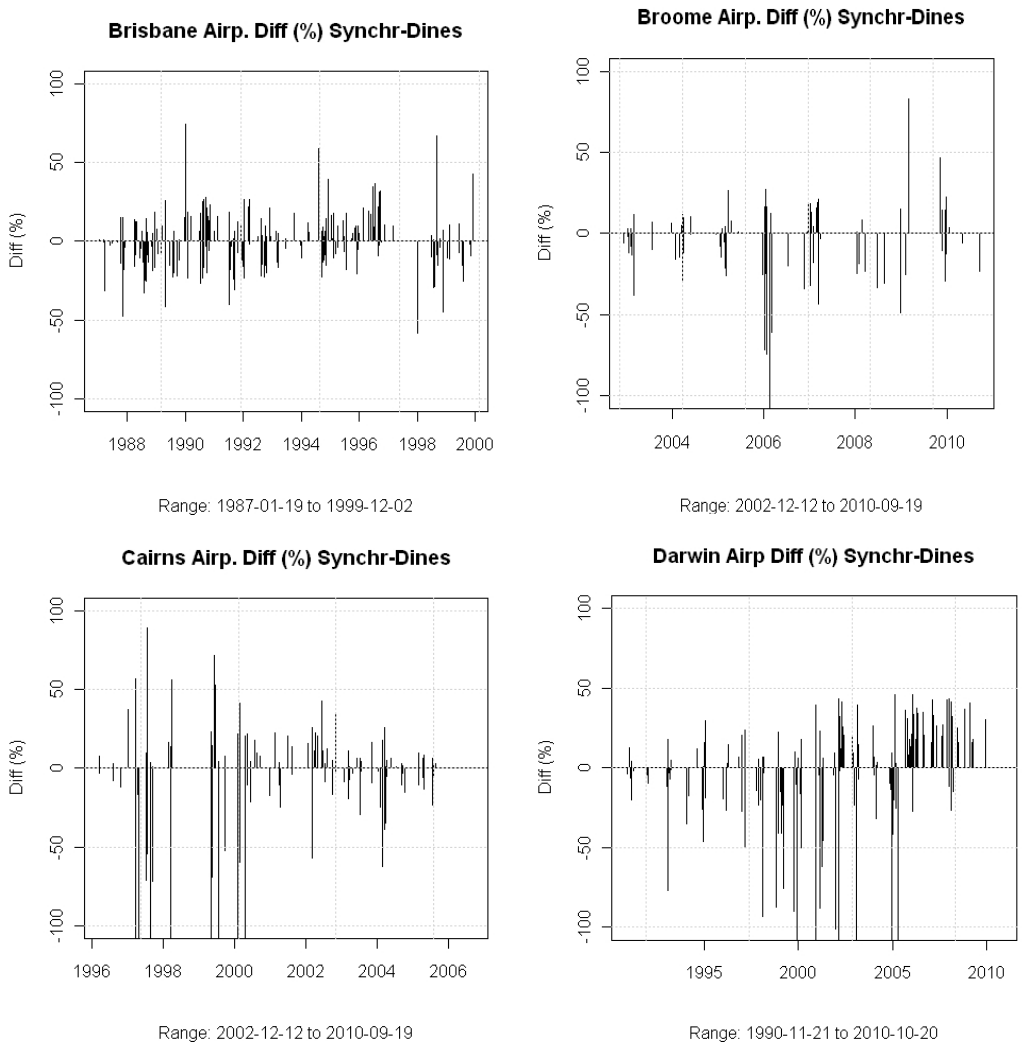

Figure C2. Time-series plot of bias between Dines and cup anemometer coincident measurements

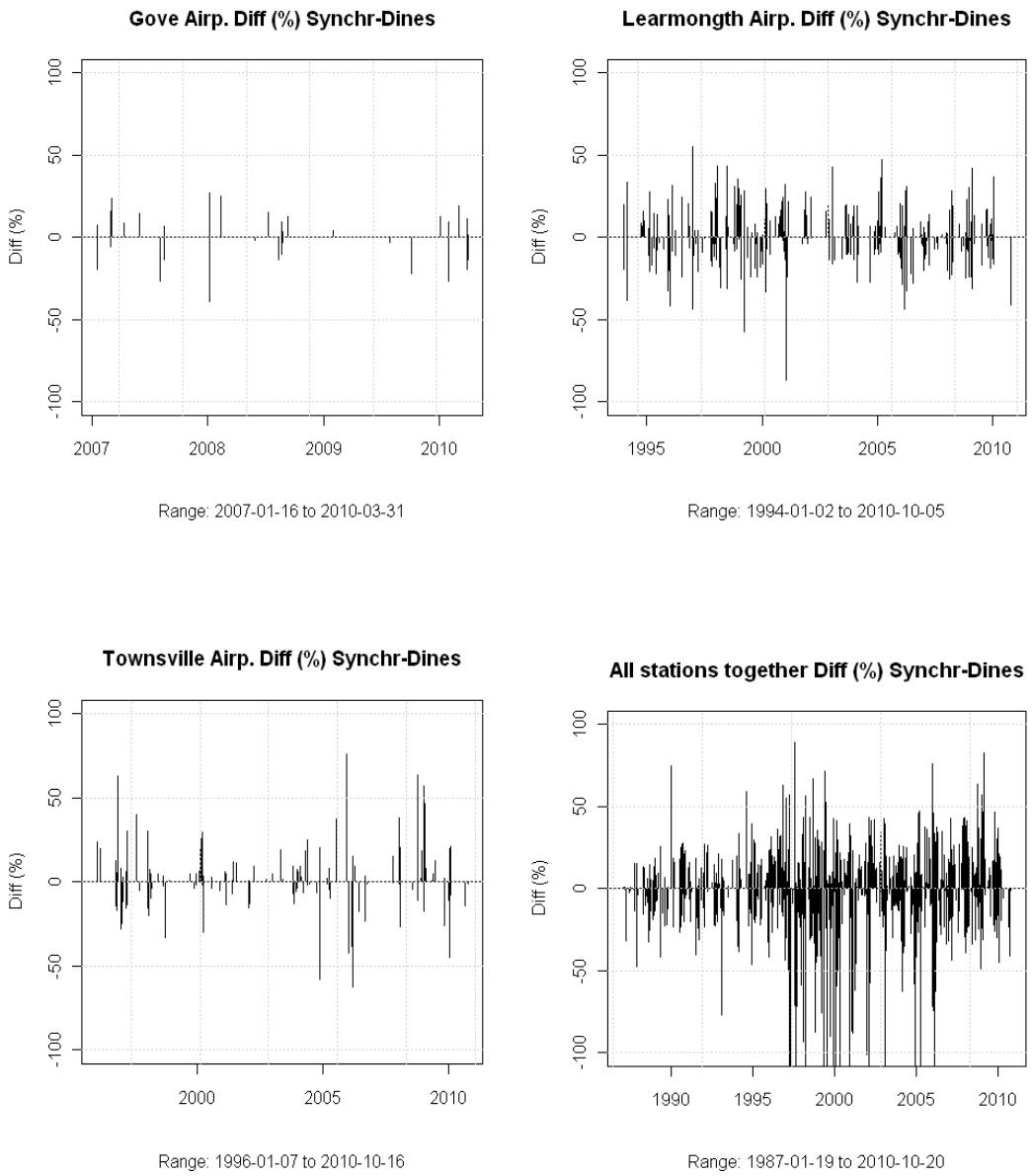

Figure C2 (Cont.). Time-series plot of bias between Dines and cup anemometer coincident measurements

Appendix II-1

Literature review of Dines anemometer response, and related studies

John Holmes
P.O. Box 269, Mentone
Victoria 3194
www.jdhconsult.com

A review of previous studies from the early 1930s to the 1980s on the dynamic response of the Dines anemometer was carried out. These included experimental studies of the response to sinusoidal pressure fluctuations and step inputs, and comparative studies of the gusts recorded by Dines anemometers and rotating cup anemometers operating in parallel in the natural wind.

The general conclusion was that the Dines anemometer probably was more responsive than most cup anemometers, but there was no definitive conclusion on the appropriate correction factors, and on the variations for the different versions of the instrument. There was also some inconclusive evidence on the effect of the connecting tubing on the response.

Gold, 1936

The classic paper by Gold (1936) is a lengthy treatise on the history of anemometry for natural winds, and gives a detailed description of the principles of operation of the standard Dines instrument. Interestingly this paper was published about the time that Dines anemometers were first imported into Australia, and may have influenced the decision of the Bureau of Meteorology to purchase that type, rather than another type, such as the Robinson cup anemometer. Gold gave a detailed exposition of the theory of the float, and derived the equation for the varying internal cross-section of the float with distance from the top, in order to give a linear (static) relationship between float vertical deflection and wind speed (or the square root of dynamic pressure). The remainder of the Gold paper consists of descriptions of installations of Dines anemometers in the U.K. and charts of a number of extreme wind events recorded by the instruments are discussed. However, Gold did not discuss the dynamic response to fluctuating winds produced by turbulent gusting.

N.P.L. Studies 1925-1934

According to Miller (2008, unpublished) extensive studies of the dynamic response of the Dines anemometer were carried out between 1925 and 1934 by the National Physical Laboratory (NPL), Teddington, England. However, information on these studies is apparently only available in a 'secondhand' form through Simmons and Johansen (1929), Giblett (1932), Goldie (1935), the Handbook of Meteorological Instruments (U.K. Met. Office, 1956), Whittingham (1964), and Miller (2008).

Two findings of the initial investigation were that the use of 1-inch diameter connecting pipes gave significantly better frequency response than when ½-inch pipes were used. It was also reported that some form of shielding was required for the pipe connections at the base of the head to avoid variations in reference pressure (suction) with varying wind direction due to interference effects from the pipework.

Goldie (1935) describes some wind-tunnel experiments carried out at the NPL, following experience with the Dines anemometer at the Bell Rock Lighthouse. The experiments compared the response of the Dines with 9m of 25mm diameter tubing, with a hot-wire anemometer. These experiments showed the presence of a resonance in the Dines response with a period of 5-7 seconds. No other information on these experiments is available.

As stated by Miller (2008), who managed to locate some of the early NPL reports in the U.K. National Archives, early work at NPL suggested that the Dines pressure-tube anemometer (PTA) became more responsive at higher frequencies as the wind speed increased. A later report was found by Miller to contain results from tests in one of the N.P.L. wind tunnels in which oscillating wind speeds with periods of 10, 4 and 2 seconds were achieved. A complete Dines PTA head, 15 metres of pipe, and a float system were installed. It was reported that there was some dependency of the frequency response on the mean wind speed, but not so large as found in earlier work with 30-metre long connecting pipes.

If a 'half-power' definition of effective gust duration is adopted (Whittingham, 1964; Miller, 2007) then the N.P.L. studies indicated the effective gust time varied from about 5 to 1.5 seconds as the wind speed increased from 10 to 37 m/s. There was apparently little effect of the length of the connecting tubing, with internal diameter of 25 mm.

Ikeda, 1937, and Sanuki, 1952

The only serious previous attempts to mathematically model the response of the Dines anemometer, including the connecting tubing, appear to have been made by Ikeda (1937) and Sanuki (1952) in Japan. The earlier reference appears to be available in Japanese only, but an English language version of the Sanuki paper is available.

Sanuki carried out a theoretical study of the movement of the float in the Dines anemometer in response to pressure changes but did not fully consider the dynamics of the float chamber. The analysis neglected compressibility and inertial effects in the tubing and derived an effective time constant ('Shrenk parameter) for the system on that basis. The expression for the response was found to depend on the cross-section area of the float, and the length and diameter of the connecting tubing. Sanuki also found that the response was independent of the mean wind speed, in contradiction to experimental evidence from the N.P.L. studies as discussed above. Another conclusion by Sanuki was that the flow in the connecting tube transmitting the pressure fluctuations is not laminar but turbulent.

The Sanuki theory has significant inconsistencies with the experimental evidence.

Whittingham 1964

Whittingham's 1964 report is of great significance in Australia for a number of reasons. He identified the various mechanisms producing extreme gusts in Australia, and was the first to carry out extreme value analyses (using the Gumbel approach) of annual maximum wind gusts from about 80 stations in Australia and its territories, all measured with anemometers of the Dines pressure-tube type.

Whittingham also discussed the response characteristics of the Dines anemometer drawing largely on the N.P.L. measurements as reported by Giblett (1932) and the U.K. Handbook of Meteorological Instruments (1956). Whittingham was the first to coin the term '2 to 3-second gust' in Australia, a concept which has been the basis for structural design in Australia ever since. Whittingham apparently based his assessment of the effective gust duration of 2 to 3 seconds, on the N.P.L. measurements of sinusoidal excitation of the Dines instrument reported by Giblett (1932), and reproduced as Table 1 in Whittingham's report. However, the 2 to 3 seconds is a period for which the amplitude ratio is still at a value of 1.0, not 0.5 as used by Miller (2007). Based on the latter definition, the effective gust duration is about 1.7 seconds, from Table 1 in Whittingham's report.

Furthermore, new measurements carried out in the present project indicate an effective gust duration (half power) of about 1.3 seconds (see Appendix II-3).

Borges, 1968

Borges (1968) investigated the frequency response of a Fuess pressure-tube anemometer, apparently copied from the Dines type, using both an impulsive excitation, and a sinusoidal excitation with an electromagnetic vibrator. He identified two distinct resonant peaks in the frequency response function of the system. These two frequencies are associated with the water and float moving in phase, and out-of phase. The frequency of the first peak had a frequency of about 0.25 Hertz and the second around 0.7 Hertz. The magnitude of the second peak increased as the mean wind speed increased and as the tubing length was made shorter. These frequencies however were about half the values found for the low-speed Dines anemometer float system in the present project, apparently reflecting physical differences between this and the Fuess instrument investigated by Borges.

Smith (1981) and Logue (1986)

In the 1980s, two studies were made in which the outputs from Dines pressure-tube anemometers were compared with cup anemometers located nearby in a turbulent natural wind environment.

Smith (1981) carried out statistical comparisons of 10-minute and 60-minute mean wind speeds recoded by Dines anemometers and Munro Mark 2 and Mark 4 cup anemometers at stations in the U.K., at which a changeover of instruments had occurred. He found that the mean wind speeds recorded by the cup anemometers exceeded those from the Dines pressure-tube type by 0.5 to 1 m/s, apparently because of the well-known 'over-speeding' characteristic of the cup type, caused by an interaction between the turbulence and the inertia of the cups. However, no comparison of gust speeds was reported by Smith.

Logue (1986) compared mean and gust speeds measured with a Dines pressure-tube anemometer and a Munro Mark 2 cup anemometer located together at Galway on the west coast of Ireland for the whole year in 1984. The mean wind speeds from the two instruments generally agreed well. However, for wind speeds exceeding 28 m/s (55 knots) the Dines read maximum gusts 5.6% higher on average than those from the cup anemometer.

Pressure measurement systems with long lengths of tubing

In the Dines anemometer system, the anemometer (pitot) head which sensed the dynamic pressure of the wind (including the fluctuations generated by atmospheric turbulence), was connected by tubing of 12- 30mm (most often 25mm, or 1 inch) internal diameter to the float chamber of the anemometer. Hence, the response of the connecting tubing to dynamic pressure fluctuations is relevant to the overall response of the Dines system,

There have been many studies of the response of pressure measurement systems, consisting of small diameter tubes connected to finite volumes, in which the pressure is measured by a diaphragm, which itself forms part of a pressure sensor, or transducer. The magnitude of the volume and the flexibility of the transducer diaphragm affect the response of such systems, as well as the length and diameter of the connecting tubing. The application of such studies during the last 50 years has been primarily for the measurement of fluctuating pressures in wind tunnels, in which tubing lengths up to about 3 metres, and internal diameters in the range of 1- 5 mm are typically used.

The work by Iberall (1950) was probably the first serious attempt to develop a comprehensive theory of pressure transmission down long tubes of small diameter. Iberall first gives an 'elementary' solution for a single tube of uniform diameter (no bends) connected to a rigid volume. The flow in the tube transmitting the pressure fluctuations is assumed to be laminar and incompressible; however, the fluid entering the volume is assumed to be compressible. Fluid inertia effects are also ignored initially. These assumptions lead to a simple linear system with 'first-order' response characteristics (analogous to an electrical R-C filter) with a time constant that is proportional to the tube length and the instrument volume, and inversely proportional to the fourth power of the tube diameter. Iberall then relaxed the assumptions and gave a series of graphical solutions.

Bergh and Tijdeman (1965) further developed the work of Iberall. They also assumed laminar flow in the connecting tube, but included fluid inertia and compressibility effects. The latter assumptions produce solutions with (damped) 'organ pipe' resonances. However the system is linear provided the pressure fluctuations are small with respect to atmospheric pressure. Bergh and Tijdeman derived a recursion formula for a series connection of tubes and volumes. This relates the amplitude of sinusoidal pressure fluctuations in volume j to that in the preceding volume j-1 and the following volume j+1. Instrument diaphragm flexibility was also accounted for.

Holmes and Lewis (1987), and Letchford (1987) carried out extensive experimental measurements with many small diameter tubing systems, and showed that Bergh and Tijdeman theory gave excellent agreement with the measurements, provided that the tubing diameters, instrument volume and diaphragm flexibility are known accurately.

Beljaars (1987)

Beljaars (1987) discussed the sampling and filtering of measured wind gusts, applying random process and linear systems theory to instrumentation systems. The level crossing theory of Rice (1944-5), and the formula of Davenport (1964) for the expected largest value of a random process, were applied to determine peak values for the gust wind speeds produced by a complete measurement system, including anemometer, digital sampling and digital filtering.

Although Beljaars did not explicitly consider the Dines anemometer, a similar approach to that of Beljaars (and Davenport, 1964) has been applied in the present project (see Appendix II-4) to determine gust factors and gust ratios, for comparison of the maximum gusts recorded by both Dines and cup anemometers.

Beljaars (1987) also proposed a new definition of 'gust duration' based on an equivalent moving averaging time, and suggested that a moving averaging filter with an averaging time of 2-5 seconds should be applied to all anemometer outputs, to provide a universally consistent maximum gust. This suggestion was later adopted by the World Meteorological Organization, and a digital moving average filter, with a time of 3 seconds, has been applied by the Australian Bureau of Meteorology for the Automatic Weather Stations (AWS). This filter has a low cut-off frequency compared with the inherent response characteristics of typical cup anemometers, and hence has had a very significant effect on the maximum gusts reported by the AWSs. Further discussion of this is given in Appendices II-3 and II-4 of this report.

Summary

Studies of the dynamic response of the Dines anemometer system, although intensive in the 1920s to 1930s period, have been sparse ever since. The early studies seemed to focus on the effect of

the tubing, which the present project has found is only a problem if very long, or very narrow, tubes are used. The most useful paper reviewed is that of Borges (1968), who focused on the response characteristics of the float movement, and identified the two natural frequencies associated with in-phase and out-of-phase motion of the float and the water; these aspects have been further studied experimentally and theoretically in the present project.

There has apparently been little interest in the U.K. in studying the comparative readings of gust wind speeds recorded by the Dines and cup anemometers, probably because of the earlier replacement of the Dines type by cup anemometers, dating back to the 1950s. Also the wind loading standard there converted from a peak gust to an hourly-mean basic wind speed, some years ago. However, the paper from Ireland by Logue (1986), in which statistical comparisons of gusts recorded over a year were compared, and higher readings of peak gusts by the Dines anemometer on average, is particularly useful for the present project.

There is an extensive literature on the response to pressure measurement systems with long connecting tubing of small diameters to fluctuating (sinusoidal pressures). The theory developed by Bergh and Tijdeman (1965) based on laminar flow, is the most comprehensive. It has been validated for measurement systems with small diameter (i.e. 1-6 mm) tubes in laboratory conditions. In this project (see Appendix II-2), this theory was applied, and validated, for tubing lengths and diameters (12-30 mm) used for the connecting tubing in Dines anemometer systems.

The use of a digital 3-second moving average filter as proposed by Beljaars (1987) is significant for this project, as such a filter has been applied in Australia to cup anemometers, and significantly reduces the maximum gusts reported, compared with those reported before 1990 from Dines anemometers.

References

A.C.M. Beljaars, 1987: The influence of sampling and filtering on measured wind gusts. *Journal of Atmospheric and Oceanic Technology*, **4**, 613-626.

H. Bergh and H. Tijdeman, 1965: Theoretical and experimental results for the dynamic response of pressure measuring systems. National Aero- and Astronautical Research Institute, Netherlands, Report NLR-TR F.238.

A.R.J. Borges, 1968: On the frequency response of floater-type anemographs, Tecnica, No. 379, pp505-511.

A.G. Davenport, 1964: Note on the distribution of the largest value of a random function with application to gust loading, *Proc., Institution of Civil Engineers (U.K.),* **28,** pp 187-196.

M.A. Giblett, 1932: The structure of wind over level country. Geophysical Memoirs 63, Meteorological Office U.K.

E. Gold, 1936: Wind in Britain – the Dines anemometer and some notable wind records during the last 40 years. *Q. J. Roy. Meteor. Soc.*, **62,** pp 167-206.

A.H.R. Goldie, 1935: Wind records from the Bell Rock Lighthouse. Geophysical Memoirs 63, Meteorological Office, London, U.K.

J.D. Holmes and R.E. Lewis, 1987: Optimization of dynamic-pressure measurement systems I. - Single point measurements. *Journal of Wind Engineering and Industrial Aerodynamics*, 25, pp 249-273.

A.S. Iberall, 1950: Attenuation of oscillatory pressures in instrument lines, *Journal of Research National Bureau of Standards*, **45**, pp85-108.

S. Ikeda, 1937: On Dines' pressure tube anemometer, *Journal of the Meteorological Society of Japan*, **15**, p 58 and 541.

C.W. Letchford, 1987: Pneumatic averaging in wind engineering, D.Phil. Thesis, University of Oxford.
J.J. Logue, 1986: Comparison of wind speeds recorded simultaneously by a pressure-tube anemograph and a cup-generator anemograph. *Met. Mag.*, **115,** pp 178-185.
Meteorological Office (U.K.) 1956: Extract from: Handbook of meteorological instruments – Part I Instruments for surface observations. pp 220-225.
C.A. Miller, 2007: Defining the effective duration of a gust. Presented at the 12th International Conference on Wind engineering, Cairns, July 1-6, 2007.
C.A. Miller, 2008: The Dines pressure-tube anemograph. 10 pp, unpublished.
M. Sanuki, 1952: A new development of the theoretical and experimental lag of Dines pressure tube exposed in fluctuating winds. *Papers in Meteorology and Geophysics*, **3,** 115-124.
L.F.G. Simmons and F.C. Johansen, 1929: Recent research on the Dines anemometer at the National Physical Laboratory. *Met. Mag.*, 64, pp 7-8.
S.G. Smith, 1981: Comparison of wind speeds recorded by pressure-tube and Meteorological Office electrical cup generator anemographs. *Met. Mag.*, **110,** pp 288-300.
H.E. Whittingham 1964: Extreme wind gusts in Australia. Bureau of Meteorology Bulletin No. 46.

Appendix II-2

Modelling of the tubing response

John Holmes
P.O. Box 269, Mentone
Victoria 3194
www.jdhconsult.com

The response of the connecting tubing from the Dines anemometer head to the float chamber to sinusoidal pressure fluctuation was studied, using a well-established theory from the 1960s. It was found that the theory agreed quite well with the measured response, obtained in Task 3, of tubing of typical length and diameter used in Australian applications of the instrument, using a representative 'rigid' volume at the end of the tubing. However the frequencies at which significant amplification of the response by the tubing were found to be significantly greater than those of the float chamber, and hence the influence of the tubing on the anemometer response was judged to be quite small. This conclusion was confirmed by measurements carried out as part of Task 3.

Introduction

In the Dines anemometer system, as generally used in Australia, the anemometer (pitot) head which sensed the dynamic pressure of the wind (including the fluctuations generated by atmospheric turbulence) was connected by approximately 10 metres of tubing of 25mm (1 inch) internal diameter to the body of the anemometer. Similar tubing connected the static holes below the anemometer head to the anemometer base. However it is known that the fluctuations in static pressure in the atmosphere are lower in magnitude than those of the dynamic (pitot) pressure, and hence response aspects of the latter tubing are of much less significance.

Also of significance is the fact that the dynamic pressure line contains three fixed points or 'elbows' at which the line changes direction by 90 degrees. These provided 'restrictions' and could affect the dynamic response of the system.

It is also noted that earlier versions of the Dines system had tubing connections with longer lengths and smaller internal diameters. These differences may have had significant effects on the response of the system to fluctuating winds. However, it is believed that such non-standard tubing arrangements were not used in Australia.

To study the effect of the connecting tubing on the Dines anemometer response, the response of a fixed volume of 100 mm diameter and 225 mm length (i.e. 0.00177 m^3) connected to a fluctuating pressure source by connecting tubing was investigated theoretically in Task 2 and experimentally in Task 3. The volume approximates the internal volume of the float chamber of the Dines anemometer.

Theory

The theoretical modelling was carried out using the Bergh and Tijdeman (1965) theory (B-T), which is based on the response of a tube-volume system of known internal dimensions, to sinusoidal pressures; laminar fluctuating flow through the tubes is assumed. The Bergh and Tijdeman (1965) theory gives the ratio of pressure amplitude in the instrument volume to the input pressure amplitude as: gives the ratio of pressure amplitude in the instrument volume to the input pressure amplitude as:

$$\frac{p_1}{p_0} = \left[\cosh(\phi L) + \left(\frac{V_v}{V_t}\right)\left(\frac{1}{k}\right) n\phi L \sinh(\phi L)\right]^{-1} \qquad (2\text{-}1)$$

where V_v is the terminating volume

V_t is the volume of the connecting tubing

L is the length of the tubing

k is a polytropic constant for the volume

n is a complex 'polytropic factor' for the tubing, with an amplitude which takes a value between 1.0 and 1.4

ϕ is a complex 'wave number' depending on the tube diameter, the ratio of specific heats, thermal conductivity, viscosity, static pressure and density of air, as well as the frequency of the pressure fluctuations.

Calculations for connecting tubing for the Dines anemometer

Calculations using the B-T theory for a length of tubing 10 metres long, 30 mm diameter and a terminating rigid volume of internal diameter 100 mm, 225 mm long, giving a volume of 0.00177 m^3 were compared with experimental data obtained using the PLA. This system was not intended to replicate the Dines system exactly. In particular, the effective volume inside the Dines float varies with the mean wind speed, and there is an additional effective volume which is dependent on the 'flexibility' of the system. Comparison of the measured tubing amplitude frequency response with the calculated response is shown in Figure 2-1.

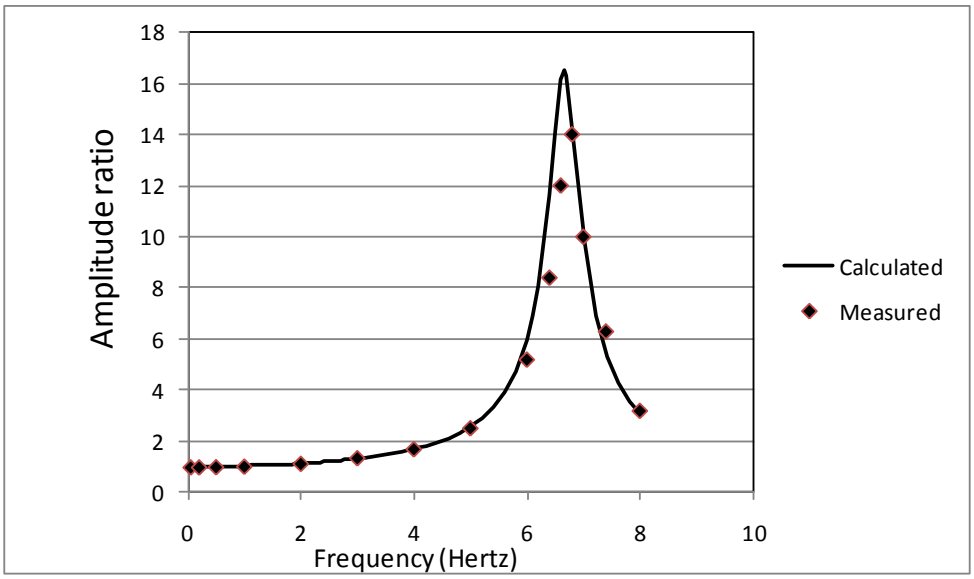

Figure 2-1. Calculated amplitude response for a system with 10m long and 30mm diameter connecting tubing

Figure 2-1 shows that good agreement is obtained. The experiments and the theory both indicate a resonant frequency of 6.6 to 6.8 Hertz. Clearly the resonant frequency resulting from the tubing is much higher than those associated with the float movement (0.5 to 1.5 Hertz), as shown in Task 3. Hence, *it can be concluded that resonance in the tubing typically used in the Dines anemometer system in Australia, has negligible effect on the response of the anemometer system*.

The good agreement between theory and experiment implies that the fluctuating flow in the tubing is laminar, an inherent assumption of the B-T theory, but contradicting a conclusion by Sanuki (1952) that the flow is turbulent.

Figure 2-2 shows the effect of the internal diameter of the tubing on the resonant frequency, and the maximum amplitude ratio at that frequency. It can be seen that both increase with increasing tubing diameter.

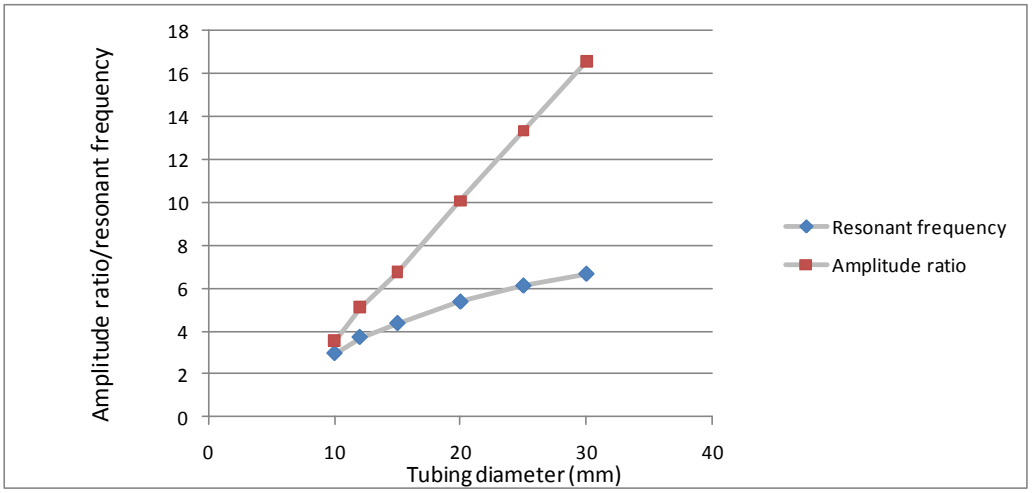

Figure 2-2. Effect of tubing internal diameter on resonant frequency and maximum amplitude (tube length: 10m; terminating volume: 0.00177 m^3)

It was also of interest to calculate the response of a system with *30m* (100 feet) of tubing of 25mm (1-inch) internal diameter, as used in the tests at NPL recorded by Giblett (1932) and reported later by Whittingham (1964). The amplitude response (to sinusoidal excitation) is shown in Figure 2-3, plotted to the same scale as Figure 2-1.

Figure 2-3 indicates resonant peaks of both lower amplitude and frequency than those for 10m long tubing. The lowest resonant frequency of 2.4 Hertz is much closer to those of the float frequencies, with the potential for some interactions. Thus, there may be some effect of a 30 metre length of connecting tubing on the response of the anemometer float system to fluctuating winds and dynamic pressures, even though a 10 metre length (or shorter) has a negligible effect.

Summary

The main conclusion of this part of the project is that the connecting tubing used on Dines anemometers in Australia, consisting of about 10 metres of tubing of 25-30mm internal diameter, has resonant frequencies considerably in excess of those of the float system. Over the range of the float frequencies the amplitude ratio in Figure 2-1 are very close to 1.0, and hence there should be negligible effect of the tubing on the overall system response. This has been confirmed by the direct measurements in this project reported elsewhere (Task 3).

Good agreement between theoretical predictions, based on laminar fluctuating flow, of the frequency response of tubing typical of that used in the Dines system with experiments, leads to the conclusion that the flow in the tubing system is essentially laminar. This contradicts a conclusion of Sanuki (1952), who suggested that the flow would be better modelled as turbulent flow.

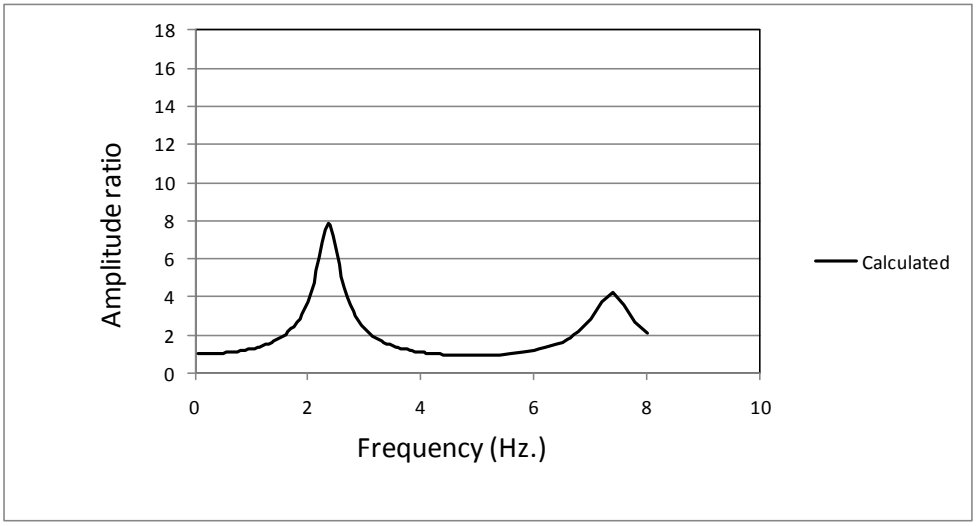

Figure 2-3. Calculated amplitude response for a system with 30m long and 25mm diameter connecting tubing (terminating volume: 0.00177 m^3)

References

H. Bergh and H. Tijdeman, 1965: Theoretical and experimental results for the dynamic response of pressure measuring systems. National Aero- and Astronautical Research Institute, Netherlands, Report NLR-TR F.238.

M.A. Giblett, 1932: The structure of wind over level country. Geophysical Memoirs 63, Meteorological Office U.K.

M. Sanuki, 1952: A new development of the theoretical and experimental lag of Dines pressure tube exposed in fluctuating winds. *Papers in Meteorology and Geophysics*, **3,** 115-124.

H.E. Whittingham 1964: Extreme wind gusts in Australia. Bureau of Meteorology Bulletin No. 46.

Appendix II-3

Statistical comparison of peak velocities recorded by Dines, cup and sonic anemometers using time histories

John Holmes
P.O. Box 269, Mentone
Victoria 3194
www.jdhconsult.com

Methodology

As part of Task 3, a state-of-the-art 'Pressure Loading Actuator' (PLA) was used to simulate accurately the actual pressure fluctuations resulting from turbulent velocities recorded by a sonic anemometer. The float movement (directly proportional to peak velocities) of a standard ('low-speed') Dines system was driven by the PLA using a pressure-time history derived from the sonic anemometer time history. The peak deflections of the float, calibrated to be directly proportional to the wind speed, were compared with the peaks recorded by the sonic anemometer, and the peaks arising from a simulated cup-anemometer response obtained by applying an exponential moving average filter to the sonic anemometer time histories.

The digitized time history from the sonic anemometer, with a mean wind speed of about 10 m/s was re-scaled, in both magnitude and time, to a mean wind speed of 25 m/s, this being more representative of the conditions producing extreme wind gusts of interest in structural design, and noting that the dynamic characteristics of the Dines float system change with wind speed. The time scale was adjusted by factoring the time increment by 10/25, to preserve turbulence length scales in the time history.

The digitized wind speed was then converted to a dynamic pressure, and supplied as a control signal to the PLA. The latter was connected through a manifold to the Dines head, and hence via 10 metres of piping, of 30 mm internal diameter, to the Dines float system. The vertical movement of the float was measured with a Linear Variable Differential Transformer (LVDT), and scaled to give the effective wind velocity, as 'seen' by the Dines anemometer. Details of the experimental set-up, calibrations, and some other results, including the response to sinusoidal pressure variations, are described in the report on Task 3

To simulate the response of a cup anemometer, the sonic anemometer time history was filtered with a moving exponential average filter with a time constant corresponding to the distance constant of the Synchrotac 706 3-cup anemometer currently used by the Bureau of Meteorology. Since the cup anemometer can be closely modelled as a first-order dynamic system, the distance constant can be defined as the time taken for the anemometer to respond to 63% of a step change in velocity, (i.e. (1-e) expressed as a percentage). The value of distance constant for the Synchrotac 706 is 13 metres (personal communication – J. Gorman, BoM). At a mean wind speed of 25 m/s, the equivalent time constant is 13/25 = 0.52 seconds.

Sixteen local maxima were selected from the Dines time history and compared with the closest maxima derived from the sonic anemometer and from the simulated cup-anemometer record, as discussed above. Ratios of these peaks were calculated and compared, as a comparison of the formerly-used Dines type, and the current cup anemometer, and an indication of the ability of both types to measure the 'true' gust peak as assumed to be recorded by the sonic anemometer system.

Results and Discussion

Figure 4 shows parts of the time histories of the Dines anemometer, and of the simulated cup anemometer traces, with some of the peaks selected for comparison. The identified peak velocities and the ratios between the Dines peak and the corresponding ones expected to be recorded by the cup anemometer system are shown in Table 1. Also shown are the ratios of the Dines peak to the 'true' peak gust recorded by the sonic anemometer.

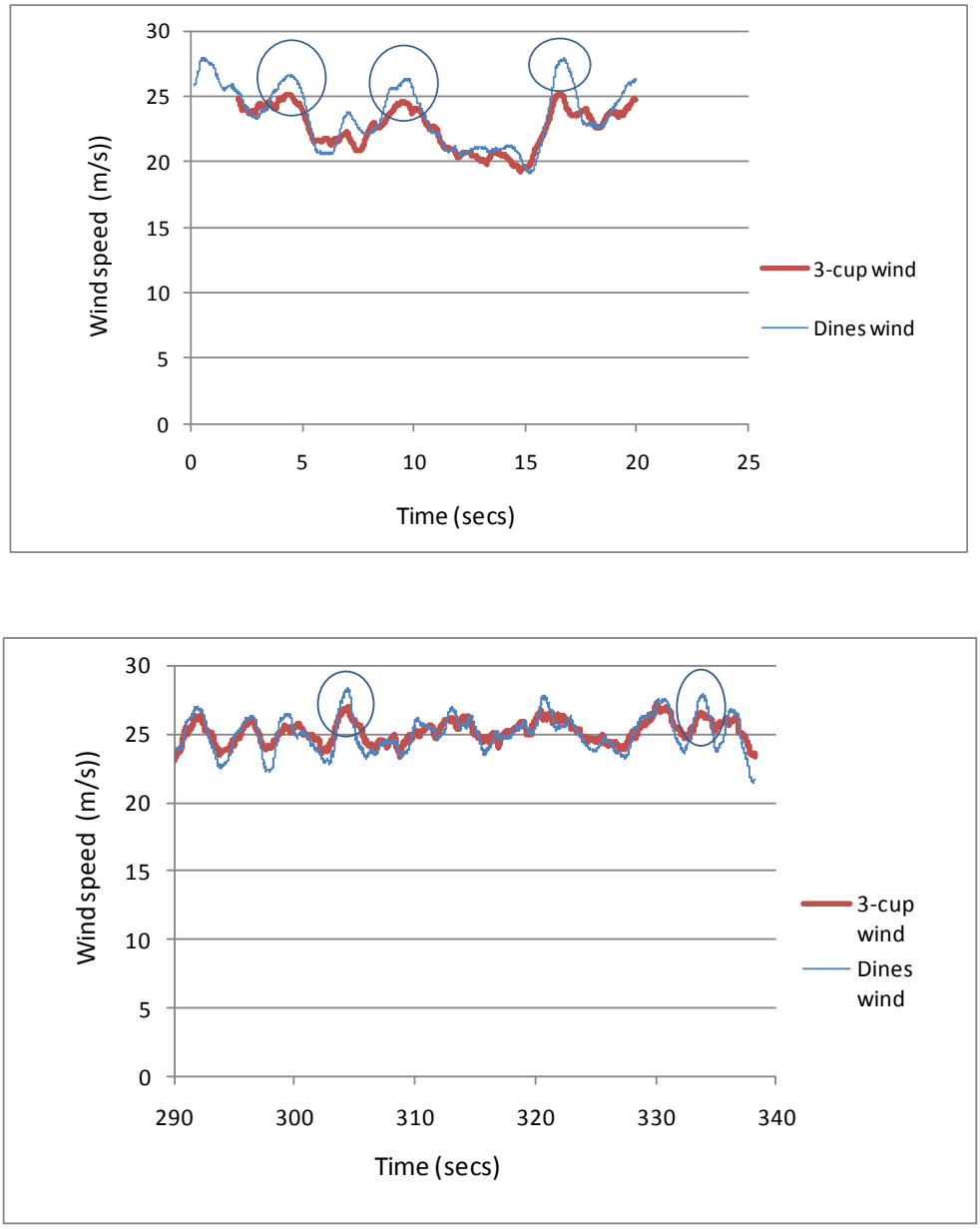

Figure 4. Extracts from wind-speed (ordinates in m/s) versus time (in seconds) histories of the Dines anemometer (blue) and of the cup anemometer (red), showing peaks selected for comparison

Table 1. Comparison of peaks recorded by different anemometer types

Peak No.	Sonic (m/s)	Simulated 3-cup	Dines	Dines/cup	Dines/sonic
1	28.65	25.17	26.32	1.045	0.919
2	26.79	24.61	26.36	1.071	0.984
3	28.45	25.03	26.77	1.070	0.941
4	30.40	27.04	28.79	1.065	0.947
5	32.45	28.70	30.75	1.072	0.948
6	32.05	28.64	30.00	1.047	0.936
7	30.40	26.47	27.57	1.042	0.907
8	28.45	26.29	27.52	1.047	0.967
9	30.58	28.07	29.67	1.057	0.970
10	31.47	28.04	29.41	1.049	0.934
11	31.93	28.79	30.24	1.050	0.947
12	30.70	27.00	28.82	1.067	0.939
13	28.71	26.41	27.31	1.034	0.951
14	28.97	26.05	27.09	1.040	0.935
15	29.97	26.96	28.30	1.049	0.944
16	28.97	26.57	27.90	1.050	0.963
Average	29.93	26.87	28.30	**1.053**	**0.946**

Table 1 shows that, for the time history of turbulence used for comparison, the Dines anemometer would have recorded peak gusts on average about 5% higher than the cup anemometer (Synchrotac 706) predominantly used with Automatic Weather Stations in Australia. This result is similar to that obtained by Logue (1986), using direct measurements of peaks from a Dines and a cup anemometer (of different type but with a similar distance constant), in atmospheric turbulence. On the other hand, the Dines would have under-predicted the sonic anemometer peaks by about 5%, for the range of peak gusts (26 to 32 m/s) compared in the time histories.

The anemometer record used for comparison had a turbulence intensity (as recorded by the sonic anemometer) of 9%. Such a value is a reasonable one for thunderstorm downdraft outflows, which probably account for more than 50% of the daily maximum gusts in Region A in Australia. However, for synoptic winds at the standard measurement conditions of 10 metres height in flat, open country, the turbulence intensity would be higher - about 20%.

To simulate the effect of a higher turbulence intensity on the ratios in Table 1, the peak velocities were re-scaled to a turbulence intensity of 20%, by subtracting the mean value (about 25 m/s), multiplying by 0.2/0.09, and then adding back the mean value. This process resulted in an average peak ratio (Dines to cup) of about 1.10.

In summary, direct measurements of the response of the low-speed Dines system using a state-of the-art pressure actuator, driven by an actual turbulent wind record, indicates an ‘overshoot’ of peaks with respect to the standard cup anemometer currently in use by the BoM of 5-11%. However, with respect to the sonic anemometer, the Dines system ‘undershoots’ the peaks by 5-10%, for the magnitude of gusts studied.

Other work for this project shows that the response of the Dines anemometer is dominated by the resonant response frequencies of the float system, particularly the first mode (although any vibrations are heavily damped). Present measurements indicate that the first-mode frequency of the low-speed type is about 0.5 Hertz, about half that measured at N.P.L. in the 1930s, and reported by Whittingham (1964).

Finally, a comment can be made about the 'effective gust duration' of the various types of anemometer. Using Whittingham's (1964) definition based on the reciprocal of the half-power frequency (also advocated recently by Miller (2007)), an 'effective gust duration', T, can be related to the time constant, or effective moving averaging time, τ, by the following (for a first-order measurement system):

$$T \cong 2\pi\,\tau = 2\pi\,(\delta/U) \qquad (1)$$

where δ is the distance constant of the anemometer.

It should be noted, however, that the World Meteorological Organization (Beljaars, 1987a) following Beljaars 1987b), has defined a 'gust duration' as equivalent to the moving average time, τ. Thus Beljaar's (1987b) definition is as follows:
'An arbitrary measuring chain produces gusts with duration t_G if the same peak factor is obtained with a moving average filter with $\tau = t_G$.'
(The terminology and symbols have been changed slightly to suit those used in this report – however the meaning is the same)

Based on the current work, the 'gust duration' (according to Beljaar's definition) of the Dines anemometer at the same wind speed, is about 0.2 seconds; however, Miller's 'effective gust duration' is about 1.3 seconds, about half that suggested by Whittingham (1964).

A Synchrotac 706 3-Cup anemometer at a wind speed of 25 m/s, with a distance constant of 13 metres, gives an 'effective gust duration'(based on Miller's definition), T, of 2π (13/25), or 3.3 seconds. However, the 'gust duration', based on Beljaar's definition, is (13/25), about 0.5 seconds.

Notwithstanding this, the Bureau of Meteorology has applied a further digital 3-second moving average filter to the output of the cup anemometers in the automatic weather stations. The effect of this filter on the response can be seen in Figure 5, in which simulated time histories of the cup anemometer, with and without the filter applied, are shown. The effect of the 3-second moving average on the measured peak gusts is discussed in Appendix II-4.

References

A.C.M. Beljaars, 1987a: The measurement of gustiness at routine wind stations – a review, Instruments and Observing Methods Report, WMO-No.31, World Meteorological Organization Geneva.
A.C.M. Beljaars, 1987b: The influence of sampling and filtering on measured wind gusts. Journal of Atmospheric and Oceanic Technology, Vol. 4, 613-626.
C.A. Miller, 2007: Defining the effective duration of a gust. presented at the 12th International Conference on Wind engineering, Cairns, July 1-6, 2007.
H.E. Whittingham 1964: Extreme wind gusts in Australia. Bureau of Meteorology Bulletin No. 46.

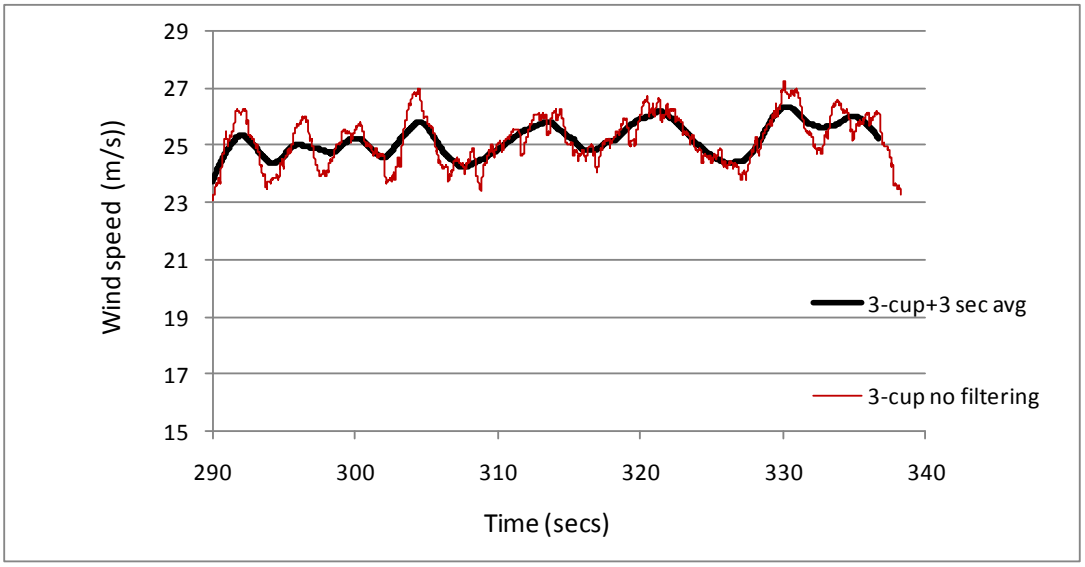

Figure 5. Simulated time histories of the cup anemometer output with no filtering (red), and with 3-second moving average filtering applied (black)

Appendix II-4

Gust factors for Dines and cup anemometers using the spectral approach

John Holmes
P.O. Box 269, Mentone
Victoria 3194
www.jdhconsult.com

Introduction

Random process and linear systems theory has been used to predict the wind gust factors recorded by 3-cup and Dines anemometers in a turbulent wind of known turbulence intensity and spectral density. This approach is similar to that previously applied to cup anemometers by Davenport (1964) and Beljaars, 1987). In the present work, the methodology has also been applied to study the average gust factors produced by the Dines anemometer.

Methodology

The procedure used was as follows:

1) The spectral density of the wind turbulence was modelled using the well-known von Karman form, which, in non-dimensional form, can be written as follows:

$$\frac{n.S_u(n)}{{\sigma_u}^2} = \frac{4\left(\frac{n\ell_u}{\overline{U}}\right)}{\left[1+70.8\left(\frac{n\ell_u}{\overline{U}}\right)^2\right]^{5/6}} \qquad (1)$$

where ℓ_u is an integral length scale, and σ_u is the standard deviation of turbulence which can be obtained from the mean wind speed and the intensity of turbulence (i.e. $\sigma_u = I_u \times \overline{U}$).

2) The effect of the anemometer is incorporated by multiplying the spectral density by a transfer function $|H_1(n)|^2$, (see Davenport, 1964). In the case of the 3-cup anemometer, the transfer function can be represented by:

$$|H_1(n)|^2 = \frac{1}{1+\left(\frac{2\pi nD}{\overline{U}}\right)^2} \qquad (2)$$

where D is the distance constant for the anemometer.

3) Following the suggestion of Beljaars (1987), and the recommendations of the World Meteorological Orgnization (WMO, 2008), the Bureau of Meteorology also applies a 3-second moving average filter to the output of the cup anemometers. This process is represented in the frequency domain by the following transfer function:

$$|H_2(n)|^2 = \left(\frac{\sin(n\pi\tau)}{(n\pi\tau)}\right)^2 \qquad (3)$$

where τ is the moving average time, in this case equal to 3 seconds.

Then the combined transfer function for the filtered cup anemometer is:

$$|H(n)|^2 = |H_1(n)|^2 . |H_2(n)|^2 \tag{4}$$

4) The cycling rate or 'average frequency', υ, of the filtered process can be calculated as follows.

$$\upsilon = \left\{ \frac{\int_0^\infty n^2 . S_u(n). |H(n)|^2 dn}{\int_0^\infty S_u(n). |H(n)|^2 dn} \right\}^{1/2} \tag{5}$$

5) The expected peak factor can then be calculated using the well-known formula for Gaussian processes of Davenport (1964):

$$g = \sqrt{2 log_e \upsilon T} + \frac{\gamma}{\sqrt{2 log_e \upsilon T}} \tag{6}$$

where γ is Euler's Constant (0.5772), and T is the sample time for which the expected peak is to be determined.

4) Finally the expected gust factor is obtained from:

$$G = 1 + g \sigma_{u,f} / \overline{U} \tag{7}$$

where $\sigma_{u,f}$ is the standard deviation of the filtered process given by:

$$\sigma_{u.f} = \left\{ \int_0^\infty S_u(n). |H(n)|^2 dn \right\}^{1/2} \tag{8}$$

Transfer functions for the Dines anemometer

For the Dines anemometer, experimental data on the transfer function is available from excitation of the Dines float system with both sinusoidal and random 'white' noise, using the pressure-load actuator (PLA). These transfer functions show a dominant low-frequency peak at about 0.3 Hertz (high speed Dines anemometer) or 0.5 Hertz (low-speed Dines). Although there is some experimental evidence that the transfer function varies slightly with the mean dynamic pressure and hence the mean wind speed, the modelling by Kepert (Appendix II-5,'Modelling of the transient response of the Dines anemometer') indicates little change in the frequency of the dominant low frequency peak with mean wind speed. Kepert found a significant increase in the frequency of the second mode with increasing mean wind speed, however this minor peak has been found to have a negligible effect on the computed gust factors in the following.

The transfer functions assumed for the calculations for low- and high-speed versions of the Dines anemometer, (based on data generated by C.A. Miller, January 2011), are shown in Figures 1 and 2, respectively. The transfer function for the low-speed Dines anemometer (Figure 1) was obtained from three runs with a mean pressure of 0.75 kiloPascals, equivalent to a mean wind speed of 29 m/s. The transfer function for the high-speed Dines anemometer, in Figure 2, was obtained with a mean

pressure of 1.0 kiloPascals, equivalent to a mean wind speed of 33 m/s. Although these were obtained experimentally for the defined mean pressures, and equivalent wind speeds, they have been assumed to be applicable for all mean wind speeds for the purposes of the calculation of gust factors and gust ratios shown following. However alternative calculations, in which frequency shifting of the transfer function was assumed (in proportion to the square root of the mean wind speed), indicated very little change in the computed gust ratios.

Comparison of gust factors and gust ratios

Using the above methodology, the expected gust factors for wind speeds recorded by a cup anemometer (Synchrotac 706 cup anemometer), and the low-speed Dines anemometer, were calculated for the following values:

$\bar{U}$ = 25 m/s; I_u = 0.09; ℓ_u = 120 m; D = 13 m; T = 600 seconds.

The value of ℓ_u of 120 metres is that specified in Equation 6.2(3) in Australian Standard AS/NZS1170.2:2011, for a height of 40 metres.

The spectral density as modified by the cup anemometer (but not filtered by a 3-second moving average) is shown in Figure 3.

The spectral density as modified by the low-speed Dines anemometer is shown in Figure 4.

The results of the calculations from the modified spectra are summarized in the following table.

Table I.

	Cup	Dines (low-speed)
Cycling rate (Hz)	0.140	0.255
Std. Devn (m/s)	2.027	2.172
Peak factor	3.17	3.35
Gust factor	1.257	1.291

It can be seen that the Dines anemometer gives a higher cycling rate, peak factor and gust factor as a result of the resonance in the float system, with a dominant frequency of about 0.5 Hertz.

A typical spectral density of the apparent wind speed recorded by the high-speed Dines anemometer is shown in Figure 5. The effect of the lower resonant frequency, and higher peak, compared with that for the low-speed anemometer in Figure 4 is clearly evident.

The ratio of expected peaks of the Dines anemometer to the 3-cup can be obtained from the ratio of gust factors. Thus, for the above conditions, this ratio is predicted to be 1.291/1.257, or 1.027. This value compares with the average ratio of 1.053 obtained directly by driving the Dines float with recorded wind velocity data converted to pressure through the PLA, and simulating the cup anemometer response with an exponential averaging filter (Appendix II-3).

Comparison with measurements of Logue (1986)

Logue (1986) compared mean and gust speeds measured with a Dines pressure-tube anemometer and a Munro Mark II cup anemometer located together at Galway on the west coast of Ireland for the whole year in 1984. The mean wind speeds from the two instruments generally agreed well. However, for wind speeds exceeding 28 m/s (55 knots) the Dines read maximum gusts 5.6% higher

on average than those from the cup anemometer. The distance constant for the U.K. Mark 2 cup anemometer is 12 metres (Sparks, 1996, 1997, communicated by C.A. Miller). As an indicator of the turbulence intensities at the site, Figure 1 in the Logue paper indicates a mean gust factor as recorded by the Dines anemometer, of about 1.7.

The following table shows the computed gust ratios, using the random process approach, for the conditions in the Logue study. The other parameters were taken the same as in the previous example.

Table II.

Mean wind speed	Turbulence intensity	Gust factor (ls. Dines)	Gust factor (Mk 2 cup)	Max. gust (cup) (m/s)	Overshoot ratio
17	0.22	1.711	1.612	27.4	1.061
20	0.22	1.711	1.622	32.4	1.055
25	0.22	1.712	1.635	40.9	1.048
				Average	**1.055**

The average gust ratio of 1.055 in the above table compares favourably with the average gust ratio of 1.056 (1/0.947) found by Logue for gusts greater than 55 knots (28 m/s).

It should be noted that this comparison does not include the effect of a 3-second digital moving average, which was not applied to the cup anemometer data in the Logue study. Thus $|H_2(n)|^2$ in Equ. (4) was taken as 1.0. However, the 3-second averaging is incorporated in the Dines-cup anemometer comparisons described following.

Evaluation of average peak gust ratios for Dines anemometer and cup anemometer

The following tables summarize the results of comparing gust factors and gust ratios for the low- and high-speed Dines anemometer with the Synchrotac 706 cup anemometer. For the latter case, gust ratios both with and without the 3-second average digital filtering are shown.

Table s III and IV show the following features:

- The overshoot ratio for the high speed Dines anemometer is greater than that for the low-speed Dines, for the same mean wind speed and turbulence intensity.
- The overshoot ratio increases with increasing mean wind speed, but relatively slowly.
- The overshoot ratio increases significantly with increasing turbulence intensity.
- The effect of the 3-second moving average filter applied to the cup anemometer output is to increase the overshoot ratio considerably – approximately doubling the increment at lower wind speeds, and trebling it at higher wind speeds. The reason for this can be seen in Figure 6, which show the effect of the 3-second averaging filter on the spectral density of the windspeed when compared with Figure 3. The high-frequency end is the spectrum is effectively truncated by the combined effect of the anemometer response and the filter.

Table III. Overshoot ratios for Low-speed Dines versus Synchrotac 706 with 3-sec averaging

Mean wind speed	Turbulence intensity	Avg. Gust factor (ls. Dines)	Avg. Gust factor (cup with 3s filter)	Max. gust (cup) (m/s)	Overshoot ratio	Overshoot Ratio (no 3s filter on cup)
20	0.10	1.3234	1.240	24.8	**1.068**	1.034
25	0.10	1.3238	1.237	30.9	**1.070**	1.030
30	0.10	1.3241	1.234	37.0	**1.073**	1.026
35	0.10	1.3242	1.231	43.1	**1.076**	1.023
20	0.15	1.4851	1.359	27.2	**1.092**	1.046
25	0.15	1.4857	1.356	33.9	**1.096**	1.040
30	0.15	1.4861	1.352	40.5	**1.100**	1.035
35	0.15	1.4863	1.347	47.1	**1.104**	1.031
20	0.20	1.6467	1.479	29.6	**1.113**	1.056
25	0.20	1.6477	1.475	36.9	**1.117**	1.049
30	0.20	1.6482	1.469	44.1	**1.122**	1.043
35	0.20	1.6484	1.462	51.2	**1.127**	1.038

Table IV. Overshoot ratios for High-speed Dines versus Synchrotac 706 with 3-sec averaging

Mean wind speed	Turbulence intensity	Avg. Gust factor (hs. Dines)	Avg. Gust factor (cup with 3s filter)	Max. gust (cup) (m/s)	Overshoot ratio	Overshoot Ratio (no 3s filter on cup)
30	0.15	1.520	1.352	40.5	**1.124**	1.059
35	0.15	1.522	1.347	47.1	**1.130**	1.056
40	0.15	1.523	1.342	53.7	**1.135**	1.053
45	0.15	1.524	1.336	60.1	**1.141**	1.051
50	0.15	1.525	1.331	66.6	**1.146**	1.049
30	0.20	1.693	1.469	44.1	**1.153**	1.071
35	0.20	1.696	1.462	51.2	**1.160**	1.068
40	0.20	1.698	1.455	58.2	**1.166**	1.065
45	0.20	1.699	1.449	65.2	**1.173**	1.062
50	0.20	1.700	1.442	72.1	**1.179**	1.059
30	0.25	1.866	1.586	47.6	**1.177**	1.082
35	0.25	1.870	1.578	55.2	**1.185**	1.077
40	0.25	1.872	1.569	62.8	**1.193**	1.074
45	0.25	1.874	1.561	70.2	**1.201**	1.070
50	0.25	1.875	1.552	77.6	**1.208**	1.067

Conclusions

The random process approach to gust factors and Dines/cup gust ratios gives good agreement with independently obtained values of gust ratios, and easily enables adjustment for varying parameters, such as mean wind speed, turbulence intensity, turbulence length scale, and the distance constant of the cup anemometer.

The approach has been applied to comparisons of the average gust factors and gust ratios recorded by the Dines and those expected from the type of cup anemometer currently used by the Bureau of Meteorology in their Automatic Weather Systems, with the 3-second moving average filter applied. As a result of the analysis, significant 'overshoots' in measured gust wind speeds are expected to occur – up to 13% for the low-speed Dines, and up to 21% for the high-speed Dines. These are compatible with statistical analyses by Geoscience Australia, and with anecdotal evidence from individual stations in the cyclone regions, where the instruments have operated in parallel.

References

A.C.M. Beljaars, 1987b: The influence of sampling and filtering on measured wind gusts. *Journal of Atmospheric and Oceanic Technology*, Vol. 4, 613-626.

A.G. Davenport, 1964: Note on the distribution of the largest value of a random function with application to gust loading, *Proc., Institution of Civil Engineers (U.K.)*, Vol. 28**,** 187-196.

E. Gold, 1936: Wind in Britain – The Dines anemometer and some notable wind records during the last 40 years, *Q. J. Roy. Meteor. Soc.*, Vol. 62, 167-206.

J.D. Holmes and D.J. Henderson, 2010: Comparison of peak velocities recorded by Dines, cup and sonic anemometers", Workshop on Southern Hemisphere Extreme Winds, Canberra, August 4, 2010.

J.J. Logue, 1986: Comparison of wind speeds recorded simultaneously by a pressure-tube anemograph and a cup-generator anemograph, *Met. Mag.*, Vol. 115, 178-185.

W.R. Sparks, 1996: The response of the Munro MK IV and Munro MK II anemometers and associated chart recorders to changes of wind speed, Final report, July 1996, UK Met Office.

W.R. Sparks, 1997: Equations of motion for Munro anemometers, Technical Report No. 11, UK Met Office. Observations (Logistics and Automation).

Standards Australia, 2011: Structural design actions. Part 2: Wind actions, Australian-New Zealand Standard, AS/NZS1170.2:2011.

WMO, 2008: Guide to meteorological instruments and methods of observation, 7th Edition, WMO-No. 8, World Meteorological Organization, Geneva.

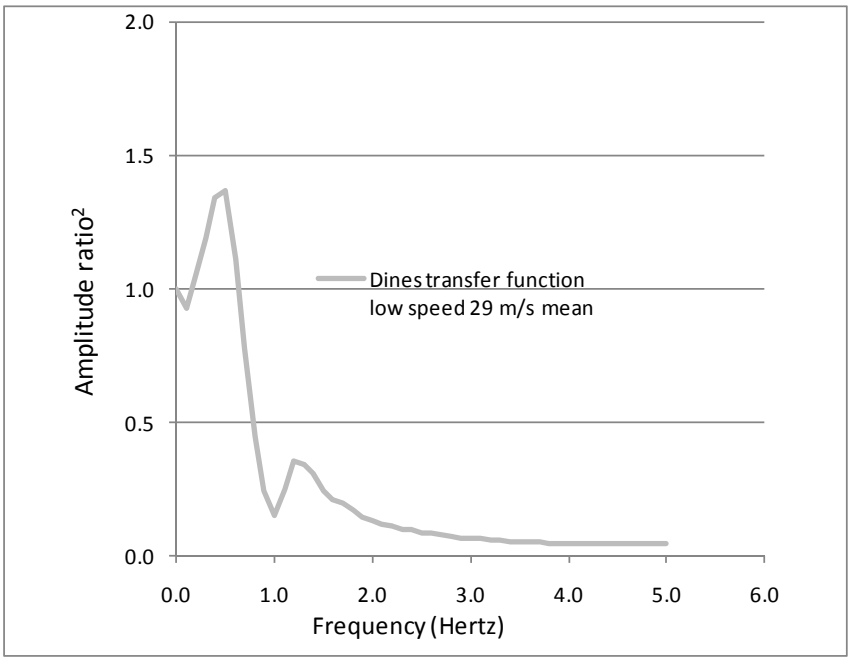

Figure 1. Transfer function for low-speed Dines – mean wind speed of 29 m/s (mean pressure of 0.75 kPa)

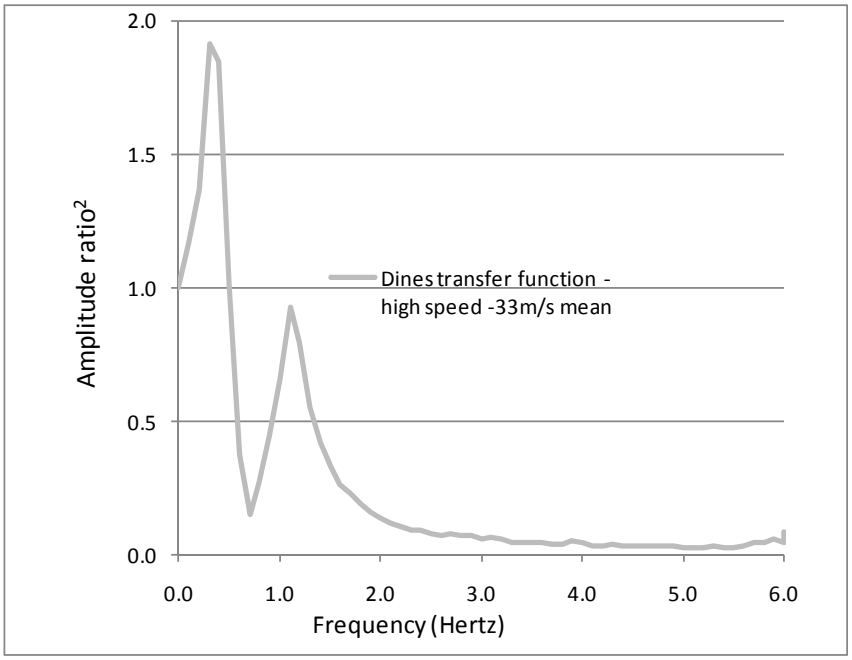

Figure 2. Transfer function for high-speed Dines – mean wind speed of 33 m/s (mean pressure of 1 kPa)

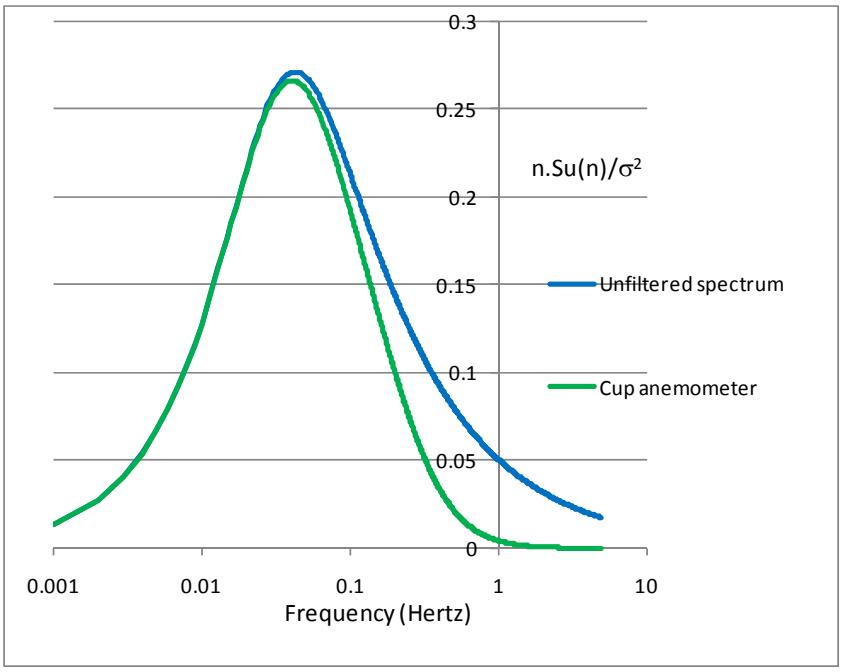

Figure 3. Spectral density as modified by the cup anemometer – mean wind speed of 25 m/s

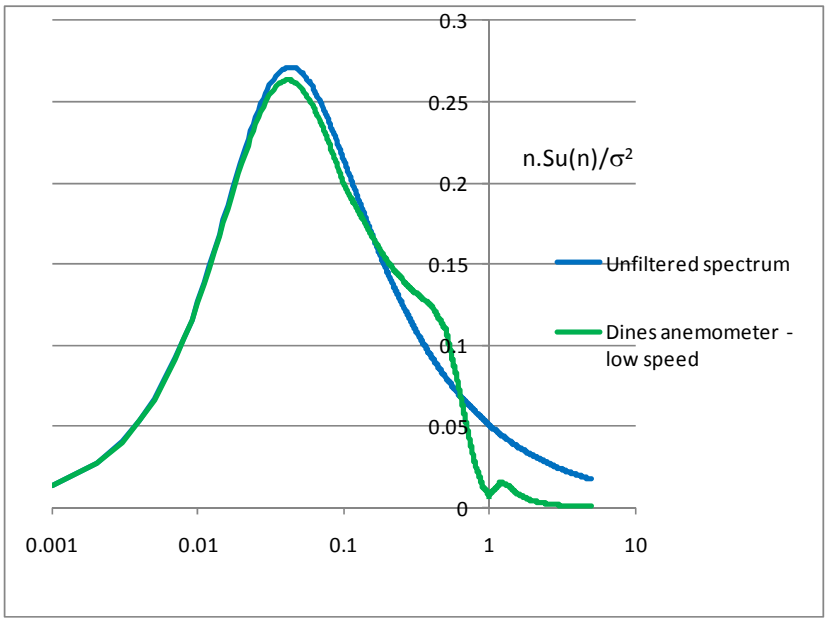

Figure 4. Spectral density as modified by the low-speed Dines anemometer – mean wind speed of 25 m/s

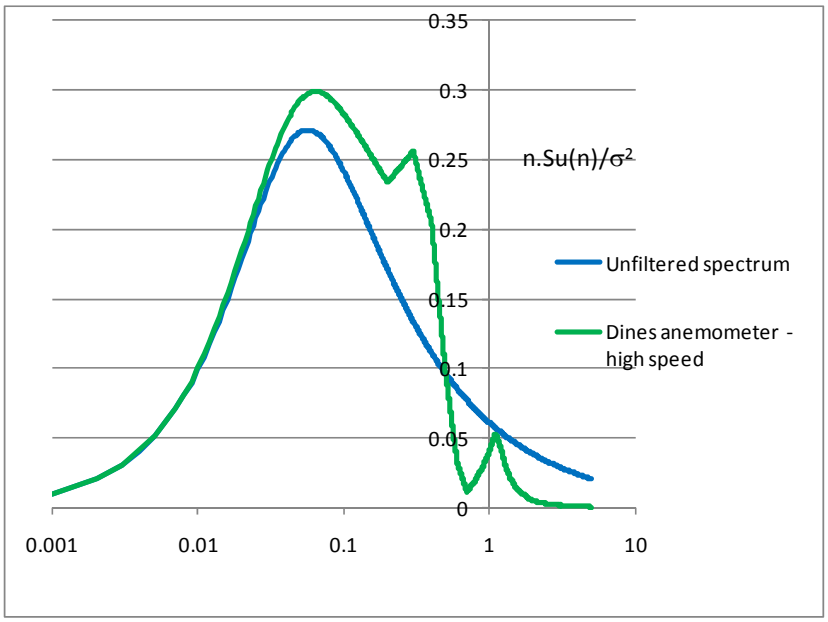

Figure 5. Spectral density as modified by the high-speed Dines anemometer – mean wind speed of 33 m/s

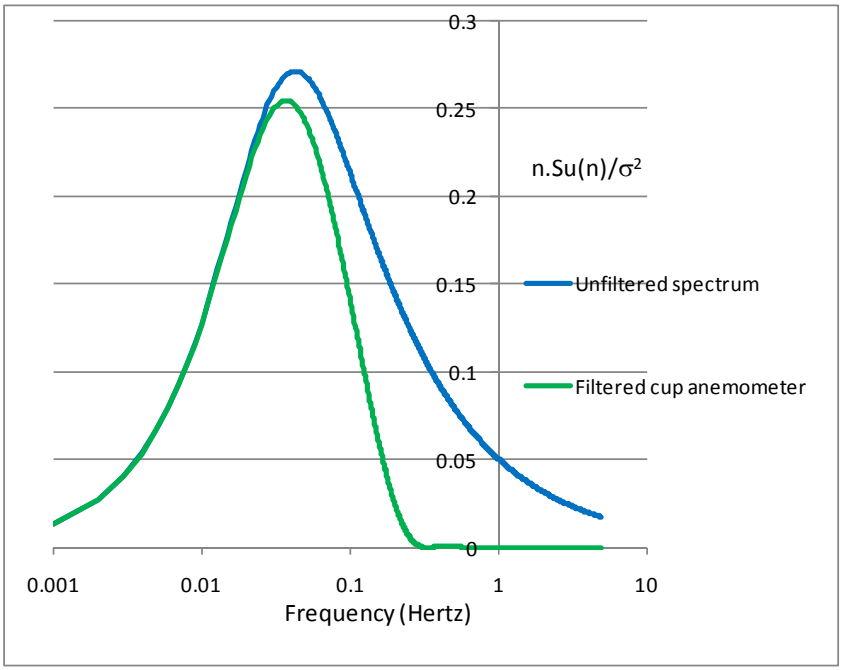

Figure 6. Spectral density as modified by Synchrotac 706 cup anemometer, filtered by a 3-second moving average filter – mean wind speed of 25 m/s

Appendix II-5: Modelling the Transient Response of the Dines Anemometer

Jeffrey D. Kepert
Centre for Australian Weather and Climate Research,
Bureau of Meteorology,
700 Collins St,
Melbourne Vic 3000.
Email: J.Kepert@bom.gov.au

April 28, 2011

1. Introduction

This report details the development of a physical model of the Dines anemometer float chamber, that can be used to study the response of the anemometer to unsteady forcing, specifically that provided by a turbulent wind field. Two models of the Dines anemometer float chamber are described, one simplified and one incorporating nearly complete physics. Linear and numerical solutions were obtained of the simplified model, showing that there are two resonances, in which the float and water move either in- or out-of-phase. The linear and numerical solutions are in good agreement for low-amplitude oscillations. Higher amplitudes result in the occurrence of additional resonances at harmonics and interharmonics of those from the linear analysis, but not in significant changes to the linear frequencies. Adding damping to this model provides good qualitative agreement with laboratory measurements. Damping of the relative motion of the float and water was found to be the most important damping mechanism for obtaining this good agreement.

Investigation of the more detailed model reveals that it has similar properties to that of the U-tube analogue, the main difference being that the variation of the resonant frequencies with wind speed is different. This change is because the effective spring constant varies with wind speed for different physical reasons.

The resonant frequencies of this model are in excellent agreement with observations, an agreement obtained without tuning – it is necessary only to insert the measureable physical dimensions and mass of the float and chamber into the model. Hence, the model is considered to reproduce the behaviour of the real anemometer to a high degree of accuracy.

The first model, with simplified geometry, is described in section 2. The second mode, which accurately represents the geometry of a real Dines anemometer, is presented in section 3.

2. Modelling the Float Chamber with Simplified Geometry

The manometer of the Dines anemometer has a complicated geometry, designed to produce a steady-state float displacement that is linear in the applied wind speed. This geometry complicates the analysis, so for convenience a simpler geometry will be assumed in this section.

This assumption is removed in section 3. In particular, the following simplifying assumptions are made:

1. The cross-sectional areas of the water inside and outside of the float are equal.
2. The float and containing vessel have parallel sides.
3. The pressure in the suction chamber is constant, or equivalently, the suction chamber is open to the atmosphere.
4. The movement of the float and liquid experience Newtonian damping with time-scales τ_1 and τ_2 respectively.
5. The relative motion of the float and liquid is Newtonian damped with time-scale τ_3, to represent the choke at the bottom of the float.

With these assumptions, the float chamber is *nearly* equivalent to a U-tube manometer with a frictionless piston supported by some trapped air in one arm, and forced by varying the amount of trapped air, as sketched in Fig 1. The piston represents the Dines float and the manometer liquid the water in the Dines float chamber. The trapped air between the piston and the manometer liquid corresponds to that inside the Dines float. It is assumed to compress isothermally, and acts as a spring between the two masses.

An important difference with the Dines manometer is that this system does not measure pressure. In a Dines manometer, the net upwards force on the float decreases as the float rises, because the area of the water surface in the bottom of the tapered float diminishes. In contrast, a parallel-sided float will rise indefinitely given an infinite supply of internal air at a fixed pressure, provided that the pressure is sufficient to lift the float. Hence the forcing in this system is better regarded as being the mass of trapped air, rather than its pressure. This simplification is helpful for understanding the transient response, but will be removed in section 3. The mass of air in the chamber will continue to be a key variable in the system, but this mass will be eventually governed by equations which describe the flow of air between the anemometer head and the chamber via the tubing.

A second difference is that the flow of the liquid around the bottom of the Dines float is possibly rather complex, while the analogous flow around the bend in the U-tube is much more simply modelled. In particular, the liquid will be assumed to move as a single mass.

The variables in the system are the positions and velocities of the piston and manometer liquid, (x_1, v_1) and (x_2, v_2) respectively, and the pressure p of the trapped air. The independent variables are the piston mass m_1, the tube area A, the amount of trapped air $c(t)$, the pressure of air in the suction chamger p_{env}, and the mass of the liquid $m_2 = 2x_eA\rho$ where x_e is the resting position of the liquid if the piston was removed and ρ is its density. All distances are measured along the tube from the bottom of the U; distances towards the piston side are positive.

The trapped air has mass m_a, pressure $p_{env} + p$ and density ρ_a. Combining the definition of density $m_a = (x_1 - x_2)A\rho_a$ with the gas law $p_e + p = \rho_a R_d T$ yields

$$c(t) \equiv R_d T m_a(t) = (p_{env} + p)A(x_1 - x_2)$$

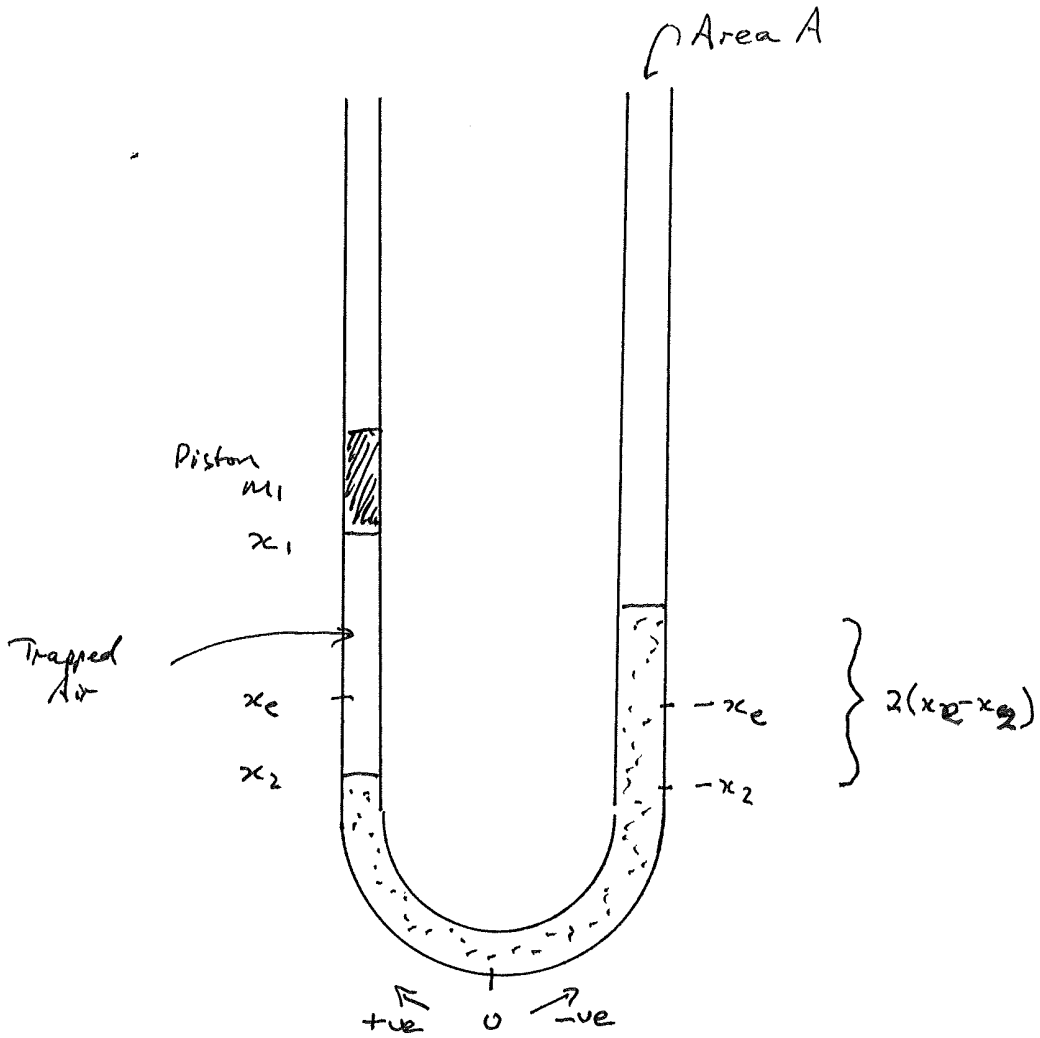

Figure 1: Sketch of the U-tube manometer with piston.

where R_d is the gas constant for dry air and T is the air temperature. We will use $c(t)$ as the principal forcing of the system.

The forces on the float are its weight gm_1, the upwards pressure of the trapped air pA, and friction which we model as a linear damping to zero with time scale τ_1, and a linear damping to the liquid motion with time scale τ_3. Newton's second law gives

$$m_1\dot{v}_1 = pA - gm_1 - m_1\tau_1 v_1 - m_1\frac{\tau_3}{2}(v_1 - v_2)\,.$$

The liquid motion is forced by the air pressure difference p between the chamber and outside, and by the hydrostatic pressure difference $2(x_e - x_2)\rho g$ due to the different liquid levels inside and outside of the float. A linear damping is again included. It is assumed that the water moves essentially as a solid mass, hence

$$2x_eA\rho\dot{v}_2 = -pA + 2(x_e - x_2)A\rho g - 2x_eA\rho\tau_2 v_2 - 2x_eA\rho\frac{\tau_3}{2}(v_2 - v_1)\,.$$

where $2x_eA\rho$ is the mass of the liquid. This last assumption is not unduly restrictive – if the channel through which the water moves is not of constant cross-section, then the greater mass per unit length in the wider sections will be exactly compensated by the lower acceleration experienced by water therein – it is the inertia that matters.

In summary, the equations governing the system are

$$x_1 - x_2 = \frac{c(t)}{A(p + p_{env})} \tag{1}$$

$$\dot{x}_1 = v_1 \tag{2}$$

$$\dot{v}_1 = \frac{pA}{m_1} - g - \tau_1 v_1 - \frac{\tau_3}{2}(v_1 - v_2) \tag{3}$$

$$\dot{x}_2 = v_2 \tag{4}$$

$$\dot{v}_2 = \frac{-pA + 2(x_e - x_2)A\rho g}{2x_eA\rho} - \tau_2 v_2 - \frac{\tau_3}{2}(v_2 - v_1) \tag{5}$$

Equation (1) is Boyle's law and (3) and (5) are Newton's second law. Equation (1) is used to eliminate pA from the remaining equations, leaving a set of four nonlinear coupled differential equations. Linear analytic solutions and numerical solutions (by fourth-order Runge-Kutta integration) will be obtained.

The equilibrium state of the system is found by solving $\dot{v}_1 = \dot{v}_2 = 0$ with $c = c_0$ constant, giving

$$x_{2e} = x_e - \frac{m_1}{2A\rho} \tag{6}$$

$$x_{1e} = x_{2e} + \frac{c_0}{gm_1} \tag{7}$$

Note that the equilibrium water level (6) is independent of c_0, as in a real Dines anemometer.

The *calibration* of the system, practically speaking, is the readings x_1 and x_2 that it would produce in response to steady forcing c_0, provided that sufficient time had elapsed for it to

reach equilibrium $v_1 = v_2 = 0$. In the absence of damping, total energy is conserved and so this state will never be met, but in reality, the anemometer will tend to this state. It is convenient to be able to discuss the calibration with respect to nonsteady forcing. Hence (6) and (7), the calibration equations of the system, will also be applied to nonsteady forcing $c(t)$, so as to compare the instantaneous readings of the instrument to that it would give in a steady state with that instantaneous forcing held constant. In particular, this interpretation is necessary for the analysis of "overshooting" and "undershooting" of gust measurements in unsteady flow.

The energy within the system is given by

$$E_K = \frac{1}{2} m_1 v_1^2 + x_e A \rho v_2^2 \tag{8}$$

$$E_{P,1} = m_1 (x_1 - x_{1e}) g \tag{9}$$

$$E_{P,2} = A\rho g \left[(x_2 - x_e)^2 - (x_{2e} - x_e)^2 \right] \tag{10}$$

$$E_{P,p} = c \log \left(\frac{x_1 - x_2}{x_{1e} - x_{2e}} \right) + p_{env} A [(x_1 - x_2) - (x_{1e} - x_{2e})] \tag{11}$$

representing respectively the kinetic energy E_K, the potential energies due to the positions of the piston $E_{P,1}$ and liquid $E_{P,2}$, and the potential energy due to the pressure of the trapped air $E_{P,p}$. . These potential energies are relative to the equilibrium states . The accuracy of the numerical solutions was checked by requiring them to conserve total energy $E_K + E_{P,1} + E_{P,2} + E_{P,p}$ to high accuracy in simulations with damping $\tau_1 = \tau_2 = \tau_3 = 0$.

2.1 *Undamped behaviour*

Some limiting, small-amplitude undamped cases are of interest. The first three are not very useful, but the fourth will turn out to explain much of the observed properties of the anemometer.

1. *Liquid stationary.* Then write $x_1 = x_2 + c/(gm_1) + \epsilon$, where the constant $c/(gm_1)$ is motivated by (7). Equations (2) and (3) with $\tau_1 = \tau_2 = \tau_3 = 0$ give

$$\ddot{\epsilon} = g \left(1 + \frac{g m_1}{c} \epsilon \right)^{-1} - g \tag{12}$$

$$\approx -\frac{g^2 m_1}{c} \epsilon \tag{13}$$

   which describes a simple harmonic oscillator with frequency

$$f_1 = g \sqrt{\frac{m_1}{c}}. \tag{14}$$

   This limit will also describe the motion of the piston relative to the liquid when the liquid is moving relatively slowly, or when the liquid is much more massive than the float. Physically, it is a mode in which the piston "bounces" on the trapped air.

2. *Piston mass negligible.* Equations (4) and (5) become

$$\ddot{x}_2 = -\frac{g}{x_e} x_2 + g \tag{15}$$

which in which the liquid oscillates with frequency

$$f_2 = \sqrt{\frac{g}{x_e}} \tag{16}$$

about mean position x_e. This is a gravitational mode.

3. *Piston and liquid move together* That is, $v_1 = v_2$, which is the same as the previous case, except that the oscillating mass has increased by m_1. The frequency is

$$f_3 = \left(\frac{2A\rho g}{2x_e A\rho + m_1} \right)^{1/2}. \tag{17}$$

This is also a gravitational mode.

4. *Coupled oscillations.* Consider oscillations of the form

$$x_1(t) = x_{1e} + \delta b e^{i\omega t} \tag{18}$$

$$x_2(t) = x_{2e} + \delta e^{i\omega t} \tag{19}$$

where $i^2 = -1$. That is, the piston and liquid are oscillating with the same frequency ω, and b describes the relative amplitude and phase of the oscillations. Substituting these equations into the governing equations (1) to (5), expanding as a Taylor series in δ and taking the first-order terms yields

$$bcm_1\omega^2 + (1-b)(gm_1)^2 = 0 \tag{20}$$

$$2Ac\rho(x_e\omega^2 - g) - (1-b)(gm_1)^2 = 0 \tag{21}$$

with solutions

$$\omega_1^2 = \frac{g^2\left(m_1^2 + 2Am_1\rho x_e + 2Ac\rho/g - \sqrt{8A\rho x_e m_1^3 + \left(m_1^2 - 2A\rho x_e m_1 + 2Ac\rho/g\right)^2}\right)}{4Ac\rho x_e} \tag{22}$$

$$b_1 = \frac{\left(m_1^2 - 2A\rho x_e m_1 + 2Ac\rho/g + \sqrt{8A\rho x_e m_1^3 + \left(m_1^2 - 2A\rho x_e m_1 + 2Ac\rho/g\right)^2}\right)}{2m_1^2} \tag{23}$$

and

$$\omega_2^2 = \frac{g^2\left(m_1^2 + 2Am_1\rho x_e + 2Ac\rho/g + \sqrt{8A\rho x_e m_1^3 + \left(m_1^2 - 2A\rho x_e m_1 + 2Ac\rho/g\right)^2}\right)}{4Ac\rho x_e} \tag{24}$$

$$b_2 = \frac{\left(m_1^2 - 2A\rho x_e m_1 + 2Ac\rho/g - \sqrt{8A\rho x_e m_1^3 + \left(m_1^2 - 2A\rho x_e m_1 + 2Ac\rho/g\right)^2}\right)}{2m_1^2}. \tag{25}$$

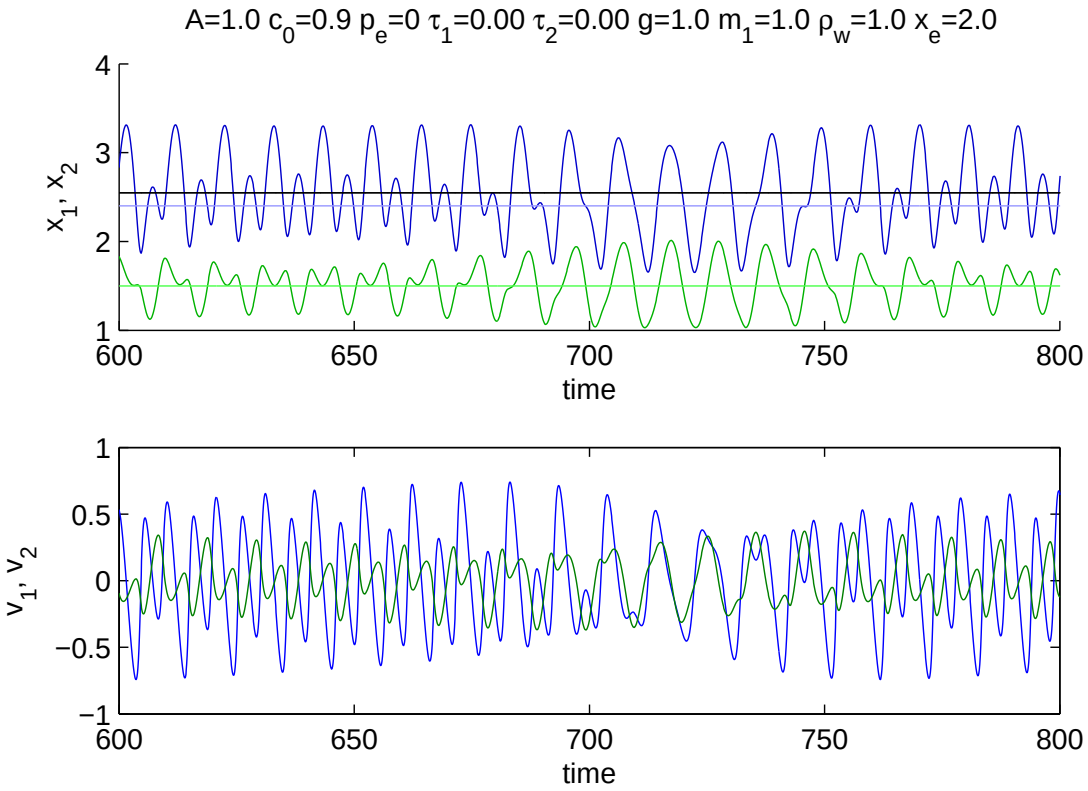

Figure 2: Time series of simulated Dines manometer. The upper panel shows the float (blue) and liquid (green) position, and the lower panel shows the respective velocities. The lighter lines in the upper panel show the equilibrium positions of the float and liquid x_{1e} and x_{2e}, and the black line shows the mean position of the float (calculated over a much longer period than that shown here). Parameters are $A = 1, c = 0.9, g = 1, m_1 = 1, \rho = 1, \tau_1 = \tau_2 = \tau_3 = 0, x_e = 2$. The initial condition was $x_1 = x_{1e} + c/(gm_1)$, $x_2 = x_{2e}$ and $v_1 = v_2 = 0$.

The argument to the square root is always positive, so b_1 and b_2 are always real. Clearly $b_1 > 0 > b_2$, so solution (b_1, ω_1) has the the piston and liquid in phase, and (b_2, ω_2) has them in opposite phase. The argument to the square root can be written

$$\left(m_1^2 + 2Am_1\rho x_e + 2Ac\rho/g\right)^2 - (16A^2cm_1\rho^2x_e)/g$$

from which it follows that ω_1 and ω_2 are always real, with $0 < \omega_1 < \omega_2$. The low frequency oscillation has the liquid and piston in phase, and the high frequency one in opposite phase.

A time-series plot of simulated motion for the full equations is shown in Fig 2. This example clearly shows periods where the liquid and piston oscillate in phase (e.g. 690 – 770), and periods where they are out-of-phase. Apparently both oscillations are present and beating is occurring. The mean position of the float (black line) is significantly displaced from its equilibrium position

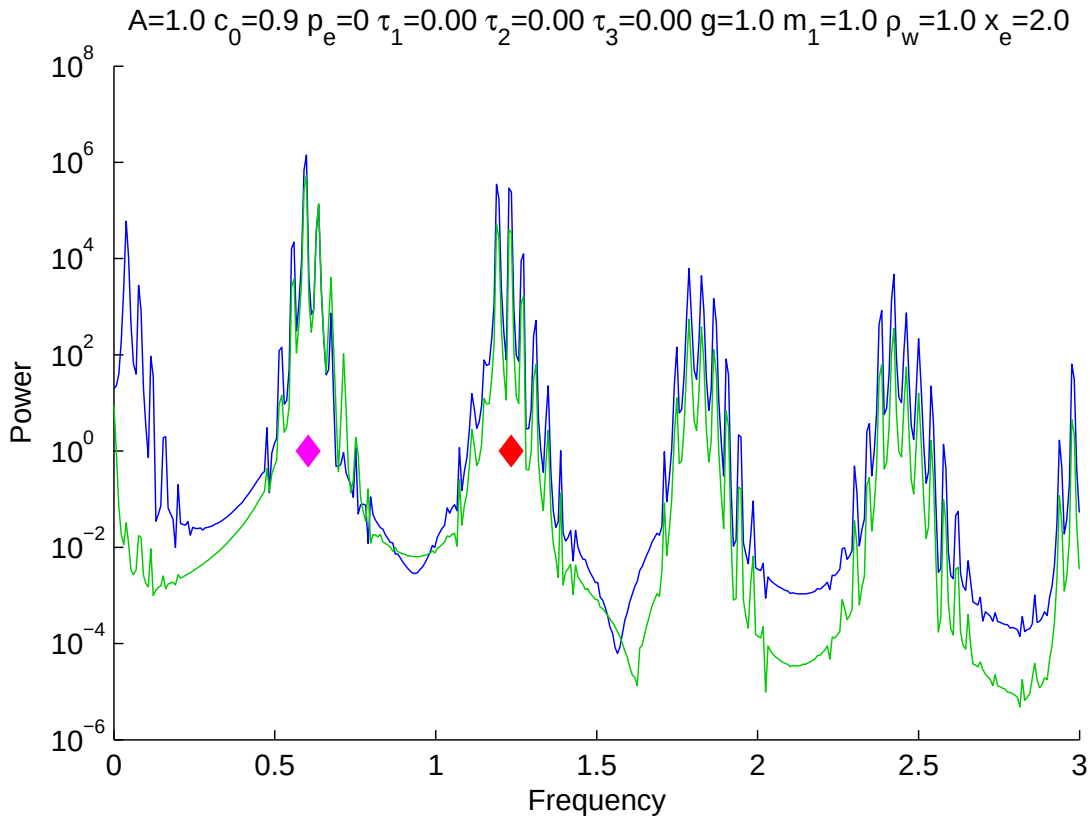

Figure 3: Power spectra of x_1 (blue curve) and x_2 (green curve) from the simulation in Fig 2. The diamonds indicate the frequencies for the coupled oscillation, ω_1 (magenta) and ω_2 (cyan).

x_{1e} (lighter blue line). In contrast, the mean liquid position is indistinguishable from x_{2e} (light green line). This offset will be analysed in due course.

The power spectra of x_1 and x_2 for this simulation are shown in Fig 3, with the coupled frequencies ω_1, ω_2 also indicated. The spectrum is dominated by a broad peaks around $\omega_1 = 0.6037$, $\omega_2 = 1.2347$, and the harmonics thereof. The nonlinearity is evident from the relatively large amplitudes of the harmonics, and from the broadness of the peaks. The broad peaks are also notably spiky; in this example the spikes are spaced at about 0.04, but when run at lower amplitude they become fewer and are spaced at $0.027 \approx \omega_2 - 2\omega_1$. It thus seems that the spikes are the result of nonlinear interactions between the frequencies ω_1 and ω_2. Reducing the amplitude of the oscillations by changing the initial condition leads to narrower spectral peaks and fewer spikes, confirming the role of nonlinearity. There is significant power in the motion of the piston, but not the liquid, at frequencies below 0.3, while the power is more similar for other peaks in the spectrum. The high piston energy and partial decoupling of float and liquid at low frequencies are less apparent when the overall amplitudes are reduced, again implying that nonlinearity may be the cause. This behaviour will be further discussed below.

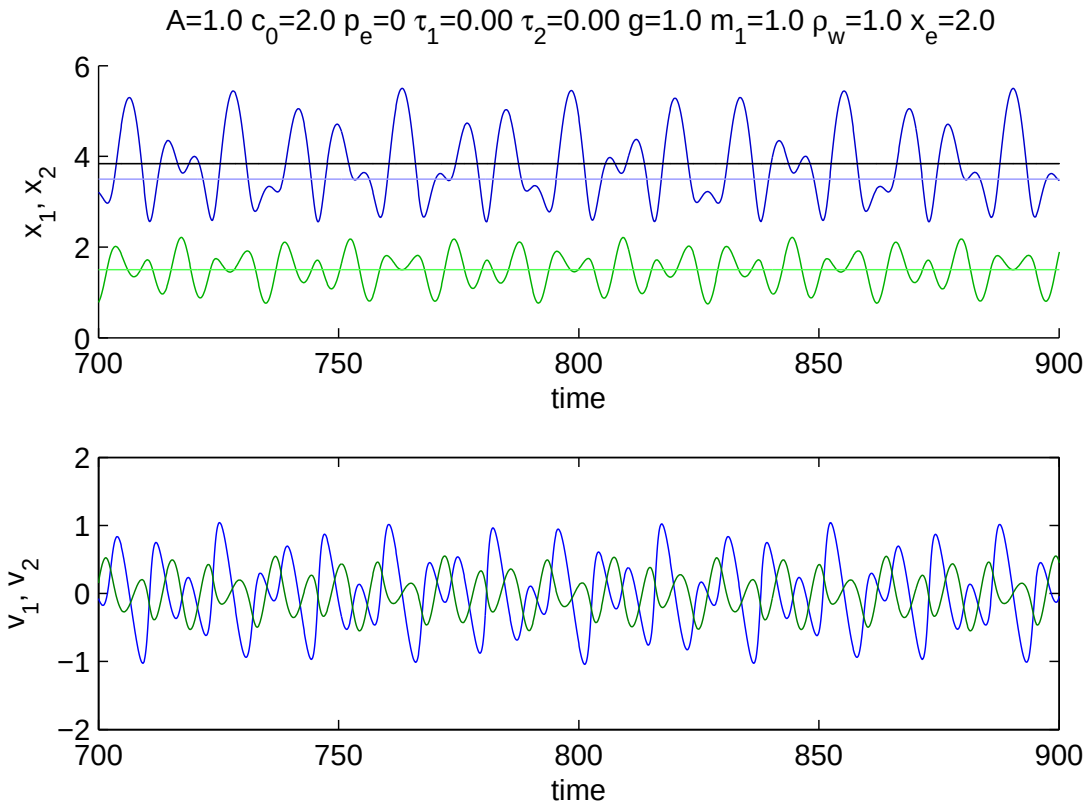

Figure 4: As for Fig 2, but with $c = 2$.

Limiting behaviour at very high wind speeds, (i.e. the limit $c_0 \to \infty$), is that $\omega_1^2 \to 0$, $b_1/c_0 \to 2A\rho/(gm_1^2)$, $\omega_2^2 \to g/x_e$ and $b_2/c_0 \to 0$. The in-phase oscillation becomes slow and predominantly in the piston, while the opposite-phase essentially becomes independent of the piston and similar to the f_2 case above.

If c_0 is increased from that show in Fig 2, then the motion becomes more complex. Time-series and spectra for $c_0 = 2$ are shown in Figs 4 and 5. The motion is approximately periodic with the section shown apparently beginning to repeat at about $t = 830$. The spectrum has many more peaks, but the linear analysis describes the strongest two. The offset of the mean float position from x_{1e} persists.

Figure 6 shows the power spectra for a range of c_0. It is clear that the linear analysis successfully picks out the dominant peaks ω_1 and ω_2 (white dotted curves), with their difference being the third prominent peak (black dotted curve). A rich range of harmonics and interharmonics are also apparent. The high power at low frequencies seen in Fig 3 is apparent in the upper panel near $c_0 = 0.9, f = 0$, from which it seems that its origin is a prominent interharmonic that happened to intersect $f = 0$ at that c_0. This intersection occurred because $\omega_2 \approx 2\omega_1$ around that c_0 (as already noted), a relationship that will presumably tend to favour relatively strong coupling between the two oscillations. The closely-spaced spikes in the spectrum seen

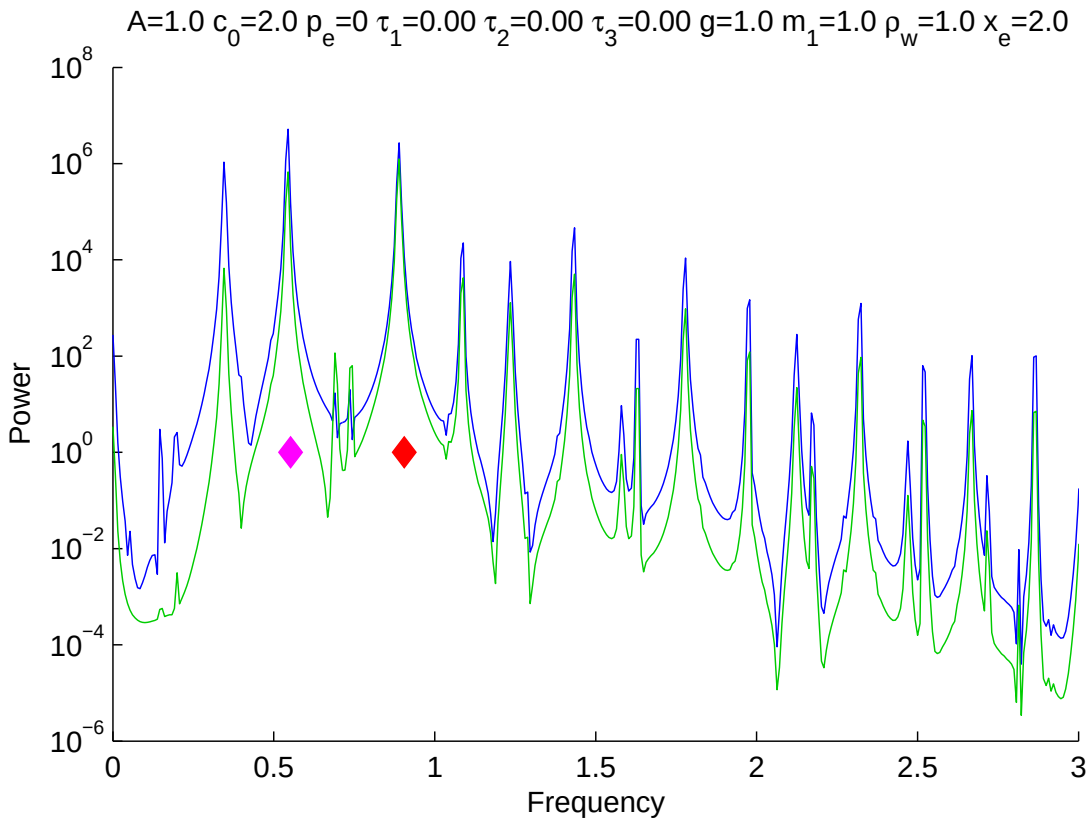

Figure 5: As for Fig 3, but with $c = 2$.

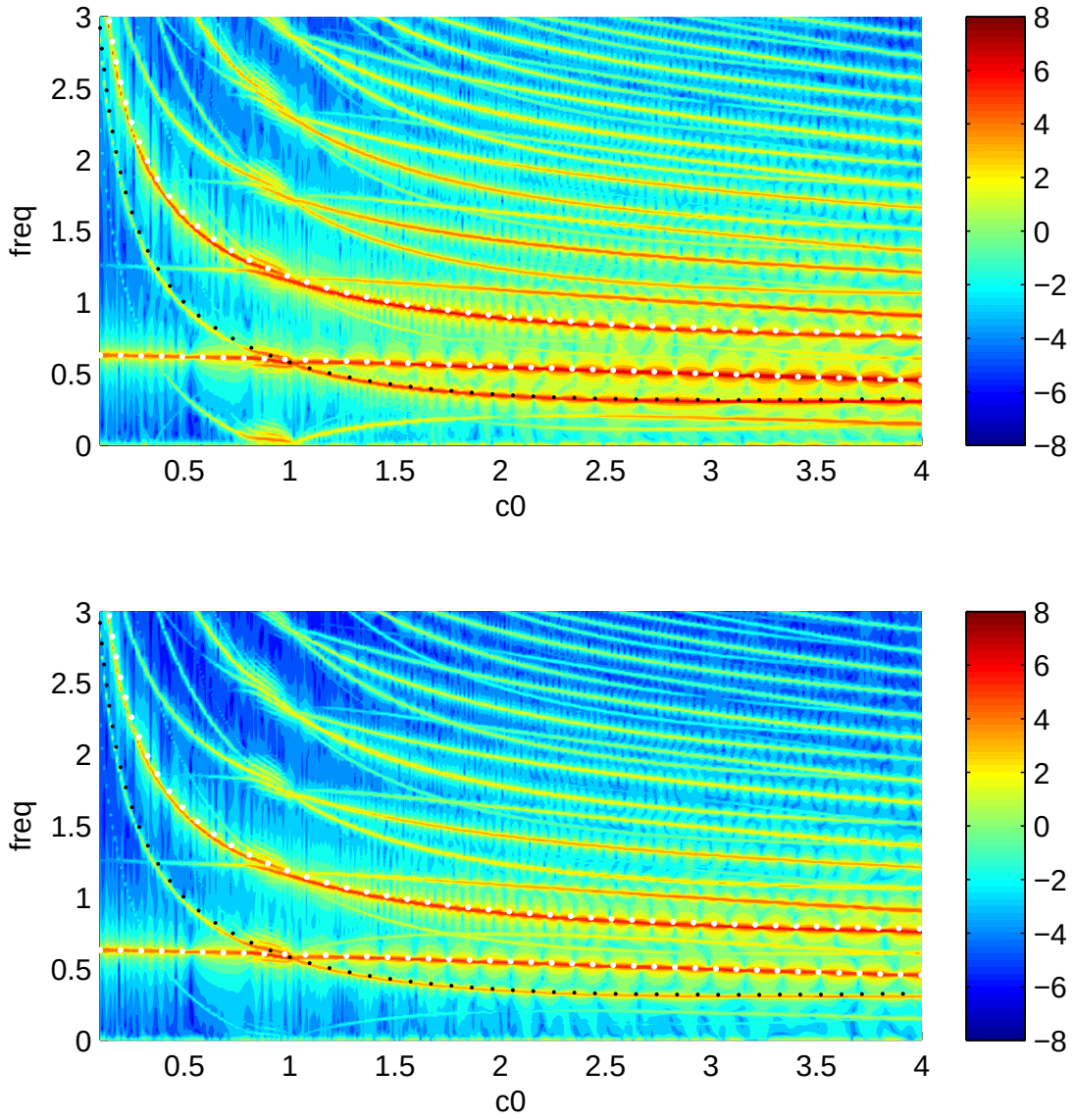

Figure 6: Logarithm base 10 of the power spectral density for x_1 (top) and x_2 (bottom) for values of c ranging from 0.02 to 4. Parameters are $A = 1, g = 1, m_1 = 1, \rho = 1, x_e = 2$. The dotted white curves are ω_1 (lower) and ω_2 (upper), and the dotted black curve is $\omega_2 - \omega_1$.

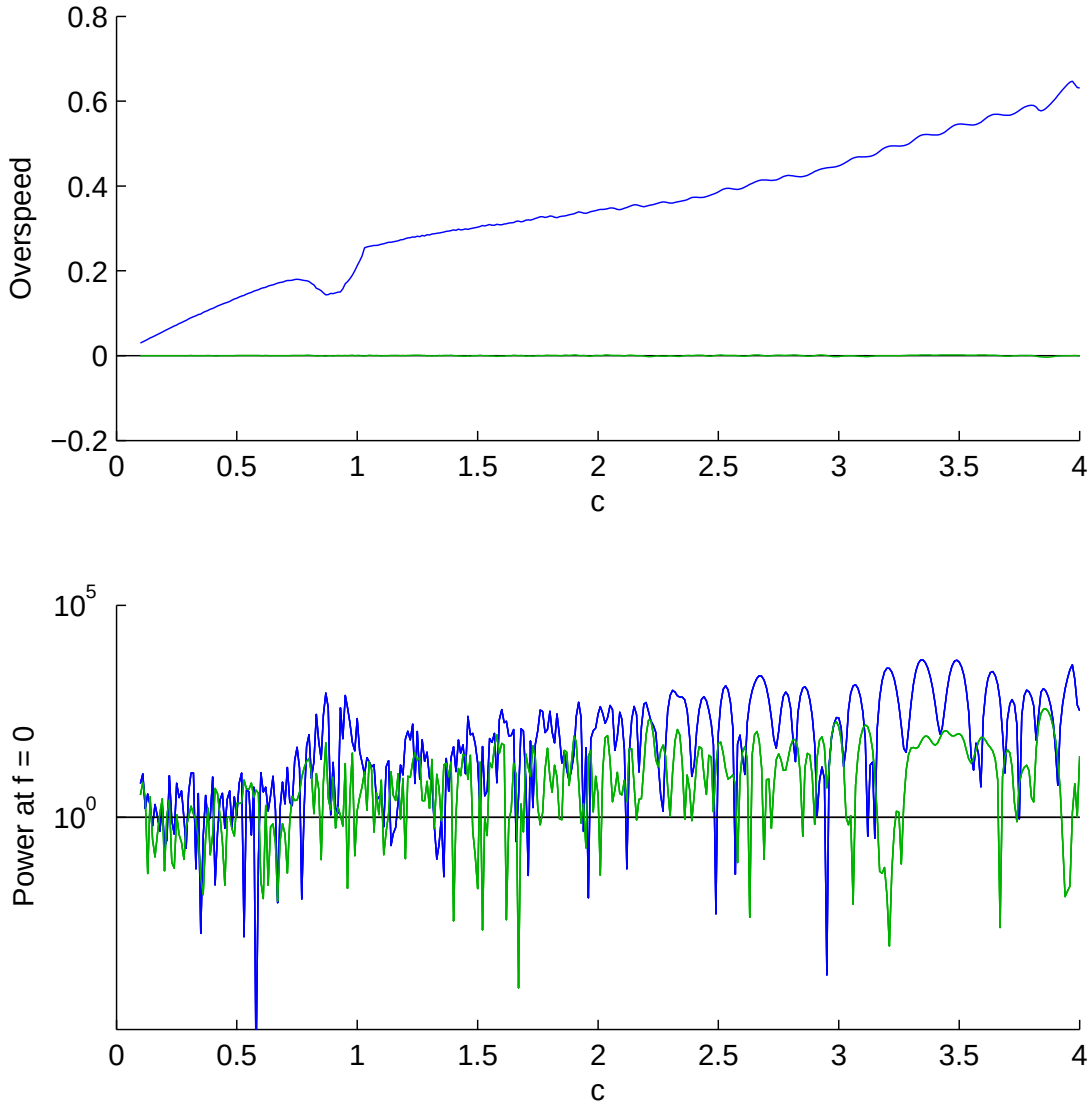

Figure 7: Upper panel: The extent to which the time-mean of x_1 (blue) and x_2 exceed their equilibrium values, in the same simulations as for Fig. 6. That is, $\overline{x_1} - x_{1e}$ (blue) and $\overline{x_2} - x_{2e}$ (green). Lower panel: The power at DC (i.e. $f = 0$) in these simulations.

in Fig 3 are also apparent. Other interesting features include the regular variation in the width of the peak about ω_1 and to a lesser extent ω_2 and the remaining lines. Similar variation is also apparent at zero frequency, and is shown more clearly in the lower panel of Fig. 7. The upper panel of that figure shows the overspeeding previously noted in Figs. 2 and 4. Relationships between the two panels are obvious, as is the systematic nature of the overspeeding. Reducing the amplitude of the initial departure from equilibrium by a factor of 10 reduces the overspeeding by about a factor of 60, suggesting that determining the cause of the overspeed will require an analysis of the nonlinearity in the system.

2.2 *The effects of damping the float*

A real float chamber has damping due to the viscosity of the water, the shaft from the float protruding through the bushing at the top of the float chamber, from the pen mechanism, and from remote read-outs. Thus such motions will be likely to be damped. On the other hand, the forcing $c(t)$ will vary due to turbulence, not be constant as in section 2.1. The behaviour when the damping $\tau_1 \neq 0$ and c varies in time is now explored. To begin with, c will oscillate sinusoidally,

$$c(t) = c_0[1 + G\sin(ft)] \tag{26}$$

where c_0 is related to the mean wind speed, G is essentially a gust factor, and f is the forcing frequency. The main diagnostic will be to compare the actual oscillation of the piston and water with that expected from the calibration equations, namely the equilibrium values expected for steady forcing. In these simulations, quite heavy damping $\tau_1 = 1$ is applied.

Interesting cases are likely to include those where f is close to one of the dominant frequencies apparent in Fig. 6, perhaps most strongly the opposite-phase oscillation $f = \omega_2$ but note that both coupled linear modes will be directly forced by oscillations in c because both involve a change in the pressure and volume of the enclosed air. A sample time-series for this case is shown in Fig 8. The water and piston are oscillating roughly in opposite phase, with relative amplitude 0.47, not too far from $|b_2| = 0.56$ for these settings. The amplitude of the piston oscillation is about 7% greater than that expected from the calibration, even with this relatively heavy damping. Evidently resonance is present at this frequency, as expected. More interestingly, the mean piston position is clearly offset slightly above its calibrated value, as also found in some undamped cases. In cup-anemometer parlance, the instrument is overspeeding. Examination of the spectrum (Fig 9) shows the now familiar peak at low frequency. A partial explanation for the overspeeding seems to be that nonlinearities are generating this peak (and many others), but that the Newtonian damping is unable to remove very low frequency (and in particular, DC) motions.

More exotic behaviour is possible, in particular in the interesting case where c_0 satisfies $\omega_2 \approx 2\omega_1$. Figure 10 shows such a case forced at a little less than twice ω_2. The amplitude was increased to $G = 0.5$ to really let the nonlinearities rip. The system resonates at $f/2$ and again overspeeds, by about 35%.

The behaviour is summarised in Fig 11. The energy (panel a) clearly depicts the resonant peak, with the overspeeding of the mean shown in panel (b). Note from panel (c) that the gusts are measured accurately at low frequencies, then tail off rapidly before being overestimated at resonance, then tailing off again. There is a frequency near 1 where the float is stationary

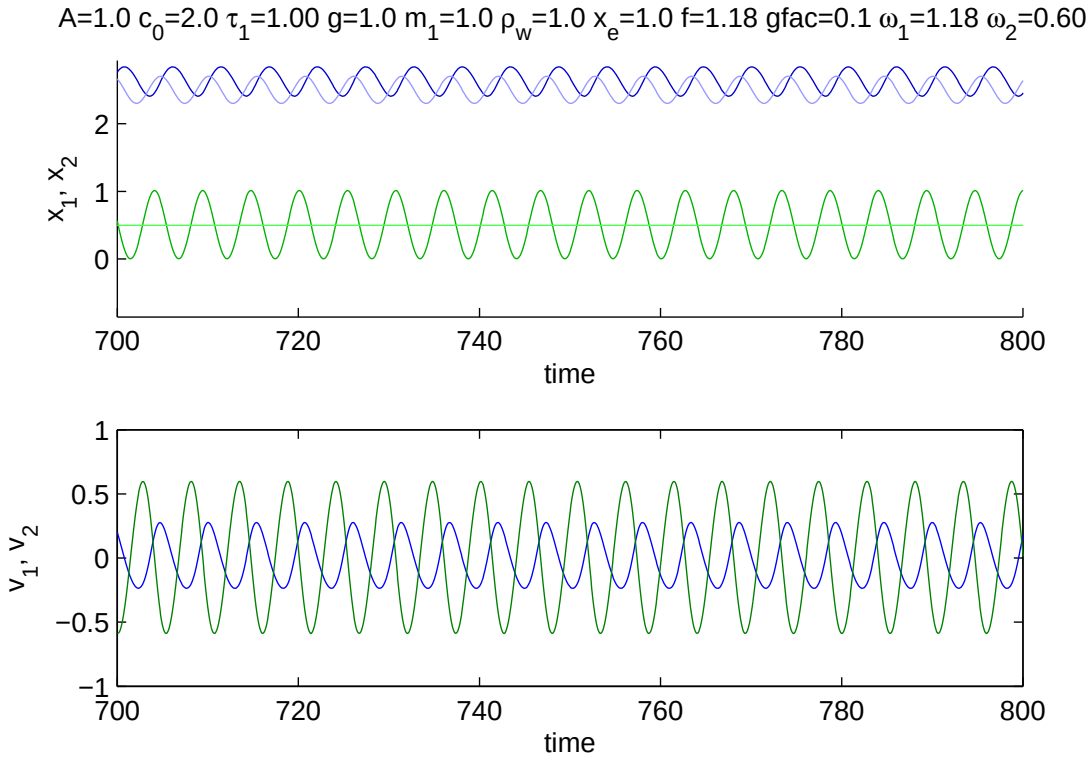

Figure 8: Time series of manometer response for sinusoidally-varying oscillation at frequency $f = \omega_2$. Upper panel, piston (blue) and water (green) positions. Dark curves show the instantaneous positions, and the lighter curves the calibrated values x_{1e} and x_{2e} calculated from $c(t)$. Lower panel, piston and water velocity. Parameters are $A = 1, c_0 = 2, \tau_1 = 1, \tau_2 = \tau_3 = 0, g = 1, m_1 = 1, \rho = 1, x_e = 1$, giving $\omega_1 = 1.18$, $\omega_2 = 0.60$, $b_1 = -0.56$ and $b_2 = 3.56$. The forcing amplitude is $G = 0.1$.

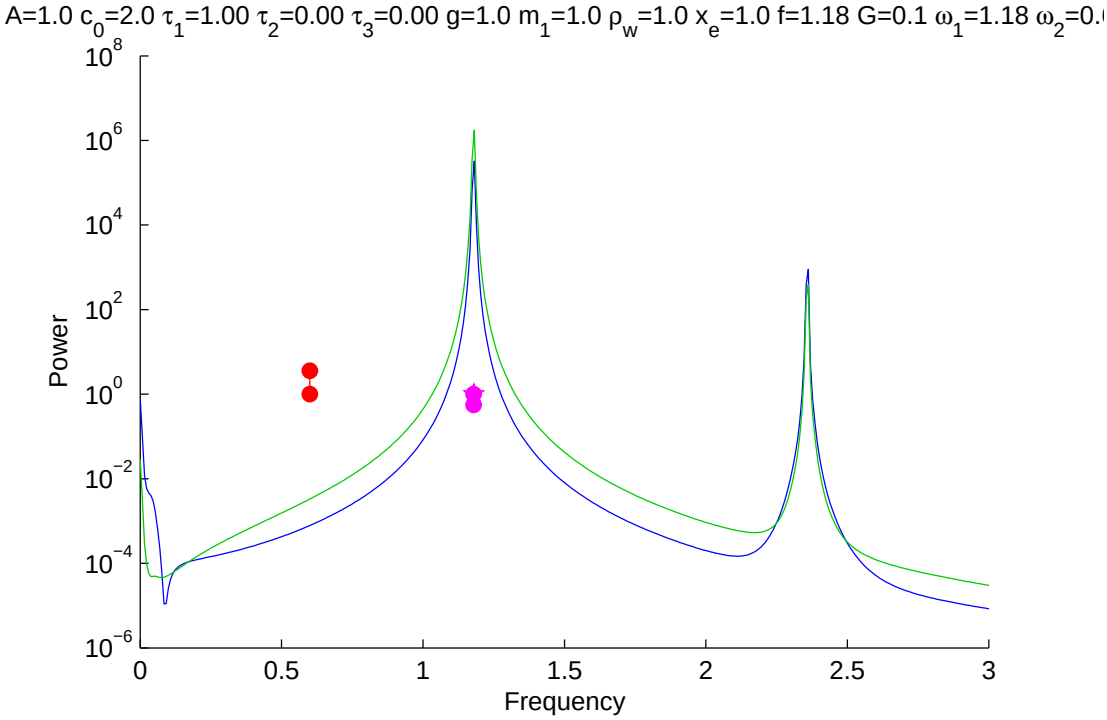

Figure 9: Power spectrum for the simulation in Fig 8. Symbols as in Fig 3, with the addition of a magenta pentagram (largely obscured) showing the forcing frequency. The lengths of the dumb-bells at ω_1 and ω_2 indicate the ratios b_1 and b_2.

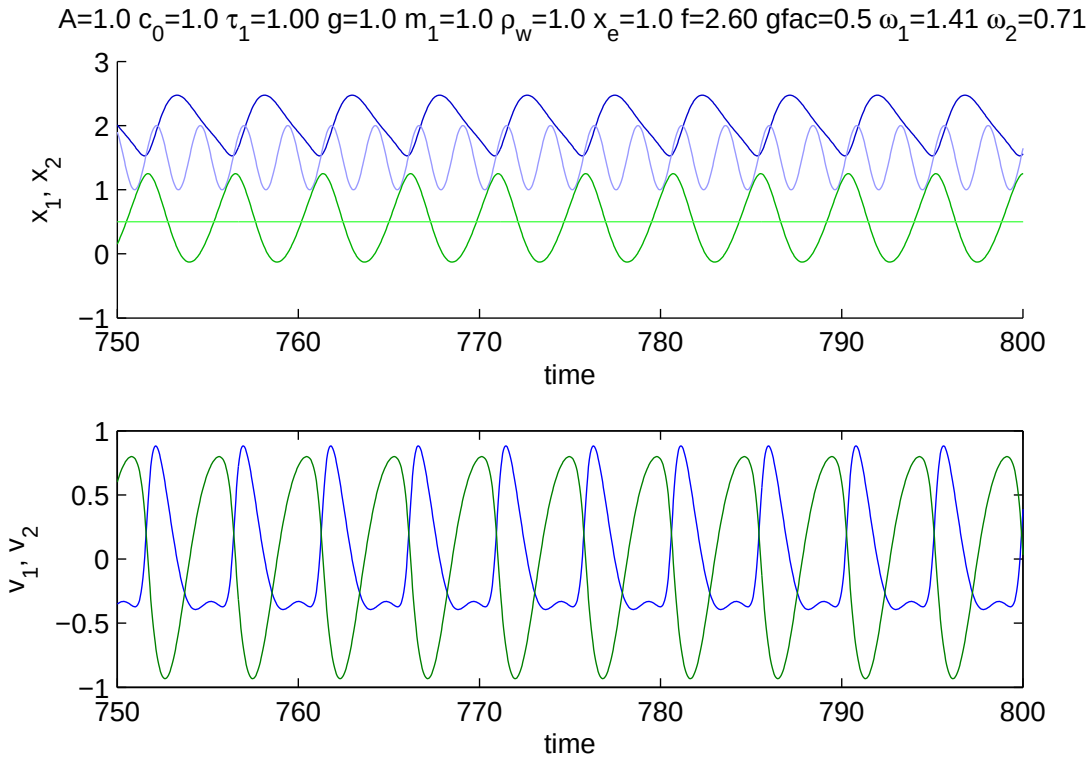

Figure 10: As for Fig 8, except with $c_0 = 1$, giving $\omega_1 = 1.41$, $\omega_2 = 0.71$, $b_1 = -1$ and $b_2 = 2$. The forcing frequency is $f = 2.6$, roughly twice ω_2 and the amplitude is increased to $G = 0.5$.

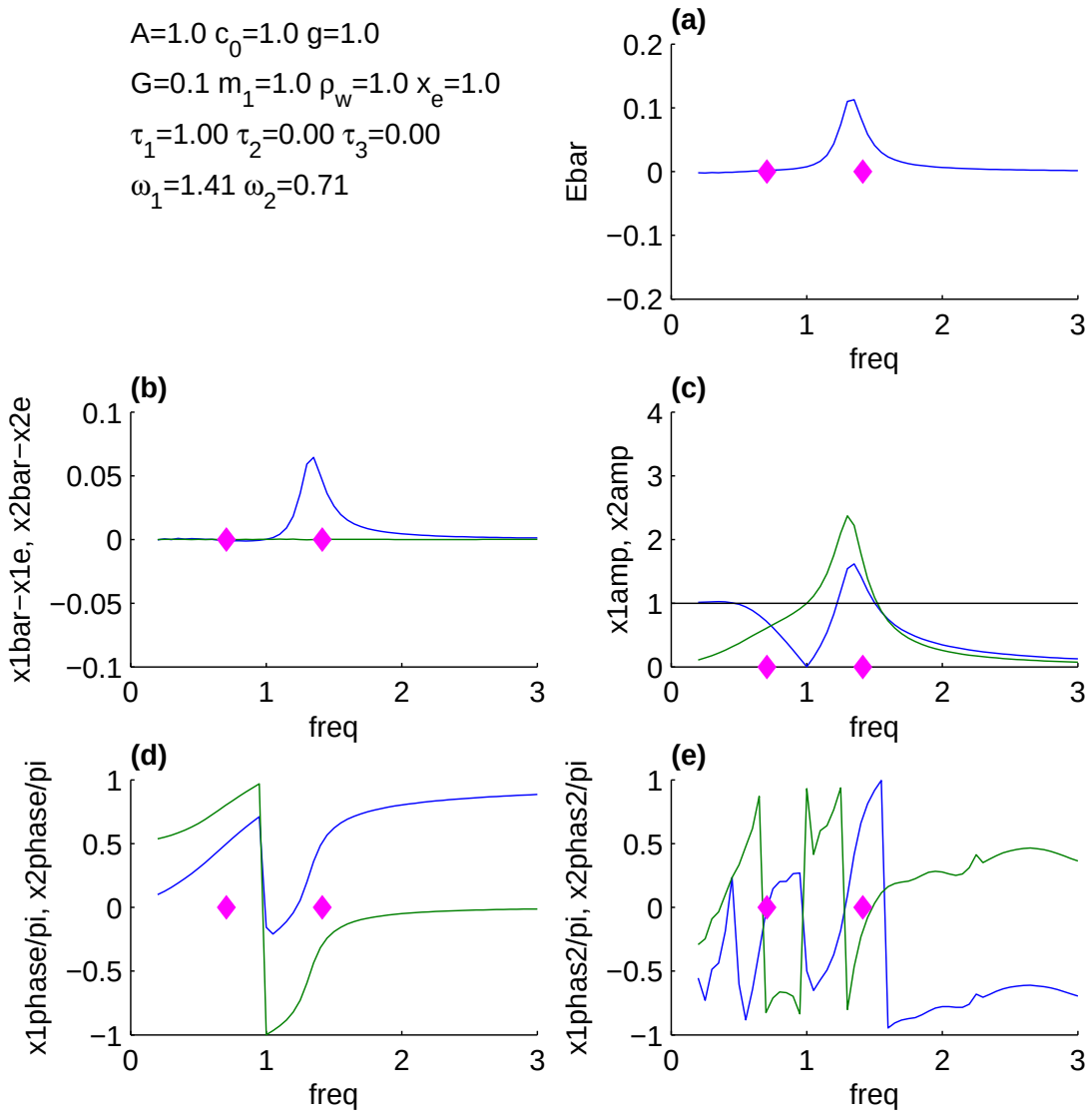

Figure 11: A summary of the behaviour for the forced damped system. Each panel shows the system behaviour as a function of forcing frequency f, with the natural frequencies ω_1 and ω_2 indicated by magenta diamonds. Paremeters are shown at top left. (a): the time-mean total energy in the system, $\overline{E_K} + \overline{E_{P,1}} + \overline{E_{P,2}} + \overline{E_{P,p}}$. (b): the mean piston and water position, relative to that expected for steady forcing c_0. (c): the amplitude of the piston and water oscillations, normalised by the calibrated oscillation for the piston. (d): is the phase difference between the forcing and the response. (e): is the same thing for the first harmonic of the forcing.

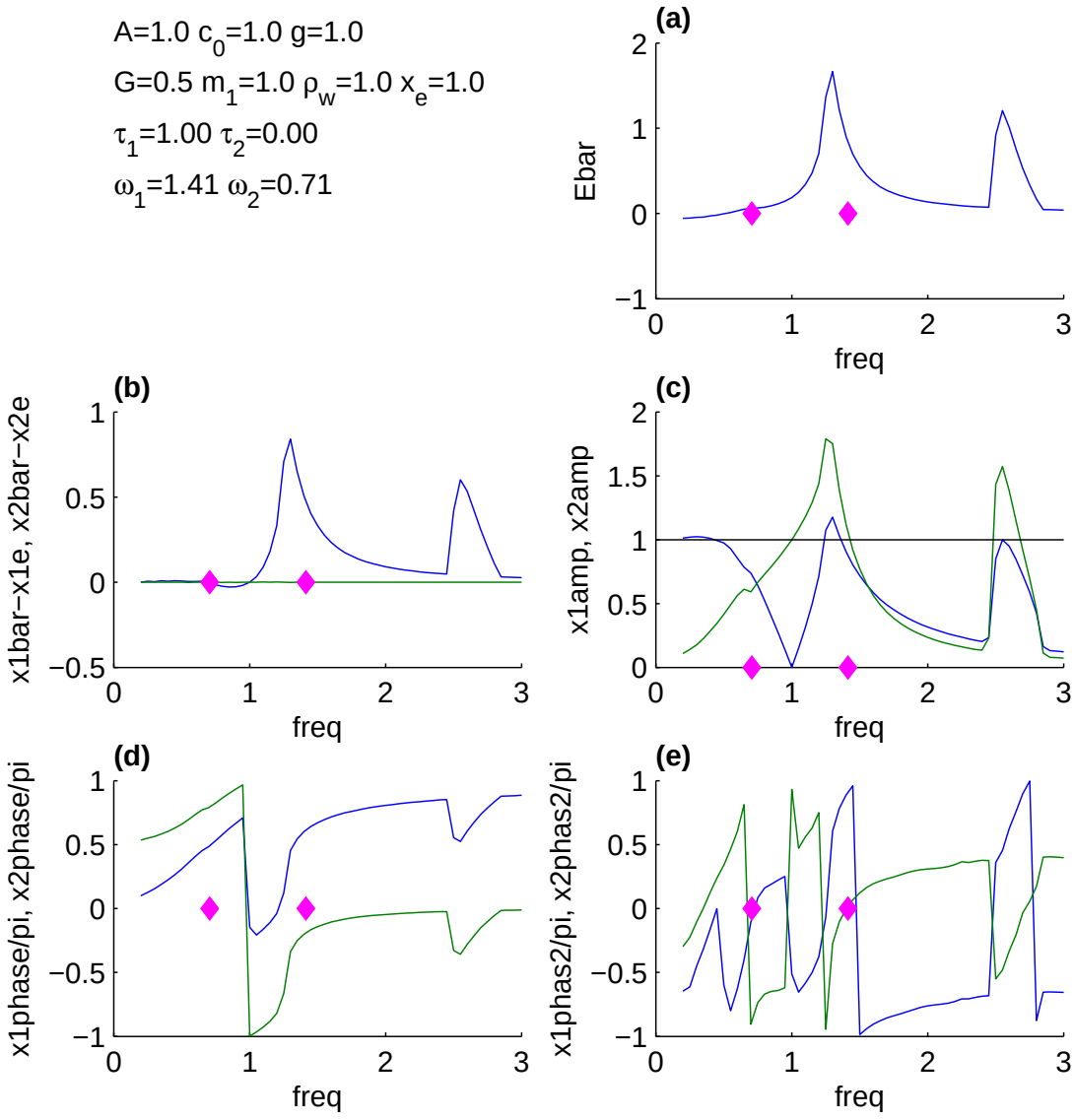

Figure 12: As for Fig 12, except with $G = 0.5$.

A=1.0 c_0=1.5 g=1.0

G=0.1 m_1=1.0 ρ_w=1.0 x_e=1.0

τ_1=0.30 τ_2=0.10 τ_3=0.50

ω_1=1.26 ω_2=0.65

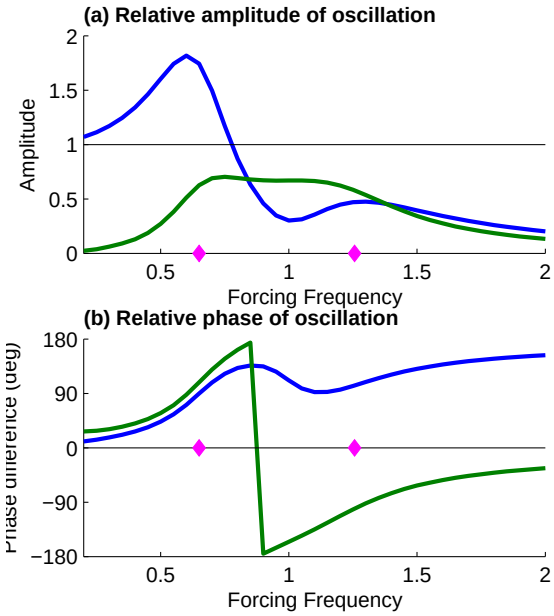

Figure 13: The (a) amplitude and (b) phase of the anemometer response in float motion (blue) and water motion (green), as a function of dimensionless forcing frequency in the simplified model. The curves have been normalised by the forcing, so an amplitude of 1 and phase of 0 implies that the float exactly follows the fluctuating wind at that frequency. The magenta diamonds show the resonant frequencies from the linear undamped theory. Parameter settings are as given at the top of the figure.

although the amplitude of the water oscillation is substantial. From panel (d), the piston and water oscillations differ in phase by $\sim \pi/3$ at low frequency, and about π at high, with the dividing frequency being that at which the piston ignores the forcing. Increasing the amplitude of the forcing (Fig 12) introduces the second resonant peak already seen in Fig 10, but not much else in the way of change.

2.3 *Comparison to measurements of Borges*

Response curves are shown for another configuration, in which the damping coefficients were tuned to give good agreement to the measurements of Borges (1968), in Fig 13. These curves show the relative amplitude and phase of the oscillation as a function of forcing frequency, with the blue curve representing the float and the green, the water. The amplitudes have been scaled by the forcing amplitude, so that amplitude=1, phase=0 means the float exactly follows the varying wind speed. The magenta diamonds indicate the linear undamped frequencies, and are clearly close to the resonant peaks. At low frequencies, the float closely follows the wind speed, with a rising response to the out-of-phase oscillation near the lower resonant frequency, and a second weaker peak near the higher resonance, with a weak trough between.

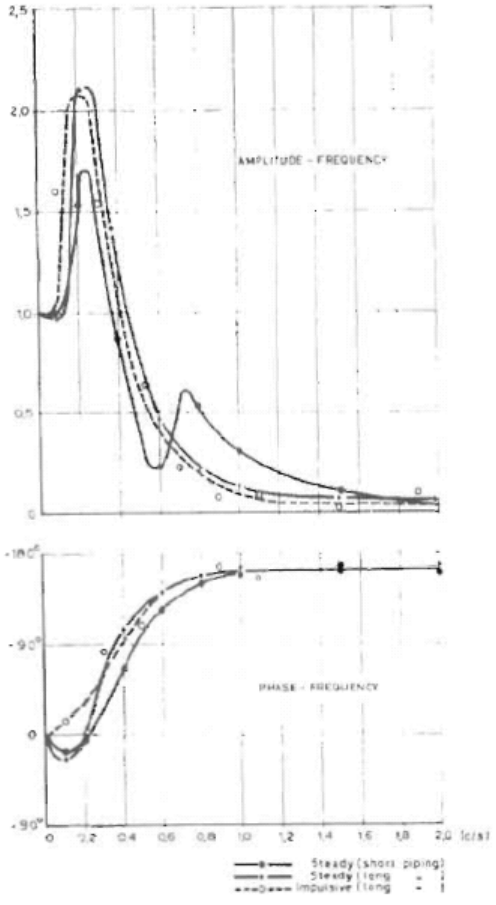

Figure 14: The relative amplitude (top) and phase (bottom) of the float movement, as a function of forcing frequency, for a Fuess anemometer with various tubing lengths. From Borges (1968).

The phase response shifts from in-phase at low frequencies, to out-of-phase at high.

Figure 13 is in very good agreement with the measurements of Borges (1968). Specifically, Fig 14 reproduces a similar curve (of the float motion only) from his laboratory experiments, showing good quantitative agreement with the model. Both the amplitude and phase of the response are well represented. The results in Fig 13 are similarly in good agreement with the measurements taken by JCU/CTS as part of Task 3 of this project, although here the agreement is more qualitative than quantitative as the higher-frequency peak is stronger. Close agreement with the Dines measurements is possible with re-tuning of the physical constants in the model equations, implying that the Fuess anemometer used by Borges has some significant differences from the Dines anemometer.

The dual peak in the response curve significantly complicates attempts to calculate the "gust period" or "response time" that the Dines anemometer measures. Such calculations are straightforward for the more usual first-order systems, but not for those with one, let alone two, significant resonances. Accordingly, due care is urged in interpreting such calculations.

2.4 *Accounting for pressure in the outer chamber*

Including a constant nonzero pressure p_{env} in the outer chamber increases the complexity of the algebra but does not require any change in the method of solution. The equilibrium water position is unchanged, while the float position becomes

$$x_{1e} = x_{2e} + \frac{c_0}{gm_1 + Ap_{env}}. \tag{27}$$

For comparison with the earlier simulations, we define

$$\Delta_0 = c_0 \left(1 + \frac{Ap_{env}}{gm_1}\right)^{-1} \tag{28}$$

which is the length that the trapped air would assume if $p_{env} = 0$. That is, we work in terms of the length or volume of trapped air, rather than its mass. Searching for coupled oscillations following the procedure in section 2.1 reveals that

$$bc\omega^2 m_1 + (1-b)(gm_1 + Ap_{env})^2 = 0 \tag{29}$$

and

$$2Ac\rho(x_e\omega^2 - g) - (1-b)(gm_1 + Ap_{env})^2 = 0 \tag{30}$$

with solutions

$$\omega_1^2 = \frac{S + 4A\rho x_e(gm_1 + Ap_{env})^2 - \sqrt{S^2 + 8Am_1\rho x_e(gm_1 + Ap_{env})^4}}{4Acm_1\rho x_e} \tag{31}$$

$$b_1 = \frac{S + \sqrt{S^2 + 8Am_1\rho x_e(gm_1 + Ap_{env})^4}}{2m_1(gm_1 + Ap_{env})^2} \tag{32}$$

and

$$\omega_2^2 = \frac{S + 4A\rho x_e(gm_1 + Ap_{env})^2 + \sqrt{S^2 + 8Am_1\rho x_e(gm_1 + Ap_{env})^4}}{4Acm_1\rho x_e} \tag{33}$$

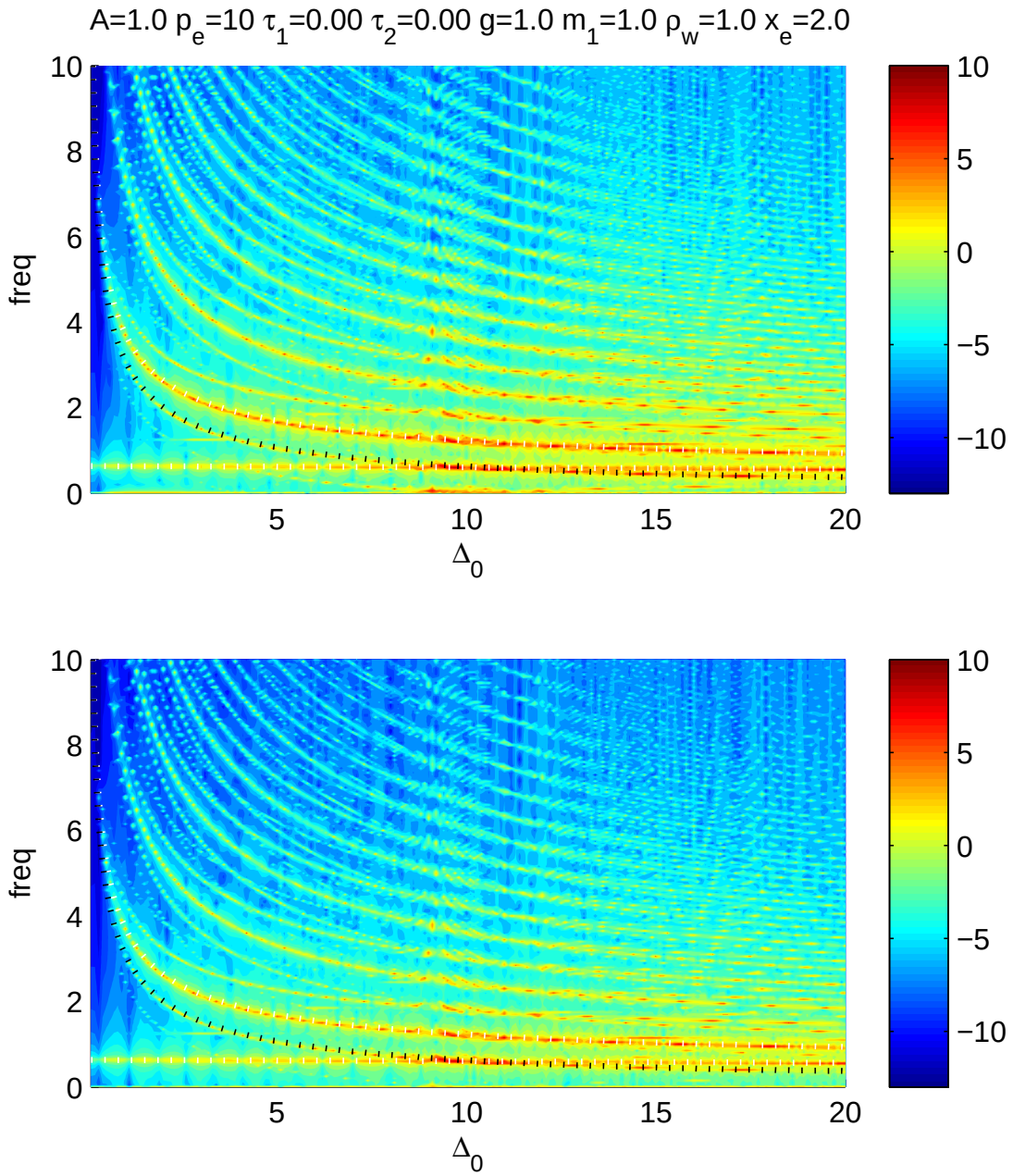

Figure 15: As for Fig 6, except with $p_{env} = 10$.

$$b_2 = \frac{S - \sqrt{S^2 + 8Am_1\rho x_e(gm_1 + Ap_{env})^4}}{2m_1(gm_1 + Ap_{env})^2} \tag{34}$$

where

$$S = (gm_1 + Ap_{env})^2(m_1 - 2A\rho x_e) + 2Agm_1\rho c \tag{35}$$

It follows from

$$\begin{aligned}[S + 4A\rho x_e(gm_1 + Ap_{env})^2]^2 - [S^2 + 8Am_1\rho x_e(gm_1 + Ap_{env})^4] \\ = 16A^2cgm_1(gm_1 + Ap_{env})^2\rho^2 x_e \\ > 0\end{aligned} \tag{36}$$

that $\omega_1^2 > 0$, so ω_1 is real.

Physically, the effect of including p_{env} is to increase the stiffness of the spring. Previously, if the volume of the trapped air halved, then p doubled. Now, p becomes $2(p_{env} + p) - p_{env} = p_{env} + 2p$. For $p_{env} \gg p$, as will usually be the case, this makes a big difference to the restoring force. The obvious effect will be to shift the oscillations to higher frequency, as is apparent in Fig. 15, which repeats the simulation of Fig. 6 except with $p_{env} = 10$. Note the different axis scales. The broad spiky spectral peaks shown in Fig 3 recur in this configuration when $\omega_1 \approx 2\omega_2$, near $\Delta_0 = 10$.

3. Modelling the float chamber with the real geometry

In this section, the simplifications present in the U-tube model are analysed and removed, leading to a model that more realistically represents the real Dines manometer.

3.1 *The system at rest*

The derivation of the shape of the float is given by Gold (1936), but that derivation is not readily extensible to the situation where the float and liquid are not stationary. The following derivation proceeds from more fundamental principles and highlights the role of the pressure within the liquid in determining the forces on the float, which will be important in modelling the unsteady case.

We work in the float-relative coordinate system outlined in Fig 16. The distance x is measured positive down from the top of the float, $x_1(v)$ and $x_2(v)$ are the water levels outside and inside the float respectively, x_3 is the bottom of the flotation chamber, and $x_d(v)$ is the bottom of the manometer chamber. At zero wind, the float just rests on the bottom, so $x_b = x_d(0)$ is the length of the float.

For the steady-state case, the pressure difference between the float and the tank is

$$\delta p = Kv^2 \tag{37}$$

where K is a constant and v the wind speed. Applying the hydrostatic equation to the liquid,

$$\delta p = \rho g(-x_1 + x_2) \tag{38}$$

whence

$$Kv^2 = \rho g(-x_1 + x_2). \tag{39}$$

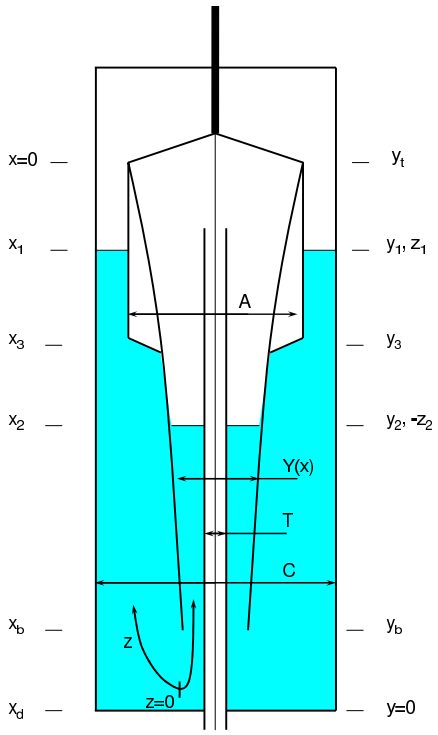

Figure 16: Cross-section of the Dines float and chamber, showing the coordinate system and variable definitions. Distances x are measured downwards from the top of the float, distances y are measured upwards from the bottom of the tank, and distances z are measured along the path of the moving water, with $z = 0$ at the bottom of the tank and $z > 0$ outside the float. The cross-sectional area of the tank is C, that of the top of the float A, that of the tube T, and that of the interior of the float $Y(x)$, where x is the distance down from the top of the tank.

The total volume of submerged air is

$$V_{sa} = A(x_3 - x_1) + \int_{x_2}^{x_3} Y(x)dx \tag{40}$$

where A is the cross-sectional area of the outside of the float, and $Y(x)$ is that of the inside of the float. The total volume of water is

$$V = -V_{sa} + C[x_d(v) - x_1(v)] - T[x_d(v) - x_2(v)] \tag{41}$$

where C and T are the cross-sectional areas of the tank and tubing respectively.

Archimedes principle states that the mass of displaced liquid is the mass of the float m

$$\rho V_{sa} = m. \tag{42}$$

It is worth recalling that this relation requires that the pressures within the liquid are hydrostatic. In particular, the net upwards force on the float due to air pressure is

$$\delta p\, Y(x_2) = \rho g(x_2 - x_1)Y(x_2) \tag{43}$$

while that due to water pressure is

$$\rho g(x_3 - x_1)[A - Y(x_3)] + \int_{x_2}^{x_3} \rho g(x - x_1)\frac{\partial Y}{\partial x}dx. \tag{44}$$

Here, the first term represents the pressure of water on the bottom of the flotation collar $\rho g(x_3 - x_1)$ times the area of that collar $A - Y(x_3)$, while the second is the pressure of water on the inner surface of the float $\rho g(x - x_1)$, in an upwards direction, integrated over the length of the float. Note the use of the hydrostatic equation in calculating the pressure within the water in (44). This integral stops at x_3, the bottom of the collar, since the forces on the inside and outside of the float below there balance. Integrating the second term of (44) by parts, the net force by the water pressure is

$$\rho g \left[A(x_3 - x_1) - \int_{x_2}^{x_3} Y(x)dx - (x_2 - x_1)Y(x_2) \right] \tag{45}$$

and adding back in the force by the enclosed air, the total upwards force on the float is

$$\rho g \left[A(x_3 - x_1) - \int_{x_2}^{x_3} Y(x)dx \right] \tag{46}$$

which is ρV_{sa} as required. This use of the hydrostatic equation in this digression emphasises that, to completely determine the forces on the float in the unsteady case, it is necessary to know the internal pressures in the moving liquid. This point will be revisited in sections 3.3 and 3.4.

Using (41) and (42),

$$\frac{m}{\rho} = -V + C[x_d(v) - x_1(v)] - T[x_d(v) - x_2(v)] \tag{47}$$

which can be differentiated with respect to v to yield

$$C[x'_d(v) - x'_1(v)] = T[x'_d(v) - x'_2(v)] \tag{48}$$

and rearranged to yield

$$x_d(v) = \frac{m + \rho[V + Cx_1(v) - Tx_2(v)]}{\rho(C - T)} \tag{49}$$

Linear calibration of the anemometer implies that

$$\alpha v = x_d(v) - x_d(0) \tag{50}$$

where the constant $\alpha = (6 \text{ inches})/(100 \text{ mph}) \approx 3.40909 \times 10^{-3}$ s for a standard Dines anemometer, and half that for a high-speed unit. Substituting (50) in (39),

$$x_1(v) + q[x_d(v) - x_d(0)]^2 = x_2(v) \tag{51}$$

where

$$q = \frac{K}{\alpha^2 \rho g}. \tag{52}$$

Gold (1936) gives $q = 0.08 \text{ cm}^{-1} = 8 \text{ m}^{-1}$ for a standard low-speed instrument; note that for a high-speed instrument q will be four times this value due to the dependency on α. Differentiating (51) with respect to v,

$$x'_1(v) + 2q[x_d(v) - x_d(0)]x'_d(v) = x'_2(v). \tag{53}$$

Using (49) to replace x_d in (51) yields

$$x_1(v) = \frac{-(C-T)^2 + 2CqTx_2(v) + (C-T)^{3/2}\sqrt{C-T+4Cqx_2(v)}}{2C^2q} \tag{54}$$

Taking (40), using (41) for V_{sa} and (47) for V gives

$$-mg + A\rho[x_3 - x_1(v)] = \rho \int_{x_2(v)}^{x_3} Y(x)dx \tag{55}$$

or, differentiating with respect to v,

$$Ax_1'(v) = Y(x_2(v))x_2'(v). \tag{56}$$

Eliminating x_1' and x_d' between (48), (53) and (56) gives an expression for $Y(x_2)$ in terms of x_d,

$$Y(x_2) = \frac{A\{C - T + 2qT[x_d(v) - x_d(0)]\}}{C - T + 2qC[x_d(v) - x_d(0)]} \tag{57}$$

or, using (49) to replace x_d then (54) to replace x_1, and writing in terms of x not x_2 for convenience,

$$Y(x) = A\,\frac{C - T + T\sqrt{1 + \frac{4Cqx}{C-T}}}{C\sqrt{1 + \frac{4Cqx}{C-T}}}. \tag{58}$$

This equation, (58), is the required expression for the shape of the float. When $T \ll C$, it reduces to

$$Y(x_2) \approx \frac{A}{\sqrt{1 + 4qx_2}} \tag{59}$$

3.2 *Some properties of* Y

Some useful properties of Y follow.

The derivative is

$$Y'(x) = -2Aq\left(1 + \frac{4Cqx}{C-T}\right)^{-3/2} \tag{60}$$

The integral is

$$\int_0^x Y = \frac{A}{2C^2q}\left[(C-T)^2\left(\sqrt{1 + 4Cqx/(C-T)} - 1\right) + 2CTqx\right] \tag{61}$$

and the inverse function of $x \to \int_0^x Y$ is

$$y \to \frac{A(C-T)^2[1 - \sqrt{1 + 4qTy/(A(C-T))}] + 2CqTy}{2AqT^2} \tag{62}$$

As the float has a tube up the middle, similar expressions for $Y - T$ are also needed. The integral is

$$\int_0^x Y - T = \frac{A(C-T)^2\left(\sqrt{1 + 4Cqx/(C-T)} - 1\right) + 2C(A-C)Tqx}{2C^2q} \tag{63}$$

and the inverse function of $x \to \int_0^x Y - T$ is

$$y \to \frac{A(C-T)^2\{(A-T) - \sqrt{(A-T)^2 + 4qTy(A-C)/(C-T)}\} - 2C(C-A)Tqy}{2(C-A)^2T^2q} \tag{64}$$

The distance x_3 (the length of the buoyancy ring surrounding the top of the float) is found as follows. At zero wind, the float is just buoyant, so the boundary conditions $x_1(0) = x_2(0) = 0$ apply together with (40) and (42). That is, we solve

$$m = \rho\left(Ax_3 - \int_0^{x_3} Y\right) \tag{65}$$

for x_3. For a tank diameter $C = 0.2032$ m, float diameter $A = 0.1524$ m, tube diameter $T = 0.0254$ m, calibration coefficient $q = 8\,\mathrm{m}^{-1}$ and float mass $m = 2.173$ kg this gives $x_3 = 0.24304$ m. Of these constants, the first four are from Gold (1936) and the latter was measured from a single sample, including the shot cup, owned by the Bureau of Meteorology. That instrument was measured to have $x_3 \approx 0.240$ m, in good agreement with the calculation[1]. A water density of $\rho = 1000$ kg m^{-3} was used.

The total volume of water required follows from (41) and either (40) or (42), again with $v = 0$ and the boundary conditions $x_1(0) = x_2(0) = 0$,

$$V = x_{d0}(C-T) - x_3A + \int_0^{x_3} Y \tag{66}$$

For the above constants, this yields $V = 0.013054$ m^3. For comparison, a somewhat crude measurement of $V \approx 0.01283$ m^3 was obtained from the same Bureau of Meteorology instrument. The discrepancy of 220 mL would disappear with a small 2 mm change in the tank diameter. The difference between measurement and calculation is therefore deemed to be negligible since factors such as wall thickness of the tubing, tank and float have been neglected. In practice, the mass of the float is adjusted by means of the shot cup to account for minor inconsistencies between V, m and x_3 in a given instrument.

3.3 *Internal pressures in the liquid. I: Is the flow hydrostatic?*

One difference between the Dines manometer and the U-tube model is that the float is not just supported by the pressure of the trapped air, but also by the buoyancy of the collar. The buoyancy force on a partially-submerged object depends on the pressure forces applied to its surface by the liquid in which it is immersed. When the liquid is stationary, the pressure therein can be calculated from the hydrostatic equation and so the buoyancy force is straightforward to determine. However, in a Dines manometer, the liquid is moving. The question, then, is whether the departures from hydrostaticity are sufficiently large to need to be accounted for.

Consider a simple system, consisting of a U-tube filled with an inviscid liquid, similar to that shown in Fig 1 but without the piston. Ignoring the small region around the bend in the

[1] A precise measurement is difficult, and the measured value is considered to only be accurate to within a few millimetres, as the bottom of the buoyancy collar is not normal to the float axis as in the model. Note that this calculation also neglects the thickness of the metal in the float.

tube, the equation of motion for the liquid is

$$\frac{\partial w}{\partial t} + w\frac{\partial w}{\partial z} = -\frac{1}{\rho}\frac{\partial p}{\partial z} - gs \tag{67}$$

where w is the speed of the fluid, z is a coordinate along the axis of the tube, g is gravity, and s is the sign of z. For an incompressible uniform fluid, $\partial w/\partial z = 0$ and ρ is constant, so (67) becomes

$$\frac{\partial w}{\partial t} = -\frac{1}{\rho}\frac{\partial p}{\partial z} - gs. \tag{68}$$

Boundary conditions for the problem are $p(z_t) = p(z_b) = 0$ where z_t and z_b are the positions of the ends of the slug of liquid. Integrating (68) from $z = 0$ to $z = z_t$, the pressure at $z = 0$ is

$$p(0) = \int_0^{z_t} \dot{w} + gs\, dz = z_t(\dot{w} + g) \tag{69}$$

Integrating along the other arm yields

$$p(0) = \int_0^{z_b} \dot{w} + gs\, dz = z_b(\dot{w} - g). \tag{70}$$

Since pressure is continuous at $z = 0$, $z_t(\dot{w} + g) = z_b(\dot{w} - g)$ and

$$\dot{w} = -g\frac{z_t + z_b}{z_t - z_b} \tag{71}$$

whence

$$p(0) = -2g\frac{z_t z_b}{z_t - z_b} \tag{72}$$

We may write (71) as

$$\dot{w} = \ddot{z}_t = -\frac{g}{L}(2z_t - L) \tag{73}$$

where $L = z_t - z_b$, a constant since the fluid is incompressible and the tube of constant cross-sectional area. This equation has solution

$$z_t = \frac{L}{2} + \beta \sin\left(\sqrt{\frac{2g}{L}}\, t\right) \tag{74}$$

where β is the amplitude and the phase has been chosen arbitrarily. Then, substituting into (72),

$$p(0) = \frac{Lg}{2} - \frac{2g\beta^2}{L}\sin^2\left(\sqrt{\frac{2g}{L}}\, t\right) \tag{75}$$

The first term on the right-hand side shows that the pressure is hydrostatic if the liquid is stationary, or at the instant when the height in both arms is equal and the liquid is oscillating. The second term gives the departure from this hydrostatic situation; the pressure at the bend oscillates with *twice* the frequency of the liquid (due to the sine-squared). The oscillating part of the pressure is negligible compared to the hydrostatic part when

$$\frac{L}{2\beta} \gg 1, \tag{76}$$

that is, the amplitude of the oscillation is small compared to the length of the slug of liquid.

As the condition (76) applies in real Dines manometers, the pressure in the tank could be assumed to be hydrostatic even though the oscillating fluid requires nonhydrostatic pressure gradients in the fluid. However, a difficulty arises with this approach. If the hydrostatic equation is integrated downwards along each arm of the manometer, two estimates for the pressure at the bottom will be obtained. The difference between these estimates is of the order of the departure from hydrostatistic balance and, while formally negligible, is an uncertainty in the model formulation. To avoid this untidiness, the nonhydrostatic pressure gradient β will be assumed to be constant, but of opposite sign inside and outside of the float.

Then

$$p_{\text{in}} = p_d - (\rho g + \beta)y \tag{77}$$

$$p_{\text{out}} = p_d - (\rho g - \beta)y \tag{78}$$

where p_{in} and p_{out} are the pressures inside and outside of the float, p_d is the pressure at the bottom of the tank, and β is the nonhydrostatic part of the vertical pressure gradient.

Applying the boundary conditions $p_{\text{in}}(y_2) = \delta p$ and $p_{\text{out}}(y_1) = 0$ yields

$$\delta p = p_d - (\rho g + \beta)y_2 \tag{79}$$

$$0 = p_d - (\rho g - \beta)y_1 \tag{80}$$

whence

$$p_d = \frac{y_1 \delta p + 2y_1 y_2 \rho g}{y_1 + y_2} \tag{81}$$

$$\beta = \frac{-\delta p + \rho g(y_1 - y_2)}{y_1 + y_2} \tag{82}$$

which are sufficient to define the internal pressure throughout the water.

3.4 *Internal pressures in the liquid. II: What is the effect of constrictions?*

The previous section analysed the departures of the pressure from hydrostatic balance due to the oscillation of the fluid, assuming a constant tube diameter. However, the flow in and around of the float in a Dines manometer has accelerations due to the varying width of the passage between the walls of the tank and the float, and within the float itself. These variations will also induce pressure perturbations. The magnitude of these perturbations is now estimated and shown to be negligible.

Consider for simplicity steady, inviscid and irrotational flow along a U-tube passageway similar to that sidcussed in section 3.4, but of varying cross-sectional area $S(z)$. Bernoulli's theorem then states that

$$H = \frac{1}{2}q^2 + \frac{p}{\rho} + g|z| \tag{83}$$

is constant along a streamline, where q is the speed of the fluid. Making the approximation that the speed is constant across the width of the tank, Sw is constant along the axis of the tube, so (83) becomes

$$H = \frac{1}{2}\left(\frac{S_0 w_0}{S}\right)^2 + \frac{p}{\rho} + g|z| \tag{84}$$

Taking the boundary condition p constant at $z = z_t$, which without loss of generality can be taken as $p(z_t) = 0$, the pressure within the fluid is

$$\frac{p}{\rho} = g(z_t - z) + \frac{S_0^2 w_0^2}{2}\left(\frac{1}{S_z^2} - \frac{1}{S_0^2}\right) \tag{85}$$

whence

$$\frac{1}{\rho}\frac{\partial p}{\partial z} = -g - \frac{1}{2}\frac{S_0^2 u_0^2}{S^3}\frac{\partial S}{\partial z} \tag{86}$$

For a typical Dines manometer with $S \sim 0.01$ m^2, $\partial S/\partial z \sim 0.005$ m, the second (i.e. perturbation) term in this equation is small provided that

$$u_0^2 < \frac{2Sg}{\partial S/\partial z} \sim 40\,\mathrm{m^2 s^{-2}} \tag{87}$$

As this condition is satisfied, there is no need to modify the pressure distribution calculated in the previous section to account for the presence of constrictions to the flow.

3.5 *Equations for the moving system*

3.5.1 *Forces on the float*

The vertical component of the forces on the float are as follows:

- The force due to the difference in air pressure,

$$F_1 = \delta p\, Y(x_2) \tag{88}$$

- The force due to water pressure on the bottom of the buoyancy collar,

$$\begin{aligned} F_2 &= p_{\text{out}}(y_3)(A - Y(x_3)) \\ &= (p_d - (\rho g + \beta)y_3)(A - Y(x_3)) \end{aligned} \tag{89}$$

- The force due to water pressure on the outside of the float below the buoyancy collar,

$$\begin{aligned} F_3 &= \int_{x_{d0}}^{x_3} p_{\text{out}} Y'(x)dx \\ &= p_d\left\{Y(x_3) - Y(x_{d0})\right\} + (\rho g - \beta)\left\{-y_3 Y(x_3) + y_b Y(x_{d0}) - \int_{x_{d0}}^{x_3} Y(x)dx\right\} \end{aligned} \tag{90}$$

- The force due to water pressure on the inside of the float

$$\begin{aligned} F_4 &= -\int_{x_{d0}}^{x_2} p_{\text{in}} Y'(x)dx \\ &= -p_d\left\{Y(x_2) - Y(x_{d0})\right\} - (\rho g + \beta)\left\{-y_2 Y(x_2) + y_b Y(x_{d0}) - \int_{x_{d0}}^{x_2} Y(x)dx\right\} \end{aligned} \tag{91}$$

- The force due to the mass of the float

$$F_5 = -mg \tag{92}$$

The net force, excluding damping, is the sum $F_1 + F_2 + F_3 + F_4 + F_5$.

3.5.2 *Forces on the water*

The acceleration of the free surface of the water outside the float is now derived. In the z-coordinate system of Fig 16, the equation of motion for the water is

$$\frac{\partial w}{\partial t} + w\frac{\partial w}{\partial z} = -\frac{1}{\rho} + gs \tag{93}$$

where s is the sign of z. Assuming that the motion is uniform across the channel,

$$Sw = S_1 w_1 \tag{94}$$

where S is the cross-sectional area of the channel, and the subscript 1 denotes conditions at the free surface outside the float. Integrating the left-hand side of 93 along the length of the water slug,

$$\begin{aligned}\int_{z_2}^{z_1} \frac{\partial w}{\partial t} + w\frac{\partial w}{\partial z}dz &= \int_{z_2}^{z_1} \frac{\partial w}{\partial t}dz + \frac{1}{2}\int_{z_2}^{z_1} \frac{\partial w^2}{\partial z}dz \\ &= \dot{w}_1 S_1 \int_{z_2}^{z_1} \frac{1}{s}dz + \frac{1}{2}\left(w_1^2 - w_2^2\right) \\ &= \dot{w}_1 S_1 \int_{z_2}^{z_1} \frac{1}{s}dz + \frac{w_1^2}{2}\left(1 - \left\{\frac{C-A}{Y(x_2)}\right\}^2\right)\end{aligned} \tag{95}$$

while the right-hand side is simply

$$-\frac{\delta p}{\rho} + g(y_1 - y_2). \tag{96}$$

Hence the acceleration of the free surface of the water outside the float, excluding damping, is

$$\ddot{y_1} = \frac{\delta p/\rho - g(y_1 - y_2) - 0.5v_1^2[1 - \{(C-A)/Y(x_2)\}^2]}{(C-A)\mathcal{S}} \tag{97}$$

where $\mathcal{S}$ is the integral of the reciprocal of the cross-sectional area of the passage through which the water passes, along the length of the water:

$$\mathcal{S} = \frac{x_3 - x_1}{C-A} + \int_{x_3}^{x_{d0}} (C-Y)^{-1} + \frac{C^{-1} - A^{-1}}{2\pi Y(x_{d0})(x_d - x_{d0})} + \int_{x_2}^{x_{d0}} (Y-T)^{-1} \tag{98}$$

where the terms on the right hand are respectively the parts of the passage between the float collar and the tank, between the tapered part of the float and the tank, below the bottom of the float, and up the interior of the float.

The water motion is written in terms of the movement of the free surface outside the float with respect to the tank, y_1. The motion inside the float, and position in float-relative co-ordinates, are diagnosed where necessary using the known volume of water and manometer geometry.

3.5.3 *Damping*

Three forms of damping are considered. The float and water each have linear damping of their motion with time-scales τ_f and τ_w respectively. In addition, the relative motion of the float and water is damped. The relative velocity of water through the choke at the bottom of the float is

$$v_{\text{choke}} = v_b + v_1 \frac{C - A}{Y(x_b)} \tag{99}$$

where v_b is the velocity of the float and v_1 is the velocity of the water level outside the float, both relative to the tank. This flow is assumed to exert a drag force

$$\rho C_{\text{choke}} |v_{\text{choke}}| v_{\text{choke}} \tag{100}$$

as it passes through the choke, leading to accelerations on the water and the tank of

$$-\rho C_{\text{choke}} |v_{\text{choke}}| v_{\text{choke}} / m \tag{101}$$

and

$$-\rho C_{\text{choke}} |v_{\text{choke}}| v_{\text{choke}} / (\rho V) \tag{102}$$

respectively.

3.6 ***Simulations with no damping***

The equations of motion of the system are solved as before, by fourth-order Runge-Kutta.

Figure 17 summarises the behaviour of the system in the absence of damping. As for the U-tube analogue, there are two dominant resonant frequencies, with the water moving in- or out-of-phase with the float. (Some care is needed in describing these, since the water position in the float, x_2, corresponds to the water position below the piston, which was x_1 in the notation of that section). The figure shows that the lower-frequency oscillation, in which the float and water inside it move in phase, has a frequency of 0.49 Hz at 10 m s^{-1}, which slowly increases with wind speed to 0.57 Hz at 25 m s^{-1} and to 0.75 Hz at 50 m s^{-1}. The higher-frequency, out-of-phase motion, has a frequency that increases from about 1 to 3 Hz as the mean wind speed increases from 10 to 50 m s^{-1}.

At a mean wind speed of 20 m s^{-1}, similar to that of the laboratory measurements conducted by the Cyclone Testing Station, the two frequencies are about 0.55 Hz and 1.45 Hz, within about 0.1 Hz of the measured resonant frequencies. This is excellent agreement; the small discrepancy is probably mainly due to the relatively crude modelling of the motion of the water, particularly around the bottom of the tank, that damping may slightly shift the frequencies, and experimental uncertainty in the measured frequencies. The first of these factors is considered to be the most likely, as the assumptions made about that flow determine the effective oscillating masses. If part of the water participates in the oscillation to a lesser degree — for example, that in the bottom corners of the tank — then this would reduce the oscillating mass and increase the resonant frequencies, possibly sufficiently to account for the discrepancy with observations.

As with the U-tube and piston analogue, there are also weaker spectral peaks at harmonics and interharmonics of the dominant resonances.

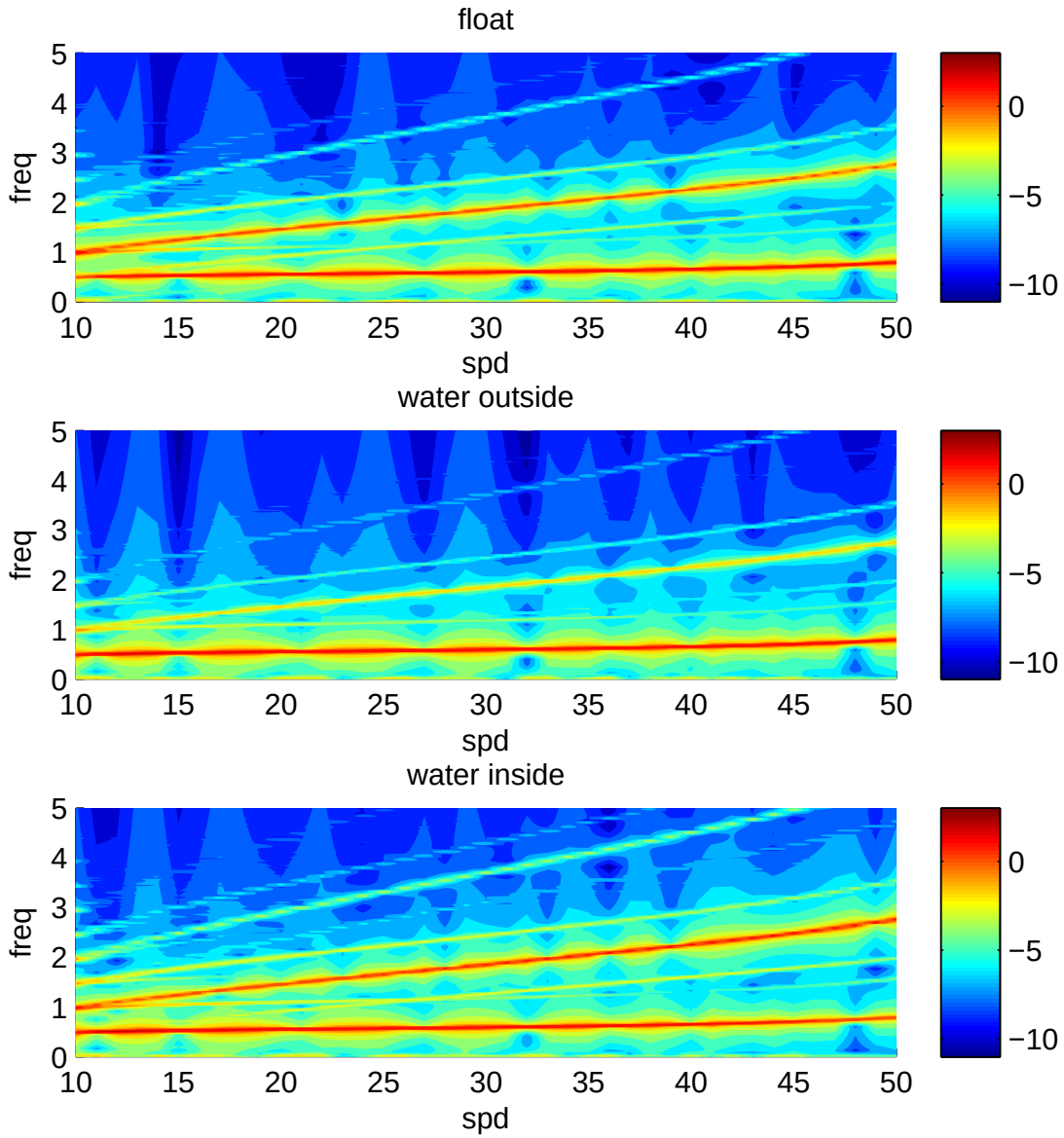

Figure 17: Logarithm base-10 of the power spectral density of the position of the float (top), water level in the tank (middle), and water level inside the float (bottom), as a function of the mean wind speed. The wind speeds are in m s^{-1} and the frequencies in Hz.

The strong agreement with the laboratory measurements provides considerable confidence in the model. There is no tuning of these results, they were obtained simply by inserting the correct float geometry and mass and chamber geometry, into the equations.

In particular, the agreement validates the decision to assume that the pressure inside the tank is equal to that at the pitot tube entrance. This decision was based on calculations and measurement showing that the tubing resonance terminated into a fixed volume was about 6 Hz, much higher than the manometer resonances. As a check, a version of the model was constructed in which the mass of air inside the float was held fixed and the pressure determined through Boyle's Law, as in the U-tube analogue. This version shifted the out-of-phase oscillation to much higher frequencies, as the effective spring constant was greatly increased, somewhat similarly to the U-tube case where the external pressure was nonzero. The poor agreement with observations of this version validates the original decision about pressure.

It is worth commenting upon the "restoring force" that enables the oscillation. In the U-tube analogue, this force is the compressed or rarefied air. Here, it is that a departure of the system from equilibrium means that the effective area on which the air pressure acts on the float and the water, $Y(x_2)$, departs from its equilibrium value, providing the necessary force imbalance. This departure has a different variation with mean wind speed than that provided by Boyle's Law in the U-tube (in that case, the spring constant reduces as the air volume increases), and is why the resonant frequencies no longer decrease with increasing wind speed.

3.7 *Tuning the damping*

Initial results indicate that good agreement with the measurements can be obtained with $\tau_f = \tau_w = 0$ and $C_{\text{choke}} = 0.5$.

3.8 *High-speed Instrument*

The previous analysis, for the low-speed instrument, is repeated for the high-speed. Unfortunately, full physical properties of the float and chamber are not known, so a hypothetical configuration of the model for a high-speed instrument was attempted. External measurements of the instrument at Learmonth Airport reveals that the normal water depth is 0.932 m, and that the tank diameter is the same as for the low-speed instrument. As a first approximation, the mass of the float is estimated to be twice that of the low-speed instrument, leading to a length of the collar $x_3 = 0.328$ m. Other float dimensions were calculated from the equations presented herein.

The resonant response of the hypothetical high-speed instrument is shown in Fig 18. Compared to the low-speed instrument, the dominant oscillation shifts to a lower frequency, about 0.3 Hz with a more marked increase at higher wind speeds, while the higher-frequency oscillation is at generally higher frequency than in the low-speed instrument. The reduction in frequency of the in-phase oscillation is in good agreement with the laboratory measurements and is consistent with the approximate doubling of the oscillating mass. However, the increase in frequency of the out-of-phase oscillation seems somewhat larger than found in the laboratory measurements. However, until firm information on the physical characteristics of the high-speed float become available, the cause for this discrepancy cannot be determined.

This sensitivity of the results to the physical characteristics of the instrument implies that

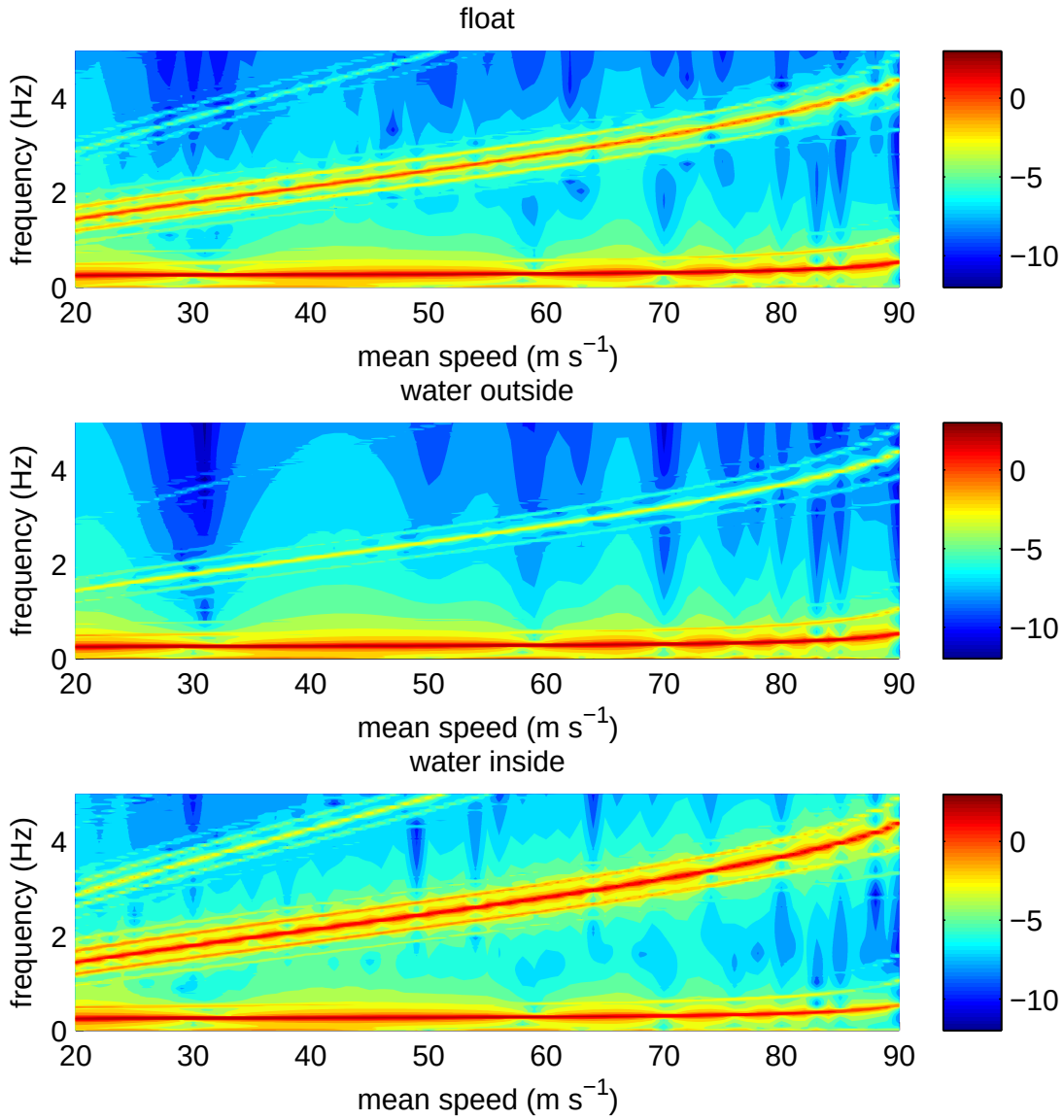

Figure 18: Logarithm base-10 of the power spectral density of the position of the float (top), water level in the tank (middle), and water level inside the float (bottom), as a function of the mean wind speed. The wind speeds are in m s^{-1} and the frequencies in Hz.

care will be needed in interpreting the results of this study to ensure that the appropriate model of Dines anemometer is considered. Of the three versions used, the most common were the low-speed and high-speed measured as part of Task 3, which had maximum readings of 100 and 200 miles per hour respectively. However, there was also an intermediate instrument, with a maximum reading of 150 m.p.h., no examples of which survive in Australia. It is apparent from the surviving chart that the winds in Cyclone Tracy were measured by the 150 m.p.h. instrument, and there is physical and anecdotal evidence for one having been previously installed at Learmonth. In addition, the Bureau's instrument laboratory have published test results on such an instrument. Unfortunately, more detailed documentary evidence has proved elusive.

Measurement of the characteristics of one of the few surviving instruments, perhaps during routine maintenance, would enable a more accurage determination of its resonances. Several enquiries to R.M. Munro, the instrument manufacturers, have not elicited detailed information on the physical characteristics of the instrument.

4. Conclusions

Two models of the Dines anemometer float chamber were developed, one simplified and one incorporating nearly complete physics. Linear and numerical solutions were obtained of the simplified model, showing that there are two resonances, in which the float and water move in- or out-of-phase. The linear and numerical solutions are in good agreement for low-amplitude oscillations. Higher amplitudes result in the occurrence of additional resonances at harmonics and interharmonics of those from the linear analysis, but not in significant changes to the linear frequencies. Adding damping to this model provides good agreement with previous laboratory measurements (Borges 1968) and with those undertaken as other tasks within this project. Damping of the relative motion of the float and water was shown to be the most important damping mechanism for obtaining this good agreement.

Investigation of the more detailed model reveals that it has quite similar properties to that of the U-tube analogue. The main difference is that the variation of the resonant frequencies with wind speed is much less, and of opposite sign, to the other case. This change is because the effective spring constant varies with wind speed for different physical reasons.

The resonant frequencies of this model are in excellent agreement with observations. This agreement is obtained without tuning – it is necessary only to insert the measureable physical dimensions and mass of the float and chamber into the model. Hence, the model is considered to reproduce the behaviour of the real anemometer to a high degree of accuracy.

The main remaining gap in this work is that the physical properties of the high-speed instrument were estimated, rather than measured. Future disassembly and measurement of one of the few remaining instruments would enable a more accurate determination of its properties, particularly its resonance frequencies.

References

Borges, A. R. J., 1968: On the frequency response of floater-type anemographs (velocity fluctuations in the direction of mean speed). *Technica*, **379**, 505–511.

Gold, E., 1936: Wind in Britain – The Dines anemometer and some notable records during the last 40 years. *Quart. J. Roy. Meteor. Soc.*, **62**, 167–206.

Appendix III: Task 3

Experimental testing of the Dines pressure tube and float for dynamic characteristics using a rapid Pressure Loading Actuator (PLA).

John Ginger and David Henderson
Cyclone Testing Station,
James Cook University
Townsville, 4811, Australia

1 Introduction

The objective of Task 3 of the project was to measure the response of low-speed and high-speed Dines systems when excited by a known pressure signal to the Dines head (inlet pitot port). The input pressure traces and the measured outputs are to provide comparison data for Task 2. A range of pressure signals with differing frequencies and amplitudes were generated using a Pressure Loading Actuator (PLA) capable of applying rapidly fluctuating realistic wind pressures.

Figure 1 shows the 3-cup anemometer at the Bureau of Meteorology at the Townsville Airport. Figures 2 to 4 show the high speed Dines anemometer tower at the site, and the float chamber with paper record drum float rod and recorder. The Dines anemometer in Townsville was replaced by the 3-cup Synchrotac anemometer and direction vane, as the official wind speed measurement device in the early 1990s. However, the Dines has been kept operational as an unofficial wind speed recording device to-date. This provides an opportunity to compare the "performance" of both instruments which are located about 100m apart, at the Airport in Townsville.

A Low Speed Dines anemometer, including the head and vane, float and chamber, from Glenlitta Victoria was loaned to the CTS by the Bureau of Meteorology. The Low Speed units were typically used in non-cyclonic regions (and in cyclonic regions prior to the mid-70s). This system was set-up in the laboratory at the CTS and series of experiments were conducted prior to testing the high-speed system at the Airport in Townsville. This enabled any potential difficulties to be identified and rectified in controlled lab conditions before conducting tests in the field.

Tests were carried out on these two instruments over a period of about five months in 2010. Details of these tests and results are provided in this appendix. The focus of these tests were to ascertain the response of these two Dines instruments, and provide test results to Task 2 of this project for calibration and validation of the mathematical models. The analysis carried out in Task 1 is also assessed against these test results.

Borges (1968) evaluated the response of a Fuess floater-type pressure tube anemometer (similar to the Dines) to sinusoidal pressures of different frequencies and showed the system amplified frequencies between 0.1 to 0.4 Hz at a mean speed of 20 m/s. The experimental setup by Borges (1968) was unable to carry out tests at frequencies less than 0.1 Hz. Recent development of the advanced Pressure Loading Actuator (PLA) that can simulate realistic fluctuating wind pressures allow the response of the Dines anemometers to be assessed for a wide range of frequencies including actual fluctuating winds.

Figure 1. 3-cup anemometer

Figure 2. Dines anemometer

Figure 3. High Speed Float Chamber

Figure 4. Float rod and speed recorder

2 Experimental setup and Data collection

Several configurations, isolating each component in turn; the Dines head, the float chamber and the 10 m tubing, were tested for assessing their contributions to the overall response of the instrument. The 10 m of tubing is the typical height of the head above ground level. The dynamic response of the Dines is complex and is dependent on the characteristics of the applied pressure fluctuations and the mass of the float/rod and the column of water in the chamber.

Pressure input to the Dines

Advanced real time pressure loading systems capable of high flow have been developed for the "Three Little Pigs" (3LP) full scale house testing facility at the University of Western Ontario

(UWO) (Kopp et al. 2010). The pressure load actuator (PLA) is used to apply actual turbulent wind pressures in an enclosure or chamber. These varying pressure time histories are obtained from measurements in a boundary layer wind tunnel or from full-scale field measurements. A Pressure Loading Actuator was used to apply a range of pressures to the Dines instruments.

The two main components of the PLA unit, shown in Figure 5, are a regenerative blower capable of delivering flows with high pressures in a large volume, and a highly reactive four port valve. The PLA's four port valve can be rapidly cycled between delivering positive pressure or negative pressure by using a rotating shaped disc. The varying shape of the holes in the disc allows the computer, via a series of lookup functions, to set the rate of flow (e.g., open the "tap" more to generate more flow). A high torque servo motor is used to rapidly position the disc.

A range of test pressure time traces were applied to the various Dines test configurations. The traces ranged from "steady" step traces, sinusoidal with frequencies from 0.2 to 6 Hz, square waves, white noise and pressure time series data representative of fluctuating velocities derived from wind tunnel data and from a sonic anemometer.

A manifold was fabricated from PVC pipe to adapt the PLA outlet hose to the Dines inlet at the head/vane unit as shown in Figure 6. The input pressure from the PLA was measured with two pressure transducers located in the manifold immediately in front of the inlet of the Dines head. One pressure transducer (PT) was used by the PLA for controlling the valve to achieve the requested pressure trace. The second PT output was recorded using the same data acquisition (DAQ) module that recorded the response of the LVDT attached to the float. The DAQ used a simultaneous sampling system ensuring that the input and output (i.e. PT and LVDT measurements) were synchronized.

Dines output

The output of the Dines float chamber is measured by the vertical rise and fall of a float rod attached to the top of the float chamber. The vertical movement is typically transcribed directly onto a chart rotated by clockwork. The chart is located adjacent to the float rod. The robust and reliable operation of the Dines and provision of repeatable output is reliant on initial and ongoing maintenance procedures, such as ensuring the free running of the float in the chamber slides and the balancing of the float chamber via the lead shot cup on top of the rod.

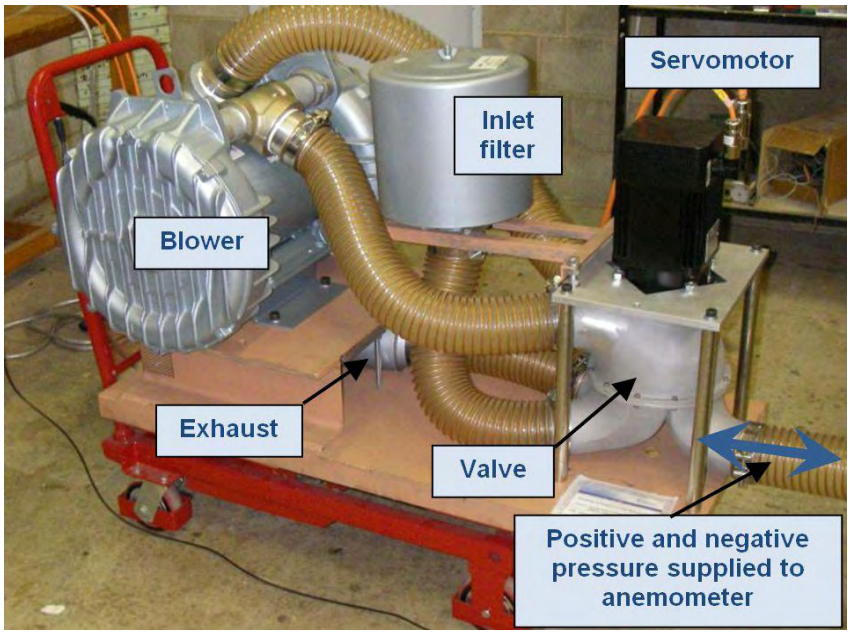

Figure 5. Pressure Load Actuator (PLA) - components

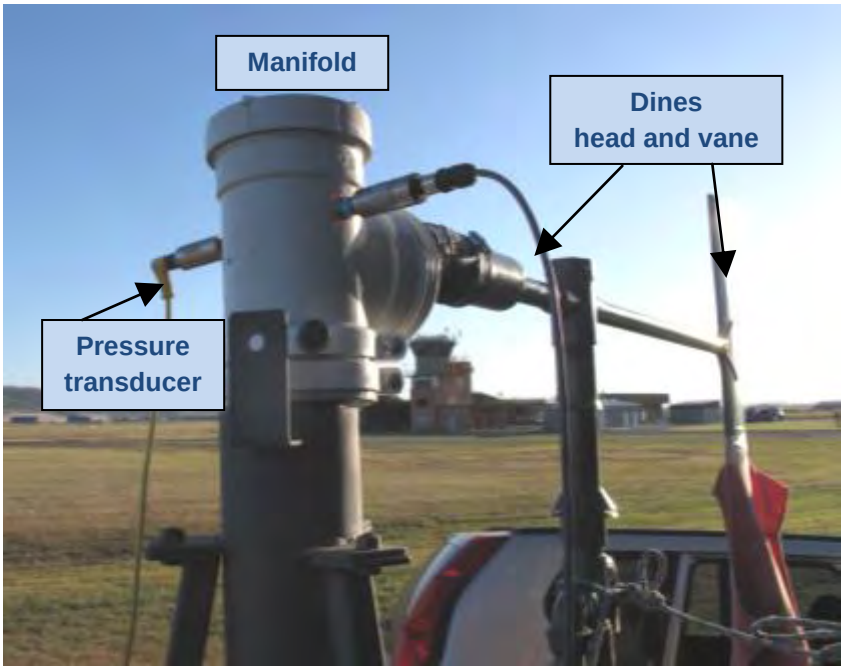

Figure 6. Manifold and stand for connection PLA to Dines head/vane. Note the two pressure transducers located at the inlet of the Dines head.

The response of the float chamber to the applied pressure was measured using a linear variable differential transformer (LVDT) connected to the shot-cup on top of the float rod as shown in Figure 7. A small universal joint was used to connect the shot-cup to the LVDT. A crucial requirement was to ensure that the weight of the universal joint, modified shot-cup and LVDT shaft was equal to the weight of the original shot-cup, lead shot and pen.

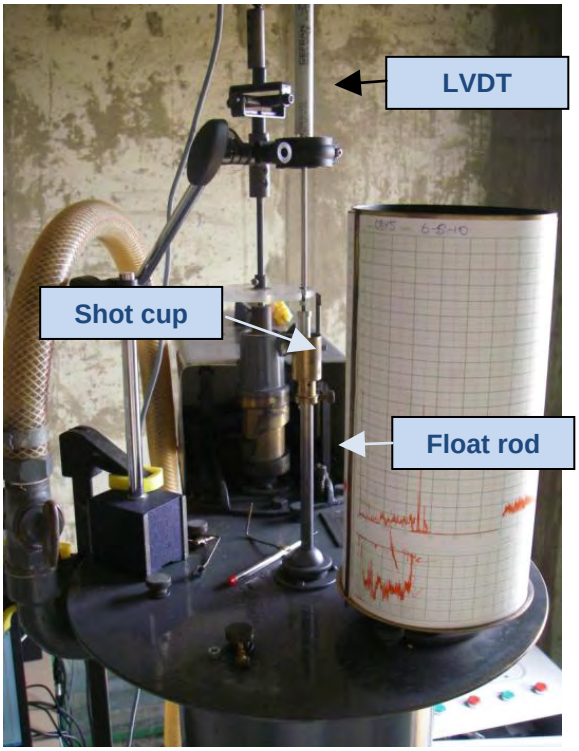

Figure 7. LVDT measuring movement of float rod

Test configurations

A range of test configurations were set-up to examine the contribution of each component of the Dines systems to the overall frequency response. The tests included assessing the response of both the high-speed and low-speed Dines float chambers, as well as investigating the contribution of the Dines Head (with associated bends), and the connecting tubing to the overall response of the system.

The test configurations were;

1. PLA connected to 10 m PVC tube (30 mm internal diameter) with 225 mm long 100 mm internal diameter *fixed* float volume at the output end (i.e. Dines head and float chamber not used)

2. PLA connected to Dines head (including right angle bends) to 8.1 m PVC tube (30 mm internal diameter) with 225 mm long 100 mm internal diameter *fixed* float volume at end (total "length of tubing" from Dines head to fixed volume remains 10 m)

3. PLA connected to Dines head (including right angle bends) to 225 mm long 100 mm internal diameter *fixed* float volume at output end (using only short flexible tube of ~ 2m)

4. PLA connected to Dines head (including right angle bends) to 10 m PVC tube (30 mm internal diameter) with low-speed Dines float chamber at the output end

5. PLA connected to Dines head (including right angle bends) to low-speed Dines float chamber (using only short flexible tube of ~ 2 m)

6. PLA connected to Dines head (including right angle bends) to high-speed Dines float chamber (using only short flexible tube of ~ 2 m)

Tests were conducted to assess for the mean (time averaged) response of the Dines to static step pressures (i.e. steady velocity) and the fluctuating (i.e. dynamic) response

3 Results

Configuration 1

A straight 10 m length of 30 mm diameter PVC pipe was connected to the PLA manifold at the input end. A PVC tube 225 mm long and 100 mm internal diameter was attached to the output end of the 10 m length of tube. This chamber nominally represents the volume of the float chamber in the Dines but does not vary in size (and is used as a base line for the experiments). The test configuration is shown in Figure 8.

The input from the PLA was measured with pressure transducers at the inlet manifold and compared to a pressure transducer measuring the pressure in the fixed volume at the end of the tube. CTM refers to the pressure transducer at the input while PTE refers to the pressure transducer at the output (i.e. the fixed volume).

(a) (b)

Figure 8. (a) Fixed volume at end of 10 m pipe and (b) inlet of 10 m straight tube

A series of cyclic and other fluctuating input pressure traces were applied. The results obtained from the cyclic pressure inputs are given in Table 1, in terms of the Standard deviation and Peak output to input pressure ratios. The amplification of pressure as the cyclic frequency approaches 6 Hz is evident with the standard deviation ratio exceeding 5.0.

Table 1. Sinusoidal traces for Configuration 1

					Ratio of output over input	
Trace	Type	Freq	Target Min	Target Max	Std dev	Peaks
		(Hz)	(kPa)	(kPa)	ratio	ratio
28-r8	Cyclic	0.05	1	3	0.99	1.03
27-r28	Cyclic	0.2	1.8	2.2	1.05	1.01
28-r5	Cyclic	0.2	1	3	0.99	1.02
28-r6	Cyclic	0.2	1	3	0.99	1.0
27-r5	Cyclic	0.3	1	3	0.995	1.02
27-r33	Cyclic	0.5	1	3	0.99	1.04
28-r3	Cyclic	0.5	1	3	1.0	1.02
27-r32	Cyclic	1.0	1	3	1.02	1.06
27-r30	Cyclic	2.0	1	3	1.13	1.08
29-r1	Cyclic	3.0	1.5	2.5	1.35	1.6
28-r4	Cyclic	4.0	1.8	2.2	1.7	1.07
29-r2	Cyclic	5.0	1.8	2.2	2.52	1.2
27-r29	Cyclic	6.0	1.8	2.2	5.2	1.3

The fluctuating component of measured input and output pressure signals for a white-noise input pressure trace are given in Figure 9. The mean values of the pressures have been calculated and subtracted from the plots in Figure 9. The spectra of both signals and the ratio of the output/input are given in Figure 10. The figures show the amplification of the input signal at higher frequencies (> 2Hz), with a resonant peak near 6Hz.

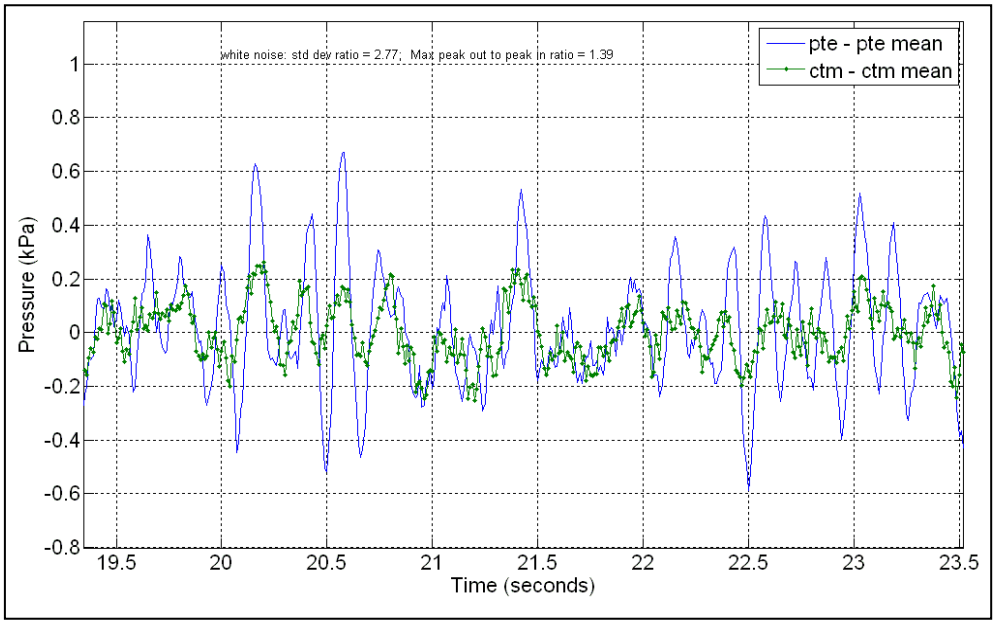

Figure 9. 27-r31 White-noise trace

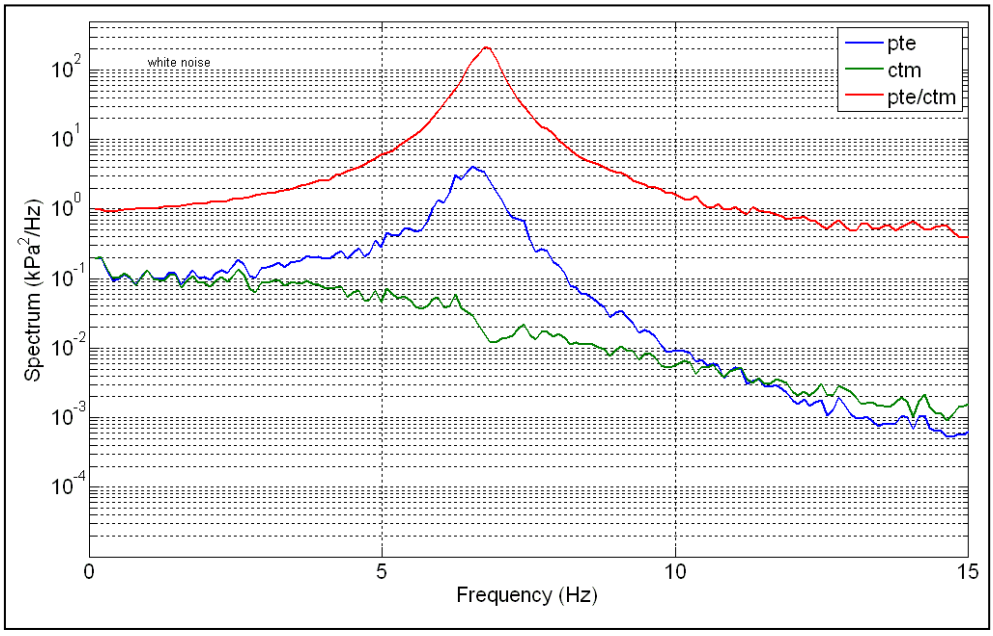

Figure 10. 27-r31 Input and output spectra Configuration 1- White-noise

Configuration 2

The Dines head with its constrictions and bends associated with the inlet tube network was incorporated into the test setup which still included the *fixed* PVC volume at the output end of the tube.

Figure 11 shows the input white-noise spectrum and output pressure spectrum. The resonant peak of frequency response of the system changed slightly from approximately 5.8 Hz to about 5.5 Hz (with the addition of the Dines head unit). The head unit had a negligible influence to the frequency response of the system.

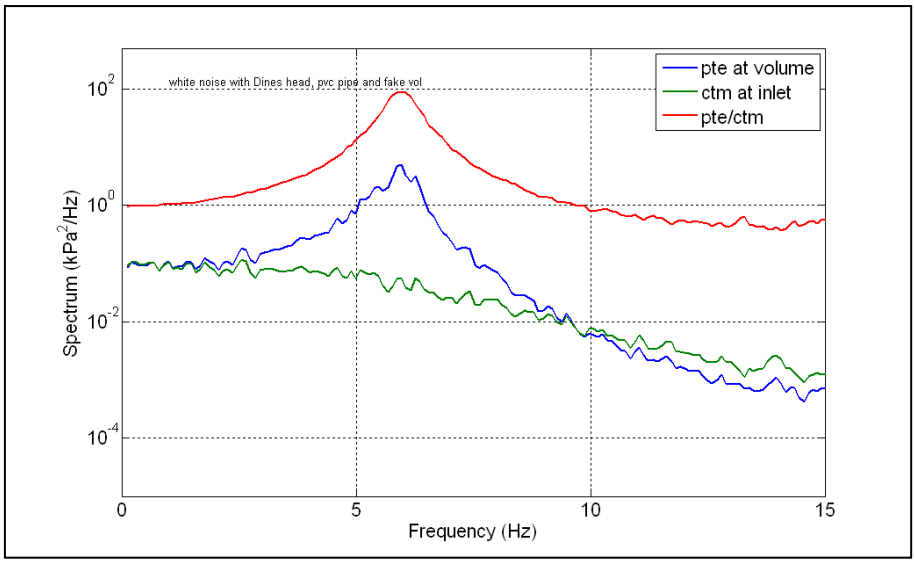

Figure 11. Input and output spectra Configuration 2- White-noise

Configuration 3

The PLA was connected to Dines head and right angle bends to 225 mm long 100 mm internal diameter *fixed* float volume (i.e. without the 10 m of tube). The test setup is shown in Figure 12.

The input white-noise spectrum and output pressure spectrum in Figure 13 show that there is no attenuation or resonance below 6 Hz. This confirms that the amplification shown at the frequency of about 6Hz is generated by the pipe (as was also demonstrated in Task 2).

Figure 12. Dines head connected to fixed float volume

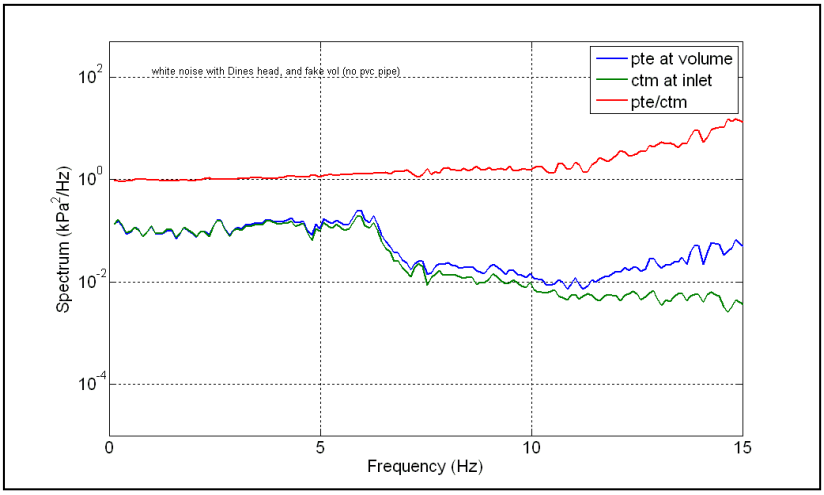

Figure 13. Input and output spectra Configuration 3- White-noise

Configuration 4

The PLA was connected to the Dines head (including right angle bends) to 10 m PVC tube (30 mm internal diameter) with standard (i.e. low-speed) Dines float chamber at the end.

Figure 14 shows the output/input standard deviation ratios for sinusoidal pressures of two different amplitude ranges, with frequencies of 0.2 to 6 Hz. The standard deviation ratios are dependent on the frequency and amplitude of the input signal. Fluctuations in the range of 0.2 to 0.4 Hz, generates an amplification of the input signal, whilst a significant trough is recoded at about 1Hz followed by a second attenuated peak at about 1.2Hz.

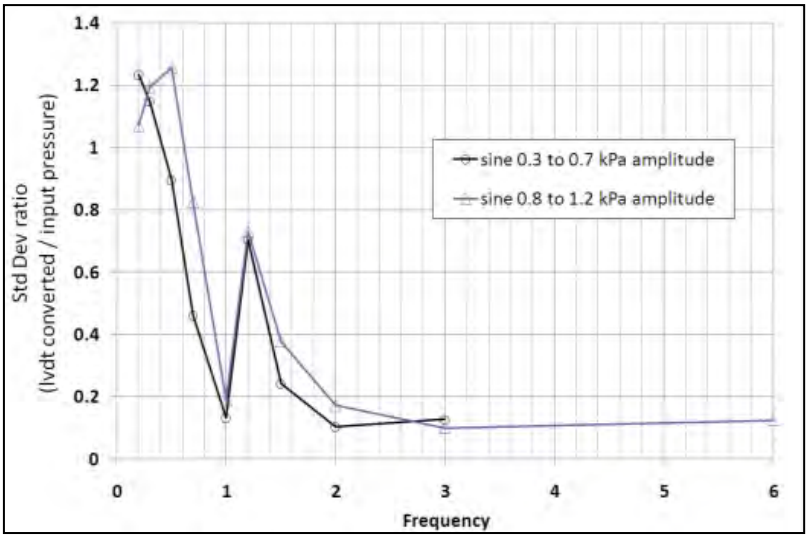

Figure 14. Output/input standard deviation ratios for sine waves two amplitude ranges – low-speed Dines float chamber

The input and output spectra for a white-noise input pressure signal with an amplitude of 0.5 to 1.0 kPa is shown Figure 15. The output spectrum shows the characteristic double peak similar to Borges (1968).

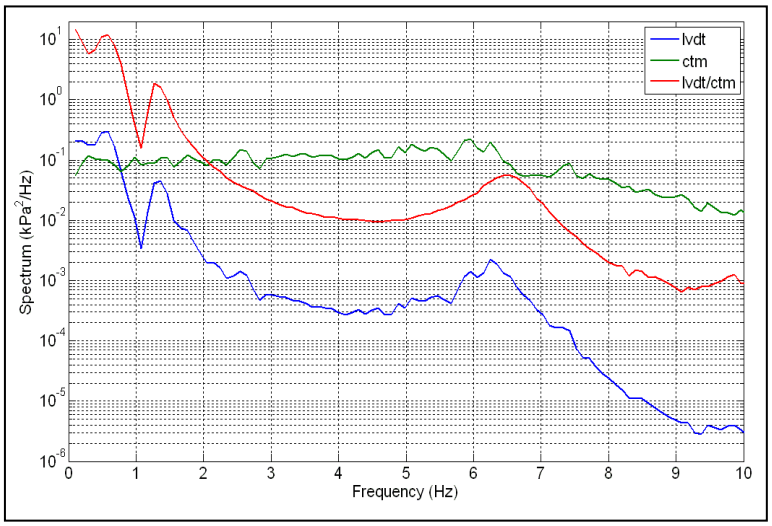

Figure 15. White noise input of 0.5 to 1.0 kPa with output of float (LVDT)

Configuration 5

The PLA is connected to Dines head (including right angle bends) to the low-speed Dines float chamber (i.e. without 10m length of tube), and subjected to white-noise input pressure of 0.5 to 1.0kPa signal. The input and output spectra shown in Figure 16 indicates the characteristic double peak at 0.8 and 1.2 Hz. Comparing Figure 15 with Figure 16, shows that 10m tube length only effects the higher frequencies around 6 Hz. That is the 10 m tube has little influence on the Dines float response for the frequencies in the range of significant wind velocity fluctuations (< 3 Hz).

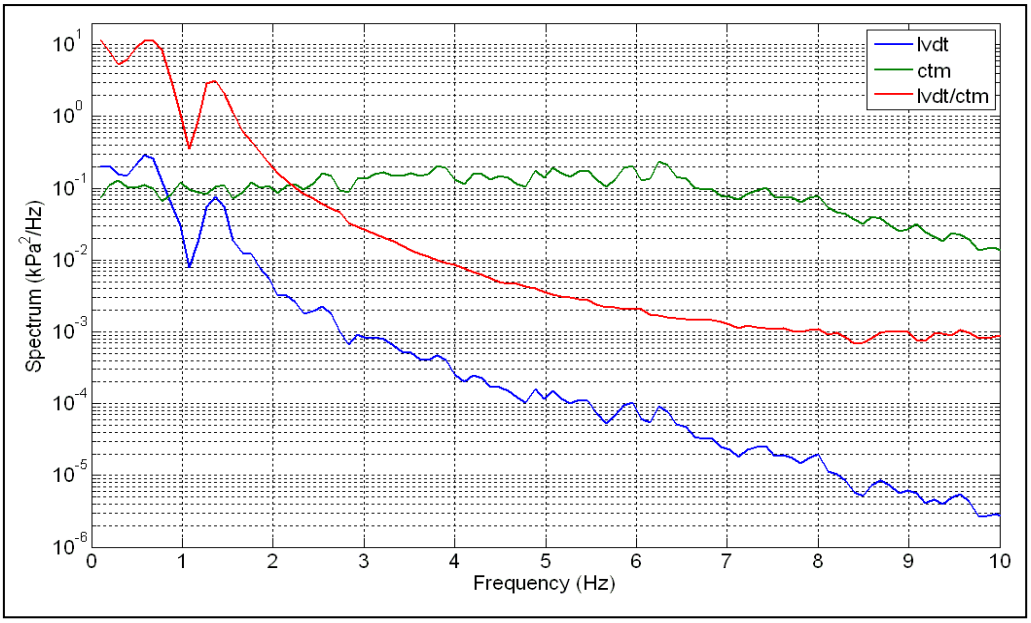

Figure 16. White noise input of 0.5 to 1.0 kPa with output of float (LVDT)

Configuration 6

The PLA is connected to Dines head (including right angle bends) and the high-speed float chamber. The tests were conducted with the Dines high-speed unit located at the Townsville airport. Figure 17 shows the test setup. A summary of these findings were presented by Henderson et al (2010)

Figure 17. PLA (in utility) connected to volume chamber which is connected to high-speed Dines

The frequency response of the high speed Dines float to a white noise input pressure with a range of 1 to 1.5 kPa is shown in Figure 18. The pressure signal is amplified at frequencies less than about 0.5 Hz and attenuated beyond that. The frequency response is of similar shape to Borges (1968) and the low-speed Dines, although the frequencies at which the peaks and troughs occur were different.

Cyclic (i.e. sinusoidal) input pressure traces generated float responses that reflected its spectrum to white noise. The displacement of the float was dependent on the magnitude of the pressure range and the frequency. Figures 19 and 20 show the response of the High speed Dines unit to a range of Sinusoidal pressure traces. The attenuation of the pressure signals at approximately 0.8 Hz and the change in phase at 1.3 Hz is evident.

Figures 21 to 24 show the response of the high-speed Dines unit to a range of square wave pressure traces of amplitudes 0 to 3 kPa and periods from 10 seconds to 2.5 seconds. The distinct "kink" and the overshooting of the response were also seen with the low-speed Dines. The time taken for the LVDT to settle depends on the amplitude.

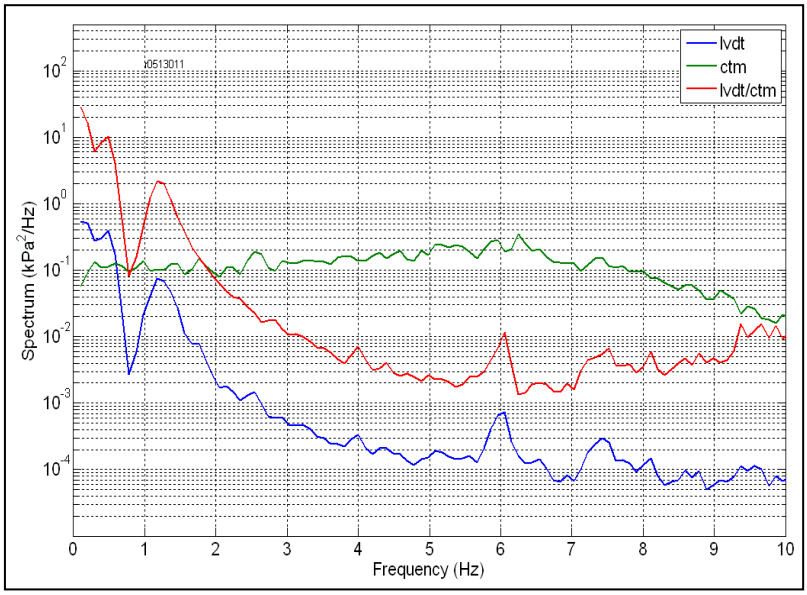

Figure 18. White-noise spectrum (mean 1 kPa, max 1.5 kPa)

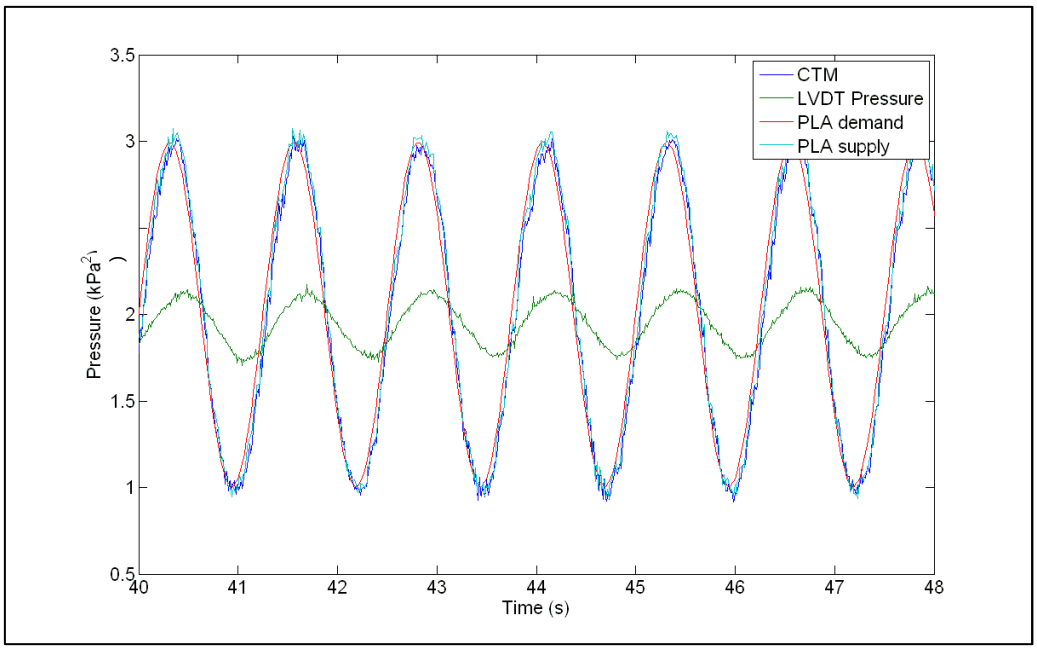

Figure 19. Input sine pressure 0.8 Hz, 1 to 3 kPa showing attenuation of Dines output

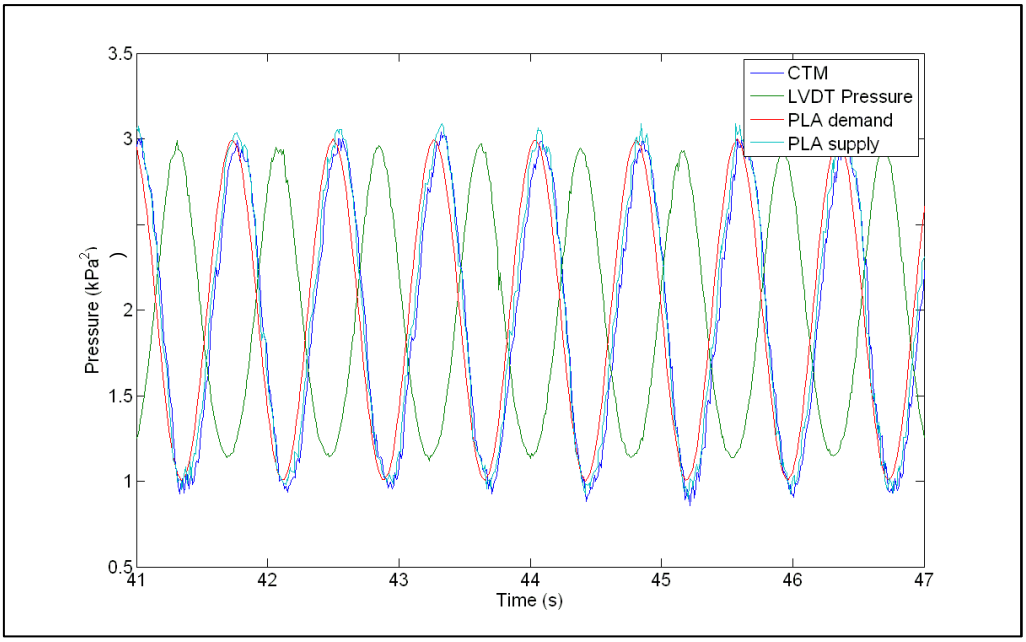

Figure 20. Input sine pressure 1.3 Hz, 1 to 3 kPa showing phase change of Dines output

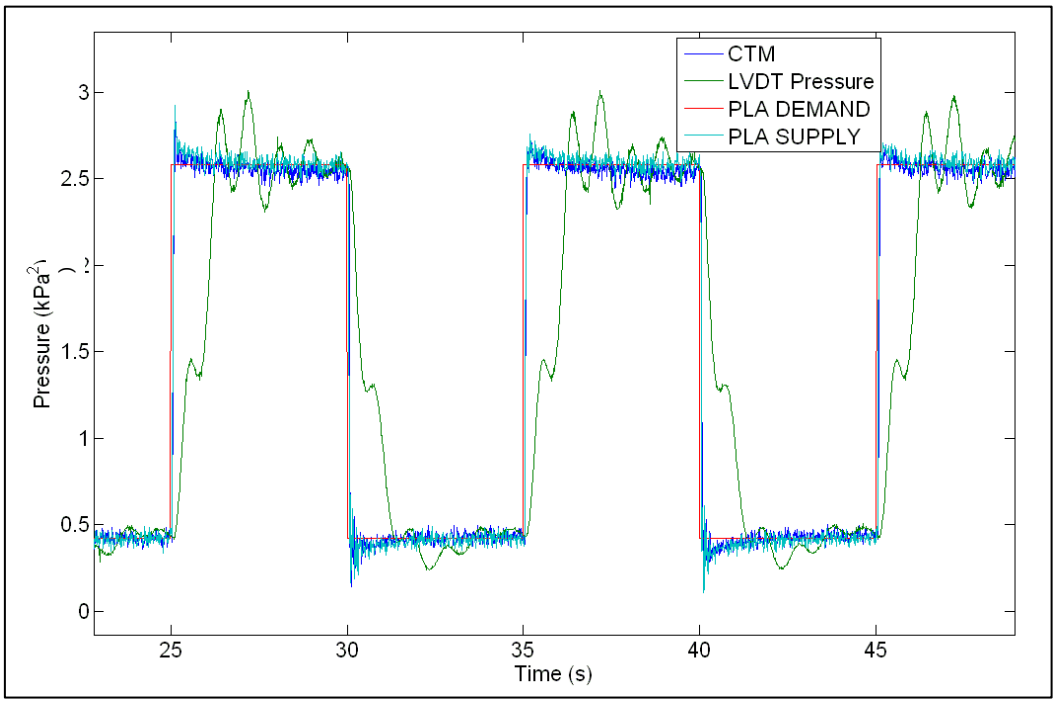

Figure 21. Input square wave pressure 2.25 kPa amplitude with period of 10s

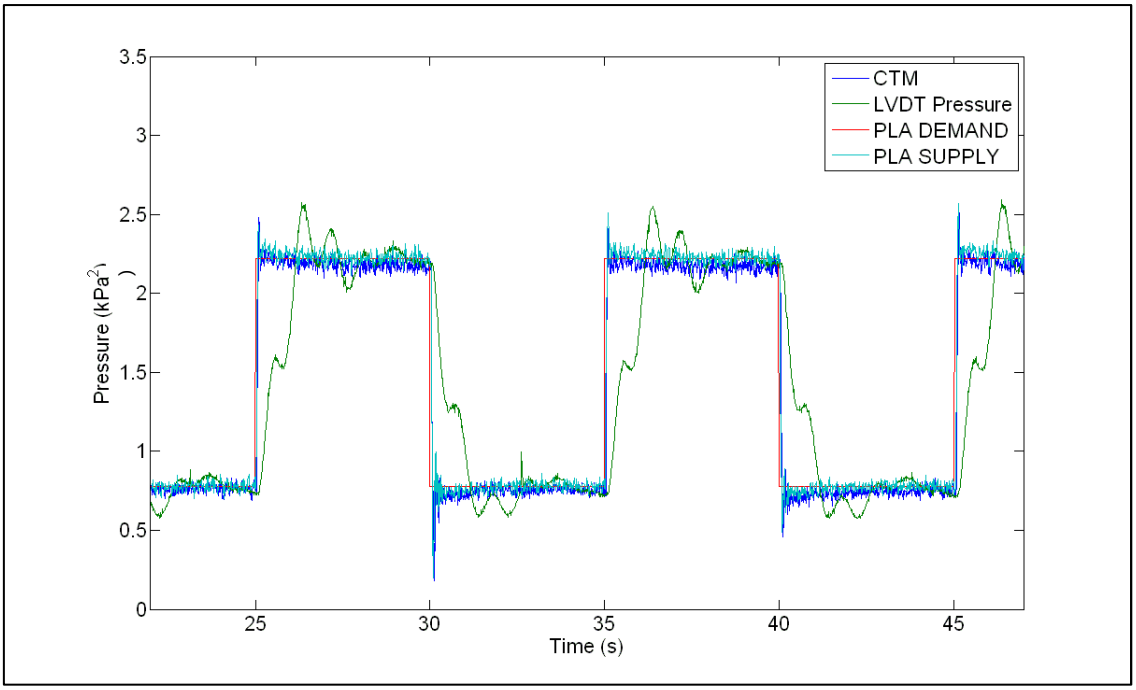

Figure 22. Input square wave pressure 1.5 kPa amplitude with period of 10s

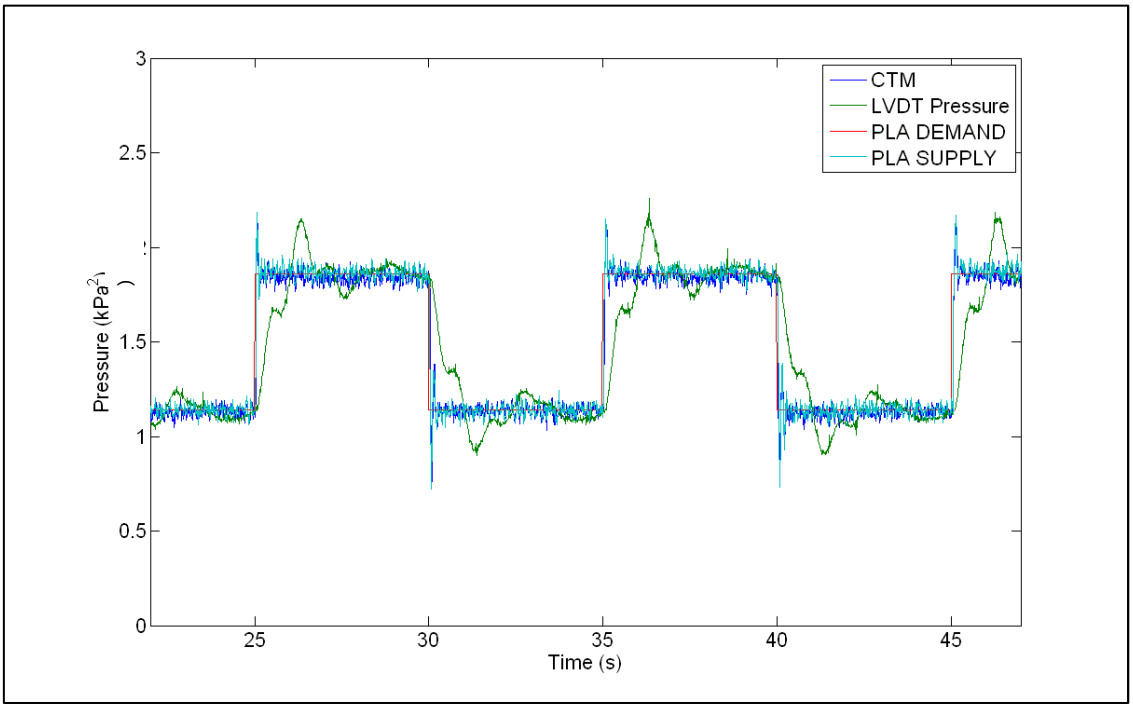

Figure 23. Input square wave pressure 0.75 kPa amplitude with period of 10s

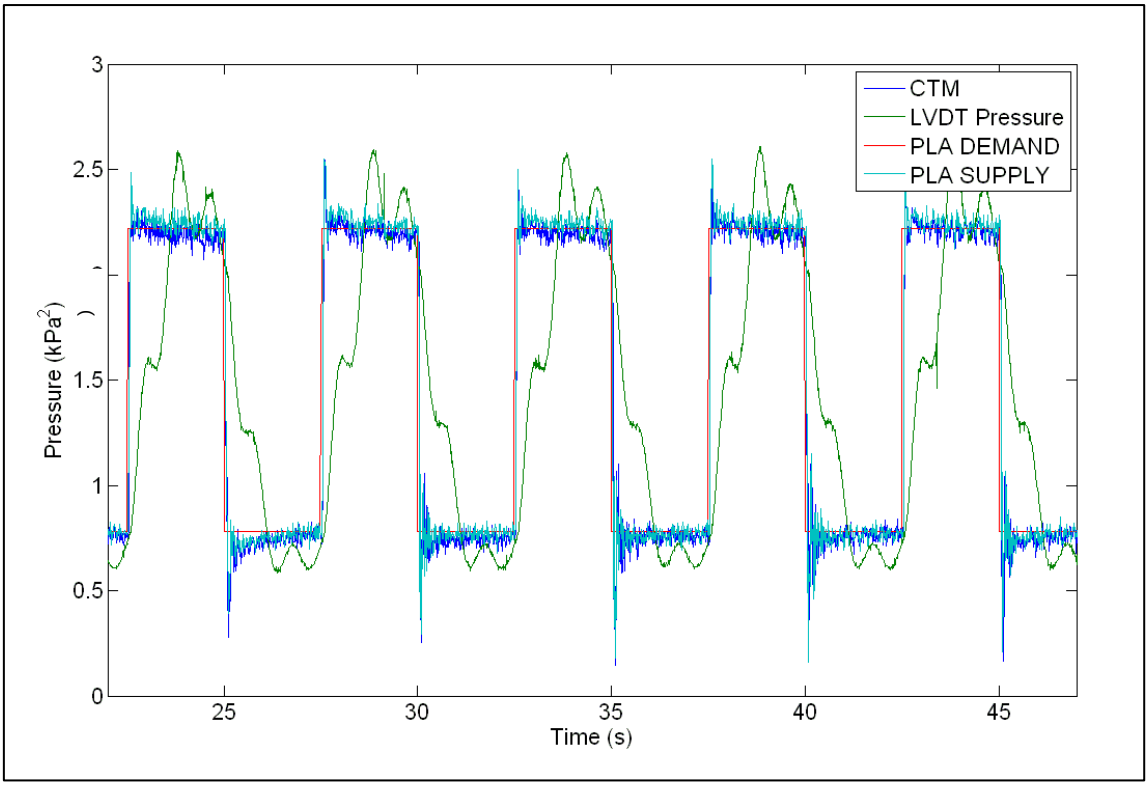

Figure 24. Input square wave pressure 1.5 kPa amplitude with period of 5 seconds

The high-speed Dines was subjected to a range of "simulated input pressure traces" based on measured wind velocity traces. The mean value of the output pressure (measured using the time averaged mean displacement of the LVDT) matched the mean input pressure. Figure 25 shows a 30sec portion of input wind pressure derived from a measured velocity signal and 1-s moving average filtered trace of the signal and the output float (or LVDT) displacement. Figure 25 shows that the Dines output effectively "follows" the input velocity fluctuations. However, the Dines misses the large peak gusts, but amplifies some of the broader peaks and was "out of phase" with some of the cycles.

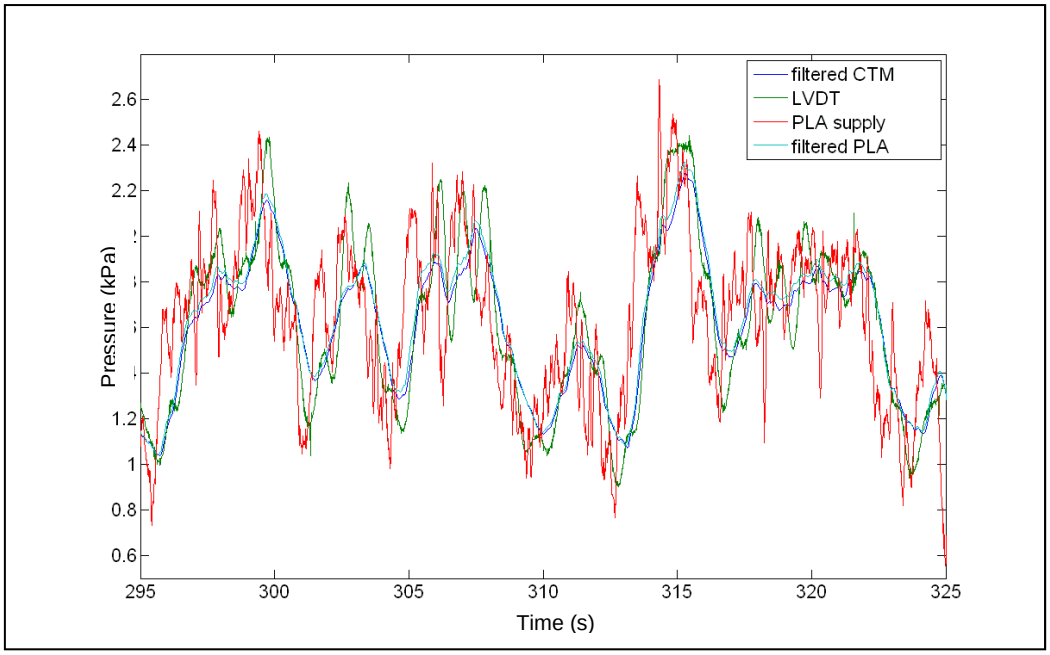

Figure 25. Portion of wind trace with 1s moving averaged filter on input pressure traces of CTM and PLA and the output of the LVDT converted to pressure

4 Discussion

The low-speed and high-speed Dines instruments were calibrated for their mean (time averaged) response to static pressures (i.e. steady velocity). The static pressure test provided a calibration factor that relates the vertical displacement of the float rod (in mm) to the applied pressure difference (in Pa) which is converted to the velocity in m/s. The calibration factors obtained are used in the series of fluctuating pressure tests (i.e. sinusoidal, square waves, white noise and pressure signals representing actual velocity), to determine their dynamic response.

The float chamber of the Dines anemometer is designed in such a way that it produces a linear displacement of the float/rod proportional to the measured velocity. The Dines anemometer responds by sensing the wind pressure at the head and relating the pressure difference between the head and reference port, Δp (in Pa) to velocity, U (in m/s) using Equation 1, as described in the "Handbook of meteorological instruments Part 1: Instruments for surface observations" (1956). Here, K =1.49 is a constant factor (i.e. a 'pressure coefficient') based on the shape and dimensions of the head, ρ is the density of air in kg/m^3.

$$\Delta p = \tfrac{1}{2} \rho K U^2 \qquad (1)$$

Following Equation 1, the displacement of the Dines float rod (i.e. the wind speed recorded) is calibrated against the pressure applied to the head. An increasing then decreasing 30 sec step pressure trace was applied to the systems. The vertical displacement of the float rod measured by the LVDT (in mm) was recorded vs Δp and converted to an equivalent velocity using Equation 1. Figures 26 and 27 show the measured response of the low- and high-speed Dines float chambers respectively, obtained by applying the "static" pressure traces. The linear relationship between the velocity, and the low- and high-speed Dines responses are 0.29 and 0.59 ms^{-1}/mm, respectively. The vertical axis (wind speed) of the actual Dines paper chart measured 177 mm for the maximum speed of 100 and 200 knots, thus each mm on the standard and high speed charts is equivalent to 0.290 and 0.583 m/s. Following calibration of the float rod with the LVDT, the vertical movement of the float rod was converted to the equivalent wind speed and then to pressure allowing direct comparison with the fluctuating input pressure traces.

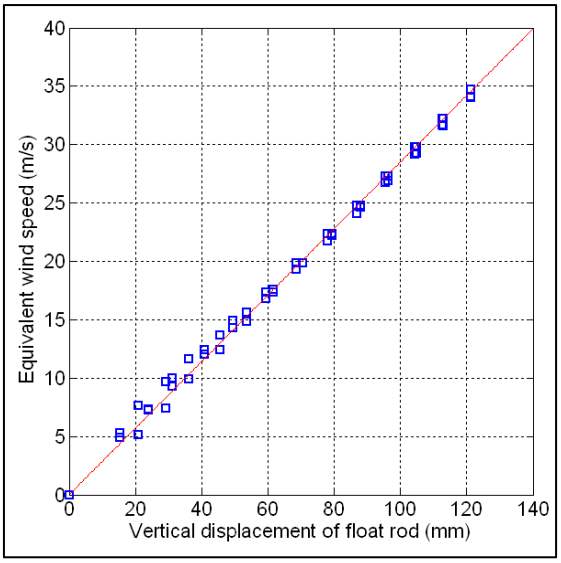

Figure 26. Wind speed converted from applied PLA pressure vs vertical displacement of float rod (measured by LVDT) –Low Speed Dines

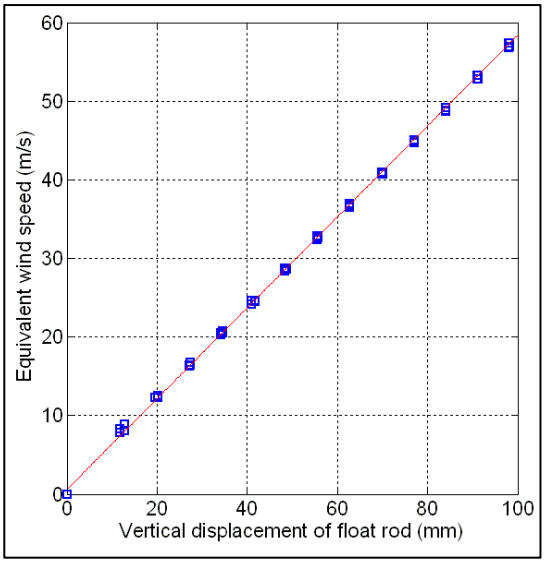

Figure 27. Wind speed converted from applied PLA pressure vs vertical displacement of float rod (measured by LVDT) – High Speed Dines

Dynamic Response

The response of the low Speed and High Speed Dines systems are summarized from tests conducted on each of the component configurations. The frequency response of the low-speed and high-speed Dines are shown in Figures 28 and 29 respectively. These functions have been utilized as a validation of the numerical analysis described in Task 2. Outcomes from these tests are summarized as;

- The 10 m length of tube connecting the inlet head to the float chamber amplifies the input signal at frequencies above 5Hz. Application of an input sinusoidal trace at this frequency showed a 90° phase change (indicating resonance), and a small lag.
- The response of the low-speed and high-speed Dines systems were dominated by their respective float chambers. Pressure fluctuations greater than 2 Hz were effectively damped by the float.
- The analysis of the low-speed and high-speed (float) response spectra to input sinusoidal, white noise and wind traces showed characteristic double peaks; an amplified peak at low frequency (< 0.8 Hz) followed by a trough and an attenuated peak at a higher frequency (~1.2Hz). These low and high frequency peaks relates to the in and out of phase motion of the float with the water column in the chamber.

The low-speed and high-speed Dines instruments were subjected to a range of input fluctuating pressures derived from wins speeds measured by a sonic anemometer. The mean wind speeds were 20, 25 and 30 m/s for the Low speed Dines and 55 and 80 m/s for the High Speed Dines. The turbulence intensities varied from ~10 to 20%. Figure 25 shows the Dines "follows" the wind speed time trace. The mean wind speed is accurately represented by the Dines and peaks are influenced by the float response.

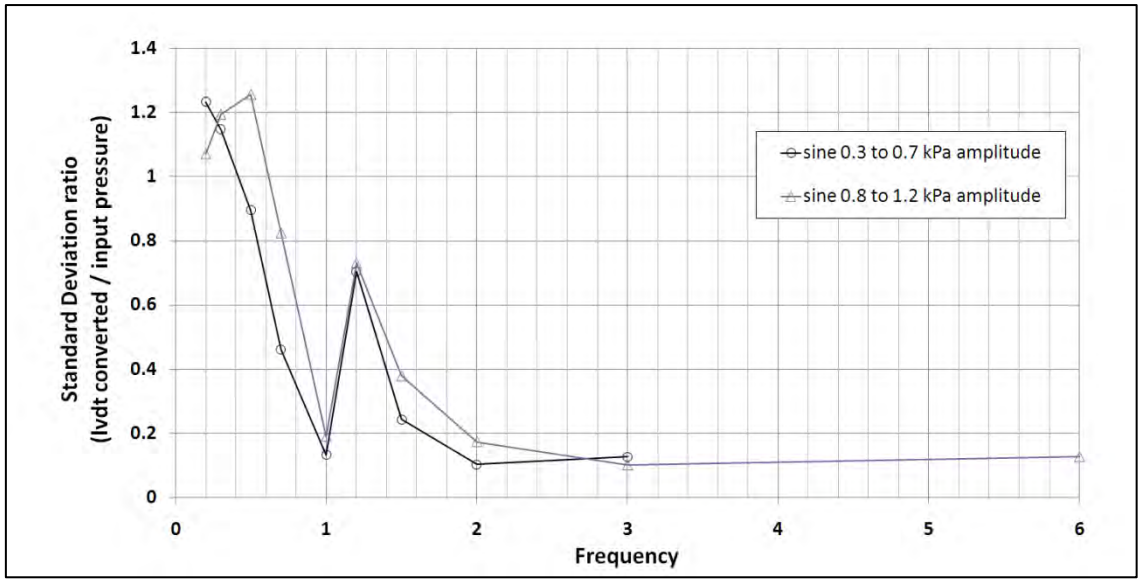

Figure 28. Frequency Response - Low speed Dines

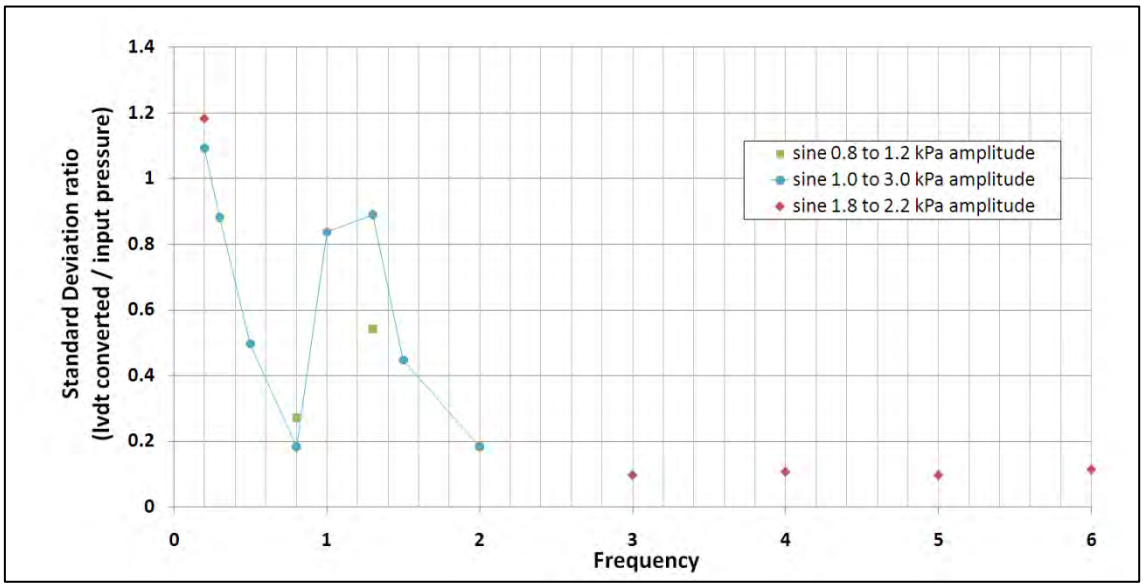

Figure 29. Frequency Response - High speed Dines

4 Conclusions

Experiments were conducted on a low-speed and a high-speed Dines anemometer using a Pressure Loading Actuator capable of simulating realistic wind pressures.

Both the low speed and high speed Dines units replicated mean winds speeds accurately. However, with the application of oscillating pressures such as sinusoidal or fluctuating pressures such as white noise or simulated wind traces, both types of Dines float chambers exhibited amplification and attenuation of some of the input signal peaks. The amount of the attenuation or amplification depended on the frequency, amplitude and mean of the input signal.

5 References

Borges, A. R. J. (1968). "On the frequency response of floater-type anemographs." Technica, 379, 7.

Henderson, D.J., Morrison M. J., Ginger, J.D. and Miller, C. A, (2010) Response of Dines Anemometer to simulated winds, 14th AWES workshop, Canberra.

Kopp, G. A., Morrison, M. J., Iizumi, E., Henderson, D., and Hong, H. P. (2010). "The 'Three Little Pigs' Project: Hurricane Risk Mitigation by Integrated Wind Tunnel and Full-Scale Laboratory Tests." ASCE Natural Hazards Review, Accepted for publication 2010.

Meteorological-Office. (1956). "Handbook of meteorological instruments Part 1: Instruments for surface observations." A. Ministry, ed., Her Majesty's Stationery Office, London.

Reardon, G., Henderson, D., and Ginger, J., (1999) "A structural assessment of the effects of Cyclone Vance on houses in Exmouth WA", Technical Report 48, Cyclone Testing Station, James Cook University, Townsville.

Test data file structure and description provided to project partners for Stage 2

Tests of PLA with PVC tube network (in CTS lab space)

PLA connected to 10 m PVC tube (30 mm internal diameter) with 225 mm long 100 mm internal diameter fixed float volume at end (i.e. NOT using Dines head or float chamber)

IRLBH2010DJHDines\dcc_pt\Test_Data\IRLBH20100427005	27-r5	27/04/2010	sine	0.3 hz at 1 to 3 kPa
IRLBH2010DJHDines\dcc_pt\Test_Data\IRLBH20100427028	27-r28	27/04/2010	sine	0.2 hz at 1.8 to 2.2 kPa
IRLBH2010DJHDines\dcc_pt\Test_Data\IRLBH20100427029	27-r29	27/04/2010	sine	6 hz at 1.8 to 2.2 kPa
IRLBH2010DJHDines\dcc_pt\Test_Data\IRLBH20100427030	27-r30	27/04/2010	sine	2 hz at 1 to 3 kPa
IRLBH2010DJHDines\dcc_pt\Test_Data\IRLBH20100427031	27-r31	27/04/2010	dynamic	white noise
IRLBH2010DJHDines\dcc_pt\Test_Data\IRLBH20100427032	27-r32	27/04/2010	sine	1 hz at 1 to 3 kPa
IRLBH2010DJHDines\dcc_pt\Test_Data\IRLBH20100427033	27-r33	27/04/2010	sine	0.5 hz at 1 to 3 kPa
IRLBH2010DJHDines\dcc_pt\Test_Data\IRLBH20100428003	28-r3	28/04/2010	sine	0.5 hz at 1 to 3 kPa
IRLBH2010DJHDines\dcc_pt\Test_Data\IRLBH20100428004	28-r4	28/04/2010	sine	4 hz at 1.8 to 2.2 kPa
IRLBH2010DJHDines\dcc_pt\Test_Data\IRLBH20100428005	28-r5	28/04/2010	sine	0.2 hz at 1 to 3 kPa
IRLBH2010DJHDines\dcc_pt\Test_Data\IRLBH20100428006	28-r6	28/04/2010	sine	0.2 hz at 1 to 3 kPa
IRLBH2010DJHDines\dcc_pt\Test_Data\IRLBH20100428008	28-r8	28/04/2010	sine	0.05 hz at 1 to 3 kPa
IRLBH2010DJHDines\dcc_pt\Test_Data\IRLBH20100429001	29-r1	29/04/2010	sine	3 hz at 1.5 to 2.5 kPa
IRLBH2010DJHDines\dcc_pt\Test_Data\IRLBH20100429002	29-r2	29/04/2010	sine	5 hz at 1.8 to 2.2 kPa

PLA connected to Glenlitta Dines head (incl right angle bends) to 8.1 m PVC tube (30 mm internal diameter) with 225 mm long 100 mm internal diameter fixed float volume at end (total “length of pipe” from Dines head to fixed volume is 10 m)

IRLBH2010DJHDines\dcc_pt\Test_Data\IRLBH20100430001	30r1	30/04/2010	dynamic	white noise
IRLBH2010DJHDines\dcc_pt\Test_Data\IRLBH20100430002	30r2	30/04/2010	sine	0.5 hz at 1 to 3 kPa
IRLBH2010DJHDines\dcc_pt\Test_Data\IRLBH20100430003	30r3	30/04/2010	sine	6 hz at 1.8 to 2.2 kPa
IRLBH2010DJHDines\dcc_pt\Test_Data\IRLBH20100430004	30r4	30/04/2010	sine	6 hz at 1.8 to 2.2 kPa
IRLBH2010DJHDines\dcc_pt\Test_Data\IRLBH20100430005	30r5	30/04/2010	sine	5.3 hz at 1.8 to 2.2 kPa

PLA connected to Dines head (incl right angle bends) to 225 mm long 100 mm internal diameter fake float volume at end (no 10m of pipe but short flexible tube)

IRLBH2010DJHDines\dcc_pt\Test_Data\IRLBH20100504001	4r1	4/05/2010	dynamic	white noise
IRLBH2010DJHDines\dcc_pt\Test_Data\IRLBH20100504002	4r2	4/05/2010	dynamic	white noise
IRLBH2010DJHDines\dcc_pt\Test_Data\IRLBH20100504003	4r3	4/05/2010	dynamic	white noise
IRLBH2010DJHDines\dcc_pt\Test_Data\IRLBH20100504004	4r4	4/05/2010	dynamic	white noise
IRLBH2010DJHDines\dcc_pt\Test	4r5	4/05/2010	dynamic	white noise

_Data\IRLBH20100504005

Tests at Bureau (airport)

PLA connected to Glenlitta Dines head (incl right angle bends) to high-speed float chamber

IRLBH2010DJHBOM\float_ctm_lvdt\Test_Data\IRLBH20100512006	12r6	40310	sine	0.2 hz at 1 to 3 kPa
IRLBH2010DJHBOM\float_ctm_lvdt\Test_Data\IRLBH20100512007	12r7	12/05/2010	dynamic	TTU_JDG
IRLBH2010DJHBOM\float_ctm_lvdt\Test_Data\IRLBH20100512008	12r8	12/05/2010	step	Step trace
IRLBH2010DJHBOM\float_ctm_lvdt\Test_Data\IRLBH20100512009	12r9	12/05/2010	sine	0.2 hz at 1.8 to 2.2 kPa
IRLBH2010DJHBOM\float_ctm_lvdt\Test_Data\IRLBH20100512011	12r11	12/05/2010	dynamic	white noise 1 kPa mean
IRLBH2010DJHBOM\float_ctm_lvdt\Test_Data\IRLBH20100512012	12r12	12/05/2010	sine	1 hz at 1 to 3 kPa
IRLBH2010DJHBOM\float_ctm_lvdt\Test_Data\IRLBH20100512013	12r13	12/05/2010	sine	0.3 hz at 1 to 3 kPa
IRLBH2010DJHBOM\float_ctm_lvdt\Test_Data\IRLBH20100512014	12r14	12/05/2010	sine	2 hz at 1 to 3 kPa
IRLBH2010DJHBOM\float_ctm_lvdt\Test_Data\IRLBH20100512015	12r15	12/05/2010	sine	3 hz at 1.5 to 2.5 kPa
IRLBH2010DJHBOM\float_ctm_lvdt\Test_Data\IRLBH20100512016	12r16	12/05/2010	sine	4 hz at 1.8 to 2.2 kPa
IRLBH2010DJHBOM\float_ctm_lvdt\Test_Data\IRLBH20100512017	12r17	12/05/2010	sine	5 hz at 1.8 to 2.2 kPa
IRLBH2010DJHBOM\float_ctm_lvdt\Test_Data\IRLBH20100512018	12r18	12/05/2010	sine	6 hz at 1.8 to 2.2 kPa
IRLBH2010DJHBOM\float_ctm_lvdt\Test_Data\IRLBH20100512019	12r19	12/05/2010	square	R 75% with 5 sec cycle
IRLBH2010DJHBOM\float_ctm_lvdt\Test_Data\IRLBH20100512020	12r20	12/05/2010	square	R 50% with 5 sec cycle
IRLBH2010DJHBOM\float_ctm_lvdt\Test_Data\IRLBH20100512021	12r21	12/05/2010	square	R 25% with 5 sec cycle
IRLBH2010DJHBOM\float_ctm_lvdt\Test_Data\IRLBH20100512022	12r22	12/05/2010	square	R 75% with 10 sec cycle
IRLBH2010DJHBOM\float_ctm_lvdt\Test_Data\IRLBH20100512023	12r23	12/05/2010	square	R 75% with 2.5 sec cycle
IRLBH2010DJHBOM\float_ctm_lvdt\Test_Data\IRLBH20100512024	12r24	12/05/2010	dynamic	wind tunnel hot wire scaled 33m/s
IRLBH2010DJHBOM\float_ctm_lvdt\Test_Data\IRLBH20100512025	12r25	12/05/2010	dynamic	wind tunnel hot wire scaled 46m/s
IRLBH2010DJHBOM\float_ctm_lvdt\Test_Data\IRLBH20100512026	12r26	12/05/2010	dynamic	wind tunnel hot wire scaled 39m/s
IRLBH2010DJHBOM\float_ctm_lvdt\Test_Data\IRLBH20100512028	12r28	12/05/2010	sine	0.5 hz at 1 to 3 kPa
IRLBH2010DJHBOM\float_ctm_lvdt\Test_Data\IRLBH20100512029	12r29	12/05/2010	sine	1.5 hz at 1 to 3 kPa
IRLBH2010DJHBOM\float_ctm_lvdt\Test_Data\IRLBH20100513001	13r1	13/05/2010	sine	0.8 hz at 0.8 to 1.2 kPa
IRLBH2010DJHBOM\float_ctm_lvdt\Test_Data\IRLBH20100513002	13r2	13/05/2010	sine	0.8 hz at 1 to 3 kPa
IRLBH2010DJHBOM\float_ctm_lvdt\Test_Data\IRLBH20100513003	13r3	13/05/2010	sine	1.3 hz at 0.8 to 1.2 kPa
IRLBH2010DJHBOM\float_ctm_lvdt\Test_Data\IRLBH20100513004	13r4	13/05/2010	sine	1.3 hz at 1 to 3 kPa
IRLBH2010DJHBOM\float_ctm_lvdt\Test_Data\IRLBH20100513005	13r5	13/05/2010	step	Step trace

Tests on Low speed Dines (in CTS lab space)

PLA connected to Dines head (incl right angle bends) to 10 m PVC tube (30 mm internal diameter) with Dines low-speed float chamber at end

IRLBH2010DJHlowspeed\float_ctm_lvdt\Test_Data\IRLBH20100521005	21r5	21/05/2010	step	Step trace
IRLBH2010DJHlowspeed	21r6	21/05/2010	dynamic	white noise
IRLBH2010DJHlowspeed	21r9	21/05/2010	dynamic	TTU_JDG
IRLBH2010DJHlowspeed\float_ctm_lvdt\Test_Data\IRLBH20100524001	24r1	24/05/2010	step	Step trace
IRLBH2010DJHlowspeed	24r2	24/05/2010	dynamic	white noise
IRLBH2010DJHlowspeed\float_ctm_lvdt\Test_Data\IRLBH20100527001	27r1	27/05/2010	dynamic	white noise
IRLBH2010DJHlowspeed	27r2	27/05/2010	dynamic	TTU_JDG
IRLBH2010DJHlowspeed	27r3	27/05/2010	dynamic	JK_sonic
IRLBH2010DJHlowspeed	27r4	27/05/2010	sine	0.2 hz at 0.8 to 1.2 kPa
IRLBH2010DJHlowspeed	27r5	27/05/2010	sine	0.3 hz at 0.8 to 1.2 kPa
IRLBH2010DJHlowspeed	27r6	27/05/2010	sine	0.5 hz at 0.8 to 1.2 kPa
IRLBH2010DJHlowspeed	27r7	27/05/2010	sine	0.7 hz at 0.8 to 1.2 kPa
IRLBH2010DJHlowspeed	27r8	27/05/2010	sine	1.0 hz at 0.8 to 1.2 kPa
IRLBH2010DJHlowspeed	27r9	27/05/2010	sine	1.2 hz at 0.8 to 1.2 kPa
IRLBH2010DJHlowspeed	27r10	27/05/2010	sine	1.5 hz at 0.8 to 1.2 kPa
IRLBH2010DJHlowspeed	27r11	27/05/2010	sine	2 hz at 0.8 to 1.2 kPa
IRLBH2010DJHlowspeed	27r12	27/05/2010	sine	3 hz at 0.8 to 1.2 kPa
IRLBH2010DJHlowspeed	27r13	27/05/2010	sine	6 hz at 0.8 to 1.2 kPa
IRLBH2010DJHlowspeed	27r14	27/05/2010	sine	0.3 hz at 0.2 to 0.6 kPa
IRLBH2010DJHlowspeed\float_ctm_lvdt\Test_Data\IRLBH20100528001	28r1	28/05/2010	sine	2 hz at 0.2 to 0.6 kPa
IRLBH2010DJHlowspeed	28r2	28/05/2010	sine	0.2 hz at 0.2 to 0.6 kPa
IRLBH2010DJHlowspeed	28r4	28/05/2010	dynamic	JK_sonic
IRLBH2010DJHlowspeed	28r5	28/05/2010	dynamic	JK_sonic
IRLBH2010DJHlowspeed	28r6	28/05/2010	dynamic	JK_sonic
IRLBH2010DJHlowspeed	28r7	28/05/2010	sine	3 hz at 0.3 to 0.7 kPa
IRLBH2010DJHlowspeed	28r8	28/05/2010	sine	2 hz at 0.3 to 0.7 kPa
IRLBH2010DJHlowspeed	28r9	28/05/2010	sine	1.5 hz at 0.3 to 0.7 kPa
IRLBH2010DJHlowspeed	28r10	28/05/2010	sine	1.2 hz at 0.3 to 0.7 kPa
IRLBH2010DJHlowspeed	28r11	28/05/2010	sine	1 hz at 0.3 to 0.7 kPa
IRLBH2010DJHlowspeed	28r12	28/05/2010	sine	0.7 hz at 0.3 to 0.7 kPa
IRLBH2010DJHlowspeed	28r13	28/05/2010	sine	0.5 hz at 0.3 to 0.7 kPa
IRLBH2010DJHlowspeed	28r14	28/05/2010	sine	0.2 hz at 0.3 to 0.7 kPa
IRLBH2010DJHlowspeed	28r15	28/05/2010	sine	0.3 hz at 0.3 to 0.7 kPa
IRLBH2010DJHDines_lowspeed_jun\float_ctm_lvdt\Test_Data\IRLBH20100607001	7r1	7/06/2010	step	step
IRLBH2010DJHDines_lowspeed_jun\float_ctm_lvdt\Test_Data\IRLBH20100607002	7r2	7/06/2010	dynamic	JK_sonic
IRLBH2010DJHDines_lowspeed_jun\float_ctm_lvdt\Test_Data\etc	7r3	7/06/2010	dynamic	JDH 3 cup

IRLBH2010DJHDines_lowspeed_jun\float_ctm_lvdt\Test_Data\etc	7r4	7/06/2010	dynamic	white noise 0.2 to 0.7 kPa
IRLBH2010DJHDines_lowspeed_jun\float_ctm_lvdt\Test_Data\etc	7r5	7/06/2010	dynamic	white noise 0.4 to 0.9 kPa
IRLBH2010DJHDines_lowspeed_jun\float_ctm_lvdt\Test_Data\etc	7r6	7/06/2010	dynamic	white noise 0.6 to 1.1 kPa
IRLBH2010DJHDines_lowspeed_jun\float_ctm_lvdt\Test_Data\etc	7r7	7/06/2010	dynamic	white noise 0.5 to 1.0 kPa
IRLBH2010DJHDines_lowspeed_jun\float_ctm_lvdt\Test_Data\etc	7r8	7/06/2010	dynamic	JK_sonic
IRLBH2010DJHDines_lowspeed_jun\float_ctm_lvdt\Test_Data\etc	7r9	7/06/2010	dynamic	white noise 0.5 to 1.0 kPa
IRLBH2010DJHDines_lowspeed_jun\float_ctm_lvdt\Test_Data\etc	7r10	7/06/2010	dynamic	white noise 0.5 to 1.0 kPa

PLA connected to Dines head (incl right angle bends) to Dines low-speed float chamber (i.e. no 10 m pipe)

IRLBH2010DJHlowspeed_nopipe\float_ctm_lvdt\Test_Data\IRLBH20100528001	28r1	28/05/2010	dynamic	white noise 0.5 to 1.0 kPa
IRLBH2010DJHlowspeed_nopipe\	28r2	28/05/2010	dynamic	white noise 0.5 to 1.0 kPa